U.PORTO

FEUP FACULDADE DE ENGENHARIA UNIVERSIDADE DO PORTO

LNEC LABORATÓRIO NACIONAL DE ENGENHARIA CIVIL

Numerical modelling of the railway track with reinforced substructure

MARGARIDA MILICIC CAMEIRA MARTINS

A Dissertation submitted in partial fulfilment of the requirements for the degree of

MASTER OF SCIENCE IN CIVIL ENGINEERING — SPECIALIZATION IN GEOTECHNICS

Supervisor: Professor Doctor Eduardo Manuel Cabrita Fortunato

Co-supervisor: Doctor André Luís Marques Paixão

SEPTEMBER 2017

MESTRADO INTEGRADO EM ENGENHARIA CIVIL 2016/2017

DEPARTAMENTO DE ENGENHARIA CIVIL

Tel. +351-22-508 1901

Fax +351-22-508 1446

✉ miec@fe.up.pt

Editado por

FACULDADE DE ENGENHARIA DA UNIVERSIDADE DO PORTO

Rua Dr. Roberto Frias

4200-465 PORTO

Portugal

Tel. +351-22-508 1400

Fax +351-22-508 1440

✉ feup@fe.up.pt

http://www.fe.up.pt

Dissertação elaborada no Laboratório Nacional de Engenharia Civil (LNEC) para obtenção do grau de Mestre em Engenharia Civil pela Faculdade de Engenharia Civil da Universidade do Porto (FEUP) no âmbito do Protocolo de Cooperação entre estas duas entidades.

To my mother

ACKNOWLEDGEMENTS

This thesis was developed at LNEC (Laboratório Nacional de Engenharia Civil) under the tutoring of Professor Doctor Eduardo Manuel Cabrita Fortunato as supervisor and Doctor André Luís Marques Paixão as co-supervisor.

This work was carried out under the R&D project GroutRail, co-funded by the European Regional Development Fund, through the POCI, in the scope of the Portugal2020 and Lisb@2020 programs [POCI-01-0247-FEDER-017978].

I would like to express my appreciation to all who have accompanied me during the elaboration of this work that, through their friendship and consideration, contributed to the elaboration of this thesis. I wish to express my sincere gratitude to:

To my supervisor, Professor Doctor Eduardo Fortunato, I would like to thank for the invitation to develop this theme at LNEC, for the encouraging words given throughout this research, for the relevant topic discussions, knowledge acquired and for his support in tough decisions.

To my co-supervisor, Doctor André Paixão, I express my gratitude for his support, constant availability, and constructive reviews, always with keen suggestions, seeking a high scientific rigor. Thank you for sharing with me relevant knowledge on numerical modelling and programming that without it, this work would not have been possible.

To LNEC, in the name of its President, Principal Researcher Carlos Alberto de Brito Pina and to LNEC's Transportation Department, in the name of its Director, Principal Researcher António Lemonde de Macedo, for providing all the conditions and means necessary to develop this work, during my period in LNEC.

To FEUP, in the name of its President, Professor João Falcão e Cunha and the Civil Engineering Department, in the name of its Director, Professor António Silva Cardoso, for all the conditions available and the high standard of education provided, allowing me to become a better professional in my future life.

To Pedro Campos, for the growing friendship demonstrated in the past years but also for the support and giggles shared in our office in LNEC.

To Catarina Mano, for the discussions and suggestions given to each other in our thesis works, but foremost for the long-lasting friendship that I hope will still carry on.

To all the people I have become friends with in LNEC, especially Vânia, Anabela, Vitor, Daniel and the other thesis writers for our entertaining lunch hours, scientific discussions and support. To Ayke and Karen, for the friendship and motivational talks.

To all my friends at FEUP that have been beside me in this 5-year journey, for the memories that will never disappear, especially to José Falcão, Pedro Campelo, Diogo Santos, Filipe Baptista, Gonçalo Cabral and the Miocenics of geotechnics.

To Mariana Amorim, for the stubbornness and for all the journeys that we have gone through as friends and colleagues, whether for the late-night study sessions and thesis discussions as well as international adventures.

Last but not least, to my mother for everything she made for me.

ABSTRACT

Today's railway infrastructures are subjected to greater demands, due to economic and social pressure, leading to an increase of the axle loads and train speeds. Despite many efforts in optimising the design and performance of railway tracks, the degradation of these structures is an intrinsic aspect of its behaviour. To restore the track's structural behaviour to desirable conditions, interventions such as ground improvement techniques are often required to guarantee a required level of performance.

In this thesis, it was decided to study a ground improvement technique that improves the subgrade characteristics underneath the ballast, due to its considerable influence in the track's overall deformation. The focus of this study was to assess the track's structural behaviour when substructure improvement is applied by means of Jet-grout columns.

For that purpose, three-dimensional FDM models designed with varied placement patterns of Jet-grout columns, were studied by carrying out parametric studies on the influence of the column diameter, column pattern and loading position. Even though geomaterials are often considered as having a linear elastic behaviour in most of structural analyses, it is known that the ballast layer has a resilient non-linear elastic behaviour, dependent of the stress levels. For this reason, two different material behaviour models for the ballast layer were considered and ultimately compared.

The results of these studies showed that, by implementing Jet-grout columns, vertical stresses are directed to the columns, following a very clear load path. In general, this results in the reduction of the stress levels at the upper layers of the substructure, as was intended with this reinforcement technique. This aspect is particularly relevant in the context of the rehabilitation of old railway lines to modern requirements. The consideration of the linear elastic behaviour of the ballast layer yielded comparable results to the non-linear elastic behaviour, in terms of vertical displacements. However, in terms of vertical stresses, results for the non-linear approach demonstrated smaller stress concentrations at the columns' positions, in comparison with the linear elastic approach. This might have to do due with the fact that the Young modulus assigned to the ballast layer in the linear approach was somewhat overestimated, which suggests the need for future work in terms of Young modulus calibrations.

KEYWORDS: railway track, substructure reinforcement, FDM modelling, non-linear constitutive laws, k- θ model

RESUMO

Atualmente, as infraestruturas ferroviárias estão sujeitas a maiores exigências, devido à pressão económica e social, levando a um aumento das cargas por eixo e da velocidade de circulação das carruagens. Apesar de vários esforços em otimizar o dimensionamento e o desempenho das ferrovias, a degradação dessas estruturas é um aspeto intrínseco do seu comportamento. Para restaurar o comportamento estrutural da via para condições desejáveis, muitas vezes são necessárias intervenções como técnicas de melhoramento do solo, de forma a garantir o nível de desempenho exigido.

Nesta tese, foi decidido estudar uma medida de fortalecimento do solo que melhore as características da subestrutura abaixo do balastro, devido à sua considerável influência na deformação geral da via. O foco deste estudo foi avaliar o comportamento estrutural da via-férrea quando a subestrutura é intervencionada por meio de colunas Jet-grout.

Para isso, foram estudados modelos FDM tridimensionais modelados com variados padrões de posicionamento das colunas Jet-grout, realizando estudos paramétricos sobre a influência do diâmetro da coluna, padrão de colunas e a posição de carga. Embora os geo-materiais sejam frequentemente considerados como tendo um comportamento elástico linear na maioria das análises estruturais, sabe-se que a camada de balastro possui um comportamento não linear elástico resiliente, dependente do estado de tensão instalado. Por esse motivo, dois modelos diferentes de comportamento do material foram considerados para a camada de balastro e, no final, comparados os resultados dessas análises.

Os resultados desses estudos mostraram que, ao implementar colunas Jet-grout, as tensões verticais são direcionadas para as colunas, sendo visivelmente criado um caminho de carga. Em geral, isso resulta na redução dos níveis de tensão nas camadas superiores da subestrutura, como era pretendido com a aplicação desta técnica de reforço. Este aspeto é particularmente relevante no contexto da reabilitação de linhas ferroviárias antigas para responder aos requisitos modernos. A consideração do comportamento elástico linear da camada de balastro produziu resultados comparáveis ao comportamento elástico não linear, em termos de deslocamentos verticais. No entanto, em termos de tensões verticais, os resultados da abordagem não linear demonstraram concentrações de tensões menores nas colunas, em comparação com a abordagem elástica linear. Verificou-se que isso poderá estar relacionado com o facto de que o módulo de Young atribuído à camada de balastro na abordagem linear ter sido ligeiramente sobreestimado, o que sugere a necessidade de trabalhos futuro em termos de calibrações de módulo de Young.

PALAVRAS-CHAVE: via-férrea, reforço da subestrutura, modelação MDF, leis constitutivas não-lineares, modelo k- θ

TABLE OF CONTENTS

LIST OF FIGURES

LIST OF TABLES

LIST OF SYMBOLS AND ABBREVIATION

k_n	Interface normal stiffness [MPa/m]
k_s	Interface shear stiffness [MPa/m]
E	Young's modulus [MPa]
G	Shear modulus [MPa]
K	Bulk modulus [MPa]
Δz	Smallest zone dimension attached to an interface (m)
δ_{ij}	Kroenecker delta symbol
α_2	Material constant related to the bulk modulus, and shear modulus
E_r	Resilient modulus [MPa]
θ	Sum of principal stresses
$\sigma_1, \sigma_2, \sigma_3$	First, second and third principal stress [MPa]
$E_r \min$	Minimum resilient modulus assigned [MPa]
k_1, k_2	k- θ model parameters
$\Delta\sigma_{ij}$	Stress increment in linear elastic behaviour in FLAC3D
σ_{ij}	Original stress values in linear elastic behaviour in FLAC3D
σ_{ij}^N	New stress values originated in linear elastic behaviour in FLAC3D
D	Jet-grout column diameter [m]
Q	Wheel load [kN]
δ_{max}	Maximum vertical rail displacement [mm]
K_v	Vertical stiffness coefficient [kN/mm]
FEM	Finite Element Method
FDM	Finite Difference Method
FLAC3D	Fast Lagrangian Analysis of Continua in 3 Dimensions
CC1	Model with columns placed in central position relatively to the sleepers and rail, with Jet-grout column under loading point
CE	Model with columns placed in external position relatively to the sleepers and rail, without Jet-grout column under loading point

CE1	Model with columns placed in external position relatively to the sleepers and rail, with Jet-grout column under loading point
CI	Model with columns placed in internal position relatively to the sleepers and rail, without Jet-grout column under loading point
CI1	Model with columns placed in internal position relatively to the sleepers and rail, with Jet-grout column under loading point
CEZZ	Model with columns placed in external position relatively to the sleepers and rail, placed in zig-zag pattern
CIZZ	Model with columns placed in internal position relatively to the sleepers and rail, placed in zig-zag pattern

1 INTRODUCTION

1.1 BACKGROUND OF THIS STUDY

Current trends in transportation show that road haulage dominates the sector, with growing operations, having a dominant position in freight transportation (see Figure 1.1). In the meanwhile, the railway's stake in the freighting market slightly decreased over the past 30 years, remaining stable over the last decade (EC, 2003). Analysing passenger and goods transportation in 2013, in Figure 1.2, we can see a clear dominance of car usage, whether for passenger or freight transportation, accounting for 83.2 % of inland passenger transport and 74.9 % of freight transported, in the EU-28. The rail sector accounted for 7.6 % and 18.2 % in passenger and freight transportation, respectively (EC, 2017).

However, due to increasing environmental awareness, attentions have turned to railway transportation since it reveals itself as the most sustainable choice, with the lowest CO_2 emissions per km.t transported (Varandas, 2013). In Figure 1.3 we can see how the railway transportation is the smallest contributor to CO_2 emissions. For instance, the White Paper on Transport for 2050 (EC, 2011) presents a strategy focused on the development of green and sustainable transportation systems, supporting the increase of rail freight and passenger transport. Many other countries such as Japan, China and Malaysia (Okada, 2007, Raju, 2003, Sunaga & Hifumi, 2001) have promoted development in this area, expanding its railway lines. Railway transport has numerous advantages over others forms of transportation, particularly road and air, related with the lower transportation costs, the lower environmental impact, as seen before, and safety (Montenegro, 2015).

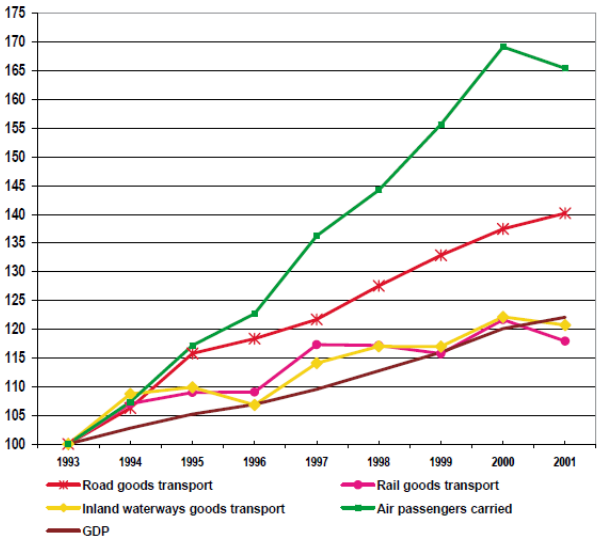

Figure 1.1 - Development of EU-15 transportation trends: growth by mode (1993=100) (after EC, 2003)

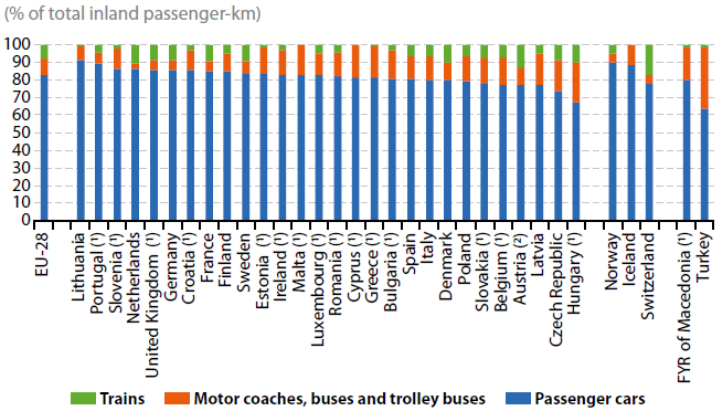

a)

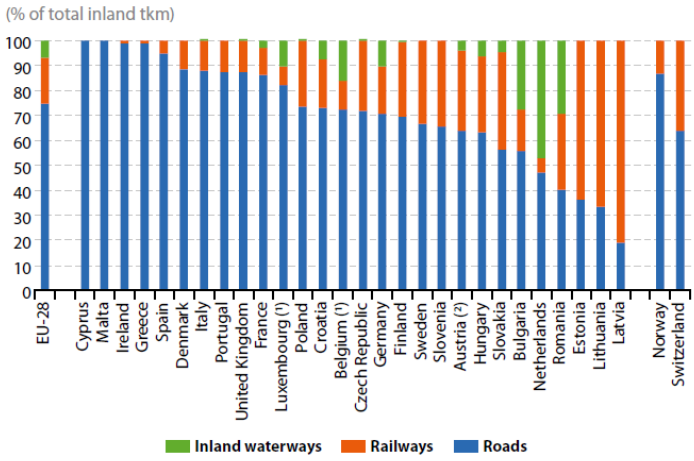

b)

Figure 1.2 - Modal split of inland transportation of a) passenger and b) cargo for 2013 (after EC,2017)

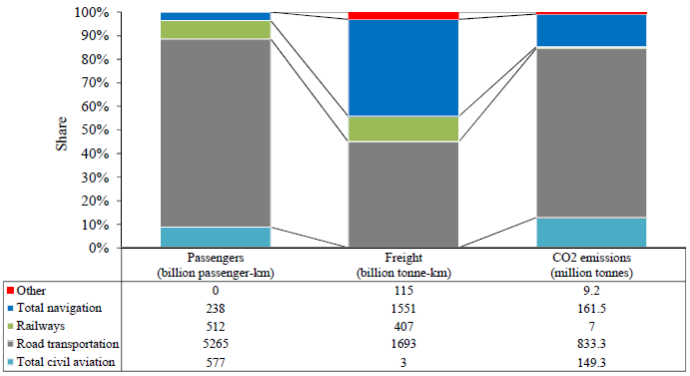

Figure 1.3 - Transportation modes and respective CO_2 emissions, EU-28 countries (after EC,2014)

More and more, the demands that current railways are subjected to are greater due to economic and social reasons, leading to an increase of the axle loads and train speeds. The railway track must have certain characteristics, allowing the safe transportation of passengers and goods, allied to comfort and quality travel levels. To do so, oscillations, noise and vibrations of the train, due to the bad conception

of the track system or due to degradation of it, must not exceed certain limits (Paixão, 2014). Despite this, it is known that, throughout its life-cycle, the railway track degrades its quality (Selig & Waters, 1994). Nowadays, many railways struggle to meet the standards of a good quality track, since its design is not appropriate nor the ground conditions are favourable (Ekberg & Paulsson, 2010). As demands for railway transportation are becoming higher and traffic is growing, there is a need to upgrade these tracks (Ekberg & Paulsson, 2010).

The main functions of the track are to guide the train correctly, to withstand the train's loads and to distribute that same load over a larger area as possible (Dahlberg, 2003), thus quickly reducing the stresses developed into the track substructure (Profillidis, 2000).

Even though there are many design methods available to properly determine the granular layer thickness of the rail track (Li & Selig, 1998), these granular materials suffer degradation, for instance, due to stresses imposed by the cyclic axle loads transferred from the track components onto the subgrade (Selig & Waters, 1994) or due to the weather conditions. To prevent this, a regular monitoring of the track conditions (i.e. in terms of track geometric quality, fault detection and component degradation, among other aspects) combined with adequate maintenance measures should be carried out in order to avoid compromising the track's correct functioning.

In general, the main causes behind track quality degradation are: i) the nature of the axle loads; ii) the variation of the characteristics of the materials that compose the rail track and iii) the environmental conditions (Fortunato, 2005, Ribeiro, Viviana 2015). From the causes mentioned above, the most severe is the nature of the load due to its high value and cyclic nature (Fortunato, 2005). The long-term behaviour of railway tracks, particularly on earth structures, is characterised by the development and accumulation of plastic deformations at different levels that result in settlements visible at the surface of the structure. It is considered that this long-term behaviour of plastic deformation has three main sources, caused either by the cyclic loads from trains or by the geostatic loads, as schematically presented in Figure 1.4, corresponding to: i) plastic deformation from the natural ground soils, primarily due the geostatic loads; ii) plastic deformations in the embankment structure, also mostly due the geostatic loads; and iii) the plastic deformations taking place at the superficial layers of the earth structure, mainly caused by the cyclic loads from trains.

Because the scope of this study is the superficial reinforcement of railway track substructures, the analysis presented herein will focus mainly on the behaviour identified in item iii) and, thus, on the deformability of the track system and stress distribution caused by traffic loads. Another observation to be made is that, with the exception of poor performing track substructures, track settlements tend to stabilise after a significant amount load cycles, normally reaching a steady value after a certain period after entering in service, as depicted in Figure 1.5.

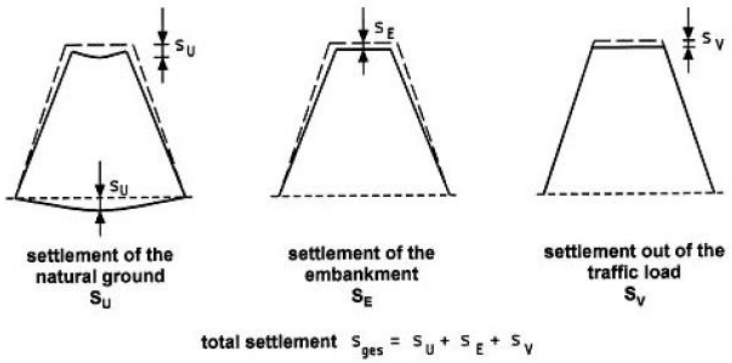

Figure 1.4 - Settlements of embankments (after UIC,2008)

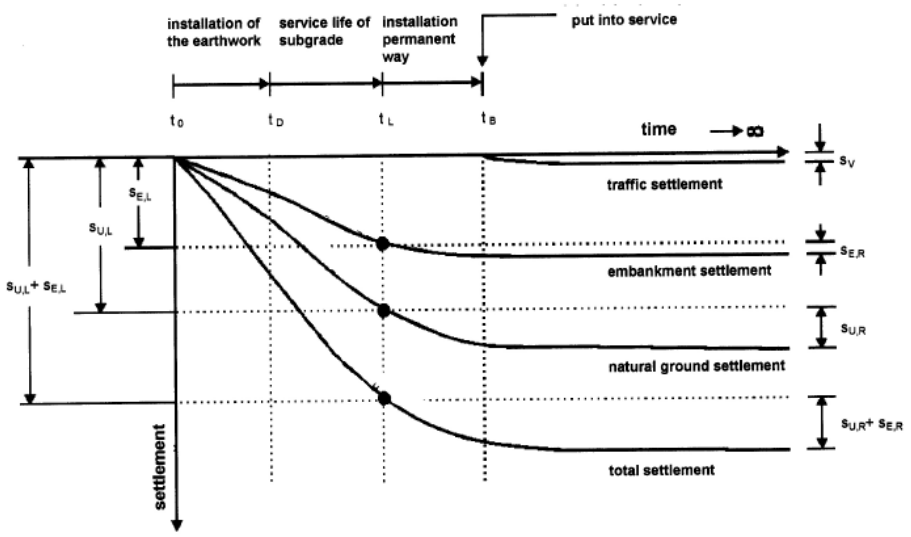

Figure 1.5 - Different settlement parts by time (after UIC,2008)

The expected total settlement that a well-performing railway track undergoes and the contribution of each of its elements to the total settlement has been studied by many authors, and an example is shown in Figure 1.6. It shows that nearly 50 % of the total settlement is due to the ballast's settlement. However, other studies on railway tracks with poor bearing conditions, have shown that only 10-30 % of the deformations have origin in the ballast or sub-ballast layer. The remaining source of deformation is due to the subgrade's low performance (Stewart, 1982).

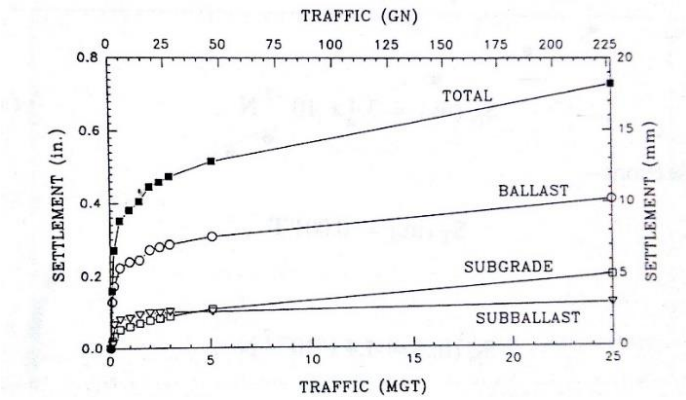

Figure 1.6 - Contribution of the track layers to the total settlement experienced by the track (after Selig & Waters,1994)

Stresses imposed by the axle loads on the subgrade may be considerable, possibly causing progressive shear failure leading, in the end, to the subgrade's overall failure (see Figure 1.7). This behaviour normally occurs in the top of the subgrade, where traffic induced stresses are higher (Selig & Waters, 1994). To reduce the probability of such phenomenon to occur one should ensure an adequate depth of load distributing granular material between the underside of the sleeper and the subgrade's surface and apply good drainage systems to maintain a low water table level (Selig & Waters, 1994).

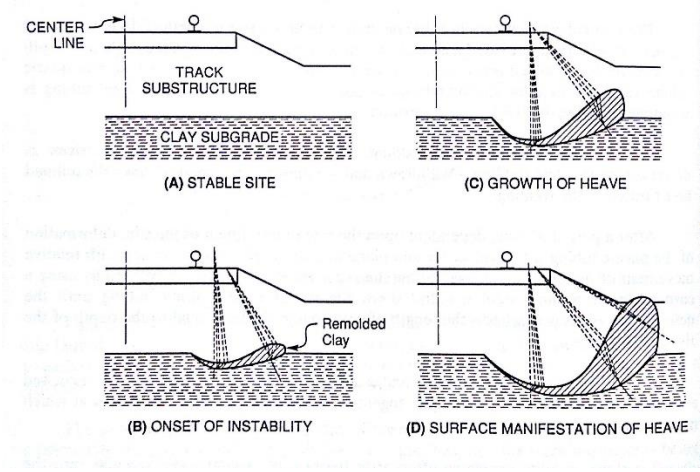

Figure 1.7 - Track subgrade failure caused by repeated loading (after Selig & Waters,1994)

Most of the times, this failure is corrected by addition of ballast underneath the track (Fortunato, 2005, Selig & Waters, 1994), which can be a costly and time consuming measure. Up to a certain level, this measure improves stability, by increasing the ballast's depth, with reduction of soil stresses, However, the ballast inclusion can form ballast pockets (see Figure 1.8) that trap water in it, reducing the improvement's potential (Selig & Waters, 1994).

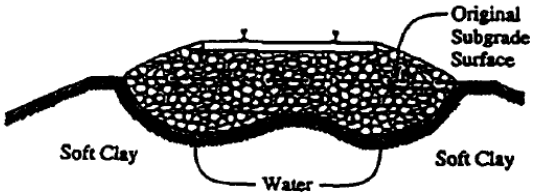

FIG. 3. Excessive Subgrade Plastic Deformation (Ballast Pocket)

Figure 1.8 – Ballast pocket caused by excessive subgrade deformation (after Li & Selig,1998Fortunato (2005))

recommended that platform improvements could consist in:

- Improving the drainage conditions of the track;
- Implementing a sub-ballast layer to reduce stresses at the subgrade's level;
- Improving the subgrade characteristics;
- Placing geosynthetics.

After a railway line is opened to traffic and functioning, the correction of settlements or other flaws can be made according to the method's technical applicability and speed of execution (UIC, 2008).

Taking into consideration the previous observations, in the scope of this thesis, it was considered pertinent to study a ground improvement technique that enhances the subgrade characteristics underneath the ballast, since it is mostly responsible for the track's overall deformation (Stewart, 1982). Track interventions not only are important to improve the railway's performance, but they also represent a substantial portion of the total railway operating cost, reaching up to 70 % of the life cycle cost (Jianmin, 2007). Independently of the subgrade's relevance in maintenance costs, track interventions have mainly been focusing on the superstructure (Ekberg & Paulsson, 2010). Besides additional axle loads and growing train speeds, track alignments frequently must cross over existing poor-quality ground, requiring ground improvement interventions. Such technique should be easy to implement, be able to reduce stresses in the upper granular layers, induced by train loads, and improve the subgrade to

achieve as closely as possible the behaviour represented in Figure 1.6. To do so, it was chosen to study the efficiency of including short Jet-grout columns placed in various patterns, as will be described later in more detail.

Recently, many studies and projects about track degradation have been developed with the purpose to upgrade the tracks to current and higher standards. Example of such projects, where ground-improvement interventions are exposed in various case studies, are the SUPERTRACK (2005), INNOTRACK (2010), SMARTRAIL (2014) and RUFEX (2011).

The analysis made in this thesis focuses on structural behaviour of a railway track after being submitted to substructure reinforcement with short columns. It is considered that the plastic deformation of the studied structures is residual, thus evidencing a quasi-elastic behaviour.

1.2 AIM OF THIS STUDY

This thesis focus is to study and evaluate the track's structural behaviour when its substructure is improved with short Jet-grout columns. To do so, detailed three-dimensional FDM models, designed with various layouts with different placement patterns of Jet-grout columns, will be studied. Parametric studies on the influence of the column diameter, column pattern and loading position will be made, considering two different material behaviour models for the ballast layer, and ultimately comparing them.

The main expected contributions are not only to obtain more insight into the behaviour of these structures and to assess the advantages and potentiality of this ground improvement technique, but also to evaluate the impact of considering non-linear elastic constitutive behaviour for the ballast layer in these advanced numerical modelling approaches.

1.3 THESIS OUTLINE

This thesis is made up by six chapters.

In Chapter 2, a general description of the ballasted track system and its components is made followed by a brief state of the art regarding soil improvement techniques, with application to railways. The methods exposed include the application of geosynthetics, vibro-techniques and grouting techniques.

In Chapter 3, a series of parametric numerical studies regarding interfaces, using FLAC3D, are analysed due to the existence, in the railway model, of certain important interactions that require accurate modelling, such as the sleeper/ballast interaction. In the first parametric study, the implications of applying an interface and how to model its behaviour was assessed. The second parametric test aimed to study the interaction between different mesh types. These parametric tests were made in simpler and smaller models, compared with the railway track models in the following chapters. Ultimately, a conclusion is reached on which software command to apply to the larger scale railway model.

In Chapter 4, a general description of the designed railway numerical models is made, detailing material characteristics, modelling procedures, assigned material constitutive behaviours and other details.

In Chapter 5, to obtain more insight into the behaviour of tracks improved by Jet-grout columns and to assess the advantages and potentiality of this ground improvement technique, the results of parametric studies regarding the influence of the column diameter, column pattern and loading position, in terms of vertical stress and displacement, are presented and discussed. Since one of the focuses of this study was to see the influence of implementing a non-linear elastic behaviour to the ballast layer, in the end of this chapter a comparison between linear elastic and non-linear elastic behaviour is established. Due to the extent of these parametric studies, a limited number of results and plots are presented in this chapter, being the remaining results presented in the digital annexes.

Lastly, in Chapter 6, the main conclusions and recommendations for future developments are mentioned.

2

THE TRACK SYSTEM AND SOIL IMPROVEMENT TECHNIQUES FOR RAILWAY TRACKS

2.1 INTRODUCTION

Currently, many railways still consist of old conventional lines where, for the most part, its design is not optimized and the subgrade is of low quality. Throughout the years, maintenance and inspections were targeted to the superstructure, neglecting the subgrade, regardless of its importance in the track maintenance costs (Ekberg & Paulsson, 2010).

As standards for railway transportation are becoming more demanding and traffic is increasing, there is a need to upgrade these tracks, applying diverse types of improvements, therefore increasing the quality and capacity of these rail lines. Subgrade improvement techniques should consider the current conditions of the track, the desirable outcome for track performance under traffic, economic impact and experience of the railway company. These methods' range is wide, extending from some meters to several kilometres of applicability, depending on the technique (Ekberg & Paulsson, 2010).

However, ground improvement techniques are very-costly, including materials, labour and traffic interruptions that can be extensive in time. Thereby, there is a need to find ground improvement methods that are cost efficient. But these methods must be verified thoroughly before being applied in actual railway tracks. This is where the importance of numerical methods steps in, justifying one of the purposes of this thesis. With numerical methods, it is possible to simulate the behaviour of certain subgrade improvement technique, predicting its behaviour before applying it in the railway line. Nevertheless, experimental field research is also very important to confirm numerical simulations (Ekberg & Paulsson, 2010).

In this chapter, the general composition of the ballasted track system is detailed followed by a general overview of some soil improvement techniques. These methods can be classified in two main categories: mechanical and chemical methods. Mechanical methods include geosynthetics, vibro-techniques, jet-grouting, deep soil mixing and micro pile installation. Chemical methods are electro-osmosis and chemical grouts. Only the mechanical methods are explained in this chapter, for a briefer overview.

2.2 THE TRACK SYSTEM COMPOSITION

To the purpose of this thesis, only the composition of the ballasted track system will be detailed, presenting the most common configuration of this structure and the function of its components. However other track configurations exist such as the slab track (Fortunato & Paixão, 2009). In Figure 2.1 a schematic representation of the difference between a ballastless and a ballasted track is shown.

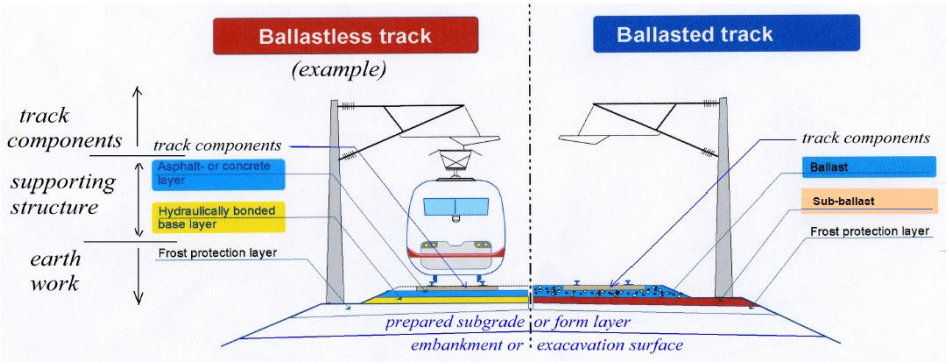

Figure 2.1 – Comparison between ballastless track and ballasted track (after UIC,2008)

2.2.1 SUPERSTRUCTURE AND SUBSTRUCTURE

The general track structure is composed of two subsystems: the superstructure and the substructure. The superstructure composes the rails, fasteners, railpads, sleepers and ballast. The substructure is composed of the subballast layer and subgrade (formation layer and the base). The superstructure is responsible for distributing train loads and is the part of the track structure that is usually submitted to maintenance or replacement operations. The substructure is where train loads are distributed and transferred from the superstructure and, in general, is not submitted to maintenance interventions (Profillidis, 2000) (see Figure 2.2).

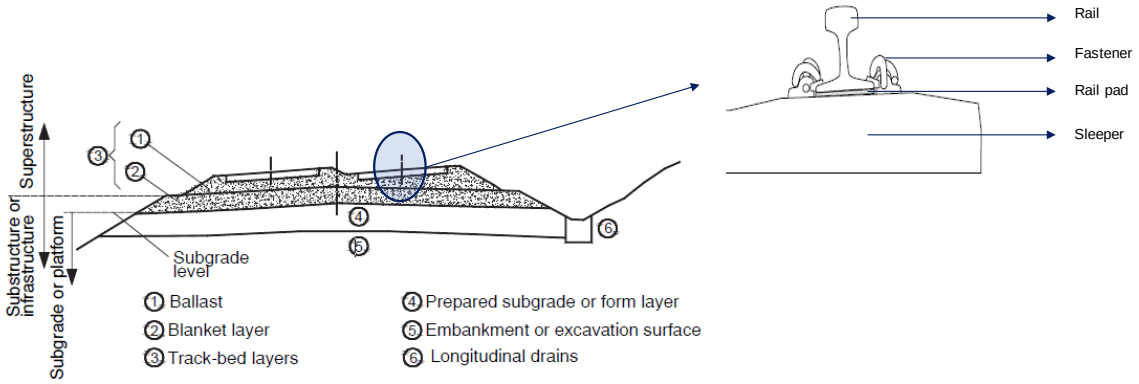

Figure 2.2 - The track structure (after UIC (2008) and Dahlberg (2003))

2.2.2 ELEMENTS OF THE TRACK SYSTEM

In the superstructure, there are the:

- Rails: guide and support the train wheels. These elements must bear and transmit the vertical, lateral and longitudinal loads from the trains to the sleepers and underlying track layers;
- Fasteners: guarantee the adequate positioning of the rails on the sleepers;
- Railpads: protect the sleepers from deteriorating due to load impact and provide electrical insulation. These are placed between the rails and sleepers and can influence track stiffness (Paixão & Fortunato, 2010);
- Sleepers: distribute the rail loads while keeping gauge, level and alignment of the track. It is where the rail and rail pads lie on. Usually made of concrete or timber, they must provide electrical insulation between rails;

- Ballast: composed of coarse granular material, with high compression resistance. Its function is to spread and damp the train loads, transferring them to the bottom layers (Powrie [et al.], 2007). It should ensure vertical elasticity and allow rapid drainage of rainwater on the track. The ballast layer supports the elements mentioned above, having the sleepers embedded in the ballast for better track stability against train loads.

In the substructure, there are the:

- Sub-ballast: it is the separation layer between the ballast and the subgrade, composed by gravel or sand materials. It should distribute further on the external loads, prevent the contamination of the subgrade and the ballast materials into one another and reduce frost penetration, while ensuring good drainage of rainwater.
- Formation layer: applied when the base soil does not have adequate quality, giving a better profile to the track bed. The ballast and sub-ballast rest on this layer.
- Base: it is the foundation of the track. It can consist of on-site soil or soil transported to the site (embankment). It supports all the elements mentioned above.

All of these elements must transfer adequately the loads imposed by the train load to the following element, from the rail to the base layer. This load transferring mechanism must be compatible with the bearing capacity of each component/layer so that they experience a quasi linear elastic or resilient behaviour (Burrow [et al.], 2007, Correia & Loizos, 2004, Jardine, 1992). With depth, the sequence of layers gradually increase its surface area, thus the effect of the train load decreases, eventually becoming neglectable (Profillidis, 2000, Selig & Waters, 1994) (see Figure 2.3).

Regarding the sub-ballast, even though both the ballast's and the sub-ballast's function is to reduce stresses, to obtain a more efficient and affordable solution, the increase of the subballast's thickness is a better approach to reduce those stresses transmitted to the subgrade, instead of increasing the thickness of the ballast layer (Fortunato, 2005).

Concerning the subgrade, it has an important function in guaranteeing the quality standards of train operation. However, it has been one of the causes of track failure and poor track quality. Despite this, the maintenance in existing tracks focuses rather on the railway track upper elements - the superstructure - rather than the subgrade (Fortunato, 2005, Profillidis, 2000). After the track is laid, alterations to improve the subgrade's characteristics are very limited (Chrismer & Read, 1994).

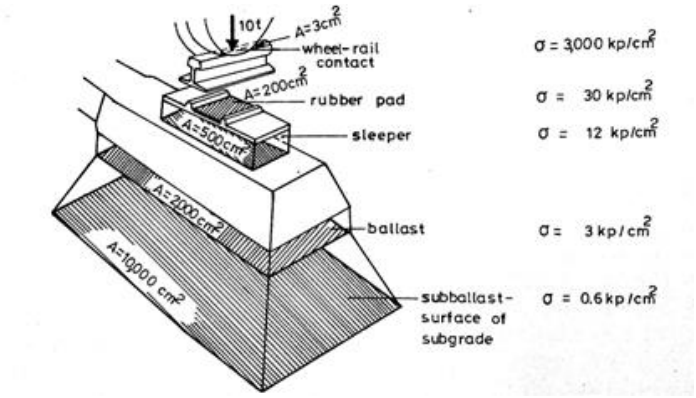

Figure 2.3 - Scheme of the base area of each track component and vertical load transfer (after Profillidis,2000)

2.3 SOIL IMPROVEMENT METHODS-GENERAL OVERVIEW

2.3.1 GEOSYNTHETICS

This technique consists in applying inside the soil mass natural or synthetic elements. Geosynthetics can be applied in the transportation field, such as roadways and railways. Focusing on railways, typical applications consist in including it in the track bed in the ballast or at the interface between the ballast and the subgrade (McGown & Brown, 2008).

The main functions of this material are separation of layers, ground reinforcement, particle filtration and water drainage and containment. With the purpose of acting as a reinforcement element, the geosynthetic must satisfy certain requirements such as high tensile strength and stiffness, durability, high level of interaction with the soil particles and good stress resistance, during construction (Pires [et al.], 2014).

The application of geosynthetics is popular due its reliable performance, durability and lower cost when compared with traditional solutions (Madhavi Latha [et al.], 2006). This is confirmed by many applications worldwide of this material, for example, in railways. For instance, by reinforcing the interaction between the subgrade and sub-ballast with geosynthetics, makes it possible to reduce the sub-ballast's thickness (Adam [et al.], 2005, Fatahi [et al.], 2011). However, such reduction should be restricted to rehabilitation of old railway lines (Adam [et al.], 2005). In Figure 2.4, an example on how to apply a geosynthetic in a railway bed is shown. Besides the economic advantage, geosynthetics are sustainable since its carbon footprint, comparing to customary materials, is distinctively lower (Koerner, 2012). Their use could instigate the recycling of discarded ballast from stockpiles, reducing the need for mining additional natural resources and reducing spoil lands in the metropolitan areas (Fatahi & Khabbaz, 2013).

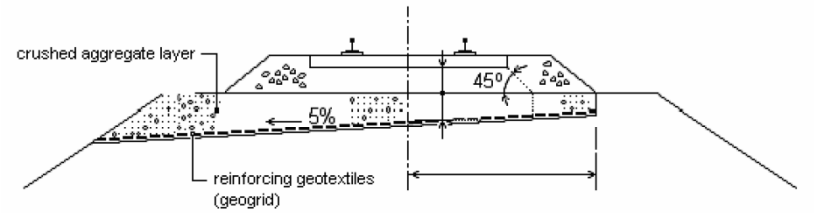

Figure 2.4 - Example of application of a geosynthetic (geogrid) in a railway (after INNOTRACK,2008)

Some known types of geosynthetics are geotextiles, geogrids, geomembranes and geocells. Geotextiles consist of synthetic fibres made into flexible and permeable fabric, by weaving machines or knitted. This material is porous to liquid flow, depending on its thickness. Biodegradation is not a problem due to its non-natural type of fibre. Geogrids are made of plastic and are assembled in a grid configuration, having large openings between individual ribs. They can be applied stretched in one or two directions for improved physical properties. Geomembranes are the main group of geosynthetics. They consist of thin and impervious sheets of polymeric material whose primary function is to contain liquid or vapour. Geocells are three-dimensional forms of geosynthetic materials with interconnected cells filled with soil (Pires [et al.], 2014). This geosynthetic is very useful for reinforcing embankments over weaker soils, it can act as an immediate working platform for construction works, thus reducing construction time and cost, and it provides short and long-term global stability to the embankment (Madhavi Latha [et al.], 2006). In Table 2.1, a general overview of these geosynthetics' functions and fields of application is presented.

Many successful cases of geosynthetic implementation are reported worldwide. In Australia, Nimbalkar & Indraratna (2016) studied the inclusion of different types of geosynthetics combined with shock mats beneath the ballast layer, alongside recycled ballast, in field trials on two rail lines in New South Wales. The placement of these materials reported a reduction in lateral displacement, lower vertical stresses in the ballast layer and smaller subgrade deformations. The European project INNOTRACK (2008) describes many railway interventions in Czech Republic with applications of geogrids, geomembranes

and geocells for increase of bearing capacity, protection of foundation weathering and improvements. Esmaeili [et al.] (2017) studied the application of a geogrid reinforcement to mitigate lateral deformation, investigating its effect on lateral resistances of both single tie and track panel via laboratory and field tests. The presence of the geogrid lead to an intertwining between the geogrid and the ballast particles, resulting in an increase in lateral resistance. Based in laboratory and field SPT, the best combination achieved for lower lateral displacement was in the tracks with a 30 cm-thick ballast layer and with one layer of geogrid positioned 10 cm beneath the tie.

Table 2.1 - Geosynthetics function and field of application (adapted from INNOTRACK (2008) and Pires [et al.] (2014))

	Function	**Field of application**
Geotextiles	Separation of subgrade layer materials Improve bearing capacity Soil reinforcement	Embankment's foundation Subgrade layers Problems in embankment stability Enlargement of railway embankment
Geogrid	Improve bearing capacity Soil reinforcement	Subgrade layers - bearing capacity improvement Embankment slopes - stability and strength protection against the weather.
Geocell	Improve bearing capacity Drainage	Embankment layer with drainage function Embankment foundation together with permeable aggregate as a filler
Geomembrane	Hydro-isolation Groundwater protection	Subgrade layers of embankment – hydro-insulative and separation Platform ground surface – protection against weathering of platform's rock ground surface

2.3.2 VIBRO-TECHNIQUES

A useful ground improvement device is the depth vibrator that can be used in various situations like seismic, static or dynamic foundation problems. The densification of loose granular soils, partial replacement of soft cohesive soils with granular material or grouted stone columns when the *in situ*'s soil lateral support is not adequate are possibilities to improve those problems.

It is essential a quality control of all these vibro-techniques, monitoring material use and power consumption of the vibrator, by adopting a well instrumented construction site (Raju, 2003).

2.3.2.1 Vibro-compaction

Vibro-compaction consists of the rearrangement of particles by reduction of void radio content, through means of a vibratory machine, achieving higher density combined with higher soil stiffness. In such a way long-term settlements can be hastened (Adam [et al.], 2005).

The vibratory machine pierces the soil through water jets. When the final depth is reached, it is gradually withdrawn and inserted again in steps, while similar material to the *in situ* soil is filled in, resulting in a column of compacted soil (Raju, 2003). A scheme of this technique's methodology is presented in Figure 2.5.

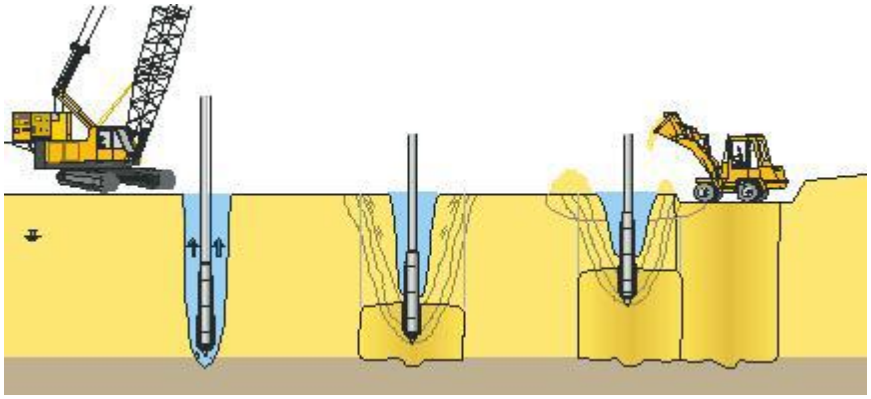

Figure 2.5 - Vibro-compaction methodology (after Raju,2003)

For this technique, there is no exact design method, so patterns for the compacted soil columns are based in field tests, such as standard or cone penetration test, heavy dynamic probing or *in situ* load tests (Adam [et al.], 2005). The most common used pattern to achieve correct soil densification is to assembly the columns in triangle or square patterns. Vibro-compaction is suited to densify granular soils such as gravel or sands, with a content of fines not above of 15% (Adam [et al.], 2005, Raju, 2003). A great advantage of this method is the reutilisation of local materials, turning it into a very economic technique (Raju, 2003).

Raju (2003) details the ground improvement of the soil for the implementation of a Malaysian rail line between Kertih to Kuantan, where vibro-compaction was used in combination with vibro-replacement. Vibro-compaction was applied where the soils consisted of clean sands, densifying those loose soils and vibro-replacement was carried out when the soils where made of soft cohesive ground, such as organic silts and clays, to a depth of up to 14 m. The application of the vibro-compaction technique effectively compacted the granular soils, registering in CPT field tests tip resistances of over 10 MPa.

2.3.2.2 Vibro-replacement

The vibro-replacement technique consists of placing large columns of coarse material in loose or soft soils, through means of specially designed depth vibrators, classifying this method as a deep vibratory compaction technique. The design method by Priebe (1995) is one of the most well-known and established methods.

There are two methods of installation: wet and dry method. In the dry method, the hole for the column is made with vibratory energy and pull down force, but it can be technically improved by applying air pressure (Adam [et al.], 2005). The wet method uses water jets to create the hole, assisting in the penetration of the vibrator (Raju, 2003), but care must be taken in cohesive soils, because it can worsen the soil's consistency (Poorooshasb & Meyerhof, 1997). The choice between these methods can depend on the proximity of water sources to the railway track (Arulrajah [et al.], 2009). However, it is preferable to choose the dry method due to environmental reasons, technological advances and broader application field (Adam [et al.], 2005, Poorooshasb & Meyerhof, 1997, Raju, 2003). After the hole is created and the desired depth is reached, it is backfilled with coarse stone with a bottom-fed vibrating device and compacted by it through impact and vibration. The compacting action of the vibrator tends to laterally displace the stone into the sides of the hole and that is why the diameter of the column can vary with

depth, being larger at the column base, at softer soil stratums and at the ground surface (Poorooshasb & Meyerhof, 1997). Diameters of the stone columns can range between 0.7 m to 1.10 m (Raju, 2003) and columns made with the dry method have smaller diameters than those made with the wet method (Poorooshasb & Meyerhof, 1997). Sometimes, the reinforcing effect obtained by the installation of the stone columns by vibro-replacement can somewhat reproduce the effect of vibro-compaction by densifying the soil between the columns (Priebe, 1995). By repeating this process, in a uniform and equally spaced pattern, the result is a load bearing improved ground made of compacted granular coarse material in columns. A representation of the vibro-replacement technique is shown in Figure 2.6.

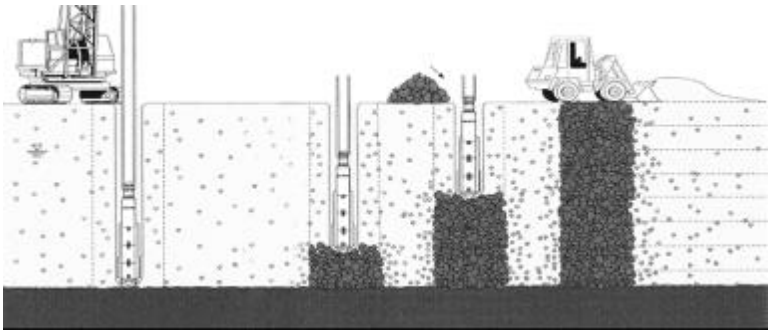

Figure 2.6 - Vibro-replacement technique (after Arulrajah [et al.],2009)

The main reasons of applying the vibro-replacement technique are to achieve better bearing capacity, to reduce settlement, improve global stability of the ground, densify the existing soil, to drain rapidly possible excess of pore water pressures and to quicken consolidation (Arulrajah [et al.], 2009, INNOTRACK, 2008, Raju, 2003). Stone columns can reduce settlements from 30 to 50 percent of the original ground response (Poorooshasb & Meyerhof, 1997). Vibro-replacement can be applied to soft soils, such as clays and silts, loose granular sandy soils and high-water table situations. It is quite an economic and very adaptable solution to most ground conditions.

Being one of the most known ground improvement techniques, there are many study cases and field tests reported. Adam [et al.] (2005) exposes in his work the rehabilitation works done in a railway line in Austria (Graz-Wies-Eibiswald) where the subgrade presented very large cavities that had to be filled to obtain good bearing capacity and reduced compressibility. Vibro-replacement was adopted because it allowed the continuous operation of the railway line during the upgrade operations, resulting in successful results. This was one of the first applications of deep ground improvement applied in an existing railway track. Raju (2003) presents details of vibro-replacement implementation in an extension of 6 km in the Hamburg – Berlin High-Speed Line on the Wittenberge section. Improvement works were applied to upgrade the existing line to a high-speed line on a rigid pavement. During the ground works, geophones were used to record vibrations at depths between 2 m and 3 m. These measurements showed that the soil deformation induced by the vibration of the installation of the stone columns was the same as the expected deformation caused by the vibrations induced by the high-speed train, because the oscillation speed of the railway is slower than the one of the ground improvement work. Vertical displacements of the rails were less than 3 mm and horizontal displacements negligible.

2.3.2.3 Grouted stone columns

When the soil cannot give enough lateral support to provide stability and bearing capacity, for example in organic soils, stone columns are not applicable. Grouted stone columns are the alternative and are obtained by adding a cemented grout suspension to the stones, while the column is being built, forming a grouted body with higher shear resistance (Adam [et al.], 2005).

The design of such columns follows the directives of normal pile design. The maximum vertical load on a column can range between 400 kN and 600 kN and largely influenced by the shape of the

compacted column base and by the column's length (Adam [et al.], 2005, Raju, 2003). In Figure 2.7, a scheme of the execution of this technique is shown.

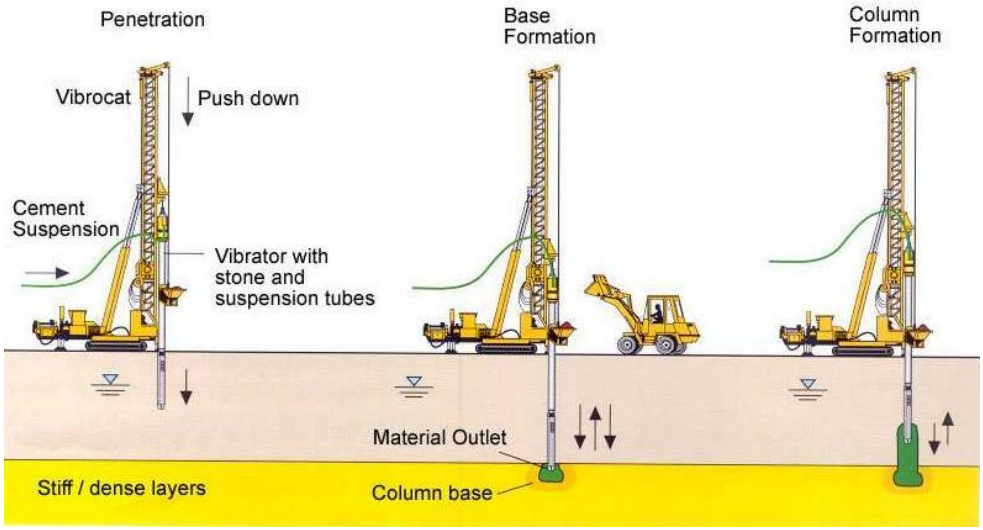

Figure 2.7 - Grouted stone columns execution (after Raju,2003) Kempfert & Raithel (2015)

presented the rehabilitation project of the railway line between Hamburg and Berlin, in the Büchen–Hamburg section, that passes through an area of soft organic soils and insufficient bearing capacity of the embankment. Track operation was maintained during improvement works, but with a train speed of 90 km/h. The ground was improved resorting to a geogrid-reinforced embankment and grouted stone columns, with the purpose to increase traffic speed to 230 km/h. Settlements were measured through geodetic measurements of the outer rail, registering data over a six-month period of train operation. The track settlement was up to 7 mm in the measurement period, which can be considered small, as generally a settlement of 10 to15 mm can occur due to the compaction of the ballast and the embankment, for favourable soil conditions. The geogrids deformed slightly to become active.

2.3.2.4 Vibro-concrete columns

Vibro-concrete columns are a variation of the previous soil improvement method. Instead of applying a cemented suspension, concrete is directly poured from the tip of the vibrator, forming a pile-like foundation column. In

Figure 2.8 the construction technique is presented.

The columns are considered to have point-bearing capacity, being able to support high service loads up to 750 kN (Adam [et al.], 2005, Raju, 2003), due to the shape of the base and the embedding of the column into the now densified soil layers. The loading capacity is related to the grade of concrete placed and the column's design is based on the concrete pile directives (Adam [et al.], 2005). Vibro-concrete columns are suitable for alluvial soils and soft clays that overly quality soil layers of gravels or soft rocks (Adam [et al.], 2005, Raju, 2003).

When these concrete columns are required to support heavily load structures, such as railways or roads, building the column with an enlarged head, by re-penetrating the vibrator, can help to reduce column length and increase column spacing, decreasing the cost of the intervention. Adam [et al.] (2005) recommends this head enlargement to be located under the railways' sleepers, serving as a direct support. Nonetheless, also recommends including a space filled with unbound material between the column's head and the ballast to prevent local stress concentration.

These two last techniques are both rigid solutions for soil improvement, normally resulting in total settlements of less than 25 mm (Raju, 2003).

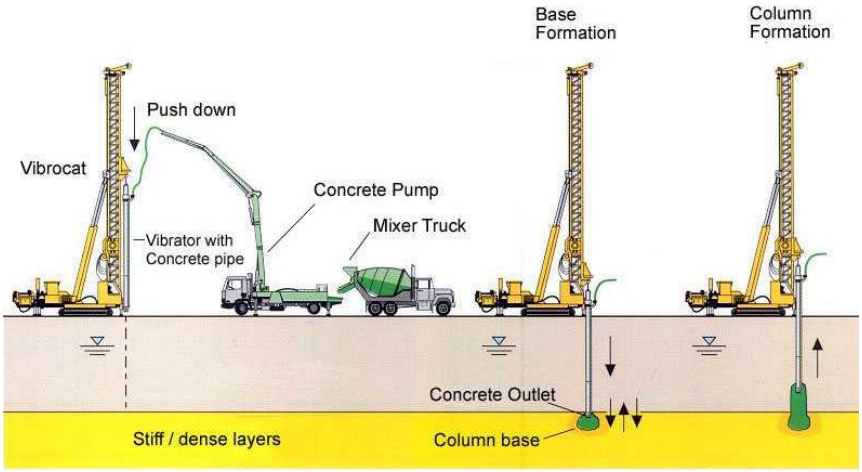

Figure 2.8 -Execution of vibro-concrete columns (after Raju,2003)

2.3.3 GROUTING TECHNIQUES

Grouting techniques are becoming a common ground improvement process applicable in underground improvement and foundations. The grouting process consists of filling pores and cavities in the ground with a liquid material, commonly cement based, to decrease permeability and improve shear strength.

The ISSMGE TC 211 classifies as ground improvement techniques with grouting type admixtures Jet Grouting, Deep Soil Mixing, Chemical Grouting, Compaction Grouting, Compensation Grouting and Particulate Grouting. For a briefer exposure, only the first two techniques will be detailed. These ground improvement approaches are applied with the purpose of enhancing embankment and global stability, mitigation of settlements and vibrations (INNOTRACK, 2008).

Guidelines for grouting projects are established in EN 12715 -"Execution of special geotechnical work – Grouting" (2000) and for deep mixing the European standard for execution is the EN 14679- "Execution of special geotechnical works – Deep Mixing"(2005) .

2.3.3.1 Deep Soil Mixing

Deep Soil Mixing is a technique engineered in Japan and in the Scandinavian countries, separately, in the 70s. It consists of mechanical mixing of *in situ* soils with a binder such as cement, lime or a mixture of both in different proportions. The mixing can be done by mixing machines or before placement (Chu [et al.], 2009). The resulting mixture of soil and binder is injected into the soil and the soil's moisture is used in the binding process. This removal of the moisture from the soil results in an improved soil surrounding the mixed one, providing in a better-quality ground with higher shear strength and low compressibility (Adam [et al.], 2005, Arulrajah [et al.], 2009, Raju, 2003).

Depending on the applications, there are various configuration types of this soil improvement method such as columns, rectangular soil-mix walls or global mass stabilization (Denies & Van Lysebetten, 2012, Essler & Kitazume, 2008). For the purpose of this thesis, the column type is of higher interest. With this method, columns of mixed soil are created, having diameters of 0.5 to 1.2 meter and depths of around 15 to 25 meters (Townsend & Anderson, 2004). In Figure 2.9 a scheme of the methodology of Deep Soil Mixing is presented.

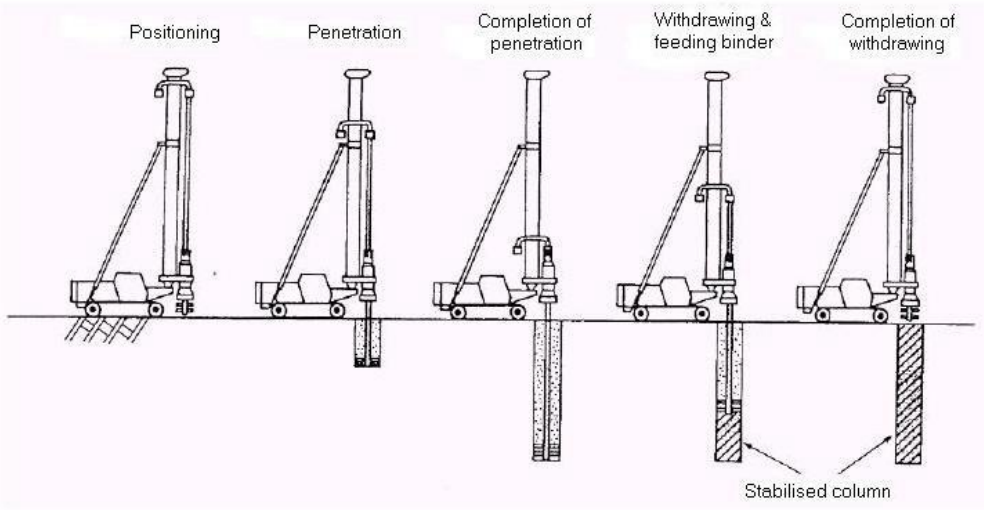

Figure 2.9 - Deep Soil Mixing technique scheme (after Raju,2003)

Regarding the procedure of binder injection into the soil, there are two approaches of installation: the wet and the dry methods. The most commonly applied, the wet mixing method, a mixture of the binder, water and occasionally sand or additives is injected and mixed with the soil. A grouted mixture is created that hardens during the hydration process (Essler & Kitazume, 2008). In the dry soil mixing process, the binder is mixed directly with the soil. The binding agents react directly with the existing soil and the contained water, forming a soil mortar (Denies & Van Lysebetten, 2012).

The strength development of the Deep Soil Mixing columns is different over time and depends on the type of soil, binder amount and proportion of the mixed materials. Generally, 90% of the final strength is reached after three weeks, succeeding the installation (Adam [et al.], 2005, Arulrajah [et al.], 2009, Raju, 2003). This time span should be taken into account, when the intervention should be restricted to a short period, especially on railways, where interruption of the lines are to be avoided (Adam [et al.], 2005).

Deep Soil Mixing technique has been applied to various soil types, focusing on soft clays and organic soils. It has been used in various structures such as foundations, retaining walls, embankments for railways or roadways or for ground water cut-off. Its application has many purposes such as settlement mitigation, increase of soil's bearing capacity and shear strength. Townsend and Anderson (2004), in their work, listed the general advantages and disadvantages of this technique, shown in Table 2.2

In railways, it may be applied to reduce vibrations caused by high-speed trains (Adam [et al.], 2005, Arulrajah [et al.], 2009, Raju, 2003). Another advantage of applying this method in railways is the possibility to apply it to operating railway tracks without track closure, while working directly on the railway's platform, using vertical drills (Calon [et al.], 2011) and to provide a more homogeneous load distribution in the subgrade layer, as well as a constant settlement profile. Additionally, the ballast and sub-ballast layers are not polluted by the grout, contrary to Jet-grouting that does so (INNOTRACK, 2009). The design approach of Deep Soil Mixing is presented by Broms (1999).

Table 2.2 - Advantages and disadvantages of Deep Soil Mixing technique (Townsend & Anderson, 2004)

Advantages	Disadvantages
Improvement depth up to 30 m Avoids costly dewatering More economical than removal and replacement of subgrade No noise or vibration problems High production rate when using multi-axis augers	High mobilization costs plus cost of batch plants Needs a thorough site investigation program. Lab tests to determine soil-reagent compatibility. Strength time durability up to 6 months Rigs require substantial headroom Deep soil mixing produces 30-50% of spoil soil volume Lack of well-developed design and analysis models

Koch & Szepesházi (2013) completed laboratory and numerical tests to implement deep-mixing in Hungarian railway projects, such as the Sárrét railway line rehabilitation, where the soil consisted of soft chalky silts. Column-type and mass stabilization scenarios were analysed using strength and compressibility data from laboratory test results. Both technologies presented settlement reduction in and increase in stability.

2.3.3.2 Jet-grout columns

The Jet-grouting technique consists of having at depth high speed jets that erode the soil and inject grout, forming columns or panels. The construction process starts with drilling a borehole, generally of 9-15 cm in diameter, until a desired depth. A machine with high pressurized jets expelling fluid is inserted in the borehole and, with its rotating movement, it erodes the soil to mix it with the cement grout, forming a mixture of "soilcrete" (cement + soil). The gradual upward movement forms a circular cement column, with diameter that ranges between 1 to 2 m, depending on the used method, but may be less. The strength and permeability characteristics of this new structure in the ground are independent from the original soil (Morteza & Mosayebi, 2011). The soil improvement technique is schemed in Figure 2.10.

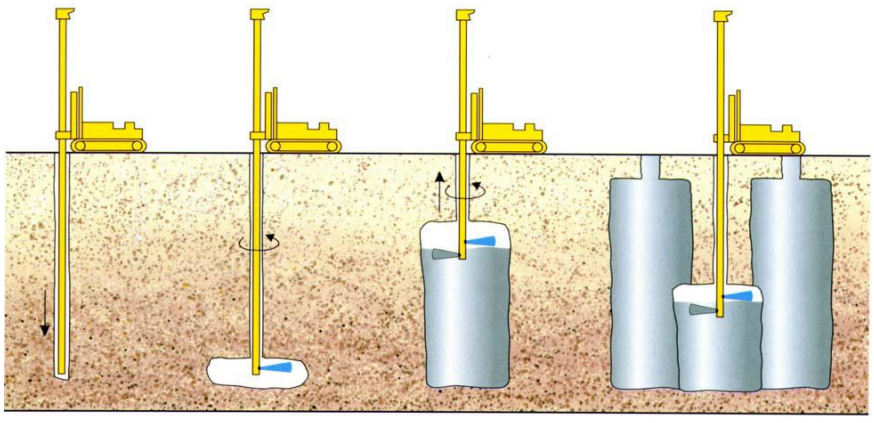

Figure 2.10 - Jet-grouting methodology (after Hayward Baker Inc,2011)

Jet-grouting comprises single, double and triple methods, being the most effective the triple method (Chu [et al.], 2009). The single method consists of the injection of grout only at high pressure. It was the first method developed and it is the most common. However, it results in small column diameters of around 1 m (Essler, 2008, Morteza & Mosayebi, 2011). In the double system, pressurized air is used in

combination with the grout at the exit nozzle point. This upgrade increases the efficiency of the jetting process, allowing to reach larger depths and obtaining greater diameters of around 2 m. Finally, triple method involves the combination of compressed air, high-pressurized water and a low-pressurized grout being expelled from the jets. The diameters obtained with this system are higher than the previous two methods, obtaining up to 2 m or higher, but the energy involved in the process is lower than with the double method (Essler, 2008). The triple method is suitable for soils that are difficult to drill, however is a more complex methodology that requires more equipment and more material (larger diameters), thus is more expensive (Morteza & Mosayebi, 2011). A scheme of these three methods if presented in Figure 2.11.

The soil range of applications for this technique is very wide, being possible to apply it to all soil types, independently from the grain or pore size and void ratio (Chu [et al.], 2009, Morteza & Mosayebi, 2011). In general, sands are the best suited soil to apply Jet-grouting because they are easily eroded. Moreover, in these soils, larger diameter columns or panels are achievable. The presence of cohesive properties in the soil affects the erosive action of the jet, so even though silts and silty sands are suitable for this technique, the grout column diameters may be smaller than in clean sands (Townsend & Anderson, 2004).

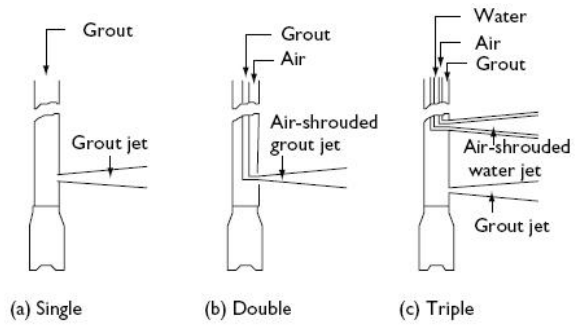

Figure 2.11- Types of Jet-grouting (after Moseley & Kirsch, 2004)

Nowadays, Jet-grouting is a multi-application tool appropriate for foundation strengthening, dam waterproofing, borehole stabilization or drilling, slope stabilization and in tunnel excavations (Morteza & Mosayebi, 2011).

This ground modification technique has many advantages such as broad range of applicability in soils and project situations, as mentioned before, work can be done directly from the ground's surface with good efficiency and performance, since large volumes and area of problematic soil can be treated (Townsend & Anderson, 2004). Particularly in railways, it is a good option since it has low damage of surrounding structures, with low noise and vibration levels (Morteza & Mosayebi, 2011, Ribeiro, Ana, 2010), it would allow to perform ground modifications while the line is working and not disrupt railway operation. Also it can be executed in conditions where space is limited or there is narrow headroom (Townsend & Anderson, 2004), making it suitable to apply in the railway structure, without the need to dismantle it. The cost of applying Jet-grout is decidedly dependent on the project's complexity, soil type and depth of treatment (Townsend & Anderson, 2004).

Due to the high pressures involved during construction and the spoil generation of it, there is an idea that Jet-grouting is a risky process. Nevertheless, with proper site control, executor and labour's experience, and proper design, the risk is no more than other ground improvement methods (Essler, 2008).

3

PARAMETRIC NUMERICAL STUDIES ON INTERFACES USING FLAC3D

3.1 GENERAL CONSIDERATIONS

One of the purposes of this thesis is to analyse the utility and performance of railway track subgrade improvement solutions, resorting to Jet-grout columns, using a three-dimensional numerical model of a railway track. However, due to the complexity of such numerical modelling, in terms of geometry, size (number of elements, nodes and degrees of freedom), different mesh types/shapes, combination of diverse materials and also due to the sleeper-ballast interaction behaviour, in some situations it may be recommended to introduce interfaces or other numerical techniques in the model (Paixão & Fortunato, 2010, Wu [et al.], 2016). Therefore, one must first study, in a smaller scale, how two generic bodies, with different soil layers and mesh type, interact using those numerical techniques to better understand how to model them further on.

The focus of the parametric studies presented in this chapter was to see if there are differences in the model behaviour, analysing stress and displacement fields, when we have different soil layers with different mesh types, especially, cylindrical zones on the bottom layer combined with brick zones (orthogonal grids) on top and their interaction.

3.2 NUMERICAL MODELLING OF THE RAILWAY TRACK STRUCTURAL BEHAVIOUR

Railway lines are rather complex structures with material and structural non-linear behaviour (Paixão & Fortunato, 2009). When studying the track's behaviour, one must consider the interaction between the various components that make up this system in order to determine accurate strain and stress results due to train loads.

Despite the existence of analytical methods that try to reproduce the effects of the train's three-dimensional loading (vertical, lateral and longitudinal), numerical methods such as the finite element method (FEM) or the finite difference method (FDM) are generally more adequate to simulate train loads and implement non-linear behaviour to the track's various materials (Fortunato, 2005, Paixão & Fortunato, 2009). Despite the train load being made up of three main components, as mentioned before, track analysis studies have been focusing rather on the effects only due to vertical loading (Fortunato, 2005, Fortunato & Resende, 2006, Varandas [et al.], 2016).

With the increase of computational capacity, the implementation of such numerical methods has become a common practice, allowing users to generate larger and more complex numerical models to achieve a better understanding of the track system's behaviour. A big advantage of implementing such numerical approaches is that it allows to perform parametric studies, analysing the effect of variation of numerous properties.

Throughout the years, many numerical models of the railway have been developed. One of the first was ILLITRACK (Tarabji & Thompson, 1976), a finite element model where two bi-dimensional models were supposed to simulate the three-dimensional effect, by calculating one of the models in the longitudinal direction and using the output results as input data for the model in the transverse direction. Until 1980 some three-dimensional FEM models were developed such as MULTA (Multilayer Track Analysis) (Prause & Kennedy, 1977) and the PSA (Prismatic Solid Analysis) model developed by Adegoke [et al.] (1979), but each presented some restrictions such as adopting linear elastic behaviour for the material models, which does not depict reality accurately. In the 80s decade, other models appeared to improve previous imperfections, such as the GEOTRACK (Chang [et al.], 1980), where it was possible to analyse non-linear stress-strain relations in the railway's materials in a three-dimensional model, with reduced computation time.

Recently many commercial software with three-dimensional capacity have appeared such as ANSYS, ABAQUS, PLAXIS 3D, FLAC3D and others (Paixão, 2014), where studies on the railway mechanical behaviour have been developed. Paixão & Fortunato (2010) report a study on the rail track structure using three-dimensional numerical models in ANSYS (FEM) and FLAC3D (FDM), comparing results with both software and establishing a tight correlation between their results.

A two dimensional numerical study developed in ANSYS on the influence of backfill settlements in the train/track interaction at transition zones of railway bridges was made by Paixão [et al.] (2016a). To simulate various settlement profiles of the backfill occurring at transition zones, numerous non-linear dynamic analyses were made on a transition zone model (Figure 3.1). By studying settlement profiles, axle vertical accelerations, frequencies and sleeper/ballast contact forces it was possible to determine the consequences of these backfill settlements and to recommend the implementation of wedge shaped backfills.

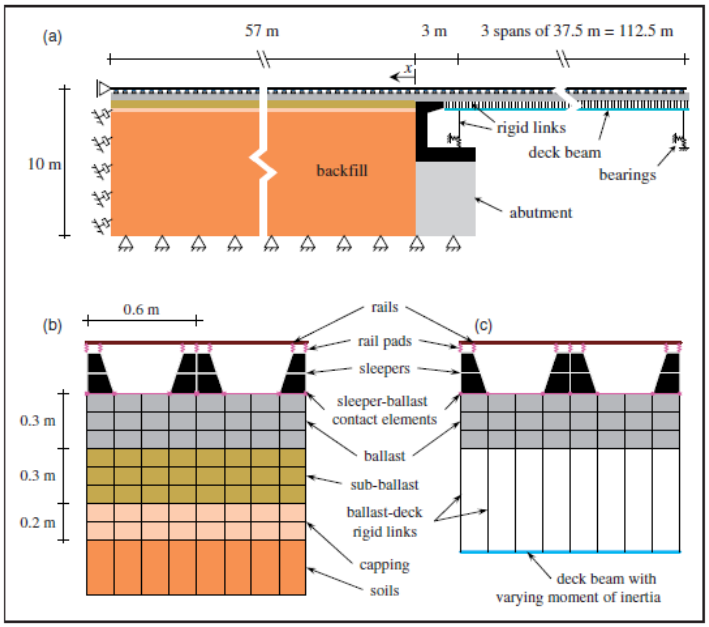

Figure 3.1 – A schematic representation of the numerical model used in a study by Paixão [et al.] (2016a)

Varandas [et al.] (2014) presented a study on the importance of the implementation of non-linear behaviour of the upper trackbed layers, in dynamic studies of railway transitions. A numerical program named Pegasus was used, where the three-dimensional model (Figure 3.2a)) was developed and fully coded in MATLAB. With this study, results demonstrated that despite the model with linear elastic behaviour provided good approximations of displacements results, the consideration of non-linear

aspects showed differences in the stress levels, due to resilient modulus variations (Figure 3.2-b)). It was concluded that it is relevant to consider the aggregates' non-linearity in the modelling of railway transitions when long-term assessment is intended.

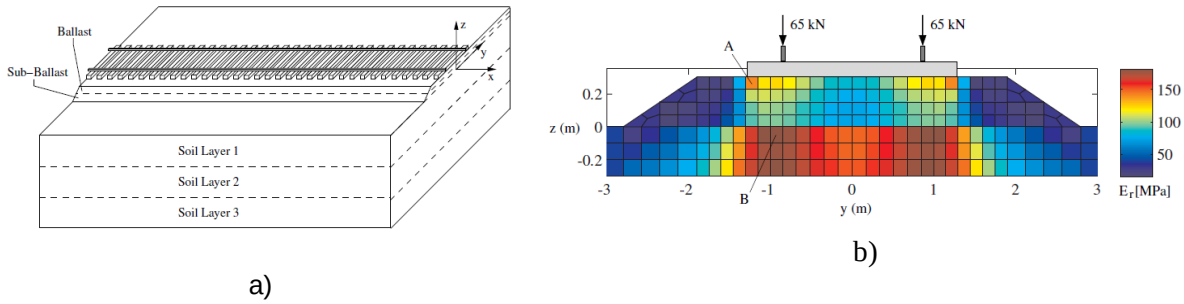

Figure 3.2 – a) Main elements considered in the finite element model in research made by Varandas [et al.] (2014) and b) distribution of maximum resilient modulus obtained inside the ballast and sub-ballast layers

Varandas [et al.] (2017) published a study on the dynamic response of the railway system when trains cross cut-fill transitions containing buried culverts (see Figure 3.3). The program used in this study was the same as in the previous study, where the train-track interaction and longitudinal level irregularities were considered. With this research, the authors concluded that differential settlements caused by permanent deformations occurring at the subgrade's level and track longitudinal irregularities were the cause of problems at cut-fill transitions, independently of vehicle loading.

In this thesis, FLAC3D was chosen to model numerically the railway track with reinforced substructure.

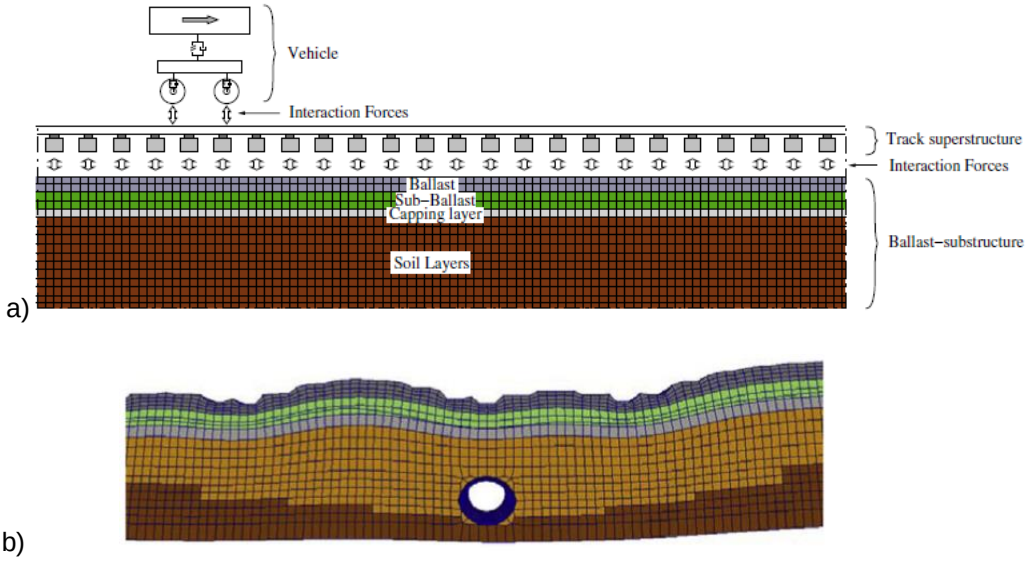

Figure 3.3 – a) Representation of the 3D FEM model and b) longitudinal view of the deformation of the ballast-substructure system with culvert (after Varandas [et al.] (2017))

3.3 FLAC3D: FAST LAGRANGIAN ANALYSIS OF CONTINUA IN 3 DIMENSIONS

In the scope of this thesis, the three-dimensional numerical modelling of the railway track was developed with a commercial software - FLAC3D, version 5.01- that uses the explicit finite difference method.

In FLAC3D, the user can simulate the behaviour of three-dimensional structures composed by soil, rock or other materials that can undergo plastic flow. The material is represented by polyhedral elements coupled together forming a user-defined grid, where each element behaves accordingly to a prescribed stress/strain law, linear or non-linear (Itasca, 2015).

The explicit Lagrangian calculation scheme and the mixed-discretization zoning technique used in FLAC3D ensure that models with complex behaviours are represented very accurately. Since no matrices are formed, large 3D calculations can be made without excessive memory requirements, offering an ideal tool for analysis of three-dimensional problems, in the geotechnical field (Itasca, 2015). It can be operated from a command-based mode, having a built-in programming language FISH, that allows the user to create other functions than the ones available, tailoring the results obtained to certain needs such as variations in time and space, custom-designed plots, automation of parametric studies and other. The layout of the software console is shown in Figure 3.4.

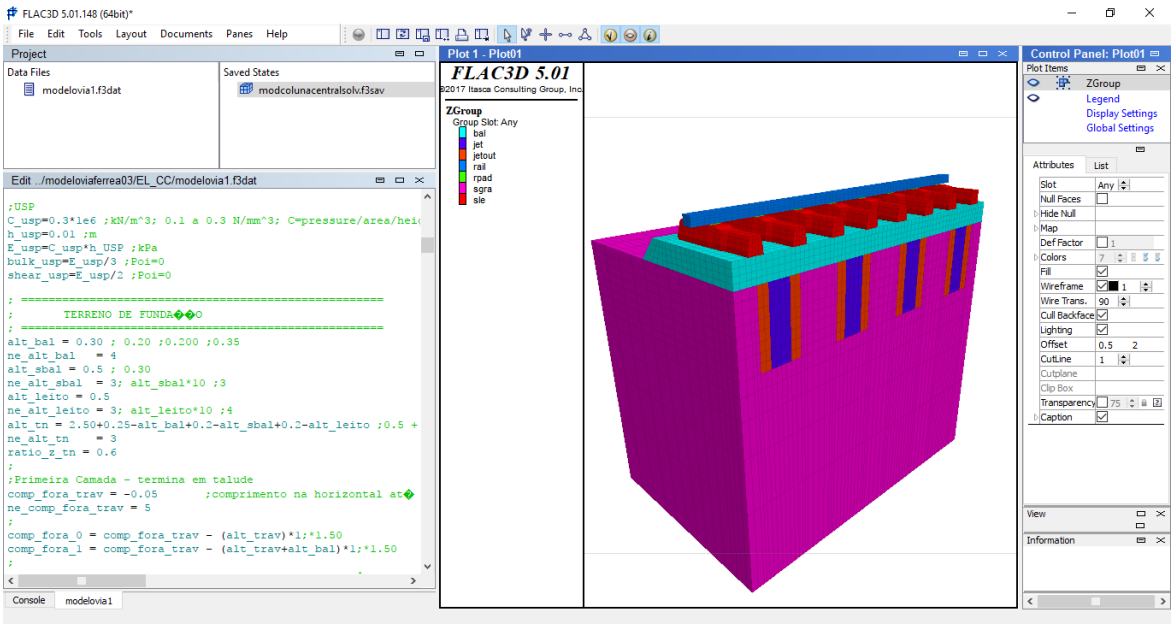

Figure 3.4 – FLAC3D layout pane

In FLAC3D (Itasca, 2015), when designing a numerical model, there are many finite difference zone generation tools available to the user. In this way, the user can build any type of model, resorting to an association of diverse types of grids and sub-grids. However, joining grids with different geometries may create an unwanted incompatibility of grid-points. To overcome this matter, the software contains two numerical techniques denoted by the commands "INTERFACE" and "ATTACH" that may be used to connect different zone type or zone size, located anywhere in space. In general, it is advisable to use the "ATTACH" command to join grids together, due to computational efficiency, rather than the "INTERFACE" command. The first command lets the user attach faces of sub-grids rigidly, forming a single grid. However, in some situations it may be more convenient to use an interface for that purpose, for example between the sleeper facets and the ballast layer to allow for eventual slip and/or separation.

The representation of an interface in FLAC3D is achieved by means of triangular elements - interface elements -, each one defined by three nodes - interface nodes. Generally, interface elements attach to the face of the target zone surface, stretching over the desired surface, causing it to become sensitive to interpenetration with any other face with which it may come into contact. Once another grid surface touches an interface element, the interaction is detected by the interface node, and is characterised by normal (k_n), shear (k_s) stiffness and sliding properties (Itasca, 2015). A good criterion, recommended by the software designers, to calculate the interface stiffness's is to set, both normal and shear stiffness, to ten times the equivalent stiffness of the neighbouring zone according to Eq. (1):

$$\max\left[\frac{K+4/3G}{\Delta z}\right] \tag{1}$$

where G and K are the shear and bulk modulus of the soil, respectively, and Δz is the smallest dimension of an attached zone in the normal direction of the interface (Esmaeili & Hakimpour, 2015, Pirapakaran & Sivakugan, 2006).

In case there are different materials adjoining the interface, the maximum value over all zones adjacent to the interface is to be used, hence "max [ ]" notation. However, if one of the materials connected to the interface is significantly stiffer than the other, then Eq. (1) should be applied to the softer side. In such manner, the deformability of the entire system will be controlled by the softer material. By setting the interface stiffness to ten times the soft-side stiffness, one will ensure that the calculation time is not significantly affected and the interface has minimal influence on the system's performance. The assignment of the interface properties (particularly stiffness) depends on the way the interface is supposed to behave. For the purpose of this thesis, the interface can behave as an artificial element to connect different mesh types so there is compatibility of the model's behaviour (Itasca, 2015).

When creating an interface element some rules should be followed such as the creation of any surface on which an interface is to be set must be generated initially or if a smaller surface area contacts a larger surface area, the interface should be attached to the smaller region. However, if there is a great difference in zone density between two adjacent grids, the interface should be attached to the grid with the greater zone density (Itasca, 2015).

To better assess how to model these interactions, regarding on which command to use ("ATTACH" or "INTERFACE") and which parameters to apply, in case we use an interface, parametric studies were carried out to study the influence of these aspects on the model's behaviour.

Since the railway track model consists of various adjoining materials, each one quite different from the other property wise, and in various positions, i.e. having stiffer or softer material on top or bottom, the influence of having different soil stiffness and whether an interface is needed to adjoin these materials had to be researched. The first parametric study had the purpose to determine the effect of applying an interface and how to model its behaviour, based on the softer soil layer or on the stiffer one. Various soil stiffness combinations were applied, with the models having always equal zone type.

Taking into account that the purpose of this thesis is to simulate the introduction of improved soil columns in the railway's subgrade, generating a complex mesh, the second parametric test was meant to assess how different mesh types interact between each other, especially cylindrical mesh types with brick zones, experimenting with equal and different soil layers and soil column material.

3.4 PARAMETRIC STUDY TO UNDERSTAND THE IMPORTANCE OF INTERFACE ELEMENTS AND ITS PARAMETERS

3.4.1 MODEL DESCRIPTION

The first model built consisted of a simple two-layered soil system. For all models, the dimensions are of a cube of 4 m x 4 m in size, with its origin at coordinates (x, y, z) = (0,0,0) on one of the bottom vertexes and equal zone type, either on top or bottom. Vertical displacements were restricted in the lower horizontal boundary, at level z = 0 m. At the centre of the lower boundary, at the grid-point with coordinates (x, y, z) = (2,2,0), the horizontal displacements were constrained to apply a query line starting from that point upwards, for future displacement analysis. The model was developed with a basic brick-shaped mesh grid, generating 9826 grid-points and 8192 zones (see Figure 3.5). To all tests, a vertical pressure of -100 MPa was applied on top of the model's surface and the considered mechanical material model was linear elastic. A query line of the vertical (z) displacement with depth, from the top surface to the bottom surface of a point in the middle of the model was drawn.

3.4.2 EQUAL SOIL LAYERS MODEL

First, to assess the influence of the interface structure, two models with equal soil layers and equal zone type were designed: one with the interaction between layers modelled with the "ATTACH" command and another with interface elements connecting the two layers. The soil and interface parameters are presented in Table 3.1.

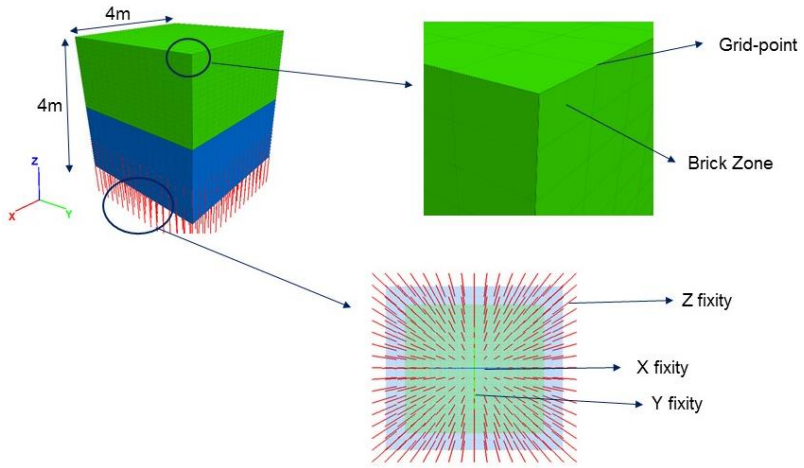

Figure 3.5 – Schematic representation of the model's configuration

Table 3.1 - Soil and interface parameters for the two-layered equal soil model

		Soil Parameters				Interface Parameters	
		Young's Modulus	Poisson's Ratio	Bulk Modulus	Shear Modulus	$\left[\frac{K+4/3\,G}{\Delta z}\right]$	$k_n=k_s=10\times\left[\frac{K+4/3\,G}{\Delta z}\right]$
Unit		MPa	-	MPa	MPa	MPa/m	MPa/m
Two-layered equal soil model	Top	160	0.3	133	615	1723	17230
	Bottom	160	0.3	133	615	1723	

3.4.2.1 Results

Analysing the Z displacements obtained with these models in Figure 3.6, it is visible, for the model with the interface, a discontinuity on the linearity of the results, at depth z = 2 m, the location of the interface element. This is due to this element that introduces an extra set of grid points resulting, for this case, in two grid-points with coordinate z = 2 m, one belonging to the interface element and first mesh block and the other to the second mesh block. This is a numerical modelling consequence of using interface elements that slightly interferes with the displacements field. However, the gap is not relevant enough to influence the behaviour of the model, representing that the top layer is interpenetrating the bottom layer. Comparing the maximum displacement values of each model, around 0.2 % higher displacements

are obtained with the model with the interface present. At the interface level, the previous observation is valid.

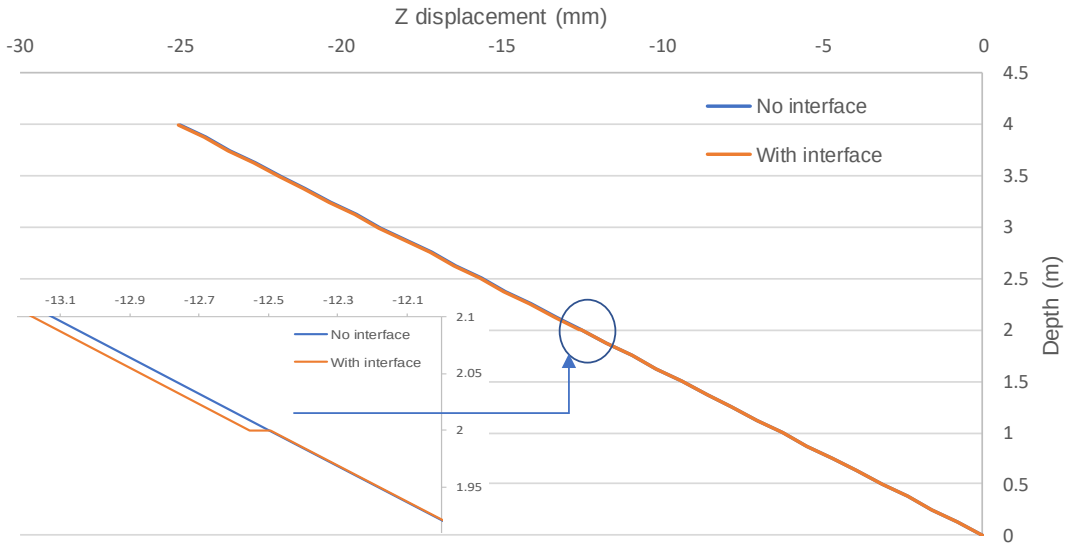

Figure 3.6 - Z displacements with depth for model without interface versus with interface, with equal soil layers

3.4.3 TWO-LAYERED DIFFERENT SOILS MODELS

Afterwards, different combinations were made by multiplying the Young's modulus of one of the soil layers by two, four and ten times the Young's modulus (E) of the material of the other layer (denoted by 2xE, 4xE and 10xE) and changing the position of the stiffer soil - on top or on the bottom -, thus creating a model with two layers of different soil and an interface element separating the layers.

However, as mentioned earlier, if the different soils stiffness is not excessively different, Eq. (1) should be applied but if they have very distinctive characteristics, the interface behaviour should be determined considering the properties of the softer soil. So, to better understand which soil should control the interface behaviour, results with a stiff interface and soft interface behaviour were analysed. The soil parameters and interface properties are presented on Table 3.2.

3.4.3.1 Results

As expected, in the presence of soils with different stiffness properties, whether the stiffer soil is on the top or bottom layer, larger displacements are observed on the softer soil and the opposite on the stiffer layer. An example of this is shown in Figure 3.7 where results for a soil layer with stiffness four times higher than the other soil layer are presented. It is visible some differences of the displacement values by choosing different interface behaviour. In general, the maximum displacement values obtained with the stiff-behaviour interface are around 0.3 % smaller than with the soft-behaviour interface. This is due to imposing the interface's behaviour to act by the stiffer layer, thus obtaining slightly smaller displacements. Independently of the type of behaviour chosen for the interface, there exists a discontinuity of displacement values at the position of the interface. However, this gap is smaller when the stiff interface behaviour is adopted (see details in Figure 3.7).

In Figure 3.8 a comparison of results for the Z displacement for different interface behaviours, soil stiffness and stiffer soil position are shown. Nevertheless, to better understand the magnitude of these differences due to the nature of the interface, a study of the absolute difference and relative difference between displacements was made

Table 3.2 - Soil and interface parameters for the two-layered different soils model

		Soil Parameters				Interface Parameters		
		Young's Modulus	Poisson's Ratio	Bulk Modulus	Shear Modulus	$\left[K+\frac{4}{3}G\right]/\Delta z$	$k_n=k_s=10\times\left[K+\frac{4}{3}G\right]/\Delta z$	
Unit		MPa	-	MPa	MPa	MPa/m	MPa/m	
Two-layered different soils model	E	160	0.3	133	615	215	-	17230
	E1=2xE	320	0.3	267	123	431	34462	
	E2=4xE	640	0.3	533	246	862	68923	
	E3=10xE	160	0.3	133E3	615	2154	172308	
Type of interface behaviour							Stiff	Soft

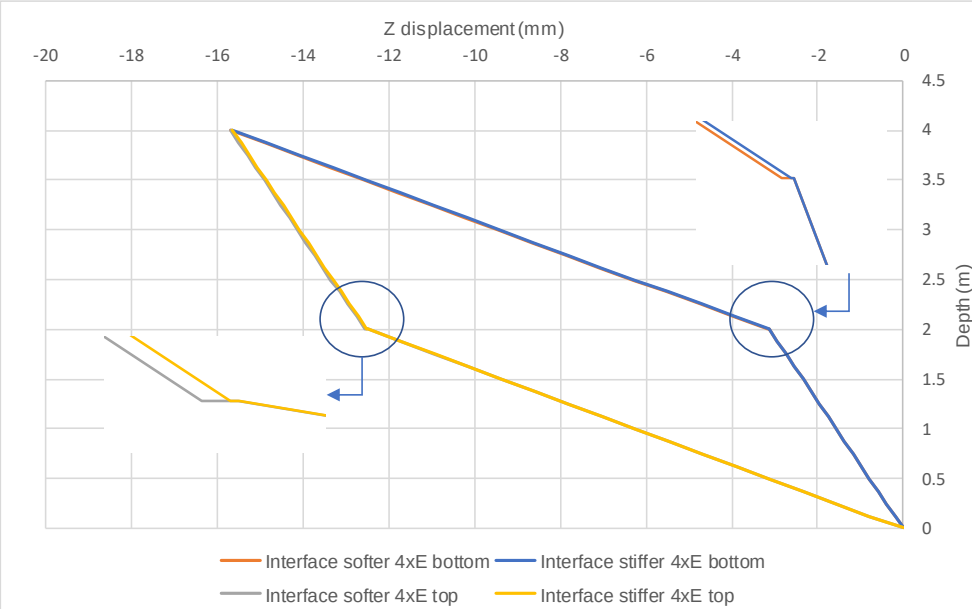

Figure 3.7 - Softer vs stiffer interface based behaviour with stiffer layer of soil (E2=4xE) in distinct location in the model

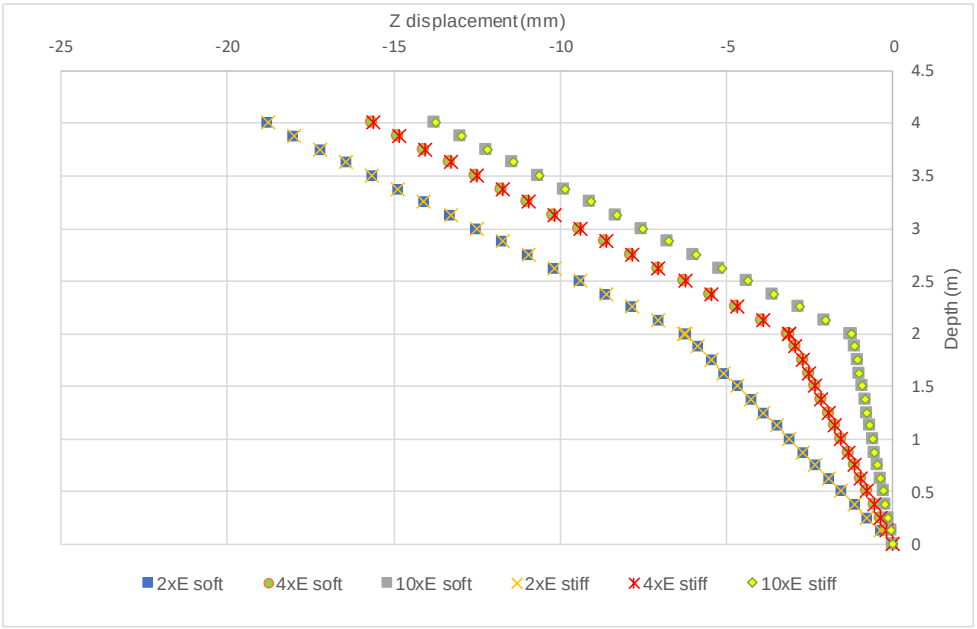

a)

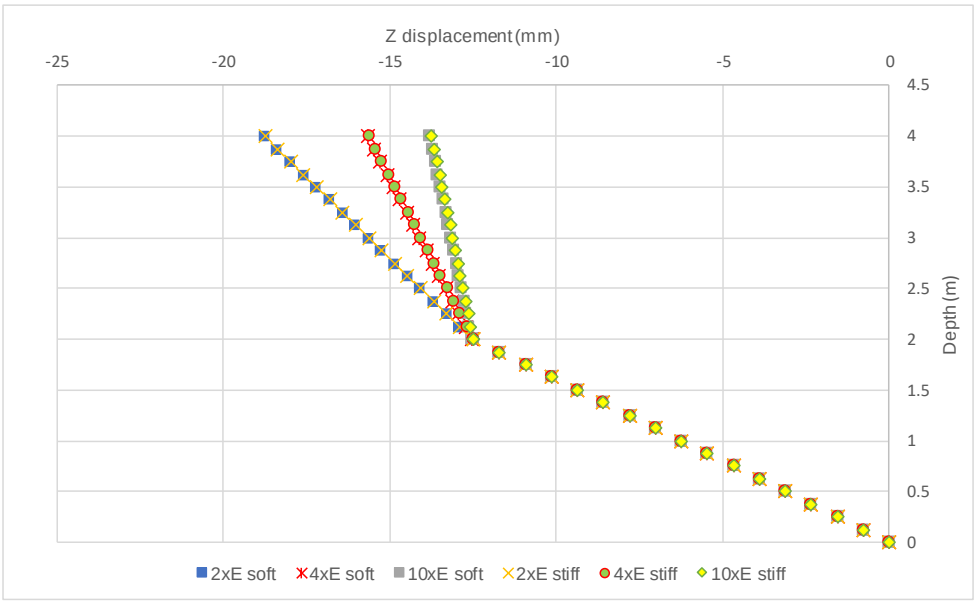

b)

Figure 3.8 - Comparison with different soil types and interface parameter with bottom stiffer soil (a) and bottom softer soil (b)

To distinguish between soft interface and stiff interface results, the absolute difference between these two is shown in Figure 3.9, where the reference is the displacement values for the stiff-interface model. By examining this plot, it is observable that on the layer above the interface there are some differences in the displacements between soft interface or stiff interface. The higher the stiffness of one of the soil layers, the bigger the difference between displacement values for the stiff-interface and soft-interface nature type. When crossing the interface, the difference between choosing stiff-interface and soft-interface is minimal (around $1x10^{-3}$), independently of soil rigidity. In other words, when presented with two different soil types, if they have similar stiffness, the choice between selecting the interface behaviour as stiff or soft based will not lead to very dissimilar results. However, as the difference between the soil stiffness grows, so will the contrast in results. Thus, it is proven the recommendation

given by the software developers for modelling the interface behaviour by the softer soil when the soil properties between two layers are very distinct.

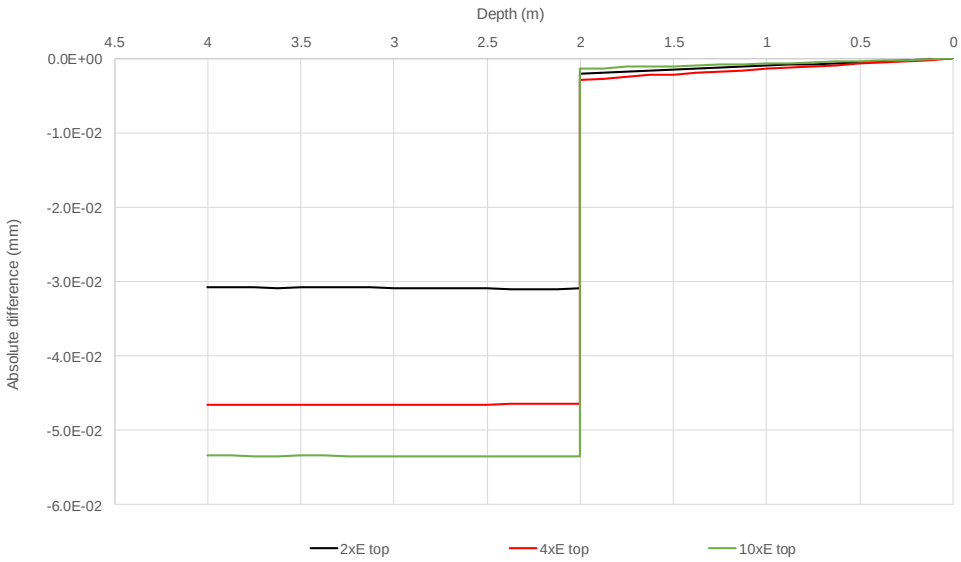

Figure 3.9 - Absolute difference between Z displacements obtained with models with soft interface and with stiff interface, for different soil types in the layers

In Figure 3.10 the relative difference between soft interface and stiff interface displacement values, with reference with the stiff interface displacement results, is plotted. As mentioned before for the absolute difference, until the interface element is reached, at depth z = 2 m, differences are evident, reaching, for example, 4% higher displacements with the soft-interface and the ten times stiffer soil layer on the bottom. After the interface element, the results are almost equal. Roughly, the soft interface yields 0.5-4% higher displacements than the stiff interface, when the stiffer soil is on the bottom and that difference increases alongside with the rigidity of the soil. When the stiffer soil is on top, the difference is smaller, ranging between 0.2-0.4% higher displacements, again with the softer interface.

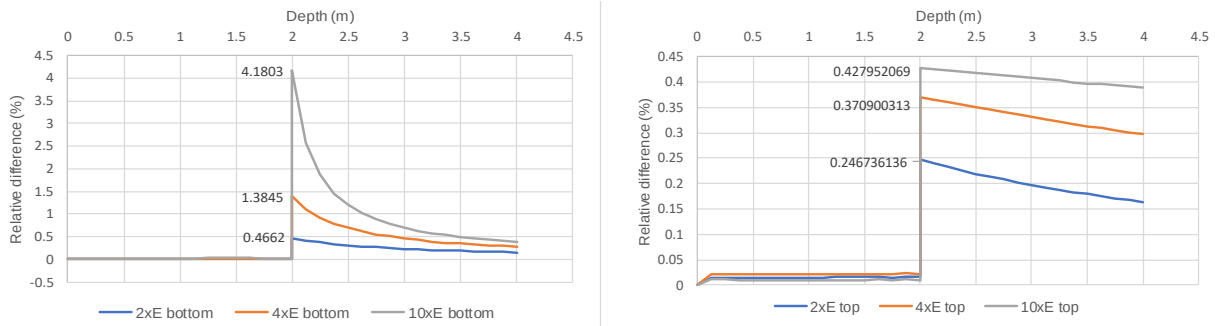

a) b)

Figure 3.10 – Relative difference between soft and stiff interface results, with stiffer bottom layer (a) and stiffer top layer (b)

After analysing the data, it is possible to say that the choice between soft or stiff interface will not influence the results very much. However, when adopting an interface, it is better to apply directly Eq. (1), in other words, to choose the stiff interface behaviour. This guarantees a better representation of the continuity of the displacements in depth by presenting a smaller gap on the values of displacement at the position of the interface, even if the deformation of the system with the stiff interface is slightly

smaller than the deformation of the soft interface system. As the difference between the soils that adjoin the interface grows, the recommendation given in the FLAC3D manual of adopting a soft behaviour interface should be followed so that the required computational effort does not increase substantially making calculation times impractical.

3.5 PARAMETRIC STUDY TO UNDERSTAND THE INTERACTION OF DIFFERENT MESHES BETWEEN SOIL LAYERS

3.5.1 MODEL DESCRIPTION

For all models in this section, the dimensions are of a prism of 12 m x 6 m x 14 m. Vertical displacements were restricted in the lower horizontal boundary, at level z = -14 m. At this same lower boundary, the horizontal displacement of the grid-point located in the centre of this face was constrained to apply a query line of the vertical (z) displacement with depth, from the top surface to the bottom surface of the model. On all models, a vertical pressure of -100 MPa was applied on the top surface, at level z = 14 m and the considered mechanical material model was linear elastic.

First, two simple models with two equal soil layers and zone type on top and bottom were designed to serve as a control example. To adjoin the top and bottom layer the "ATTACH" (model A1) and "INTERFACE" (model I1) commands were applied. The model was developed with a basic brick-shaped mesh grid on both layers, generating 10830 grid-points and 9072 zones (see Figure 3.11).

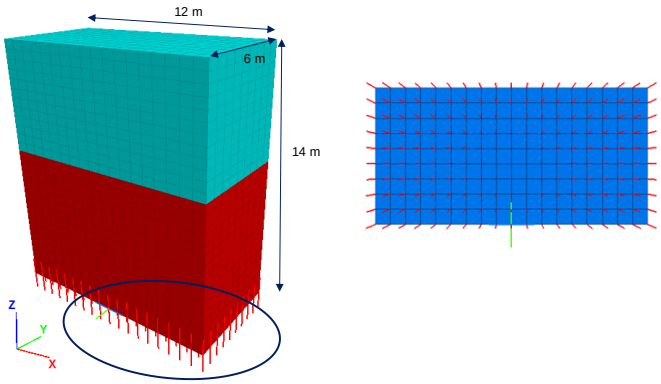

Figure 3.11 – Schematic representation of half of the simple model and its fixities

3.5.2 EQUAL SOIL LAYERS AND DIFFERENT ZONE TYPE

Afterwards, two models were made with two equal soil layers but the top layer with simple brick zone elements and the bottom layer with a cylindrical grid, to simulate the soil column, combined with a radially cylindrical brick mesh type, around the cylindrical grid (Figure 3.12). The difference between these two models was the method the different zones are joined together. One was modelled with the "ATTACH" command (model A2) and the other with "INTERFACE" (model I2) (see Figure 3.12 – b) for the model with the interface elements). Both models were generated with 18740 grid-points and 16616 zones. The soil parameters and interface properties are presented in Table 3.3.

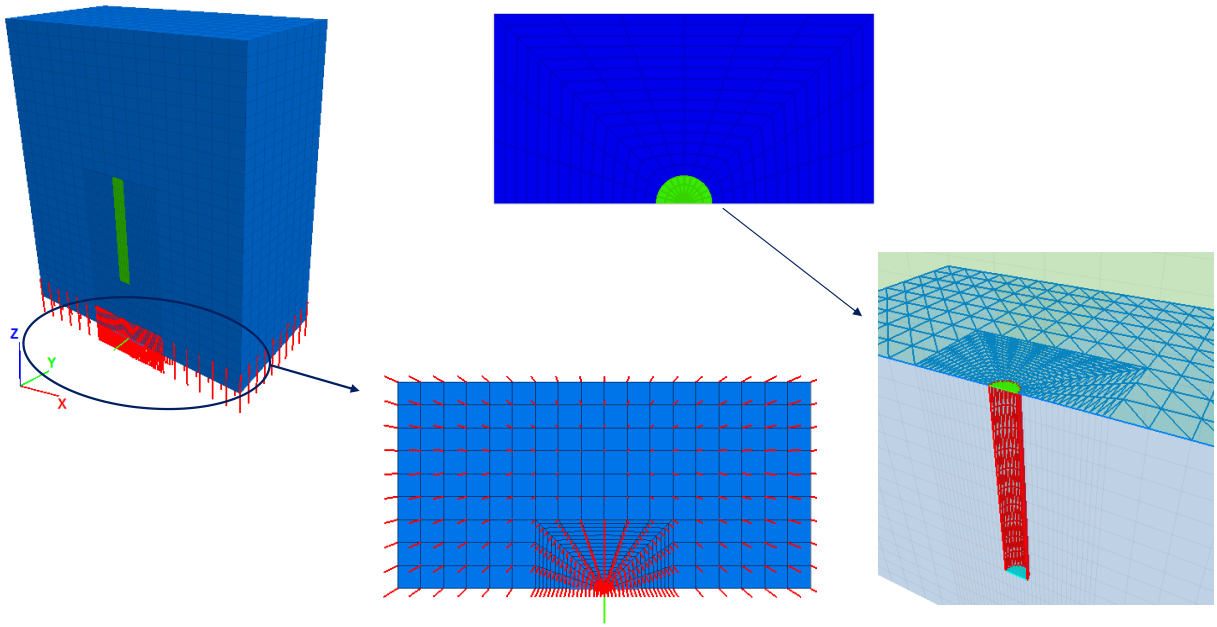

Figure 3.12 – Schematic representation of half of the column model, its boundary conditions and interface elements

Table 3.3 - Soil and interface parameters for the two-layered equal soils model

		Soil Parameters				Interface Parameters	
		Young's Modulus	Poisson's Ratio	Bulk Modulus	Shear Modulus	$\left[\frac{K+4/3\,G}{\Delta z}\right]$	$k_n=k_s=10\times\left[\frac{K+4/3\,G}{\Delta z}\right]$
Unit		MPa	-	MPa	MPa	MPa/m	MPa/m
Two-layered equal soil model	Top	60	0.25	40	24	144	1440
	Bottom	60	0.25	40	24	144	

3.5.2.1 Results

As expected, the behaviour of the four models is almost identical when observing the displacement curve with depth in Figure 3.13. However, as mentioned before, the results with the "INTERFACE" command show a discontinuity at its location, while this does not happen in the model with the "ATTACH" command.

Comparing between models with or without a column on the bottom, independently of the command used to join the different grids, the displacements values are similar between different meshes. However, the displacements obtained with the column model are a little higher than off the control, until the interface element is reached. After the interface, the opposite happens, having smaller displacements with the column model, when comparing with the control example. This can be seen in the plot of relative difference of results in Figure 3.14 , where a comparison between models with different meshes is made, having as reference the control example model. The minor difference that exists between results might be due to the different mesh discretization.

Between the model I2 and model A2 there are also very small differences, resulting in around 0.37 % larger displacement obtained by applying the “INTERFACE” command rather than the other one, until the interface element is reached. After the interface element, differences between both models become even more insignificant, reaching to 0.02%. (see Figure 3.15).

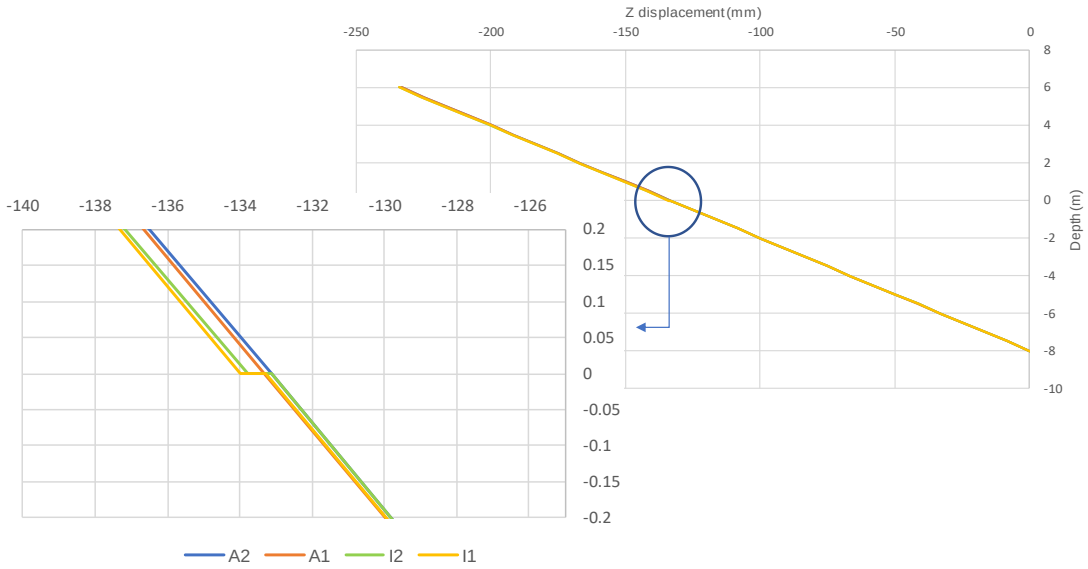

Figure 3.13 - Displacement curve for different meshes and different commands to adjoin grids

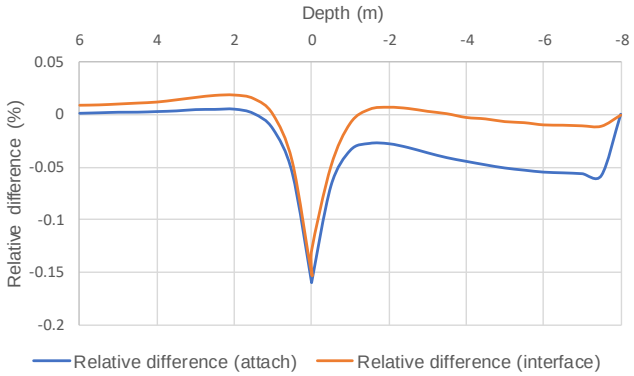

Figure 3.14 – Plot of relative difference between the control model and the models with the cylindrical mesh column, for different commands

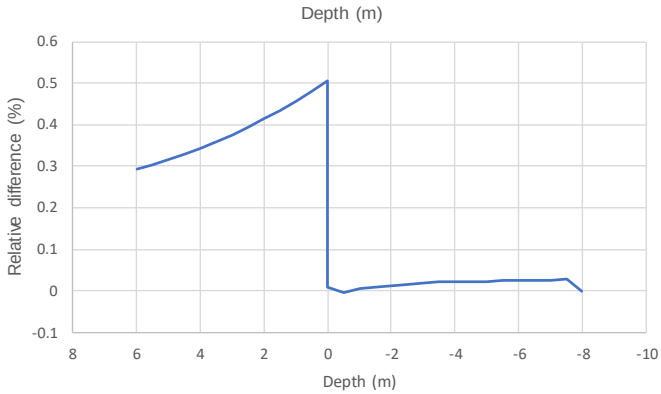

Figure 3.15 - Relative difference of results between the “ATTACH” command and “INTERFACE” command, in the model with the cylindrical mesh column (model A2 vs model I2)

3.5.3 DIFFERENT SOIL LAYERS AND ZONE TYPE

After the previous tests, where the interface elements acted only as a means to connect different mesh types, one must study how this interface acts when in presence of different soil layers and mesh types, on top and at the bottom, and its effect.

3.5.3.1 Different soil layers (column included in bottom layer)

Four models with the geometric properties of the previous ones were created, however, with different soil properties on top and at the bottom. Two of them were made with regular mesh types on both layers, one having the "ATTACH" command and other the "INTERFACE" command separating the soils (models A1 and I1) (see Figure 3.16). The other two models had the mixed mesh type, also one with the "ATTACH" and another with the "INTERFACE" separating the layers (model A2 and model I2) as shown in Figure 3.17. The interface properties were based in the stiffer soil and the ground and interface attributes are presented in Table 3.4.

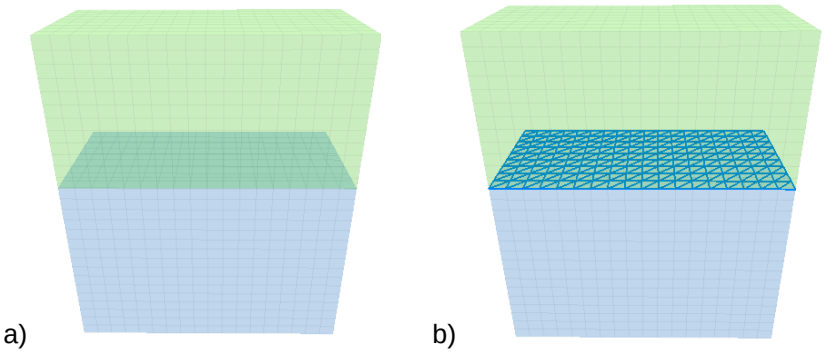

a) b)

Figure 3.16 - Different soil layers with regular mesh models: a) "attach" command (model A1); b) "interface" command (model I1)

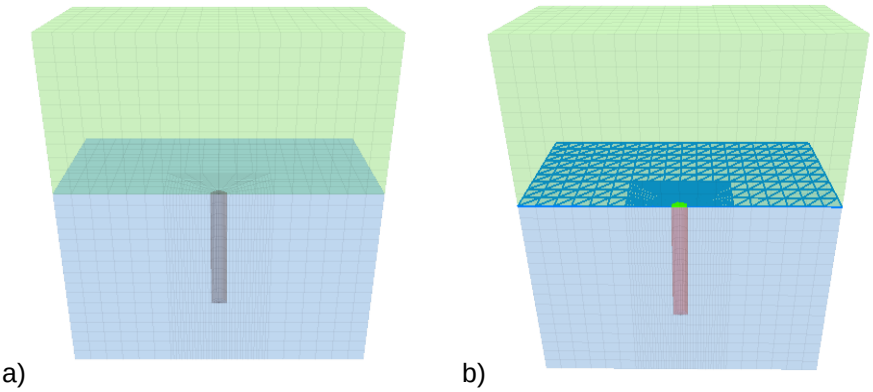

a) b)

Figure 3.17 - Different soil layers with mixed mesh models: a) "attach" command (model A2); b) "interface" command (model I2)

Table 3.4 - Soil and interface parameters for the two-layered different soils model

		Soil Parameters				Interface Parameters	
		Young's Modulus	Poisson's Ratio	Bulk Modulus	Shear Modulus	$\left[K+\frac{4}{3}G\right]/\Delta z$	$k_n=k_s=10\times\left[K+\frac{4}{3}G\right]/\Delta z$
Unit		MPa	-	MPa	MPa	MPa/m	MPa/m
Two-layered equal soil model	Top	60	0.25	40	24	144	2880
	Bottom	120	0.25	80	48	288	

3.5.3.2 Results

As in the previous tests made with equal mesh types but different soil layers, when analysing the displacements in depth there is a change in the curve' slope due to the different stiffness's of the layers. Hence lower displacements where the layer is stiffer, thus steeper curve. This is observable in Figure 3.18.

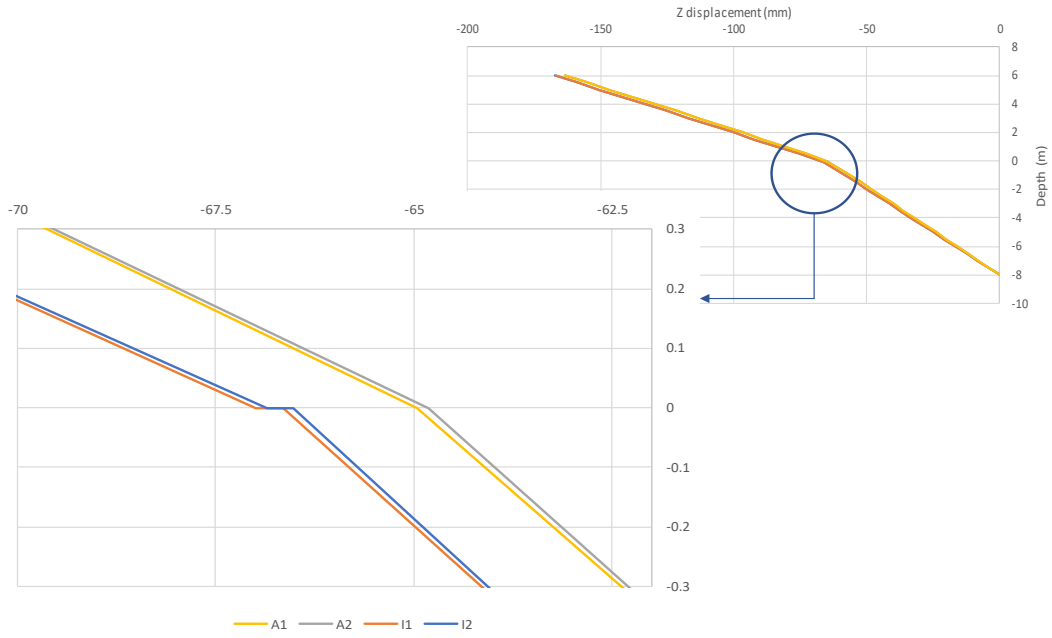

Figure 3.18- Displacement curve for different meshes and different soil types

In general, all four models produced very comparable outcomes, as seen in Figure 3.18. When comparing the results between the models A1 and A2, generated with the "ATTACH" command, the model with the mesh column has slightly larger displacements comparing with model A1, before the interface element is reached. From z = 0 m to z = -8 m, model A2 has somewhat smaller displacements than the one with the regular mesh on the lower layer, around 0.04% smaller. This might be due to the mesh refinement on the lower layer when the mesh column is present. Comparing models I1 and I2 generated with the "INTERFACE" command, the difference between results is minimal and the previous conclusions are valid.

Regarding the difference between the "INTERFACE" or "ATTACH" command, either for the mesh without or with column, the displacements are around 3.4 % higher when the interface element is present (see Figure 3.19).

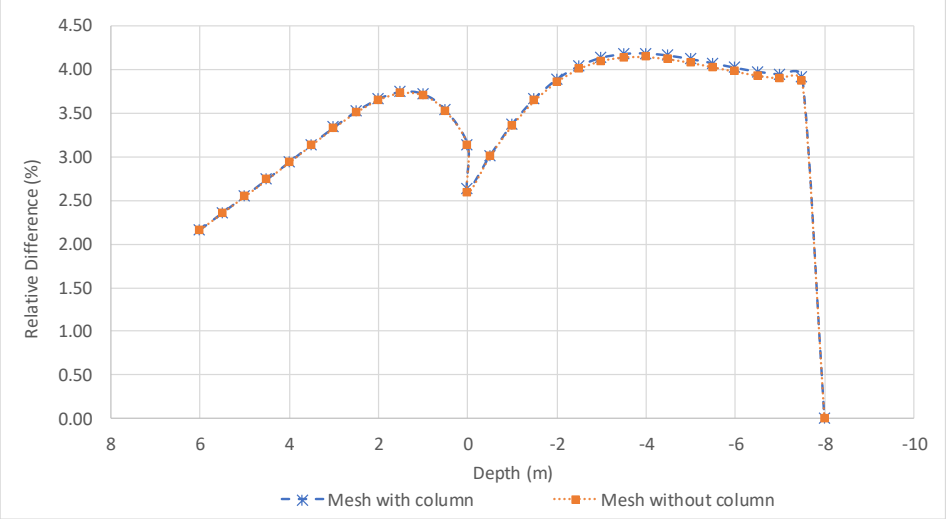

Figure 3.19 - Plot of relative difference between "INTERFACE" vs "ATTACH" command, for the mesh models with and without column

3.5.3.3 Different soil layers and soil column properties

The later purpose of these parametric studies is to introduce the elements studied in this chapter on a larger model of the railway. Thus, three models were designed with different stiffness properties in the top layer, bottom layer and the soil column. The ground and interface parameters are presented in Table 3.5. One model was designed with the "ATTACH" command (model A) and the other two with the "INTERFACE" command (model I1 and I2) to adjoin the different soil layers.

On model I1 only two interfaces were applied: one of them at the top tip of the soil column in contact with the upper layer and the other one separating the soil layers, similarly to Figure 3.17-b). Regarding model I2, four different interfaces were generated as can be seen in Figure 3.20: the first one was placed separating the soil layers horizontally, the second one was the bottom tip of the soil column, the third enveloped the perimeter of the column and the last one was the top tip of the column. The purpose of the model I2 was to see if, when we have compatible grids but dissimilar materials, it is more efficient to apply the "ATTACH" command rather than placing an interface, an element that is quite tricky to model when it comes to a cylindrical surface.

The interface properties were assigned as a stiff layer controlled behaviour. Regarding model I2, the first and fourth interface were assigned properties $k_n=k_s=2880$ MPa/m and the second and third $k_n=k_s=4800$ MPa/m.

Table 3.5 - Soil and interface parameters for the two-layered different soils model

		Young's Modulus	Poisson's Ratio	Bulk Modulus	Shear Modulus	$\left[\frac{K+4/3\,G}{\Delta z}\right]$	$k_n=k_s=10\times\left[\frac{K+4/3\,G}{\Delta z}\right]$
Unit		MPa	-	MPa	MPa	MPa/m	MPa/m
Two-layered equal soil model	Top	60	0.25	40	24	144	1440
	Bottom	120	0.25	80	48	288	2880
	Column	200	0.25	133	80	480	4800

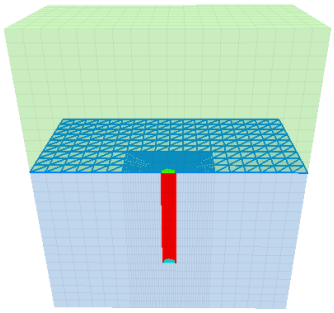

Figure 3.20 – Scheme of model I2 for different soil layers properties and mesh types

3.5.3.4 Results

By observing Figure 3.21, it is visible that the difference between the three models is very small. As mentioned before, with the presence of an interface there is a discontinuity on the displacement values, suggesting a very small interpenetration of the upper layer on the lower layer.

Comparing the results between models I1 and A, the displacement values obtained with the "INTERFACE" command are circa 3.5 % higher than with the "ATTACH" command. The plot of the relative difference of model I1 vs model A, with reference the displacement values of model A, is shown in Figure 3.22.

Regarding models I1 and I2, the results obtained are exactly the same in terms of displacement field, as it can be seen, in Figure 3.21, that the displacement curves coincide. Although not shown here, other models with the same characteristics as these last three, but with grid-point incompatibility, were tested and the same conclusions were reached, by analysing the stress and displacement field. This allows us to conclude that interface elements and the "ATTACH" command can perform very similarly, and one might implement the interfaces when mesh types or materials are very different. Having in mind that the "INTERFACE" command may significantly increase computational effort and computation time, the "ATTACH" command seems to be preferable and can be implemented when grids are compatible, even if material properties are slightly different.

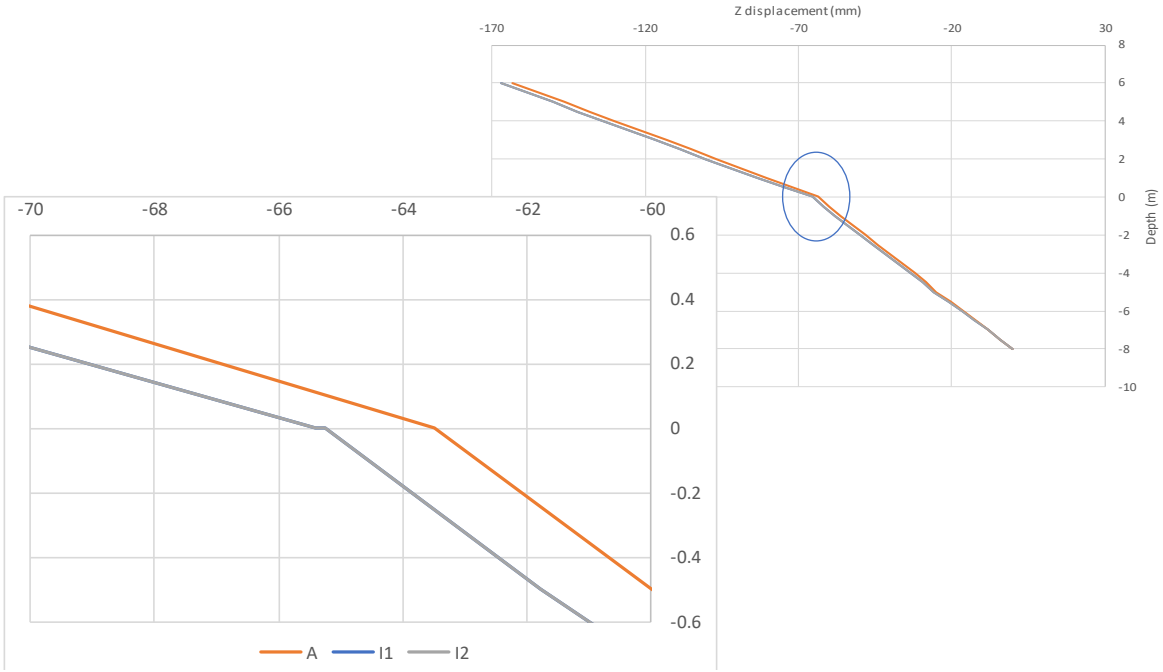

Figure 3.21 -Displacement curves for models A, I1 and I2

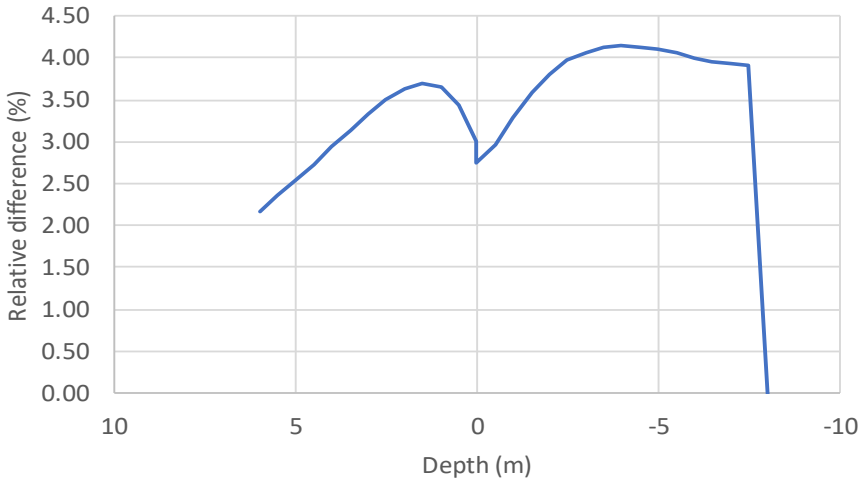

Figure 3.22 – Relative difference plot between "INTERFACE" and "ATTACH" command for models I1 and A

3.6 CONCLUDING REMARKS

With these parametric tests, a better understanding on FLAC3D's commands "ATTACH" or "INTERFACE" was obtained and practical knowledge was acquired that will be used in the following chapters to support the decision on how to implement these commands on the larger scale model.

With the first parametric tests, it became clear that choosing between a stiff behaviour or soft behaviour interface is almost irrelevant when the materials that adjoin the interface are similar, being wiser to adopt a stiff interface behaviour. However, as suggested in the manual, if material properties significantly different, one should choose a soft interface behaviour to limit the increase in computational effort and time.

With the second parametric tests, considering the applications under study, it was visible that the choice between “ATTACH” or “INTERFACE” will not influence results very much. The demonstration that choosing between an “ATTACH” to join compatible sub-grids but with different materials was a very useful conclusion for later application on the railway model.

Between both commands, if no slip or separation is expected, it is better to choose the “ATTACH” command because it is easier to implement comparing with the “INTERFACE” command. In the case of the interface elements, their geometry must be created carefully and attributed certain characteristics, whereas by implementing the “ATTACH” command, calculation time is more efficient and the results produced are satisfactory, when compared with interface models results.

4

NUMERICAL MODELLING OF THE RAILWAY TRACK

4.1 GENERAL CONSIDERATIONS

In this study, the three-dimensional numerical modelling of the railway track was developed with FLAC3D to study the structural behaviour of the railway track with reinforced substructure by means of Jet-grout columns. In this chapter, a brief description of the characteristics of the generated models is made.

4.2 DESCRIPTION OF THE NUMERICAL MODELS

4.2.1 GEOMETRIC PROPERTIES

Nine types of models were generated, with different column layout and loading configuration.

The first model (model N) represented the original railway track, without ground improvement to examine the upgrade achieved by the Jet-Grout piles. Six of the models had a row-like pattern, with the Jet-Grout columns in a central, interior or external position relatively to the rail and sleepers (models CC, CC1, CI, CI1, CE and CE1 – see Figure 4.1), while the remaining two had a zig-zag configuration of the columns position, being placed externally or internally to the rail (models CEZZ and CIZZ – see Figure 4.1). By studying different column patterns, it enables us to better understand the influence of the columns and their pattern in the structural response of the track and, ultimately, to obtain information that allows us to identify the most adequate solution for a given scenario.

To study the response of the railway system in different extensions of the track, for each column pattern, two types of loading configuration were established regarding the relative position of a single axle of a freight train to the position of the reinforcement columns. Both loadings were applied on the rail at the transverse plane of symmetry of the model, at the span between two consecutive sleepers (Figure 4.1): i) at a span without column reinforcement; ii) at a span with a Jet-Grout column.

In all model types, when applicable, the existing symmetry of the railway in the transverse and longitudinal directions was considered, guaranteeing a reduction of the problem's domain, thus reducing computation effort and time. Seven of the models consisted of a double symmetry, reducing the problem's domain to a quarter of its original size and the remaining two, due to the zig-zag column configuration scheme, with a single symmetry. In Figure 4.1 the details mentioned above are represented.

For the double symmetry models, the mesh's length was 4.8 m in the longitudinal direction, parallel to the rail, 2.2 m in the transverse direction, parallel to the sleepers and with a depth of 4 m below the base of the sleepers. For the single symmetry models, in the transverse direction, the length was twice of the double symmetry model's length (see Figure 4.2). Regarding boundary conditions, horizontal

displacements were restrained in the model's vertical planes and at level z = - 4.3 m, in the lower horizontal boundary, all displacements were restricted.

The models were developed with an 8-node hexahedral and 6-node polyhedral grid, having each model different number of grid points and zones. In Table 4.1 a summary of the amount of grid points and zones generated is presented. A mixed discretisation technique was used, having a higher number of grid points and zones in regions where higher stress gradients were expected and the analysis should be more thorough, such as under the sleepers and at the ballast layer.

Concerning the vertical loading, as mentioned above, a single axis load of 200 kN was considered as a reference for all the analyses carried out. Due to the symmetry conditions, a quarter of the loading (i.e. 50 kN) was applied on top of the rail, in the transverse vertical plane of symmetry.

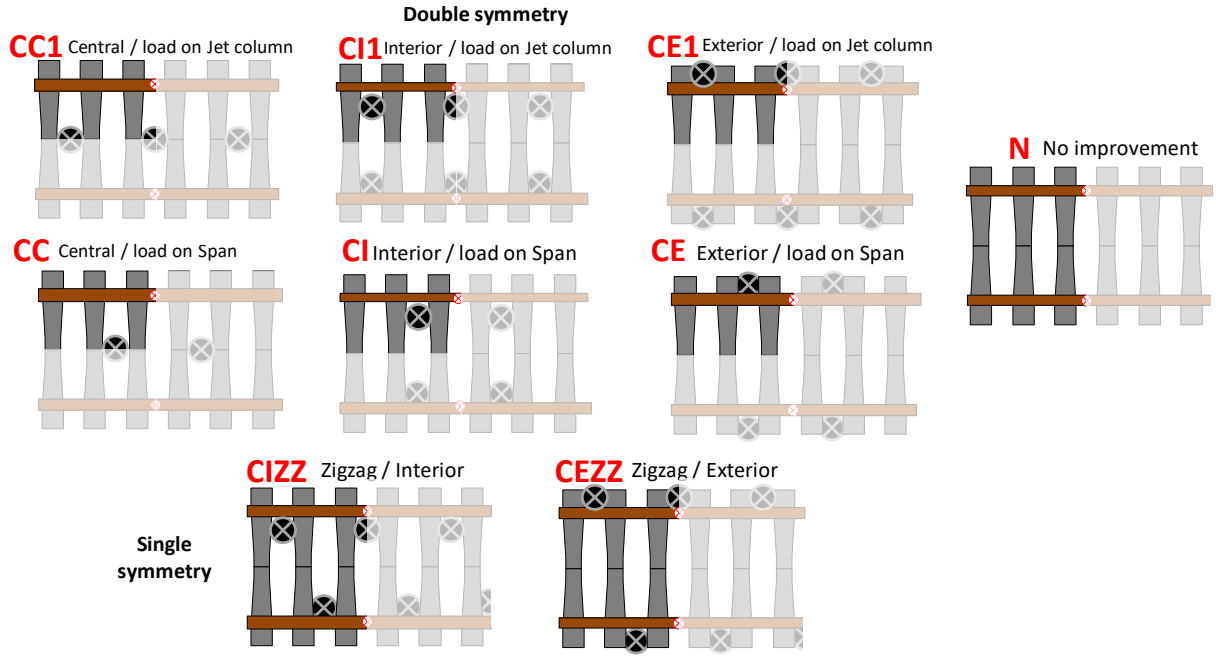

Figure 4.1 – Model's different configurations regarding column pattern and load position (the number of sleepers in this schematic representation of the different configurations is only illustrative, being that for all models a total of 8 sleepers were modelled)

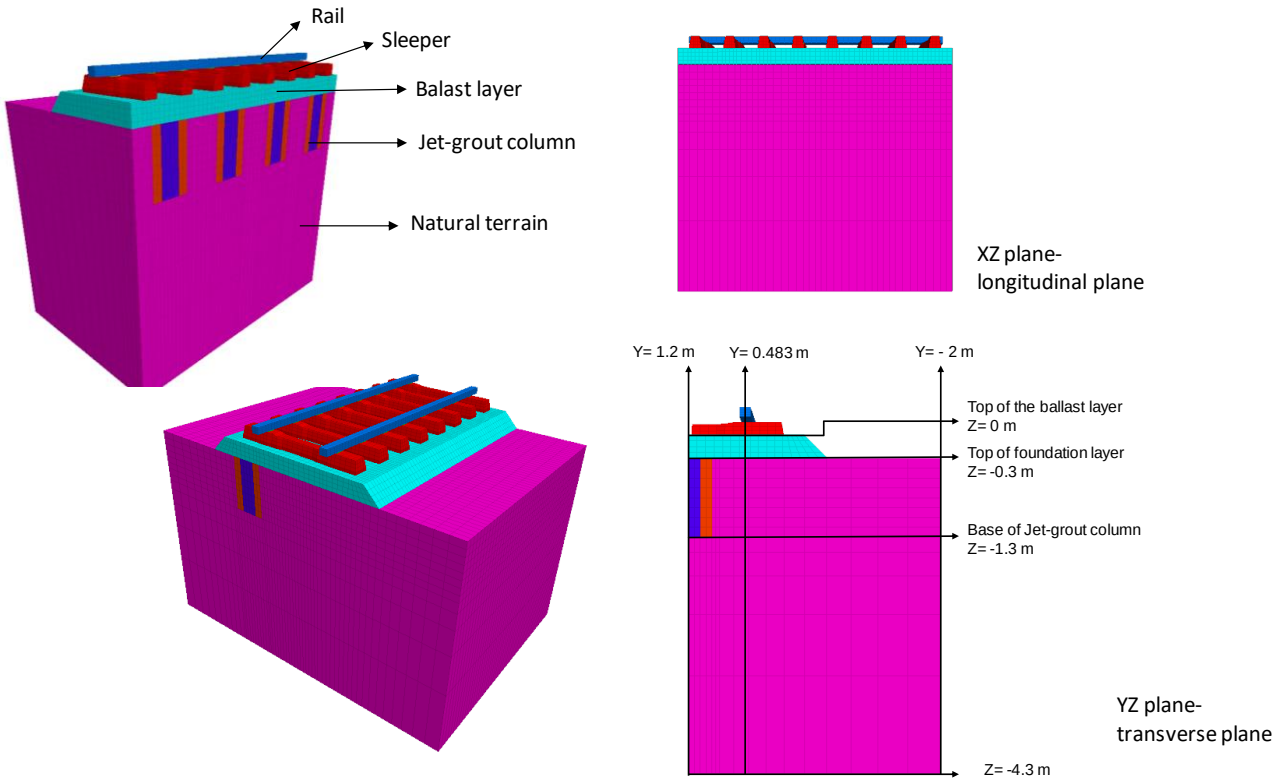

Figure 4.2 – Schematic representation of the railway track model generated with FLAC3D

Table 4.1 – Number of grid points (GPs) and zone generated for each model

Model	N	CC	CC1	CI	CI1	CE	CE1	CIZZ	CEZZ
Nº of GPs	29417	22963	22991	29417	29473	34219	34275	57679	67283
Nº of zones	24944	18496	18496	24944	24944	29312	29312	49888	58624

4.2.2 MODELLING THE RAILWAY COMPONENTS

When loading the track with a single axle, the load distribution between sleepers is intensely reliant on the system's vertical stiffness. By misjudging the load transferred to the sleeper located right under the axle load, lower stress levels will emerge at the sub-grade, leading to a non-conservative analysis (Paixão & Fortunato, 2010). Thus, a proper modelling of the superstructure should be made to reduce these aspects. The railway track components modelled were the rail, rail pads, eight sleepers, the ballast and foundation layers and the Jet-Grout columns. A detail of the representation of these elements is shown in Figure 4.3.

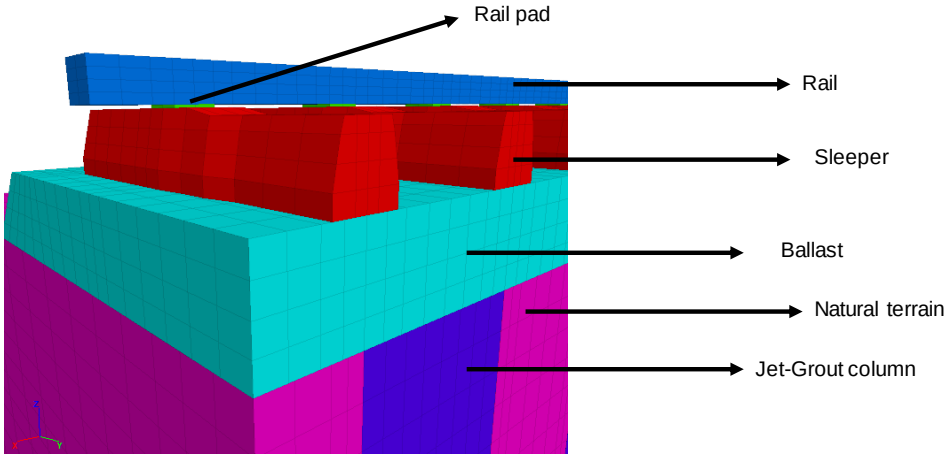

Figure 4.3 – Schematic representation of the modelled elements of the railway

4.2.2.1 Superstructure

To replicate the rail's cross section, a rectangular shape with brick zone elements was modelled (Figure 4.3). The width was of the rail foot and the height was determined so to obtain the bending stiffness of the actual rail type modelled. In all models, a rail type UIC 60 was modelled, with 0.14 m width and an equivalent height of 0.1222 m, spaced with a gauge of 1.435 m. An equivalent density was given to these elements to reproduce the actual rail weight.

Regarding the rail pads, these elements were modelled with brick zone elements placed in between the rail and sleepers. The load distribution between sleepers is highly dependent of the rail pad's vertical stiffness (Paixão & Fortunato, 2010) so proper properties should be given to this element. Paixão & Fortunato (2010) expose a study of the rail pad's stiffness and its influence on the system's vertical stress in the ballast layer. From this study, it was concluded that higher vertical stiffness of the rail pad leads to high stresses at the top layers and higher load concentration under the first sleeper. For this study, a vertical stiffness of 500 KN/mm was given to the rail pad and it was designed with a 0.01m height. An equivalent Young modulus was determined so that the adopted vertical stiffness would be obtained.

The sleepers, spaced 0.6 m, were modelled with brick elements, moulded to resemble the actual geometry of concrete monobloc structures (Figure 4.3). A schematic plane view from the top of the superstructure is represented in Figure 4.4.

Between the sleeper's bottom face and ballast layer, interface elements were placed to better model the interaction between these elements and to allow for possible slip/separation, thus providing a more realistic load distribution between sleepers (Alves Ribeiro, 2014, Varandas, 2013). As mentioned in Chapter 3, if two materials adjoining an interface are quite different from one another, the interface behaviour should be assigned to act by the softer material that adjoins that element. Since the sleeper's stiffness is much higher than the ballast's (400 times higher), the interface stiffness parameters k_n and k_s were determined based in the parameters of the ballast layer, by applying Eq. (1). The applied interface parameters were $k_n = k_s = 32323.23$ MPa/m, cohesion of 1000 kPa and tensile strength of 0 kPa.

The ballast layer was modelled with a thickness of 30 cm bellow the sleepers, made up of crushed granite aggregate. As in other studies, the crib (space between the sleepers) was not modelled here given that it presents little importance in the track's vertical structural behaviour and additional contact elements placed on the sleeper sides would be necessary to avoid obtaining unrealistic results (Paixão & Fortunato, 2010). Concerning the ballast's Young modulus, it was considered initially to have a value of 160 MPa for the linear elastic behaviour, since previous studies (Paixão [et al.], 2016b, Varandas,

2013) have determined that assigning a value between 130 MPa and 160 MPa yields good approximations to the track's behaviour. Far ahead, the non-linear behaviour of the ballast layer will be considered. The ballast's shoulders were represented with a 1% slope.

The elastic parameters and other properties of these elements are detailed in Table 4.2.

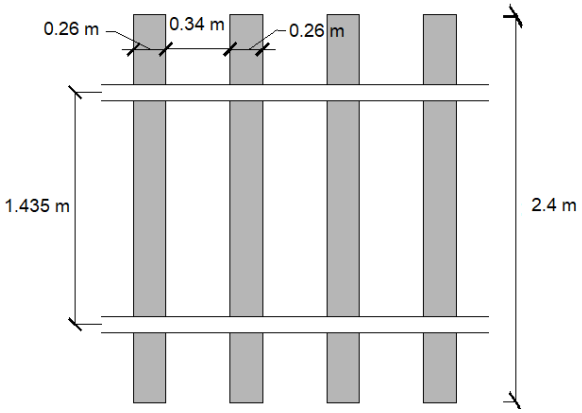

Figure 4.4 – Plane view of superstructure and depiction of unit lengths

Table 4.2 – Stiffness and other parameters of the modelled superstructure elements

	Young's modulus	Poisson's ratio	Bulk modulus	Shear modulus	Density
Unit	MPa	-	MPa	MPa	kN/m^3
Rail	210000	0.3	175000	80800	23.6
Rail pad	275	-	91.6	137	10
Sleeper	64000	0.25	42667	25600	25
Ballast	160	0.2	88.9	66.7	17.7

4.2.2.2 Substructure

The substructure is composed by the natural terrain and, when applicable, the Jet-Grout columns.

The natural terrain, assumed to be a soft ground layer, with a thickness of 4 m, was modelled with brick elements conjugated with a radially cylindrical mesh that surrounded the soil columns, as can be seen in Figure 4.5. The combination of these two mesh types was to enable the use of a cylindrical mesh, guaranteeing mesh compatibility. However, with this geometry, the mesh of the substructure is not fully compatible with the orthogonal mesh considered in the superstructure, as described above. This issue was solved with FLAC3D's "ATTACH" command, as will be addressed later.

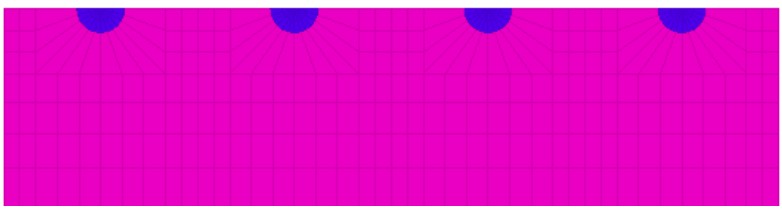

Figure 4.5 – Depiction of the foundation's mesh for the CC model (XY plane view)

The Jet-Grout columns were modelled with a cylindrical-shaped mesh, spaced by 1.2 m, placed alternately between sleepers, with a length of 1 m bellow the bottom of the ballast layer. Each model had a different layout pattern for the columns, as mentioned earlier. Furthermore, for each layout, two diameters were considered and modelled: 0.3 m and 0.6 m. These diameters were chosen to fall in the most common range of diameters that are likely to be achieved using the available injection methods and other techniques (Calon [et al.], 2011, Le Kouby [et al.], 2010). The choice of such spacing and column depth is related to the need of implementing this ground improvement solution as quickly and economically as possible, without disrupting the railway line's operation. Implementing a dense and complex layout pattern of columns may increase the project's complexity and execution time. This observation is valid for the columns' spacing, since it is more efficient, in terms of work progression, to implement a wider and simpler spacing pattern. Another remark is the fact that the diameter of each column may be sufficient to cover and receive the load from two consecutive sleepers. This reduces the need of implementing columns between every sleeper, thus reducing costs and time of work. Regarding the column's depth, since the cost of such ground improvement increases with the column's depth, a more economic approach was investigated in this study compared to other studies (Le Kouby [et al.], 2010).

Although the pile skin friction contribution influences the columns' loading and overall system behaviour (Jenck [et al.], 2009), this interaction was not studied in these numerical models. Between the piles and the foundation ground no interface elements were considered, assuming that a perfect bond exists between these soils.

To model the column, two distinct stiffness were assigned to its core and exterior. The core was assigned a stiffer material and the exterior a softer one to represent the range of treated area, since there is a diminution on the amount of grout from its injection axle to the outside.

The stiffness parameters and other properties of these elements are detailed in Table 4.3.

Table 4.3 - Stiffness and other parameters of the modelled substructure elements

	Young's modulus	Poisson's ratio	Bulk modulus	Shear modulus	Density
Unit	MPa	-	MPa	MPa	kN/m3
Natural terrain	40	0.4	66.7	14.29	19.9
Jet-Grout column (interior)	1000	0.25	666.7	400	20
Jet-Grout column (exterior)	400	0.25	266.7	160	19

4.2.3 TRACK COMPONENTS AND GROUND CONSTITUTIVE MODELS

It is important to correctly assign material properties and constitutive models to reach a realistic system behaviour. In general, when modelling the railway system, it has been considered that the layers underlying the track have linear elastic behaviour (Paixão & Fortunato, 2010, Paixão [et al.], 2016b). However, such consideration may not be precise for the upper layers (i.e. ballast, sub-ballast) since a faulty stress distribution in depth may be obtained (Paixão & Fortunato, 2010, Paixão [et al.], 2016b). Such hypothesis is valid for deeper soil stratums, where the materials undergo many load cycles with low strain increments and are considered to remain in an elastic regime (Paixão [et al.], 2016b).

It is known that ballasted railway tracks have non-linear elastic behaviour (Fortunato & Resende, 2006, Lekarp [et al.], 2000, Paixão & Fortunato, 2009, Paixão [et al.], 2016b). In particular, the ballast layer

undergoes various loading cycles that induce considerable stress changes, resulting in stiffness variations in this layer (Paixão [et al.], 2016b, Powrie [et al.], 2007). While linear elastic models require by far lower computational effort and are able to reproduce approximately the overall track's response, the stress levels inside the ballast layer may be highly underestimated (Paixão [et al.], 2016b).

4.2.3.1 Linear elastic behaviour

Materials that follow a linear elastic behaviour are characterized by reversible deformations under loading, where stress-strain relations are linear and path-independent. In an elastic isotropic model, a stress increment is generated by a strain increment according to Hooke's linear and reversible law.

In FLAC3D, the formulation of Hooke's law is:

$$\Delta\sigma_{ij}=2G\,\Delta\epsilon_{ij}+\alpha_2\,\Delta\epsilon_{kk}\,\delta_{ij} \tag{2}$$

where the Einstein summation convention applies, δ_{ij} is the Kroenecker delta symbol, and α_2 is a material constant related to the bulk modulus, K, and shear modulus, G, as

$$\alpha_2 = K - 2/3G \tag{3}$$

New stress values are then obtained from the relation

$$\sigma_{ij}^{N}=\sigma_{ij}+\Delta\sigma_{ij} \tag{4}$$

4.2.3.2 Non-linear elastic behaviour: k-θ model

The ballast layer is formed by unbound granular material, whose deformational resistance depends on the applied stress (Brecciaroli & Kolisoja, 2006). In track layers, the stress induced by moving wheel loads is quite complex, consisting of vertical, horizontal, and shear components (Lekarp [et al.], 2000).

This leads to the appearance of different stress levels at different points throughout the upper layers, where a linear elastic law may no longer be valid (Brecciaroli & Kolisoja, 2006). When materials in the upper track beds undergo a large number of load cycles, the deformational response is characterized by a recoverable – resilient - deformation and a residual – permanent - deformation. The deformation undergone by these materials is initially inelastic, reducing the plastic deformations with load cycling, until the resilient response is almost totally recovered after each loading cycle (Brecciaroli & Kolisoja, 2006, Huang, 1993, Paixão, 2014, Taciroglu, 1998). The resilient deformational response is crucial for the load-carrying capacity of the track, while the permanent strain define the track's long-term performance (Brecciaroli & Kolisoja, 2006).

Due to this behaviour, the stress-strain relationship curve is non-linear (see Figure 4.6), performing a hysteresis loop that represents the permanent strain that occurs throughout the loading cycle (Brecciaroli & Kolisoja, 2006) (see Figure 4.7).

Varandas [et al.] (2016) published a numerical study on the stress changes on the ballast layer due to train loads. By considering the k-θ model for the ballast layer, results showed a significant difference on the stress distribution, compared with a linear elastic behaviour, where unrealistic tensile stresses appeared in the track's upper layers. With the non-linear elastic model, the phenomena of principal stress rotation decreased, since the elements under the loaded sleeper are stiffer than the ones located between the sleepers, inducing a higher vertical stress transmission, reducing the principal stress rotation effect.

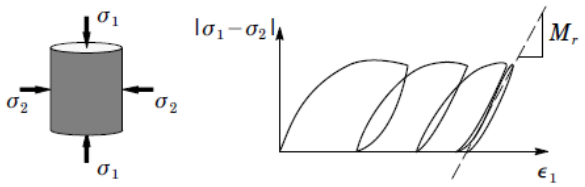

Figure 4.6 – Triaxial test with repeated loading and its response, for a granular soil sample (after Taciroglu ,1998)

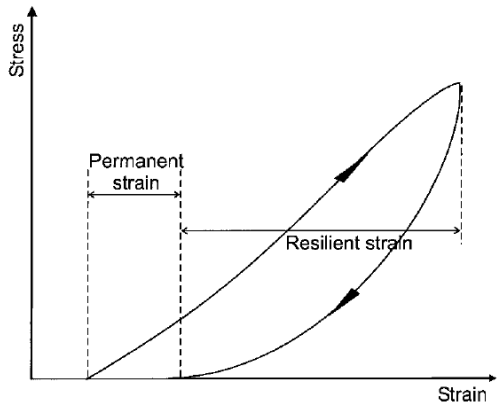

Figure 4.7 – Stress strain curve for granular materials during one cycle of load application (hysteresis loop) (after Lekarp [et al.],2000)

The non-linear elastic model k-θ formulated by Brown & Pell (1967) has been used to model the reversible behaviour of granular materials, where its simple formulation is:

$$E_r = k_1 \, \theta^{k_2} \qquad (5)$$

where E_r is the resilient modulus, θ is the sum of the principal stresses ($\theta = \sigma_1 + \sigma_2 + \sigma_3$), and k_1 and k_2 are model parameters based on cyclic load triaxial tests of the material. This model is an approximation of the granular material's resilient behaviour under cyclic loading, assuming that ultimately it quickly shakedowns to an elastic response under repeated loading (Taciroglu, 1998). This elastic modulus is not constant, varying with the stress and strain level (Brecciaroli & Kolisoja, 2006). The iterative nature of the k-θ model must part from a minimum value of Young modulus assigned to the ballast layer and due to loading cycles reaches a certain value, which is higher than the previous one. This minimum value (E_r min) may be assigned as low as required to keep tensile stresses reasonably small (Allaart, 1992). In Figure 4.8 is shown a typical variation of the resilient modulus with the sum of principal stresses (represented as bulk stress), resulting from a study undertaken by Zeghal (2004), where an investigation of the resilient behaviour of granular materials using Discrete-Element Method was made.

For this study, when considering a non-linear behaviour for the ballast layer, the parameters adopted are shown in Table 4.4.

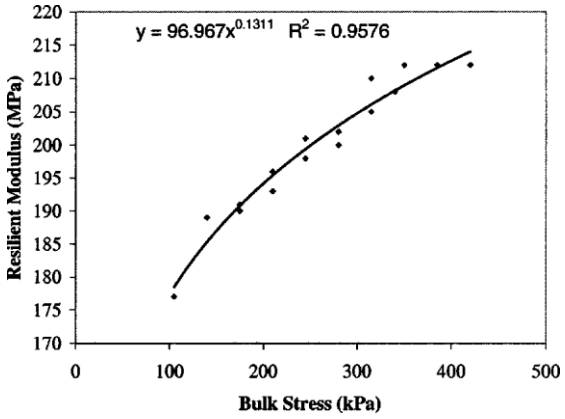

Figure 4.8 -Variation of E with θ (after Zeghal (2004))

Table 4.4 – Parameters used for the k- θ formulation applied to the ballast layer

	E_r min	k_1	k_2
Unit	MPa	MPa	-
	50	22.7	0.3

4.2.4 MODELLING PROCEDURE

The entire model is set up in one phase, which constitutes the initial state, thus the effect of the construction of the superstructure and pile installation was not considered. This is because the study aims at analysing the quasi-elastic behaviour of the track, corresponding to scenario after a sufficient number of cyclic loads (due to passing trains) have induced most of the plastic deformation. That is, in a scenario where the behaviour of the track is governed by an elastic regime.

As referred in Chapter 3, there are some rules on the creation of interface elements, such as the interface element should be attached to the smaller block of two adjoining blocks. That being so, the interface sleeper/ballast was attached to the sleeper, with the properties mentioned before.

To adjoin the ballast layer and the subgrade, the "ATTACH" command was implemented. Between these two layers, there is some grid-point incompatibility due to different mesh types applied on the ballast layer and the foundation. However, by applying the "ATTACH" command and as verified in Chapter 3, this will not have relevant interference in the calculation results.

In FLAC3D, the steady-state solution is detected when the mechanical ratio reaches 1×10^{-5} (default value). The ratio is defined as the maximum unbalanced force magnitude for all grid-points in the model divided by the average applied force magnitude for all the grid-points. The unbalanced force indicates when a mechanical equilibrium state or the onset of plastic flow is reached for a static analysis, being monitored throughout the calculation, never reaching exactly zero for a numerical analysis. The model is considered to be in equilibrium when the value of the maximum unbalanced force is small compared to the total applied forces in the problem. When the ratio falls below a certain value during the calculation process, the mechanical calculation will stop (Itasca, 2015, Jenck [et al.], 2009). All calculations were made in small strain mode.

In this thesis two types of analysis were made: i) one considering a linear elastic behaviour for all model components and ii) the other considering a non-linear behaviour for the ballast layer, keeping a linear elastic model for the other geomaterial and track components.

For the linear elastic calculations, all material properties were assigned with that behaviour and calculations were made without considering the gravitational force. Equilibrium was achieved when the mechanical ratio reached 1×10^{-5}.

For the non-linear calculations, system attributes are dependent on the actual stresses existing among components (Varandas [et al.], 2016). This requires that the initial stress state is calculated before applying the train load. Firstly, the gravitational force was activated so the weight of the materials would be considered, calculating this stage considering an elastic model type for all materials (view Figure 4.9). After achieving equilibrium of the initial stress state, the k-θ model was assigned to the ballast, through a script written in FISH language (Fortunato, 2005, Fortunato & Resende, 2006), where through cycle calculations, the new stiffness properties of this layer were determined taking into account the stresses originated in the initial state. The parameters considered for the non-linear law were $k_1=22.682$ MPa and $k_2=0.3$, assuming a constant Poisson's ratio of 0.30 (an intrinsic requirement of the k-θ model) and a minimum value of E_r min= 50 MPa.

Afterwards, the train load was applied in two stages, splitting the total load in half and applying it at each stage (see Figure 4.10 for stresses developed in the ballast layer when applying each load step). This procedure was established to ensure adequate converging of the numerical calculations, because applying the entire load at once could lead to unrealistic results. If solutions increments are small enough, all solution strategies ought to return similar results. Yet, by increasing increment size, solutions can output very inaccurate results (Potts [et al.], 2001). This technique of "sub stepping" is usually applied in FEM models to calculate non-linear constitutive models but the same principle is applicable in FDM.

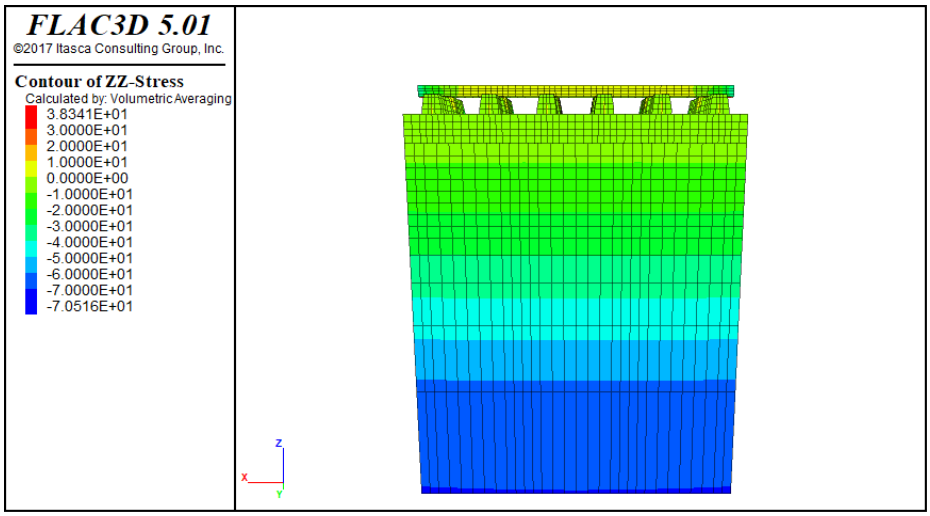

Figure 4.9 - Initial stress state generated with the k-θ model

a)

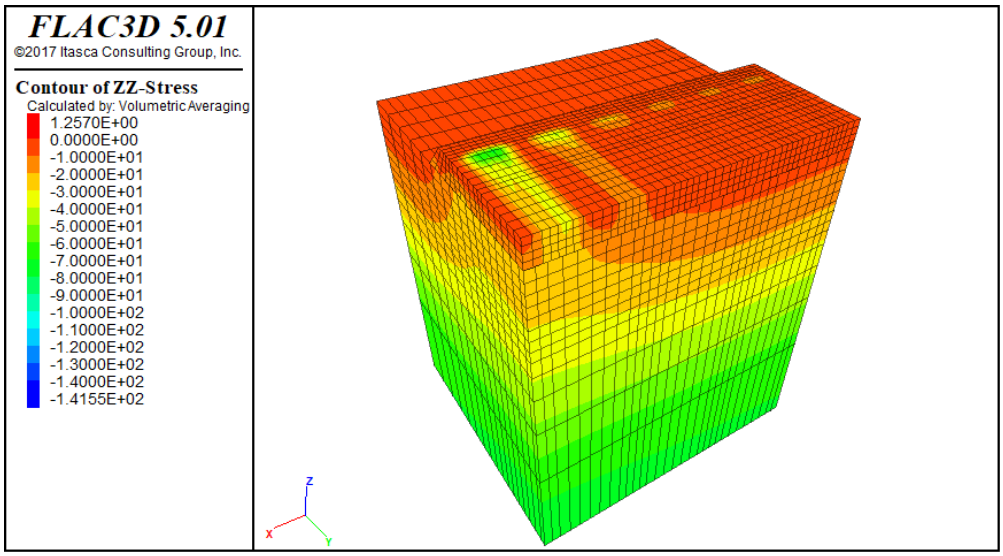

b)

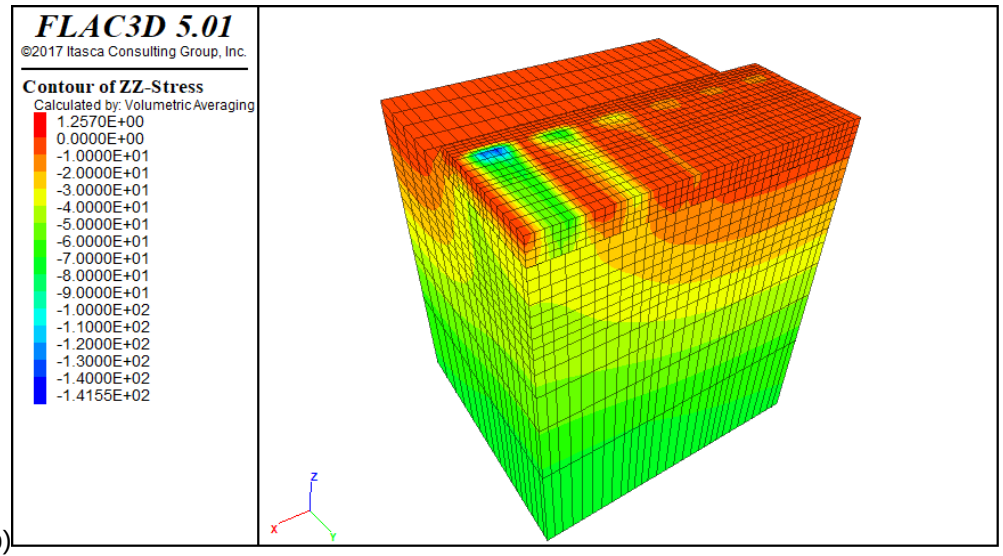

Figure 4.10 - Stress state originated at the ballast layer: a) in first load step and b) second load step

5

PARAMETRIC STUDY ON THE STRUCTURAL BEHAVIOUR OF RAILWAY TRACKS WITH REINFORCED SUBSTRUCTURE

5.1 GENERAL ASPECTS

To evaluate the potential of subgrade improvement by means of Jet-grout columns, various layouts with different placement patterns of the columns within the subgrade were designed and studied, generating different structures. In this chapter, the results of a parametric study on the influence of the column diameter, column pattern and loading position are presented and discussed to obtain more insight into the behaviour of these structures and to assess the advantages and potentiality of this ground improvement technique.

The generated models were designed as described in Chapter 4. The parametric study also focused on analysing the influence of assigning non-linear elastic constitutive behaviour to some geomaterials to achieve a more realistic representation of the actual behaviour of the track system. Firstly, results considering the linear elastic behaviour only will be analysed and discussed. Then, the non-linear elastic behaviour will be introduced in the ballast layer following a k-θ law and subsequent analysis and discussion of the results will be presented. This chapter will conclude with a comparison between these two approaches and an overall summary of results.

In general, the analysis of results was made in terms of vertical stress and vertical displacement values. The rail's vertical displacements, as well as the displacements and stresses developed in depth in the geomaterials, were analysed at the XZ plane aligned with the rail. The stresses and displacements on the top and at the bottom of the ballast layer, on the top of the foundation and slightly beneath the Jet column were analysed at specific XY planes, (see Figure 5.1).

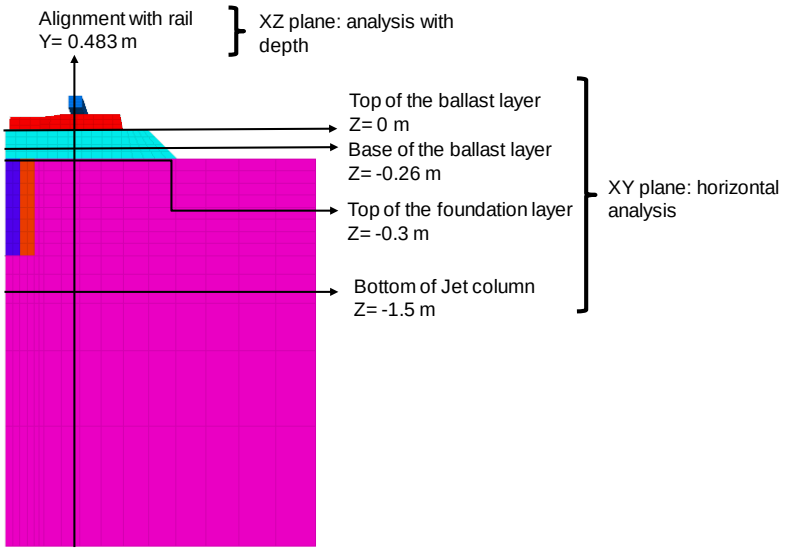

Figure 5.1 – Schematic representation of the XZ and XY planes where the analyses were made

The displacement and stress values were obtained through scripts written in FISH language and ran in FLAC3D. For displacement values, a query line is made through a set of grid-points. For stress values, a volume-weight averaging of subzone stress components is made (Itasca, 2015). In other words, displacements are evaluated at the grid-point level whereas stresses are obtained by a zone average.

When running the scripts, a starting query point in the middle of a zone is assigned moving to next closest query point, within a certain tolerance interval distance. By increasing the tolerance, more zones are enveloped and a larger number of zones is taken into consideration in the stress averaging procedure, which may alter the results presented (see Figure 5.2). The adopted tolerance interval is shown in Figure 5.2-b), so a smaller number of zones would be considered in the stress averaging procedure. Also since the mesh on the foundation is rather complex and not totally designed with brick elements, when reaching the column's surrounding, the query line will register stress values a little further or closer to the column (not on a straight line). This is observable when increasing the column's diameter as shown in Figure 5.3.

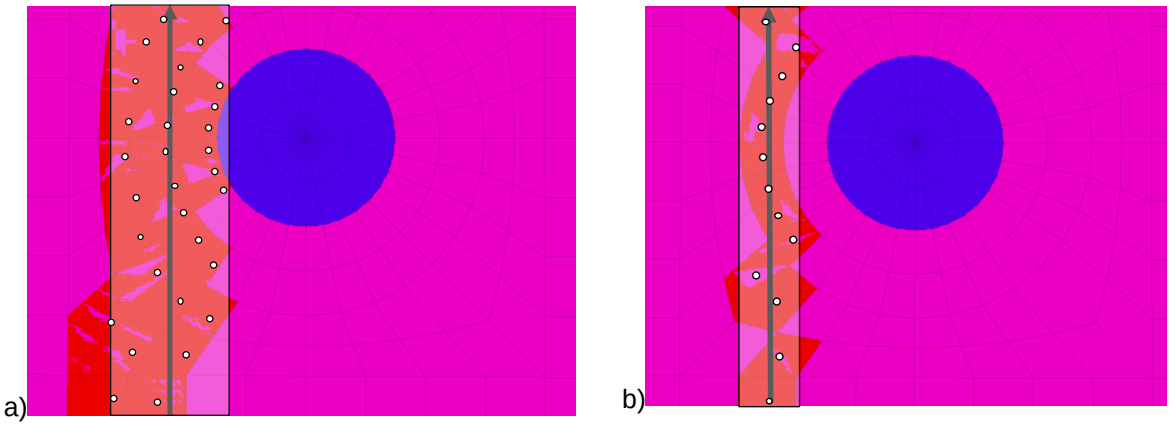

Figure 5.2 -Queried zones for stress values considering a) a larger and b) smaller tolerance interval (XY plane view)

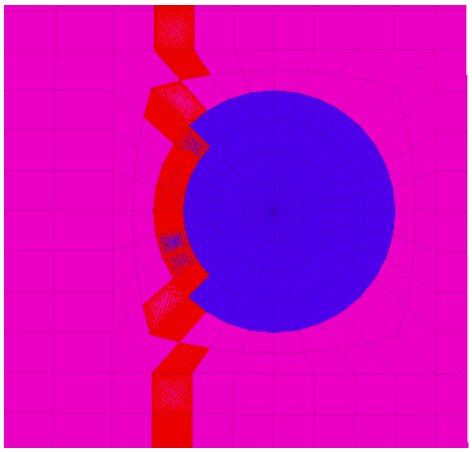

Figure 5.3 -Queried zones for stress values with a column radius of 0.3 m (XY plane view)

Herein the representation of results was generally made by means of contour charts of vertical displacements and vertical stresses. It was chosen to represent results in such manner due to existing differences in grid-point positions between models. Since each generated model had a different layout of Jet-grout column, the generation of the mesh for the foundation was completely different from model to model, becoming nearly impossible to design a mesh for the foundation that would be compatible with the mesh on the ballast layer and with all columns placement patterns. Thus, each model became difficult to compare with the others since most grid-points did not have a direct coordinate match from model to model. Despite this mesh incompatibility, the interconnection between the ballast and foundation grids was made by the "ATTACH" command, as explained in the previous chapter. This mesh mismatch of the foundation is visible in Figure 5.4, where a transverse plane of the CI and CC model (see Figure 4.1) is shown.

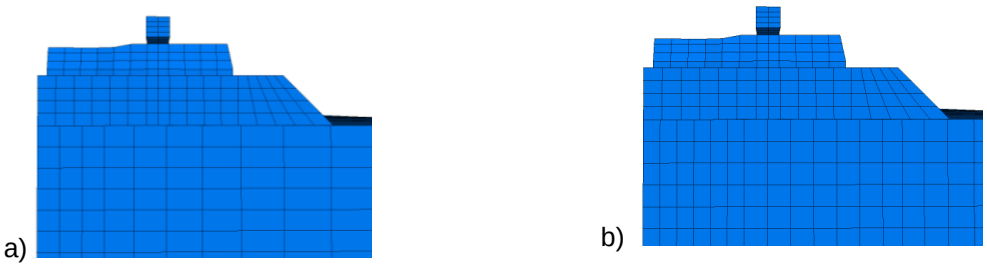

Figure 5.4 – Mesh incompatibility representation in the transverse plane for models a) CI and b) CE (YZ plane view)

When trying to represent results through charts for each model, these would not be representing the same point, due to mesh differences. In Figure 5.5 it is visible how similar coordinates refer to distinct locations in the mesh. For example, if analysing the displacement value in the point represented in Figure 5.5- b) and comparing with the point in Figure 5.5-a), the displacement values would be very different since one is quite close to the jet column and the other is not.

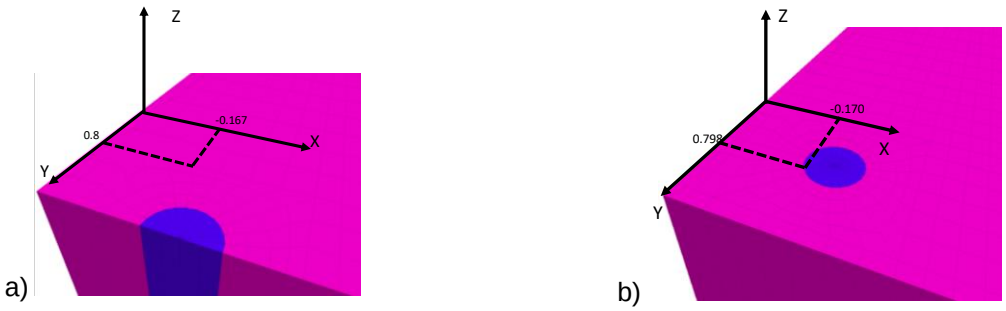

Figure 5.5 -Mesh incompatibility between model CC a) and CI b)

The solution to this was the representation of results by contour plots since contour lines represent lines of connecting points where a function has the same particular value (Hughes-Hallet [et al.], 2013), allowing us to have comparable results. All contour charts were developed in MATLAB, resorting to a three-dimensional representation of results by means of Delaunay triangulation using `delaunay` function[1], transforming then into a two-dimensional representation using the `trisurf` function[2]. However, when performing a study of the difference of values between different models, the incompatibility between grid-points was an issue. To overcome this, a linear interpolation between the x and y coordinates of each model was made, for example, when analysing the XY cut plane.

5.2 LINEAR ELASTIC BEHAVIOUR

5.2.1 INFLUENCE OF COLUMN DIAMETER

In this study, two Jet-grout column diameters (D) were considered and modelled: 0.3 m and 0.6 m (see Figure 5.6).

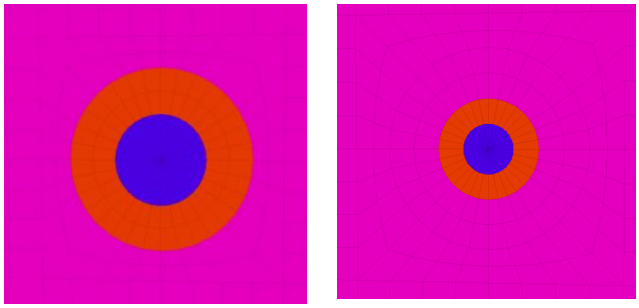

a) b)

Figure 5.6 – Identical mesh geometry for direct comparison between different column diameters: a) D = 0.6 m; b) D = 0.3 m (XY plane view)

[1] https://www.mathworks.com/help/matlab/ref/delaunay.html
[2] https://www.mathworks.com/help/matlab/ref/trisurf.html

5.2.1.1 Results at the XY planes

In general, with a larger column diameter, smaller vertical displacements are obtained, both for the top of the ballast layer or the foundation, and larger displacements beneath the Jet column.

Since this observation is valid for most of the model configurations, the results for the CE pattern will be presented in this subchapter. For the other models, results are presented in the digital annexes, presented separately in CD format.

5.2.1.1.1 Vertical displacements on top of the ballast layer

Regarding the vertical displacements on top of the ballast layer, they are larger under the first sleeper (nearest to the axle load position) for both diameters. With the increase of the column's diameter, the magnitude of the maximum displacement decreases, as expected, from 1.2 mm to 1.1 mm (see Figure 5.7). The location of the maximum vertical displacement, for both diameters, is in the middle of the sleepers. This may be due to the existence of the columns at an exterior position to the rail, giving higher support to the extremities of the sleepers, thus smaller deformations on the ballast layer on that section. In this way, the sleeper is likely deforming as a simply supported beam. This behaviour is typical for softer foundations soils (Selig & Waters, 1994).

To compare both diameters, difference plots were made regarding displacements and stresses, and all had as reference the results for 0.3 m diameter, as shown in Figure 5.8. If we look closely, it is possible to identify the position of the sleepers by analysing the contours, being visible that the first three sleepers show smaller displacements for the 0.6 m diameter. This difference between displacement results diminishes as we go further away from the position of the point load due to the reduction of the load's influence. It is visible that the larger difference lies underneath the first sleeper, existing smaller displacements beneath this element for D=0.6 m. The maximum difference between results is of 0.1107 mm larger displacements for the D=0.3 m, in position in x = -0.2150 m and y=0.3094 m. This difference is not very high, meaning that even though with a higher diameter, displacements are smaller but the improvement obtained is not that substantial in terms of vertical track deformability, that is, track vertical stiffness.

The maximum displacement values and the position of those maxima, for different column patterns and column diameter, are presented in Figure 5.9. Considering that some models have double symmetry it would be expected that the maximum displacement values would fall aligned with the longitudinal symmetry axis of the model. Apparently, this is not the case for some models such as the CC model, since it has a column placed in a central position relatively to the sleeper. This may be due to some minor numerical errors, obtained either in the calculation or during the post-processing of the results.

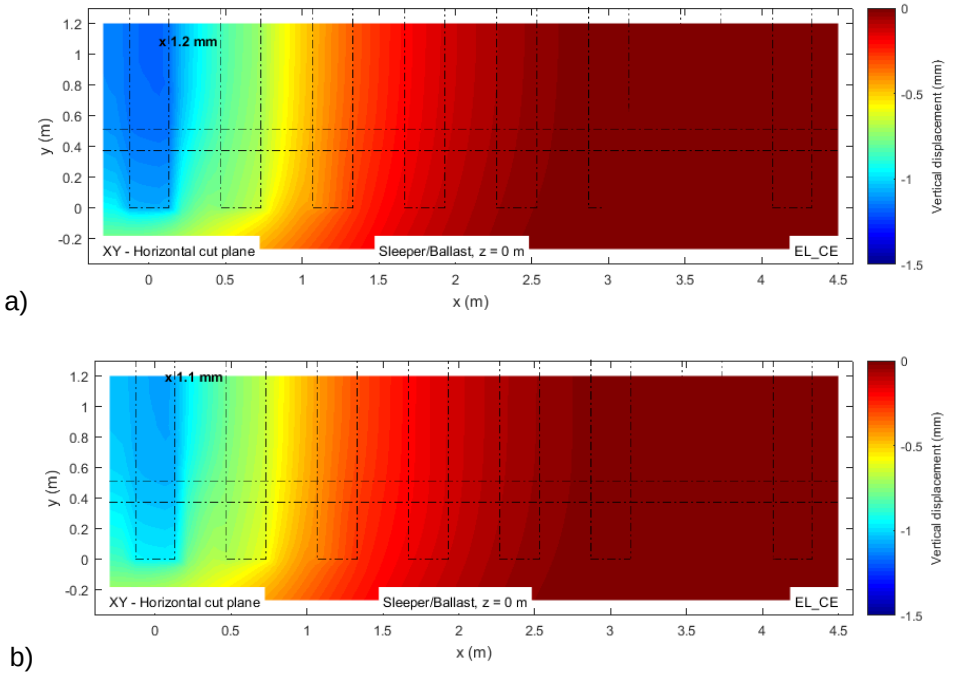

Figure 5.7 - Vertical displacement distribution on top of the ballast layer in pattern CE for a diameter of 0.3 m a) and 0.6 m b)

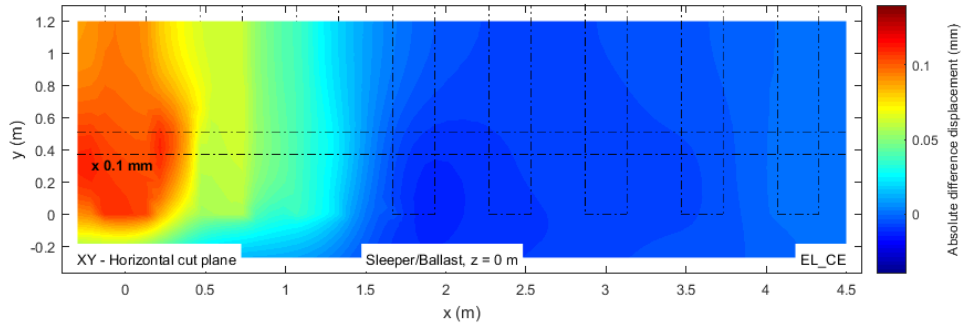

Figure 5.8 -Difference of results of vertical displacement distribution on top of the ballast layer between different diameters in pattern CE

5.2.1.1.2 Vertical displacements on top of the foundation

On top of the foundation, the observations are analogous to the ones for the top of ballast layer. Displacements are higher under the first sleeper, closer to the point load, and decrease as we go further away in the longitudinal direction of the track as depicted in Figure 5.10. Again, regarding the maximum displacement for both columns, increasing the column's diameter does not deliver significant improvement.

The difference between displacements for the top of the foundation, with reference to the results for a 0.3 m diameter, is shown in Figure 5.11. The displacement results with the larger column are in overall smaller, as expected, and it is noticeable a circular region between the first sleepers, where a column is positioned that displays a more evident difference in the displacements. That region displays higher differences since it appears that the loading is affecting displacements on the surrounding of the column closer to the loading point. The presence of stiffer substructure under the sleeper reduces deflections under this element. By implementing a larger diameter, a reduction of 0.2 mm in the deflection value, of the substructure under the first sleeper, is obtained.

The maximum displacement values and the position of those maxima on top of the foundation, for different column layouts and column diameter, are presented in Figure 5.12.

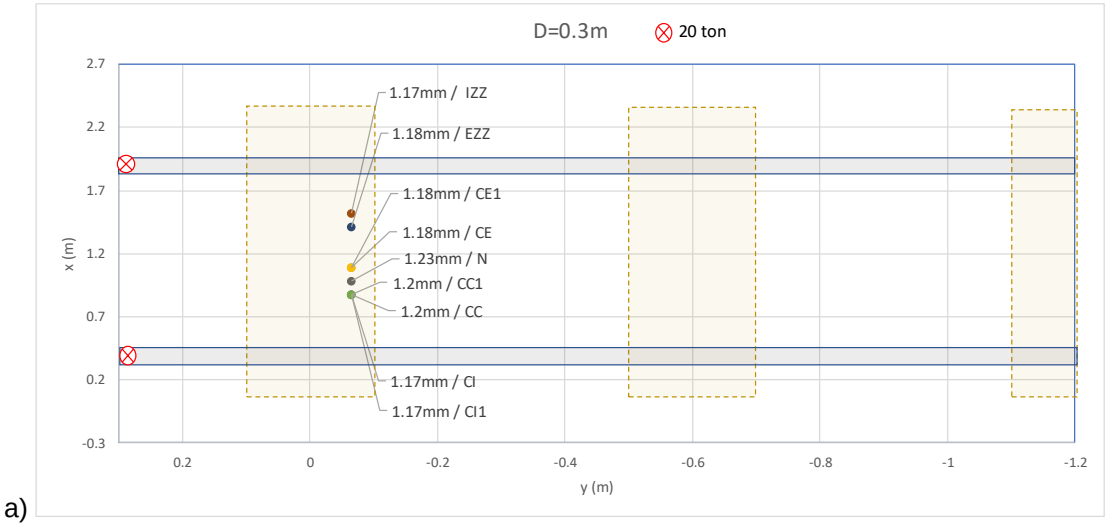

a)

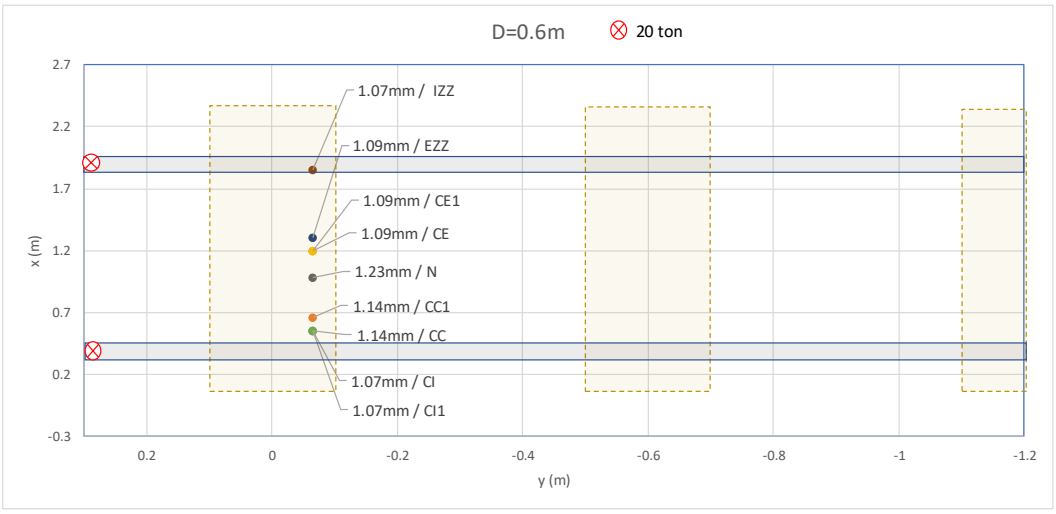

b)

Figure 5.9 -Maximum displacement values and their position for different column layouts and diameters (a) D=0.3m and b) D=0.6m) on top of the ballast layer.

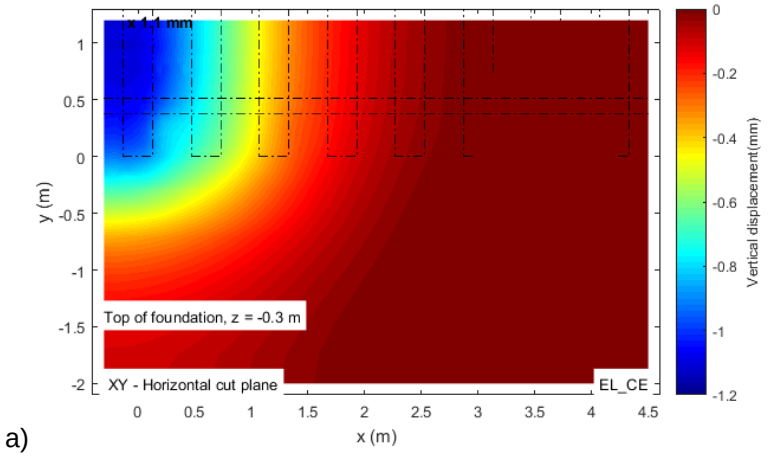

a)

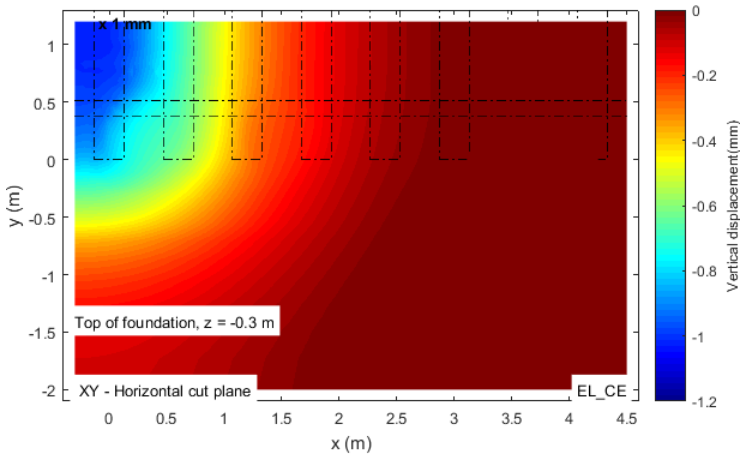

b)

Figure 5.10 - Vertical displacement on top of the foundation in pattern CE for a diameter of a) 0.3 m and b) 0.6 m

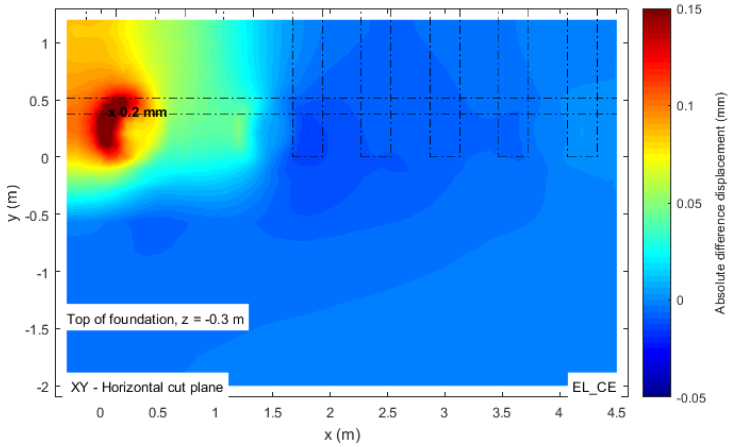

Figure 5.11 - Difference of results of vertical displacement distribution on top of the foundation between different diameters in the pattern CE

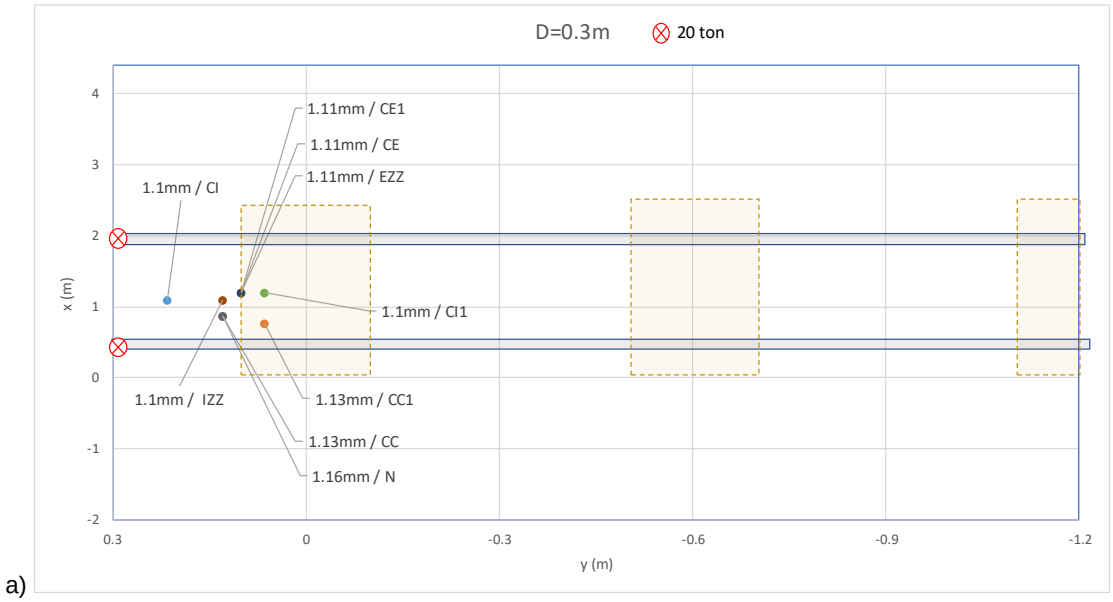

a)

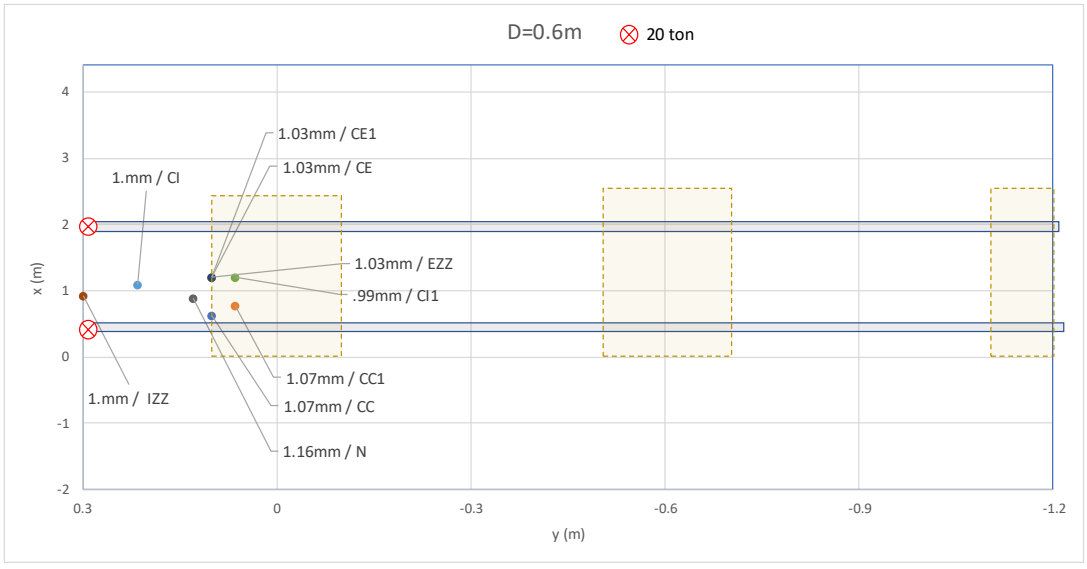

b)

Figure 5.12 - Maximum displacement values and their position for different column patterns and diameters (a) D=0.3m and b) D=0.6m) on top of the foundation.

5.2.1.1.3 Vertical displacements under the columns

The displacement contours at a depth just under the Jet column, for both diameters, are presented in Figure 5.13. Underneath the Jet-grout column, the displacements are slightly higher for the 0.6 m diameter. This remark is more evident when analysing the plot of difference in Figure 5.14 where it is visible circular regions at the positions of the columns, where it shows that for the D=0.6 m underneath the column, displacements are 0.1 mm higher. In between the sleepers, at that depth, smaller displacements are visible, for a larger diameter.

The maximum displacement values and the position of those maxima at a level beneath the Jet-grout column, for different column patterns and column diameter, are presented in Figure 5.15.

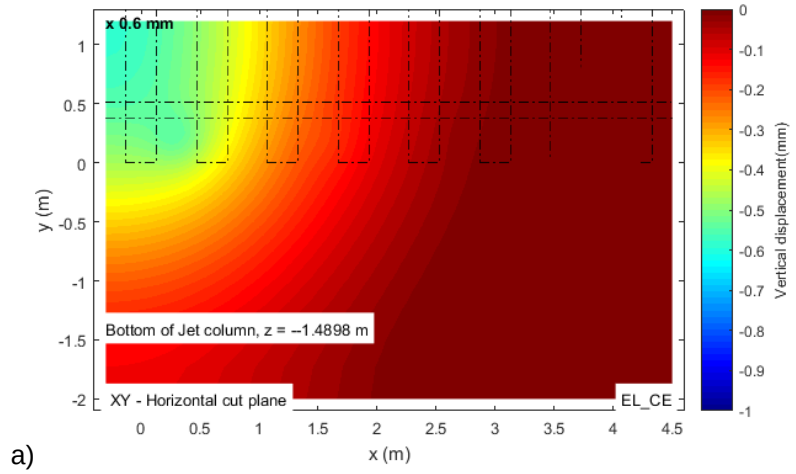

a)

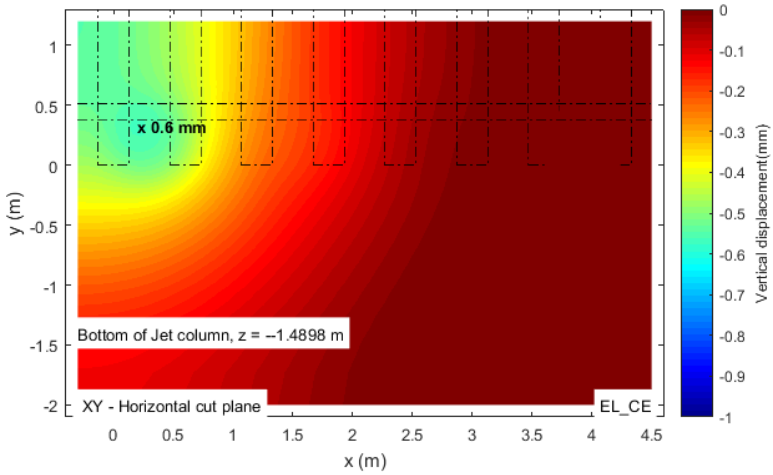

b)

Figure 5.13 – Vertical displacement at the bottom of Jet column in pattern CE, for a diameter of a) 0.3 m and b) 0.6 m

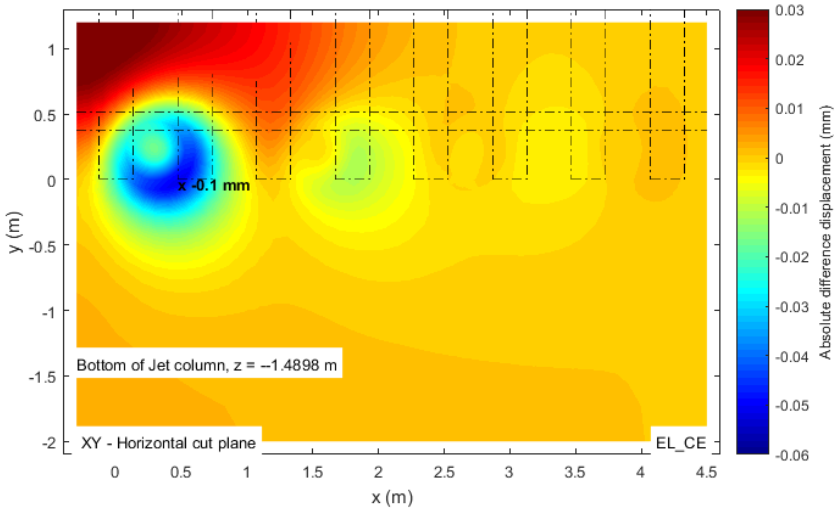

Figure 5.14 -Difference of results of vertical displacement at the base of the Jet column in pattern CE

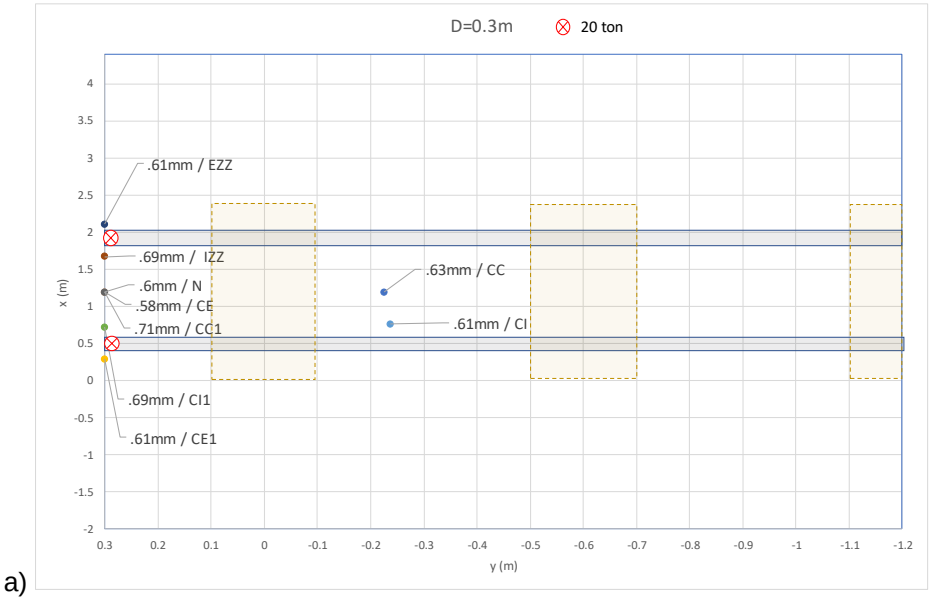

a)

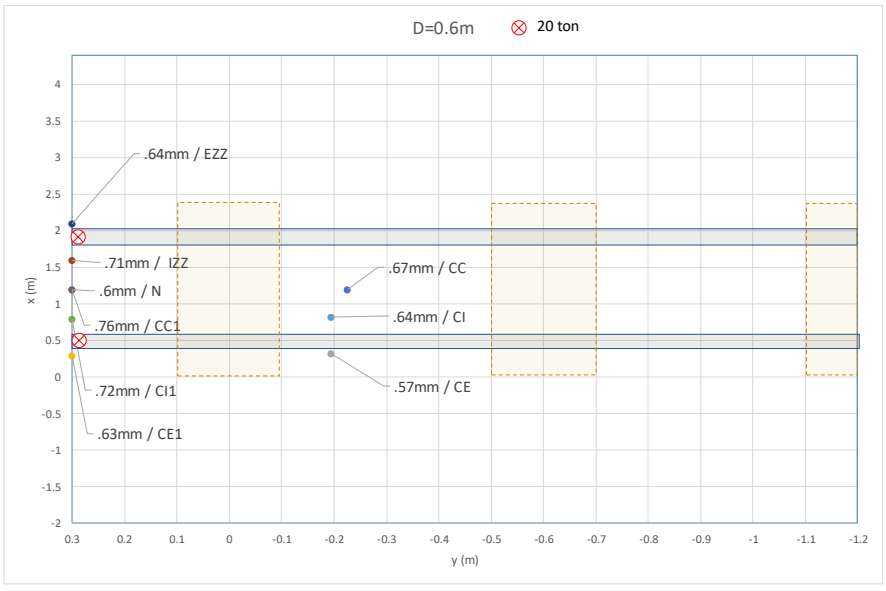

b)

Figure 5.15 - Maximum displacement values and their position for different column patterns and diameters (a) D=0.3m and b) D=0.6m) at a position beneath the Jet-grout column.

5.2.1.1.4 Vertical stresses on top of the ballast layer

Regarding the maximum vertical stress on the top of the ballast layer, for all the layouts modelled, lower stress values are developed with a diameter of 0.6 m, as it would be expected. In this layer, the contour plots showed a higher concentration of stress at the edges of the first sleeper. At the bottom of the ballast layer, most of the models showed that with a larger diameter, a higher concentration of vertical stress would appear in the places where columns are positioned. On top of the foundation, most of the results demonstrated that when the column diameter increases, smaller stress concentrations appear at the column's position. Regarding the stresses developed at a position underneath the Jet column, in general, stresses increase with the column's diameter, at its position.

In resemblance to the vertical displacements analysis, the results for CE will be described in this subchapter and for the other models, results are rendered in the digital annexes.

Analysing the results for vertical stress on top of the ballast layer for model CE, there is a slight reduction in the maximum stress value when a larger diameter is chosen for the Jet column. When loaded, the ballast layer shows higher stresses under the first sleeper, especially at its external edges (see Figure 5.16). This reduction of the maximum stress value when the diameter increases might be related to the load transfer arching effect. The arching effect allows partial load transfer onto the pile as well as reduction of surface settlement (Jenck [et al.], 2009), transferring loads from weaker zones to stiffer ones (see Figure 5.17). By increasing the column's diameter, a larger area of stiffer substructure is created, allowing a larger amount of load to be transferred from the weaker layers, such as the ballast, to the jet column, thus such reduction. However, that reduction was only of 0.8 % compared with the maximum value for D=0.3 m (relative difference between maximum stress results, taking as reference the value for the smallest diameter).

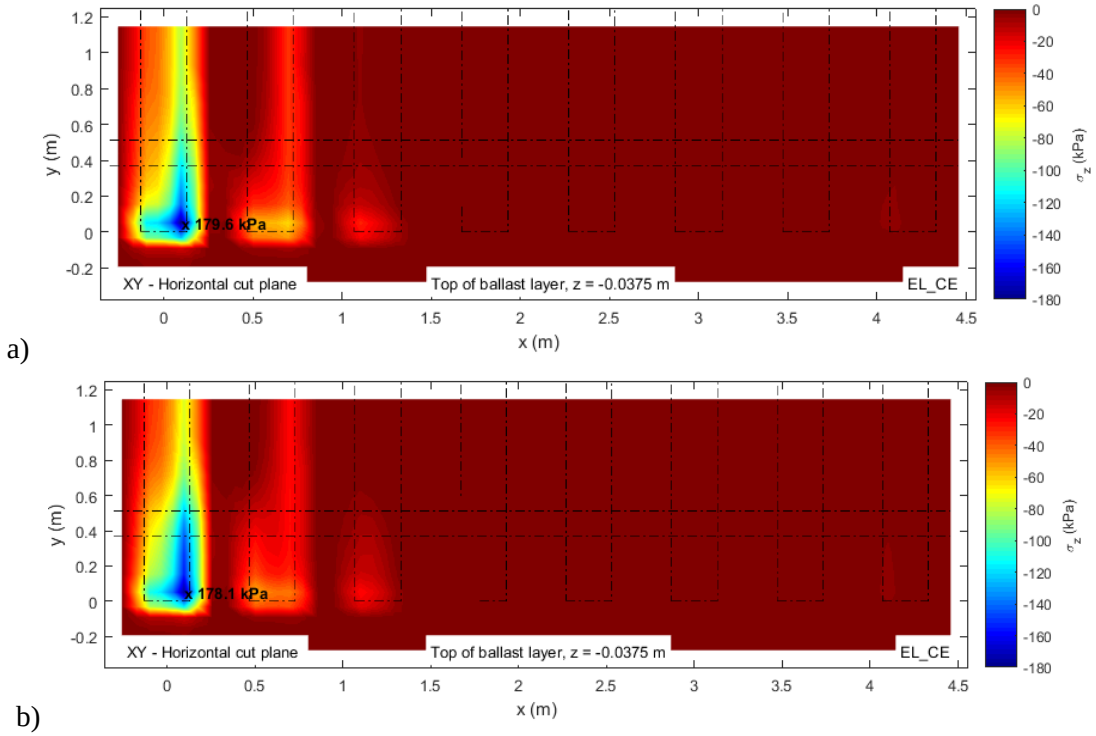

Figure 5.16 - Vertical stress distribution on top of the ballast layer in pattern CE for a diameter of a) 0.3 m and b) 0.6 m

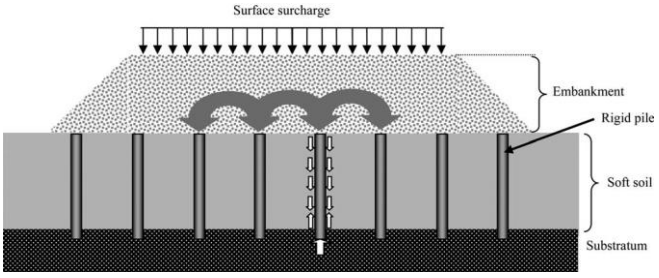

Figure 5.17 - Schematic representation of arching effect principle on a piled embankment (after Jenck [et al.],2009)

On the difference plot in Figure 5.18, it is visible an area beneath the sleeper where the vertical stress is 24.9 kPa higher for the larger diameter relatively to the smaller one. This might be due to the arching effect explained earlier, where larger amounts of stress are being transferred to the column, creating a

concentrated stress path. Regarding the edges of the sleepers, smaller stress concentrations appear with the D=0.6 m. The maximum vertical stress values and the position of those maxima on top of the ballast layer, for different column patterns and column diameters, are presented in Figure 5.19.

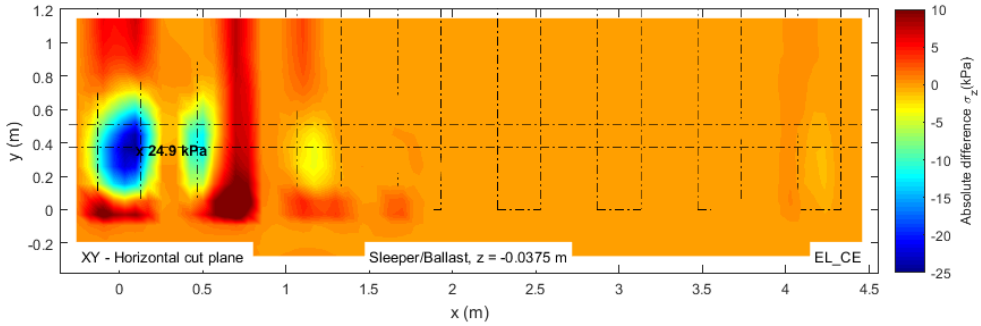

Figure 5.18 - Difference of results of vertical stress distribution on top of the ballast layer between different diameters in pattern CE

a)

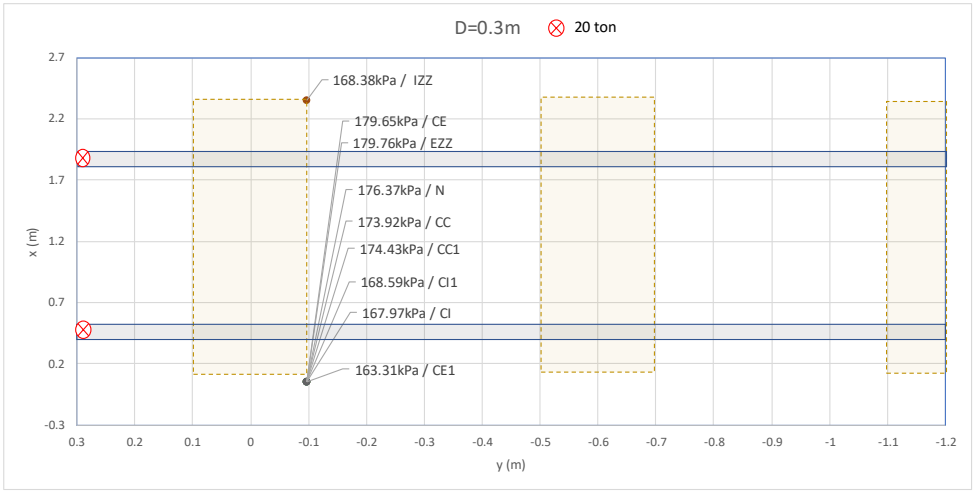

b)

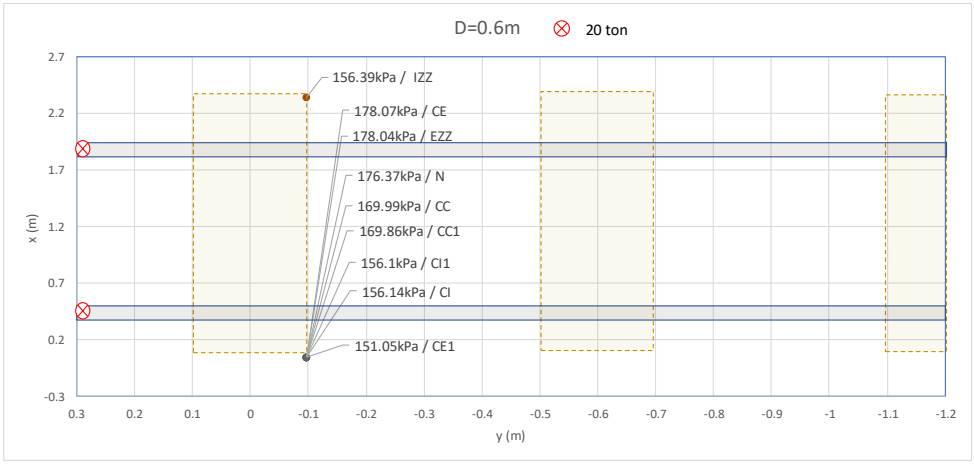

Figure 5.19 - Maximum vertical stress values and their position for different column layouts and diameters (a) D=0.3m and b) D=0.6m) on top of the ballast layer.

5.2.1.1.5 Vertical stresses at the bottom of the ballast layer

When studying the vertical stress that develops at the bottom of the ballast layer, by analysing Figure 5.20, an area of stress concentration is visible at the approximate location of the column closer to the load point. This stress concentration is slightly higher when a larger diameter is modelled for the column. This stress increment might be explained by the arching phenomena, being the column more loaded on the external side under the sleeper, where stresses are higher.

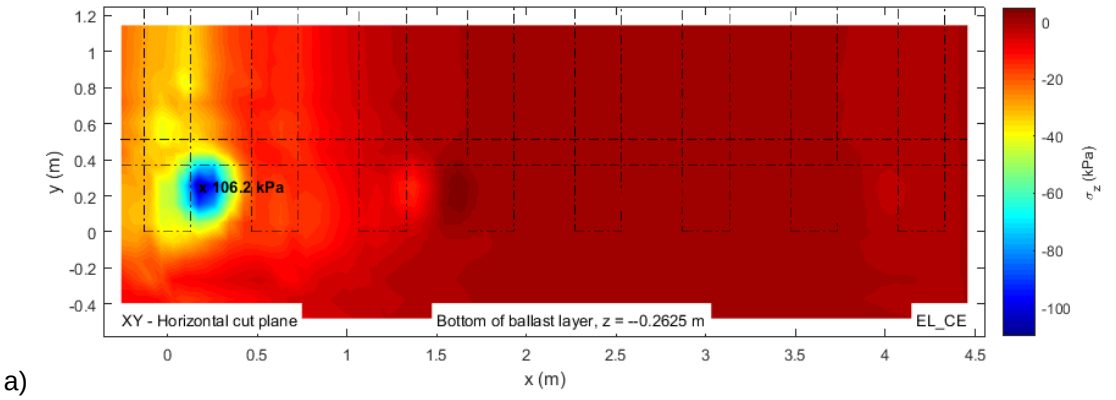

a)

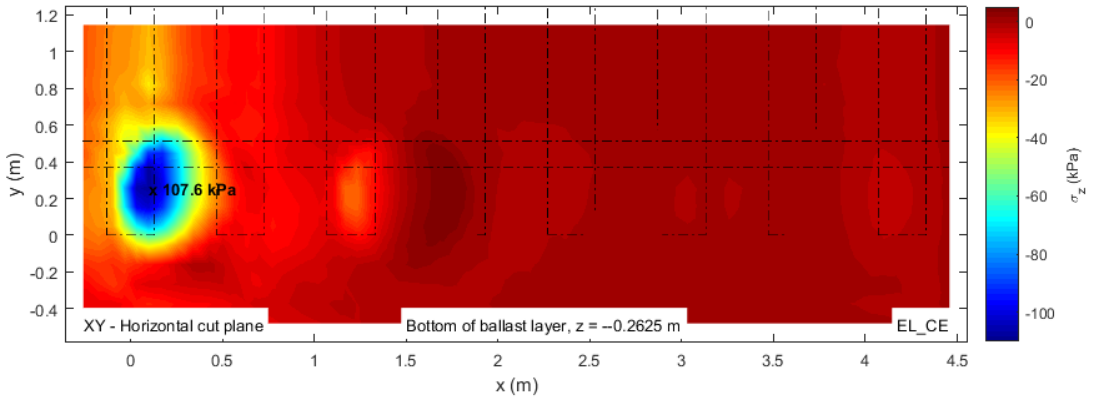

b)

Figure 5.20 - Vertical stress at the bottom of the ballast layer in pattern CE for a diameter of 0.3 m a) and 0.6 m b)

In Figure 5.21, the difference of vertical stress is plotted. It is visible the columns pattern, suggesting that implementing a higher diameter introduces higher stresses on the column's location. Under the first sleeper, there are higher stress levels for D=0.6 m demonstrating that by opting for a larger diameter, part of the column's cross section will be placed under the sleeper and developed stresses under the sleepers will be lead to the column. This is visible in the second sleeper as well, however on a smaller scale since the first sleeper is the most loaded one.

The maximum vertical stress values and the position of those maxima on the bottom of the ballast layer, for different column layouts and column diameters, are presented in Figure 5.22.

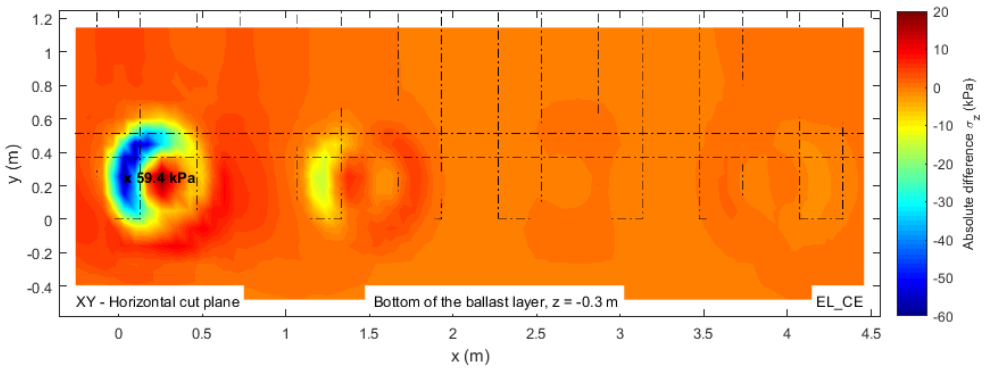

Figure 5.21 - Difference of results of vertical stress distribution at the bottom of the ballast layer for different diameters in pattern CE

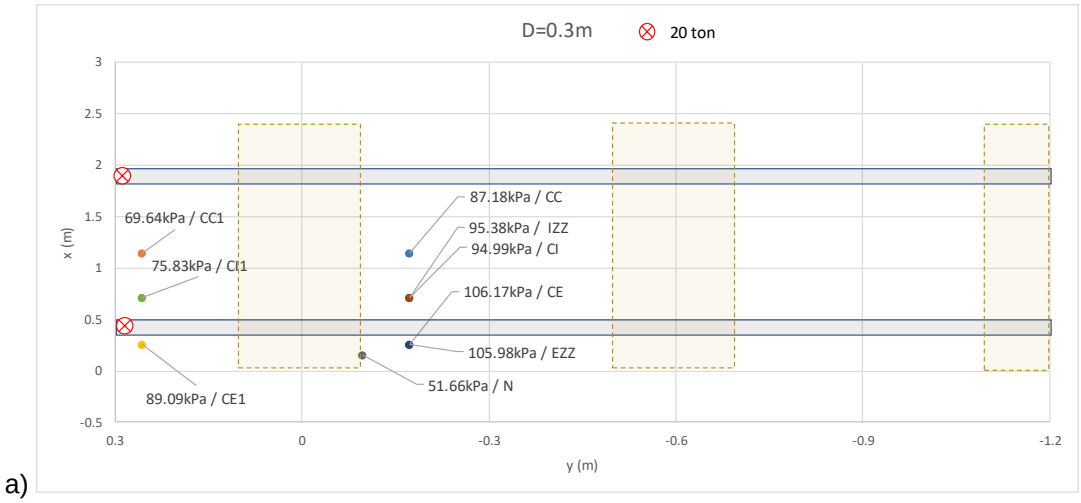

a)

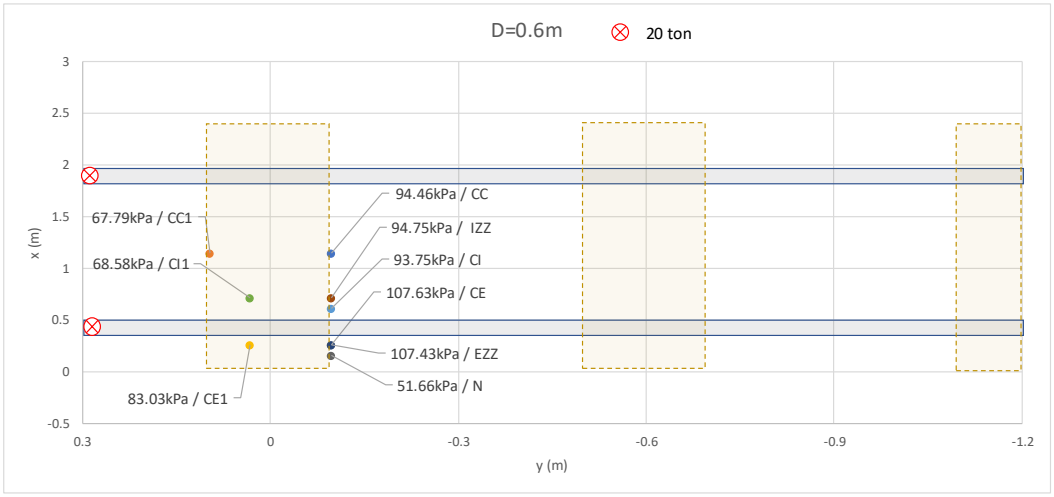

b)

Figure 5.22 - Maximum vertical stress values and their position for different column layouts and diameters (a) D=0.3m and b) D=0.6m) on the bottom of the ballast layer.

5.2.1.1.6 Vertical stresses on top of the foundation

For both diameters, the stress distribution on top of the foundation is shown in Figure 5.23. By comparing Figure 5.23-a) and Figure 5.23-b), it is visible how a column is larger than the other and how stresses spread in each configuration. For the diameter of 0.3 m, a higher stress concentration is visible at the centre of the column, when compared with the larger diameter. This is related to the column's size since, with a larger column diameter, there is a larger area where the stresses can be spread, reducing its value. Since the left side of the D=0.6 m column is placed under the sleeper, where higher stresses occur, it is there where the maximum stress value appears.

Analysing Figure 5.24, the previous statement is confirmed since the larger difference in stress values remains at the column's position. It is visible how at the centre of the first column, stresses are considerably higher for the smaller diameter, around 105 kPa higher. The blue region around the column demonstrates how higher stresses occur under the first sleeper for the larger diameter, in comparison with the smaller one. This difference might have to do with the fact that two regions, one with improved substructure, with a stress value of around 145 kPa, and another without (the external region of the smaller column), with nearly null stresses, are being compared.

The maximum vertical stress values and the position of those maxima on top of the foundation, for different column layouts and column diameters, are presented in Figure 5.25.

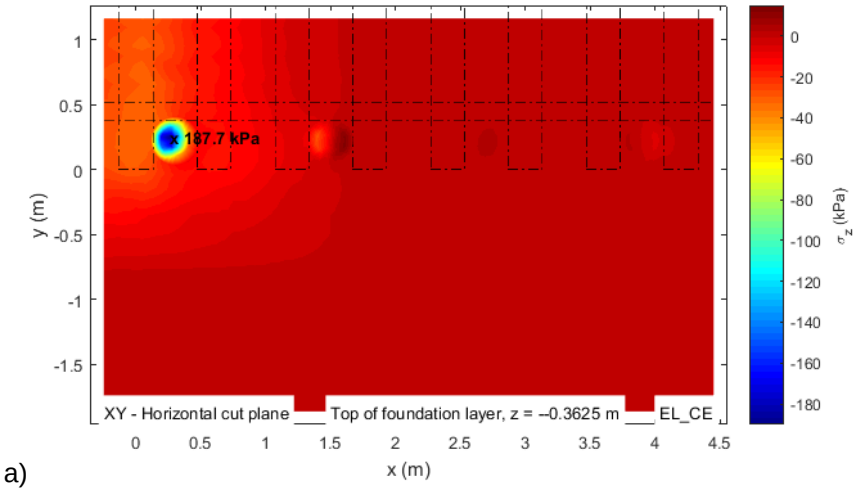

a)

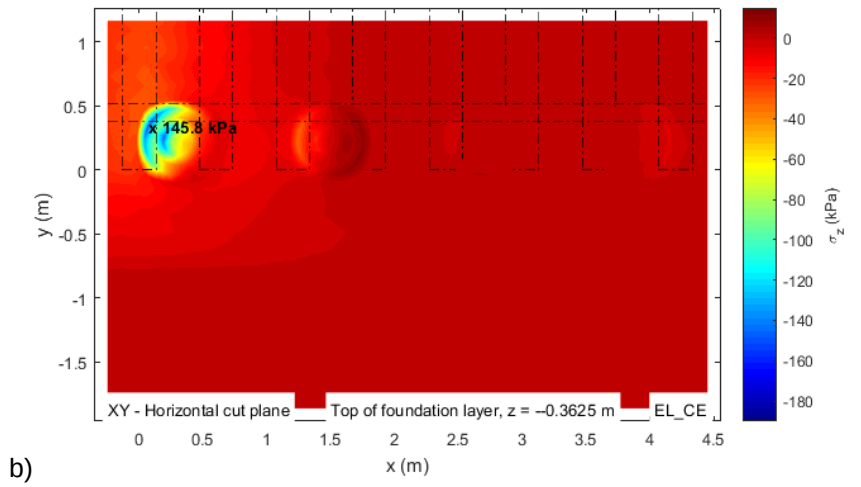

b)

Figure 5.23 - Vertical stress on top of the foundation in pattern CE for a diameter of 0.3 m a) and 0.6 m b)

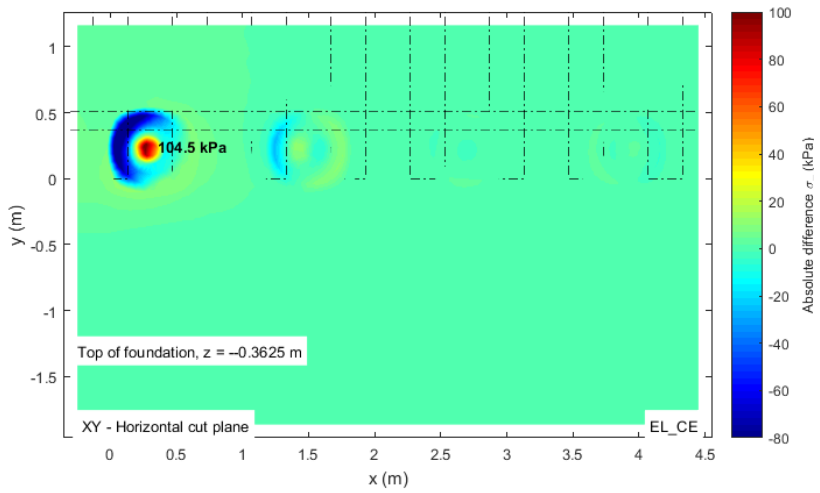

Figure 5.24 - Difference of results of vertical stress distribution on top of the foundation for different diameters in pattern CE

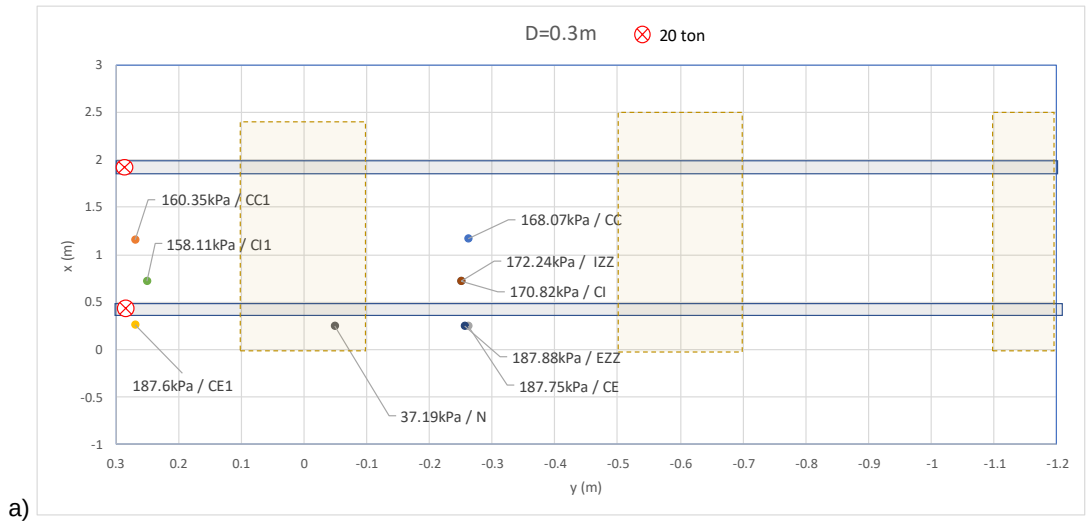

a)

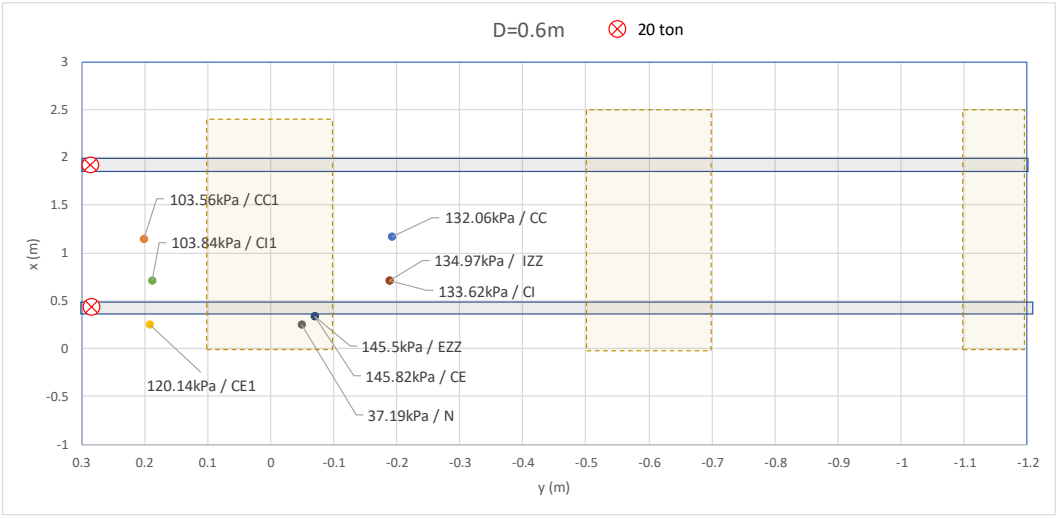

b)

Figure 5.25 - Maximum vertical stress values and their position for different column layouts and diameters (a) D=0.3m and b) D=0.6m) on top of the foundation.

5.2.1.1.7 Vertical stresses under the columns

Concerning the stresses developed at a position underneath the Jet column, the contour plots are presented in Figure 5.26. It is visible a circular region regarding the first column where higher stresses are concentrated. Comparing Figure 5.26 a) and b), with a larger diameter, there are slightly higher stress concentrations at the first column's position. By observing Figure 5.26 two sets of blue circular regions can be seen at the column's position. This horizontal plane cut lets us see a portion of the pressure bulb that is forming underneath the Jet pile. The darker region, placed in the centre of the column, bears higher stress values. This might be due to the property of the interior of the Jet column that was assigned higher stiffness properties Table 4.3, thus bearing higher stresses. Around this darker blue region, there is a halo zone of light blue, meaning the soil is lightly stressed, likely due to the less stiff material assigned to the column's exterior zone. The difference plot between vertical stress values for different diameters, at this depth, is displayed in Figure 5.27.

The maximum vertical stress values and the position of those maxima on top of the foundation, for different column layouts and column diameter, are presented in Figure 5.28. The maximum stress values are positioned, as expected, where columns are positioned. For instance, the CC, CE and CI models present higher stress values between the first two sleepers, because it is where a column was placed.

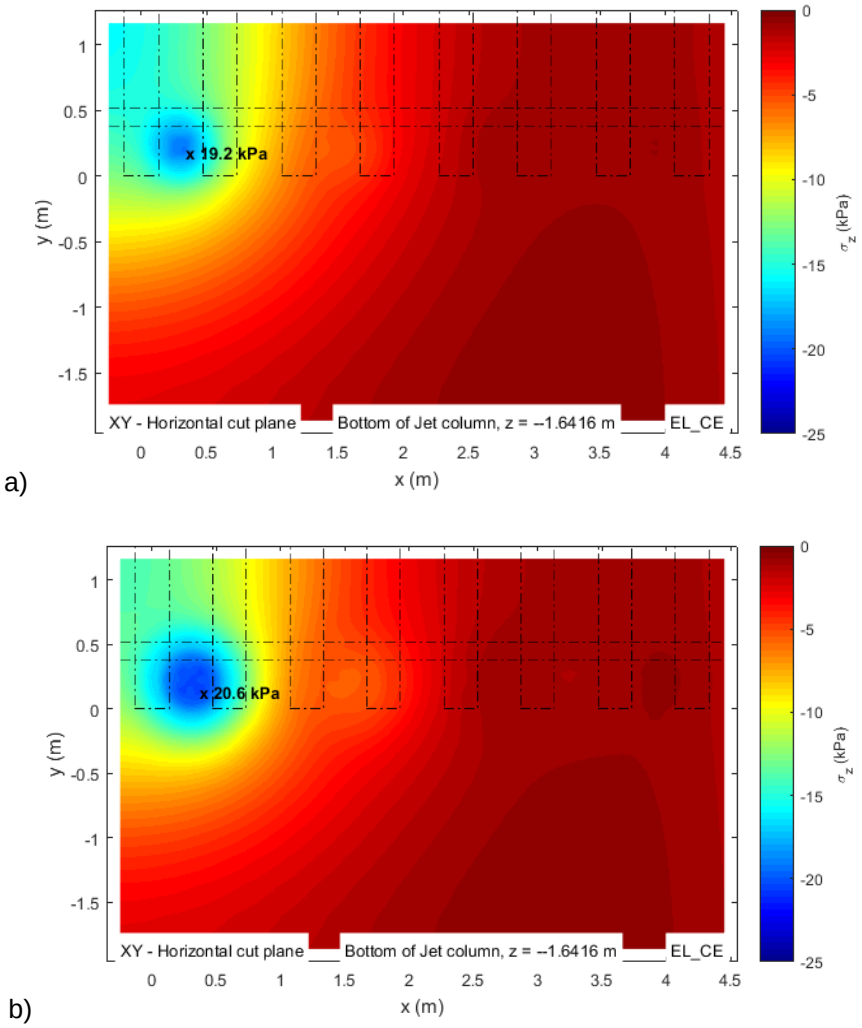

Figure 5.26 - Vertical stress at the bottom of the Jet-grout column in pattern CE for a diameter of 0.3 m a) and 0.6 m b)

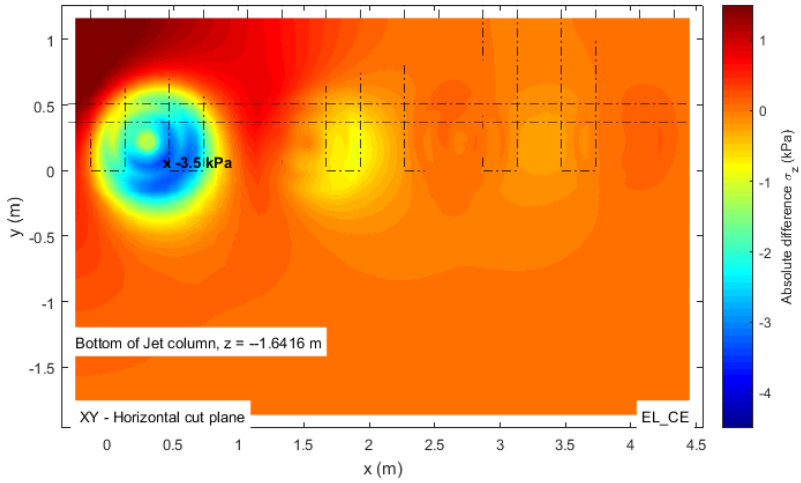

Figure 5.27 - Difference of results of vertical stress distribution at the bottom of the Jet-grout column for different diameters in pattern CE

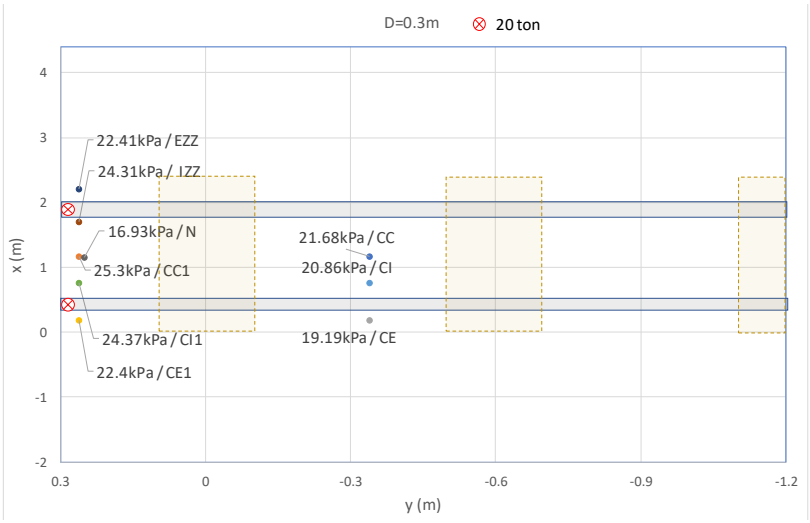

a)

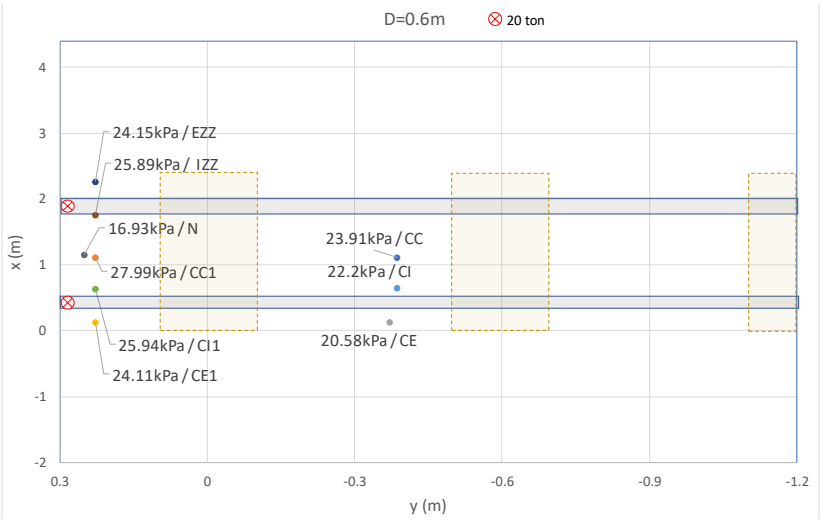

b)

Figure 5.28 - Maximum vertical stress values and their position for different column layouts and diameters (a) D=0.3m and b) D=0.6m) at the bottom of the Jet-grout column.

5.2.1.2 Results at the XZ plane aligned with the rail

5.2.1.2.1 Vertical rail displacements in the longitudinal alignment

The vertical rail displacements in the longitudinal alignment, for column diameters of 0.3 m and 0.6 m, are shown in Figure 5.29 and the maximum rail displacement values are presented Table 5.1. For all model configurations, the increase of the columns radius led to a reduction of the rail's displacement. As expected, the maximum displacement occurs at the position of the point load and decreases as we go further away in the longitudinal direction. For both column diameters, between point load distance of 2.5 m and 3 m, it is observable the typical an upward vertical displacement of the rail.

To analyse the improvement in the rail displacement, the difference of results is presented in Figure 5.30. From all models, the one that showed less improvement with the increase of the column's diameter was the central column pattern, probably because it is the one with the least number of columns per sleeper. Moreover, given that the position of the jet columns in this pattern is in the middle of the span in between sleepers, the improvement obtained from the Jet-gout on the deflection does not encompass the rail since the columns are somewhat far from it and not under the sleepers, not being able to reduce sufficiently the rail's displacement.

The patterns that showed better performance with the diameter's increase were the ones where the columns are placed closer to the rail such as the models CE or CI. The pattern that showed the most improvement by increasing the radius of the column was model CEZZ. As mentioned earlier, by increasing the column's diameter, part of it envelops the surface under the sleepers adjacent to it. This creates a larger support to the sleepers, reducing deflections under it. By implementing a zig-zag pattern and diameter increase, the sleepers support will be improved from both of its edges as explained in Figure 5.31.

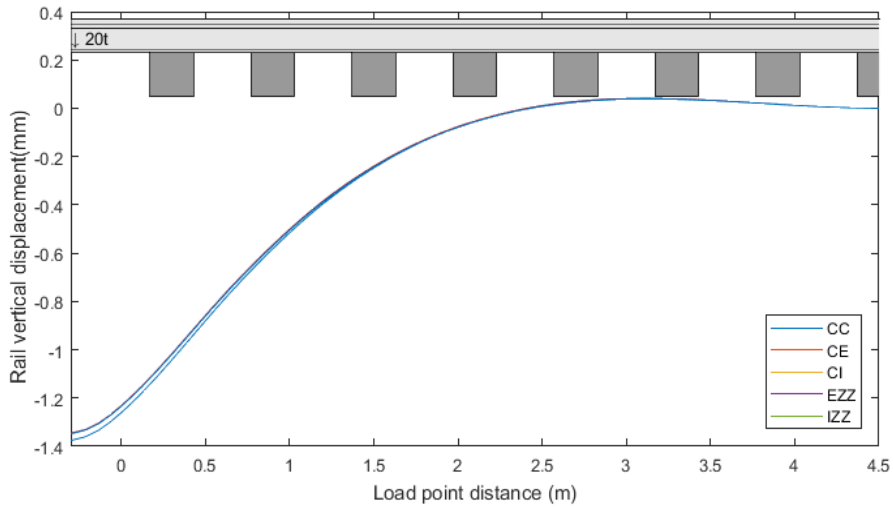

a)

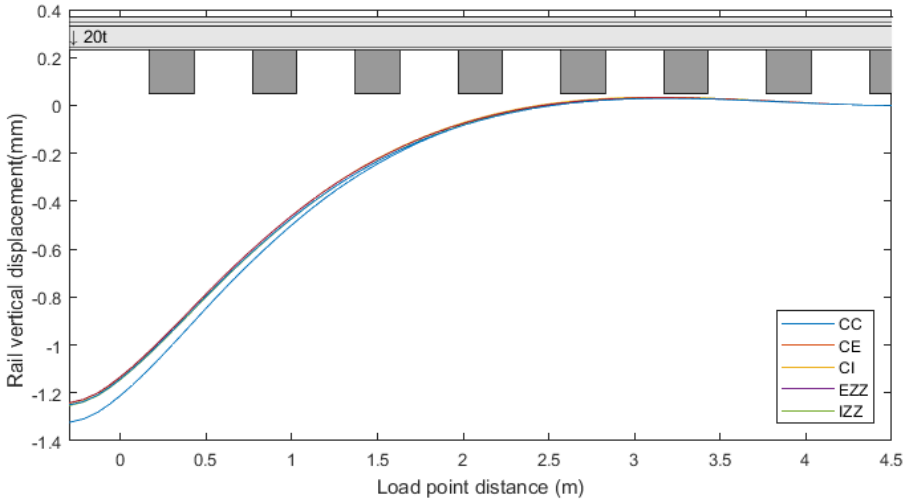

b)

Figure 5.29 -Longitudinal rail displacement for the different models with diameter of a) 0.3 m and b) 0.6 m

Table 5.1 – Maximum rail displacement for different models and diameters

	Diameter	Unit	CC	CC1	CE	CE1	CI	CI1	CEZZ	CIZZ	N
Rail displacement	0.3 m	mm	1.38	1.38	1.35	1.35	1.35	1.35	1.35	1.35	1.41
	0.6 m		1.32	1.33	1.24	1.24	1.25	1.26	1.24	1.25	1.41

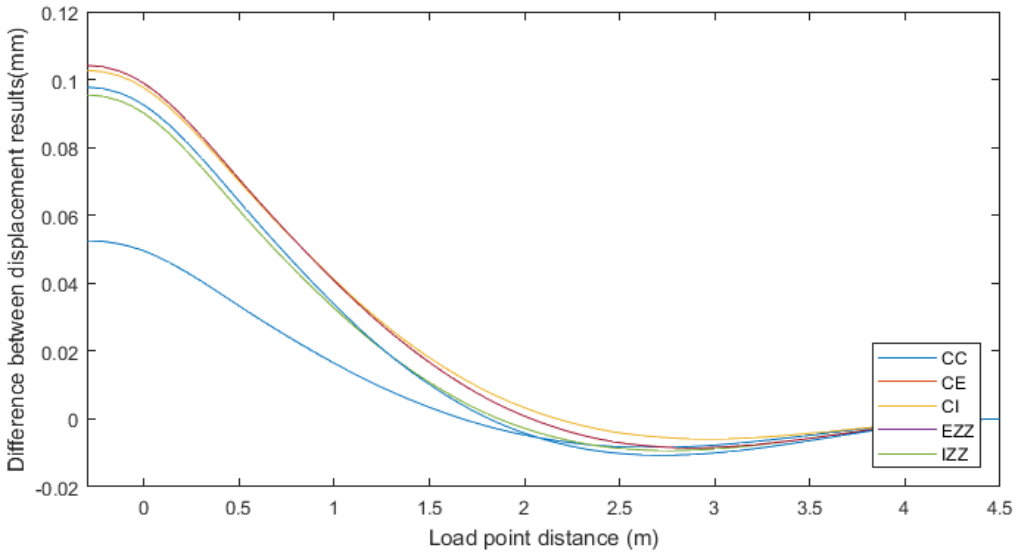

Figure 5.30 - Difference plot between different diameters for results of longitudinal rail displacement

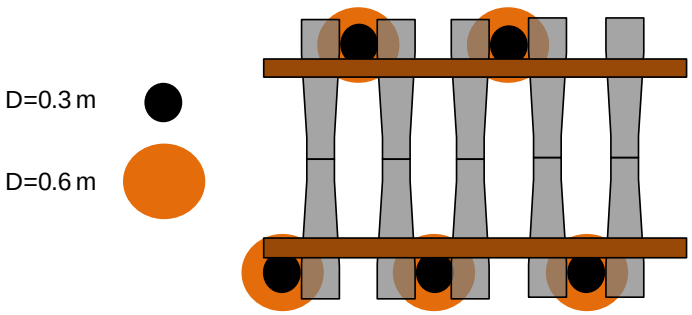

Figure 5.31 - Column's diameter area of influence in model CEZZ

5.2.1.2.2 Vertical stresses under the rail alignment

The vertical stress distribution with depth under the rail for both diameters modelled is shown in Figure 5.32. It is visible, for both diameters, a zone of higher stresses under the first sleeper on the ballast layer. By increasing the diameter, the load path from the bottom of the sleepers to the jet column becomes visible, being the right side of the column more loaded. For a smaller diameter, this stress path is not visible, since the queried zones do not cross column zones, as explained earlier (see Figure 5.3 for queried zones for the D=0.6 m). It is possible that with a larger radius, the train load is being more effectively transferred to the column since it has a larger area.

The difference plot in Figure 5.33 clearly shows higher stress concentrations on the columns positions when a larger diameter is chosen, in comparison with D=0.3 m, existing nearly 100 kPa higher stresses on the left side of the columns when diameter 0.6 m is modelled.

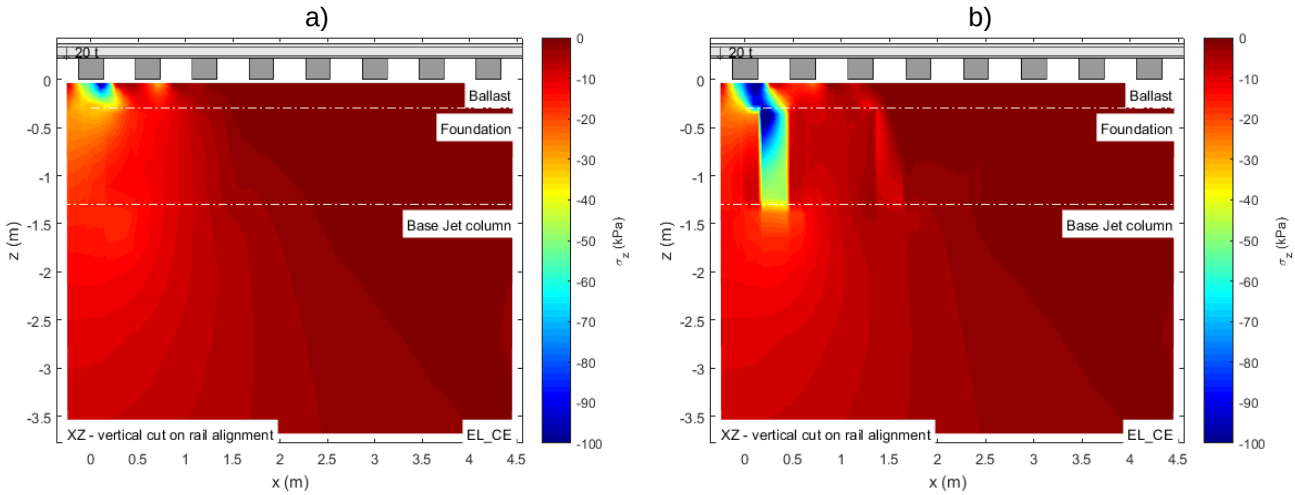

Figure 5.32 - Vertical stress distribution with depth under the rail, in pattern CE, for diameter a) 0.3 m and b) 0.6 m

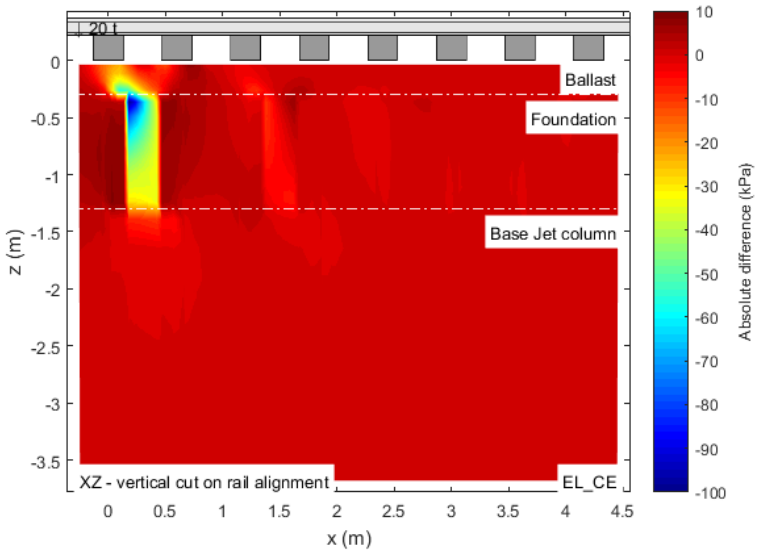

Figure 5.33 - Difference of vertical stress distribution with depth under the rail between different diameters in pattern CE

5.2.1.2.3 Vertical displacements under the rail alignment

Analysing Figure 5.34, with a larger diameter there is a reduction of the vertical deflections underneath the first sleeper. In Figure 5.34-b) a larger area with a displacement of around 0.7 mm appears on the position of the column suggesting that a differential settlement of the column might be occurring, as was suggested in the horizontal plane analysis of a depth just beneath the Jet-grout column. Berthelot [et al.] (2003) explains how this mechanism functions saying that in the upper portion surrounding the column, the softer soil has a larger deflection than the pile, creating negative skin friction that increases the load transferred onto the pile. At the lower part, as the pile strikes the substratum, it settles more than the softer soil, leading to positive skin friction and development of tip resistance.

In Figure 5.35, the previous remarks are validated when analysing the plot of difference.

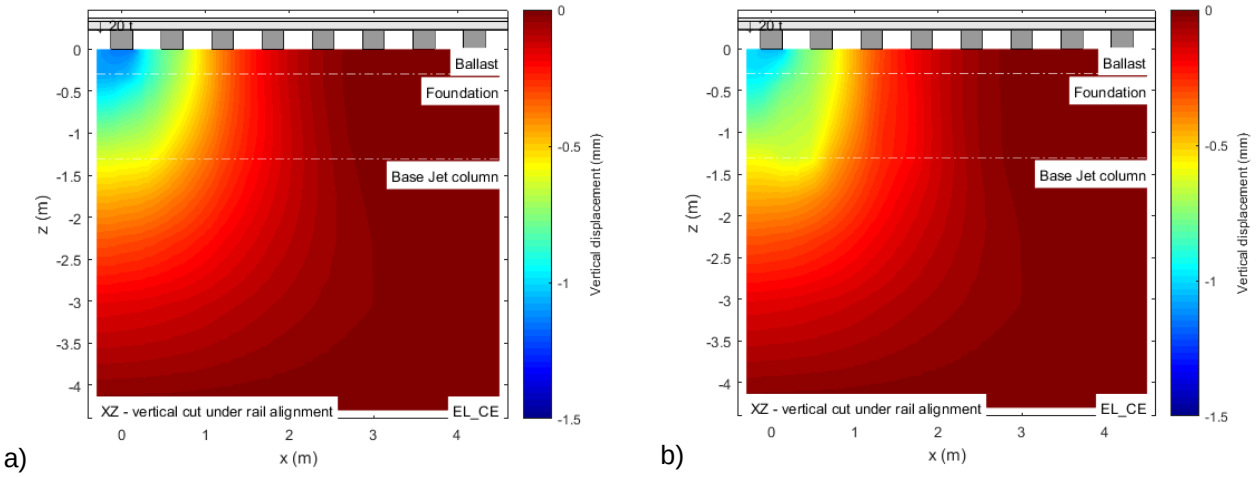

Figure 5.34 - Vertical displacement distribution with depth under the rail, in pattern CE, for diameter a) 0.3 m and b) 0.6 m

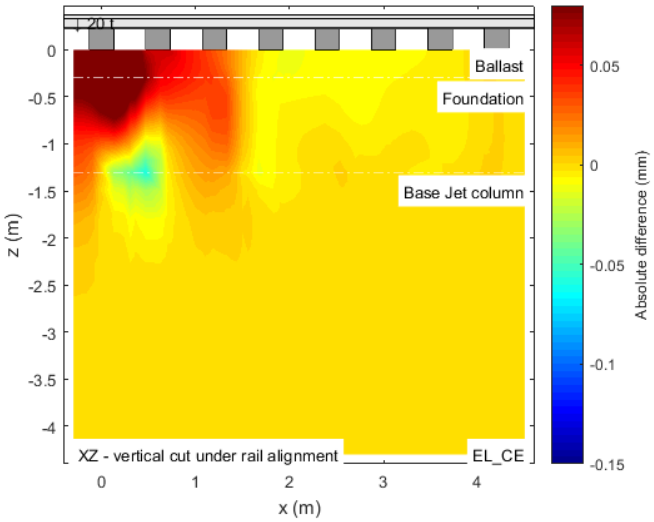

Figure 5.35 - Difference of vertical displacement distribution with depth under the rail between different diameters in pattern CE

5.2.2 REINFORCED SUBSTRUCTURE VS NO REINFORCEMENT

In this analysis, five different patterns of column layout were considered: CC, CE, CI, CEZZ and CIZZ (see Figure 5.36). These different configurations were compared with a model where the foundation had no reinforcement, being composed totally of soft soil. For the zig-zag models, due to their single symmetry, the analysis focused only on one-half of the model, from y = 1.2 m to y = -2 m, to become comparable with N model.

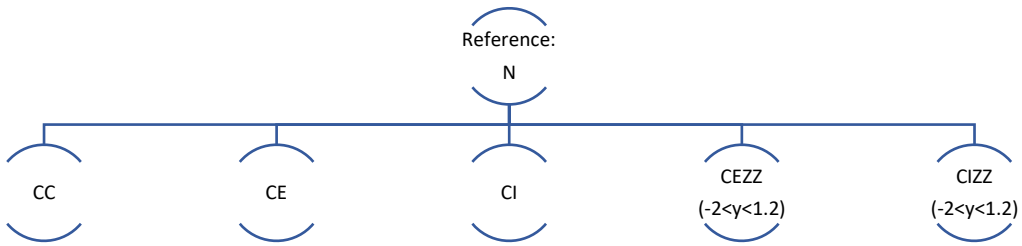

Figure 5.36 – Scheme of comparison established between reinforced substructures and no reinforcement

5.2.2.1 Vertical stresses and vertical displacements at the XY planes

An analysis of the displacements results showed that, in general, with an improved substructure, slightly smaller displacements are obtained at the top of the ballast and foundation. At the bottom of the columns, displacements of the improved substructure at that level are roughly higher than the simple non-improved model. Seeing that these observations are valid for all configurations, the results for the CE pattern will be presented in this subchapter. For the other models, results are presented in the digital annexes.

Concerning vertical displacements on top of the ballast layer, we can perform a comparison between Figure 5.7 a) and b), and Figure 5.37. With a larger column diameter of improved substructure, displacements reduce more efficiently than with the smaller diameter. This is evident when analysing the difference plot in Figure 5.38, with reference the results for model N. All plots of difference were calculated with this same reference. By applying substructure improvement, deflections undergo a stronger reduction under the first sleeper and on the ballast right above the column. This might be due to the presence of a stiffer substructure due to the column. This enhancement extends till the third sleeper, reducing the improvement obtained as we increase the distance from the axle load. Despite this, the maximum deflection underwent by the simple model is not reduced substantially with the substructure improvement, regardless of the diameter chosen.

The previous conclusions can be applied for the displacements analysis on the top of the foundation. By examining Figure 5.10 a) and b), and Figure 5.39, it is observable how displacements reduce at the columns' positions, due to its stiffer nature. Figure 5.40 presents the difference plots for both column diameters. For a wider diameter, a larger area of improvement of the displacement value at the column's position is obtained. However, the improvement achieved by implementing Jet-columns is not that significant, achieving a maximum reduction of only about 0.14 mm, for the greater diameter.

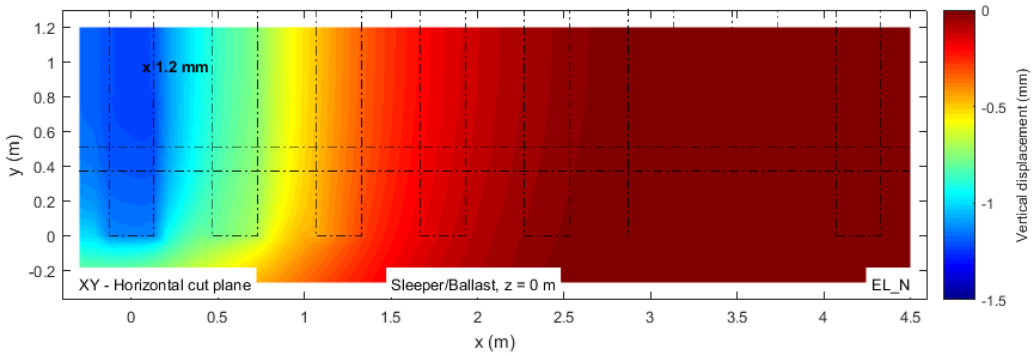

Figure 5.37 - Vertical displacement distribution on top of the ballast layer in pattern N

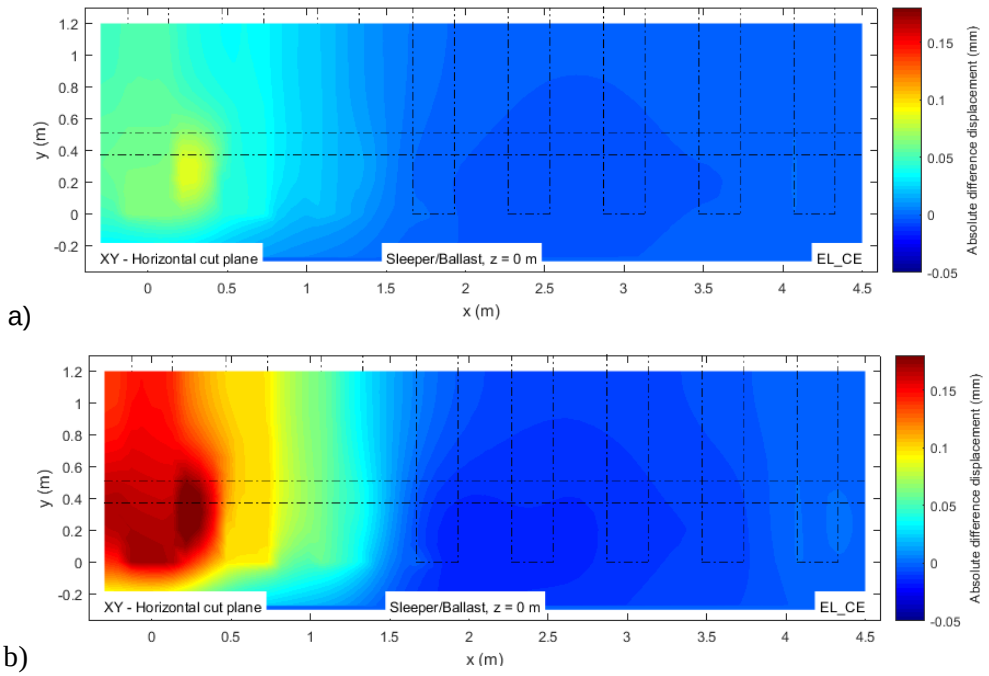

Figure 5.38 - Difference of vertical displacement distribution on top of the ballast layer between models CE and N, for a) D=0.3 m and b) D=0.6 m

At a depth just beneath the Jet-columns, vertical deflection results are higher at the columns' positions for the improved substructure models. This fact is not so evident when comparing singly Figure 5.13 and Figure 5.41, but by analysing the difference plots in Figure 5.42, this remark becomes clear. However, this difference between displacement results is not so big (the maximum difference is of around 0.1 mm higher, for D= 0.6 m). In the middle of the sleepers, in between rails, displacements reduce in this region when the substructure is improved. These occurrences are more noticeable when having a larger diameter.

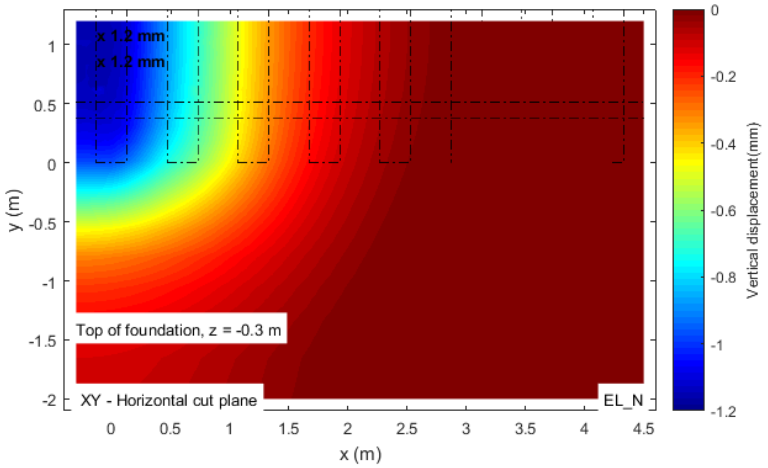

Figure 5.39 - Vertical displacement on top of foundation in pattern N

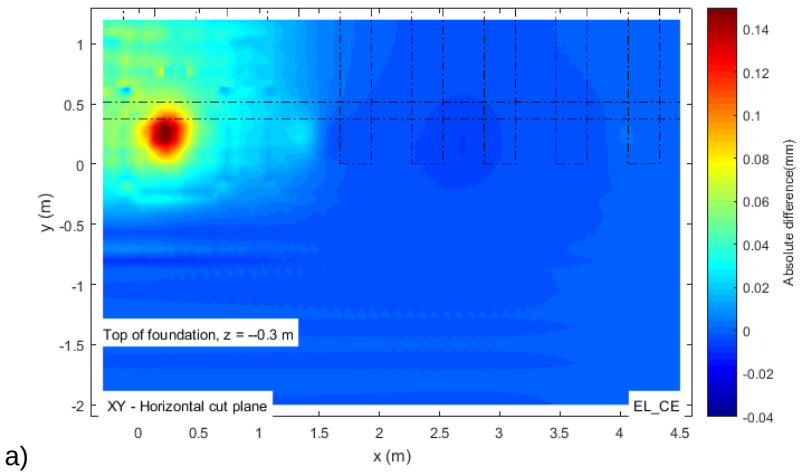

a)

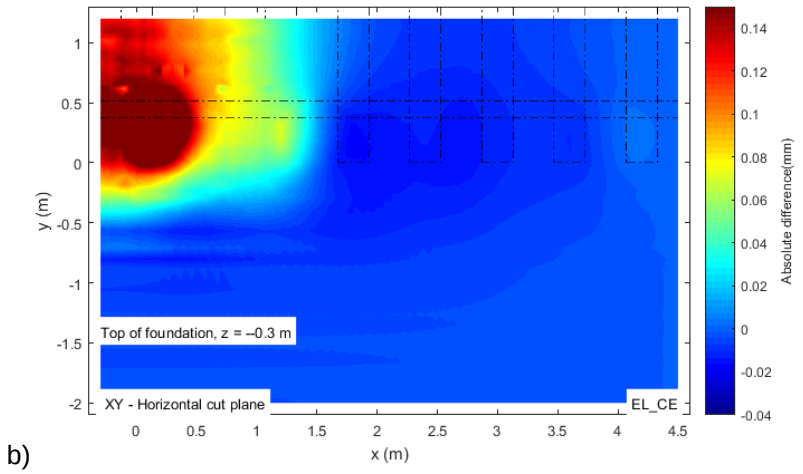

b)

Figure 5.40 - Difference of vertical displacement distribution on top of the foundation between models CE and N, for a) D=0.3 m and b) D=0.6 m

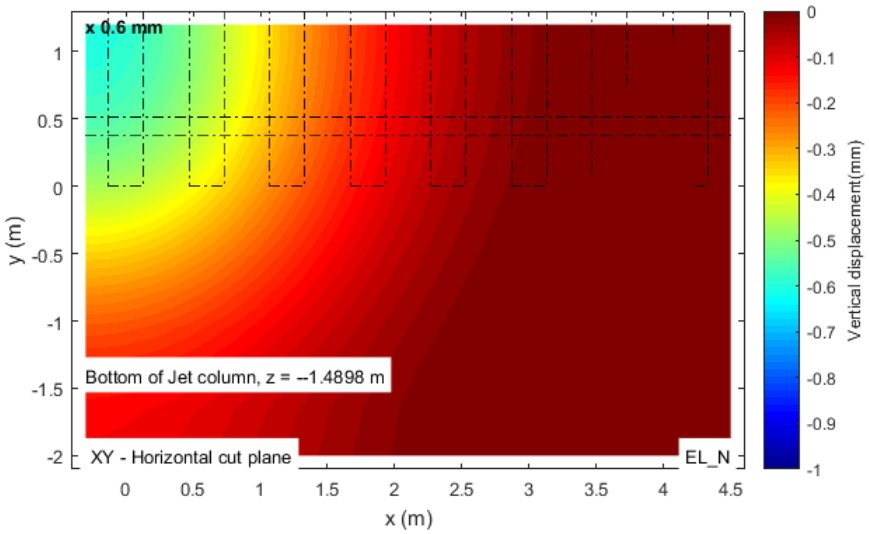

Figure 5.41 - Vertical displacement at the bottom of Jet column in pattern N

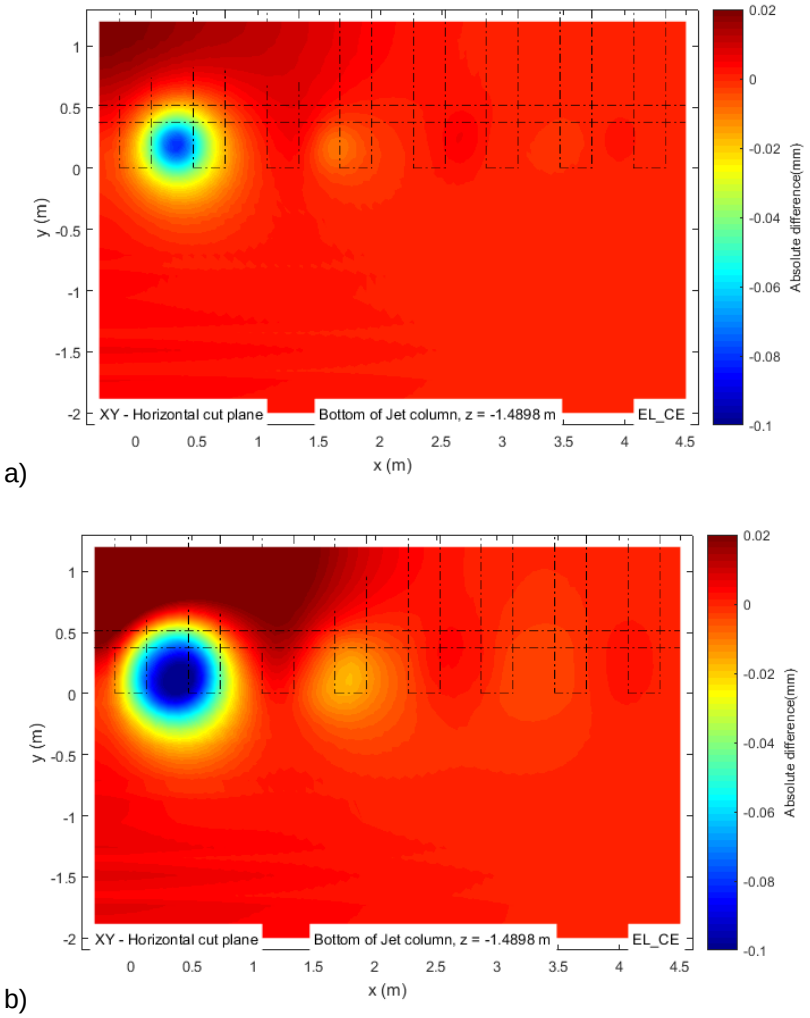

Figure 5.42 - Difference of vertical displacement distribution at the bottom of the Jet-grout column between models CE and N, for a) D=0.3 m and b) D=0.6 m

Concerning vertical stresses, the conclusions obtained from one model are generally valid for the others, thus only the results for CE will be described in this subchapter and for the other models, results are presented in the digital annexes.

The contour plot of vertical stress on top of the ballast layer, for model N, is presented in Figure 5.43. By comparing Figure 5.43 with Figure 5.16, it is noticeable that the maximum stress value for the improved substructure models is higher than the maximum value for the simple model, independently of the diameter chosen for the column improvement. A curious observation is the fact that the maximum stress value obtained for the models with columns positioned interiorly relatively to the rail (CC, CI and CIZZ) is smaller than the maximum stress value of the model without improvement. The opposite occurs for the model CE and CEZZ. This only happens for the maximum stress value. By analysing the difference plot in Figure 5.44, when a column pattern is placed externally to the rail, we can observe that there is a slight stress reduction at the edges and middle of the first sleepers, in comparison to the stresses developed in a model without substructure improvement.

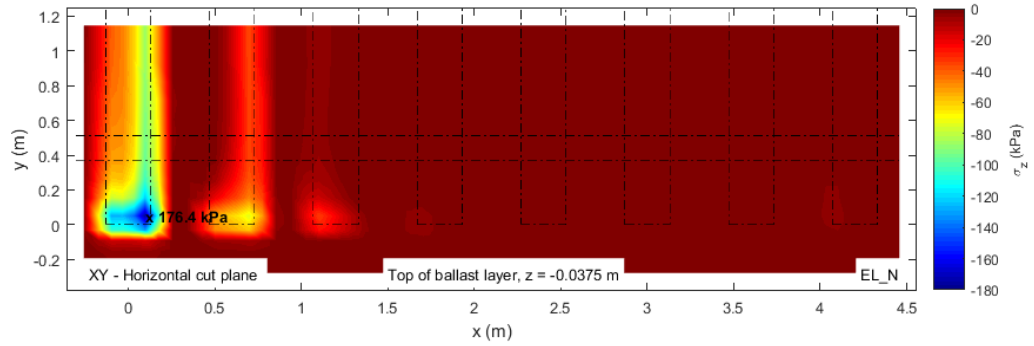

Figure 5.43 - Vertical stress distribution on top of the ballast layer in pattern N.

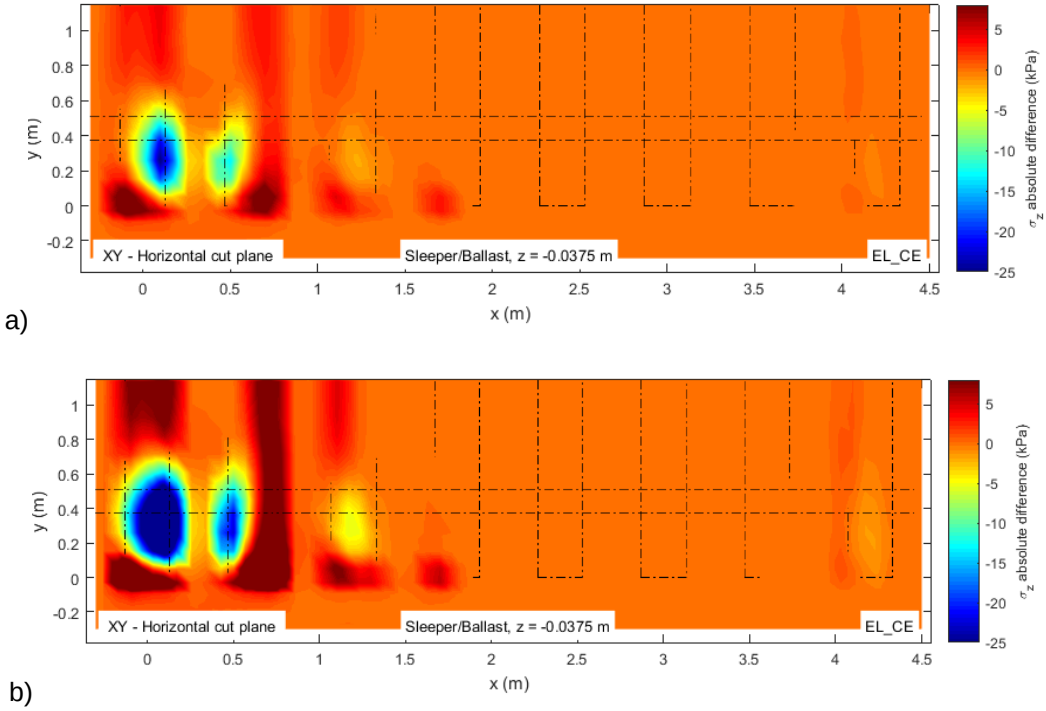

Figure 5.44 - Difference of vertical stress distribution at the top of the ballast layer between models CE and N, for a) D=0.3 m and b) D=0.6 m

On the other hand, at the positions where a column is placed, higher stresses develop for the CE model, possibly meaning that due to the presence of the stiffer substructure, stresses are being directed into that region, a mechanism that does not happen for the simple model. In Figure 5.44, the circular region has a centre zone clearly more stressed than the surrounding. This may be due to the stiffer central zone of the jet column that undergoes higher stresses, as mentioned before, due to the arching effect. With a larger diameter, these observations are more evident.

The contour plot of vertical stress for model N, at the bottom of the ballast layer, is shown in Figure 5.45, where we can see that the higher stress concentration occurs near the edge of the first sleeper. Comparing this figure with Figure 5.20, by the difference plots in Figure 5.46 it is visible that higher stresses are concentrating at the columns' positions (around 60 kPa higher) and that the stresses throughout the rest of the foundation are practically the same for models with improvement or without.

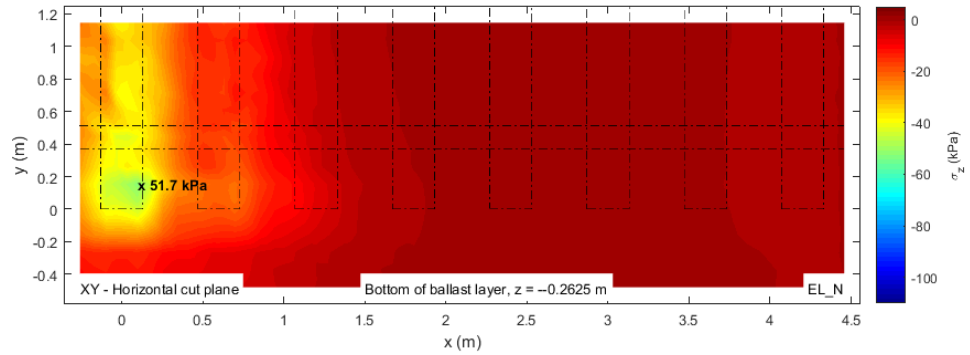

Figure 5.45 - Vertical stress distribution on bottom of the ballast layer in pattern N

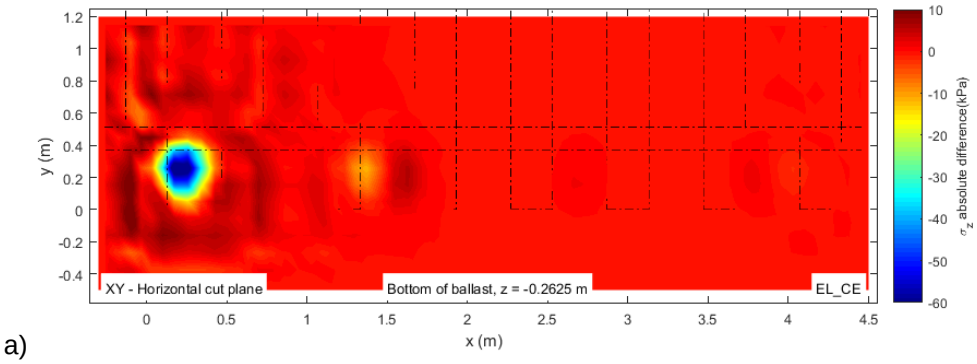

a)

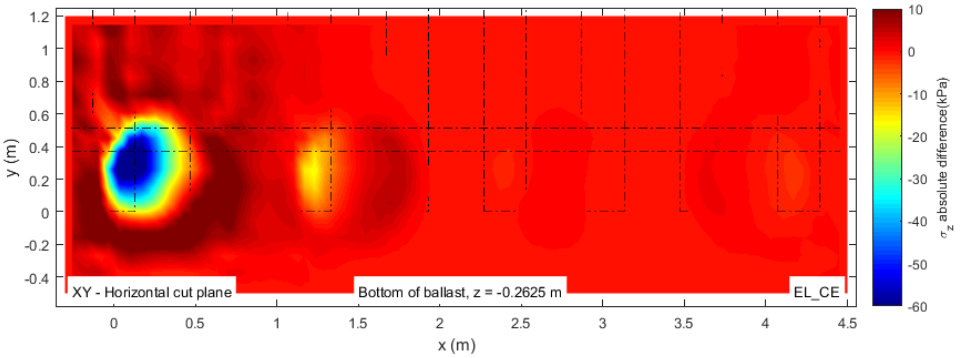

b)

Figure 5.46 - Difference of vertical stress distribution on bottom of the ballast layer between models CE and N, for a) D=0.3 m and b) D=0.6 m

Analysing the stresses developed on top of the foundation, by implementing Jet-grout columns, we can observe that higher stresses develop in specific locations in comparison to model N (see Figure 5.47 and Figure 5.23). In Figure 5.48, it is visible that throughout this layer, stress values maintained practically the same, with the exception at the positions where Jet-grout columns were placed. This might be the result of a load path that has appeared, directing the load to stiffer zones where columns are placed.

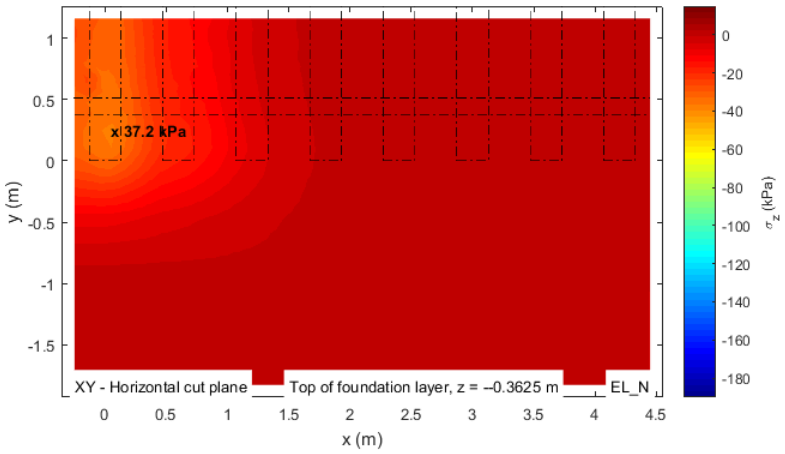

Figure 5.47 - Vertical stress distribution on top of the foundation in pattern N

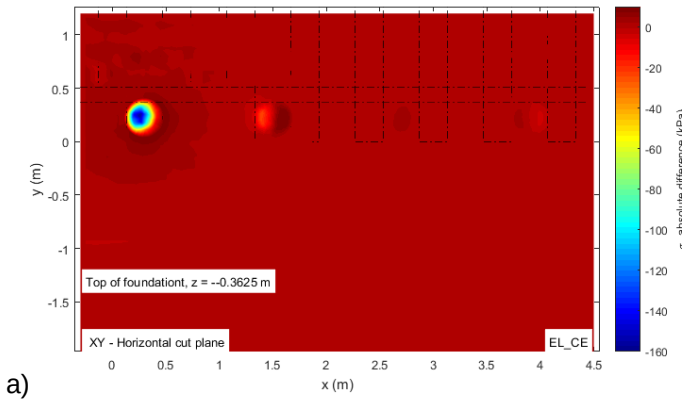

a)

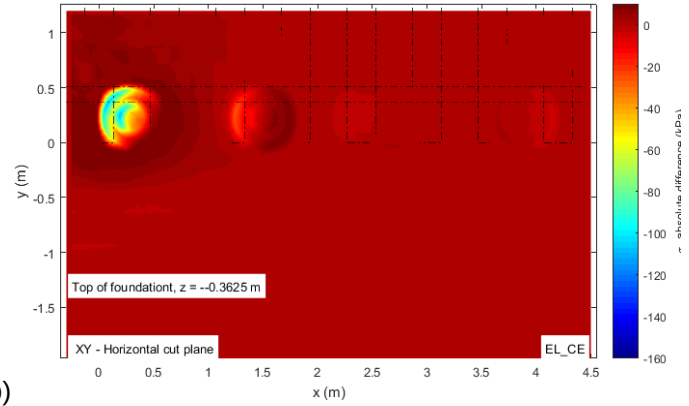

b)

Figure 5.48 - Difference of vertical stress distribution on the top of the foundation between models CE and N, for a) D=0.3 m and b) D=0.6 m

The vertical stress distribution underneath the Jet-grout columns in the pattern N is presented in Figure 5.49. By comparing this figure with Figure 5.26, we can see differences in the stress contours, appearing certain circular regions, when the substructure is improved, which may represent the pressure bulbs that develop beneath the column. The difference plot in Figure 5.50 clearly evidences the previous statement, being visible that a larger column diameter originates a larger pressure bulb.

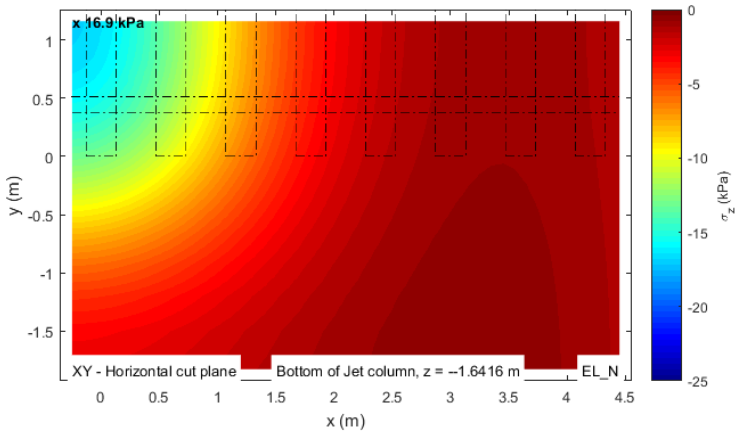

Figure 5.49 - Vertical stress distribution at a depth underneath the Jet-grout column in pattern N

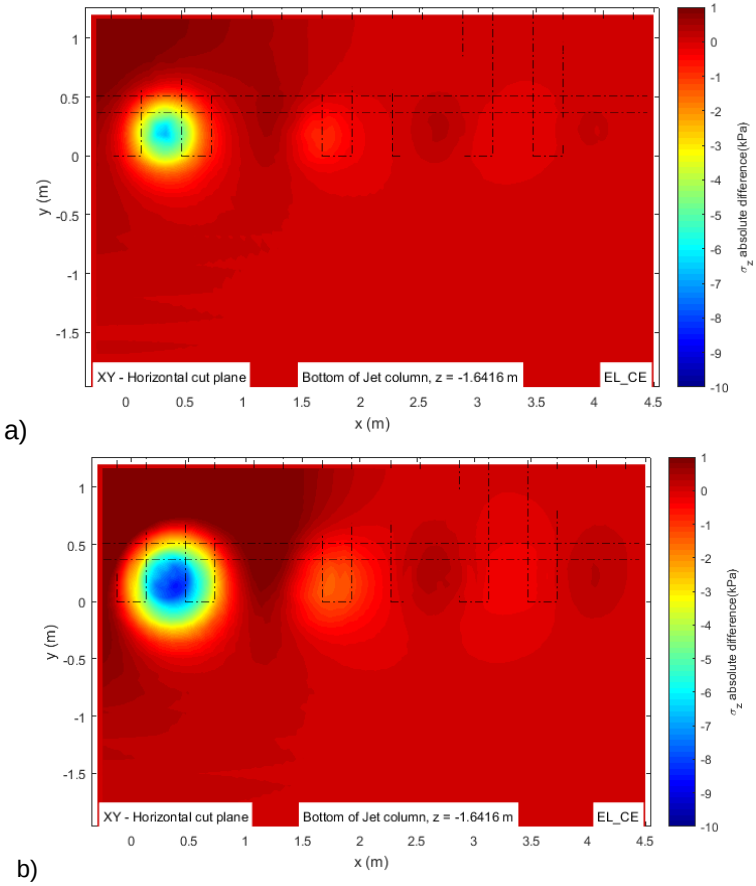

Figure 5.50 - Difference of vertical stress distribution at a depth underneath the Jet-grout column between models CE and N, for a) D=0.3 m and b) D=0.6 m

5.2.2.2 Vertical stresses and vertical displacements at the XZ plane aligned with the rail

Regarding the rail's vertical displacements in the longitudinal alignment, by implementing the Jet-grout columns, smaller rail displacements were obtained for all models. The model CEZZ was the one that showed better performance, slightly reducing the maximum deflection registered for model N (see Figure 5.51) by 0.16 mm (see Figure 5.52), for a larger diameter. The models that have columns closer

to the rail demonstrate better results, as mentioned in the previous analysis for the diameter comparison (see Figure 5.31)

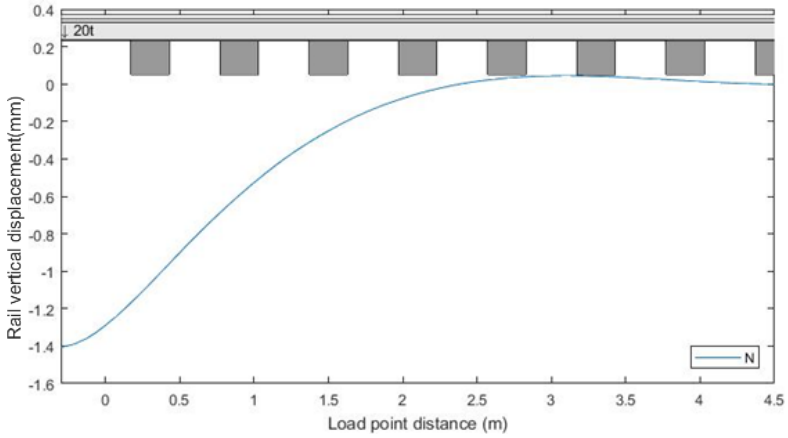

Figure 5.51 - Longitudinal rail displacement for the model N

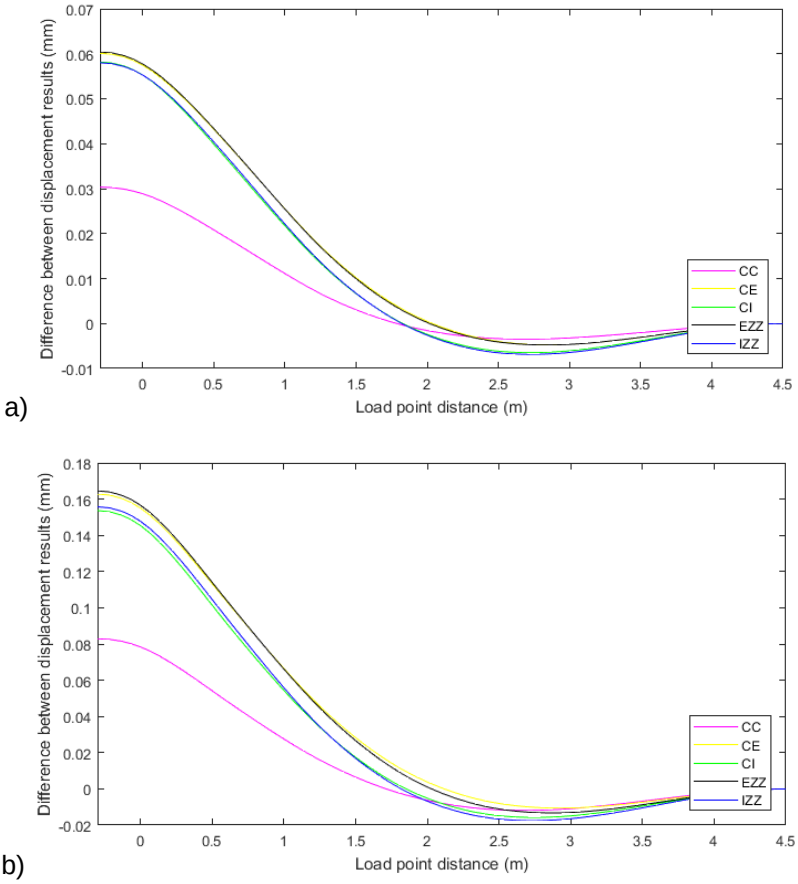

Figure 5.52 - Difference plot between models with substructure improvement and model without improvement, for results of longitudinal rail displacement, for a) D=0.3 m and b) D=0.6 m

The vertical stress distribution with depth for model N is shown in Figure 5.53. It is visible a zone of higher stress concentration on the ballast layer, under the first sleeper (which is the most loaded). Through the installation of a Jet-grout column in the foundation, when the model is loaded, a stress path from the base of the sleepers to the column is created, being the right side of the column, which is closest to the first sleeper, more loaded (see Figure 5.32-b)). With the presence of such columns, the stresses

being developed by the train load, instead of spreading in depth over the foundation, are being concentrated in limited zones of stiffer nature.

The difference plot in Figure 5.54 clearly shows higher stress concentrations at the column positions, yielding around 50 kPa higher stresses at the foundation, when a larger column is placed. It may seem that a larger diameter has higher stress concentrations, however, the difference between Figure 5.54-a) and Figure 5.54-b) may result from selected queried zones, as mentioned before.

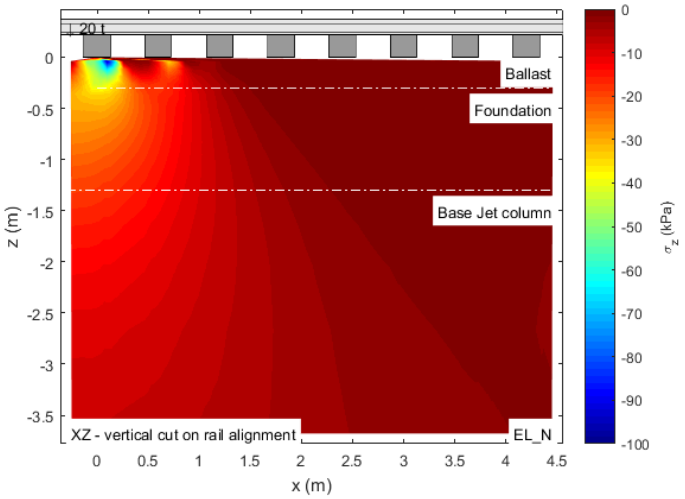

Figure 5.53 – Vertical stress distribution with depth under the rail, in pattern N

a) b)

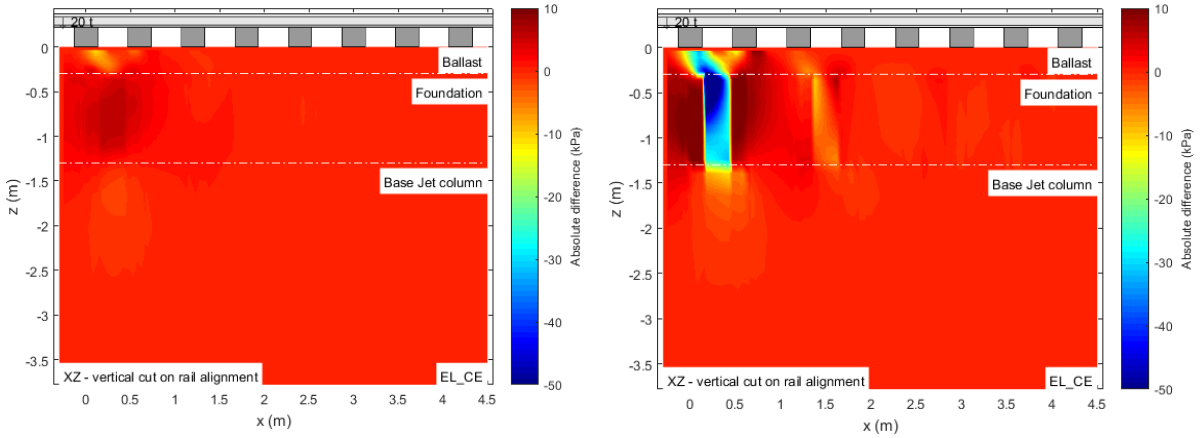

Figure 5.54 - Difference of vertical stress distribution with depth under the rail, between models CE and N, for a) D=0.3 m and b) D=0.6 m

Analysing Figure 5.55, concerning the vertical displacements with depth for model N, it is observable a larger displacements zone underneath the first sleeper and how displacements decrease with depth. To determine the magnitude of deflection reduction obtained by implementing this ground improvement technique, in Figure 5.56 the plot of difference of results is presented. By improving the substructure, deflections under the first sleeper are reduced but only to a very low extent (around 1.00 to 0.08 mm). Underneath the position of the Jet-grout column, a zone of higher displacements appears. This could suggest that the column is settling more than the surrounding soil. These observations become more evident and have a higher representation when a larger diameter is chosen for the column.

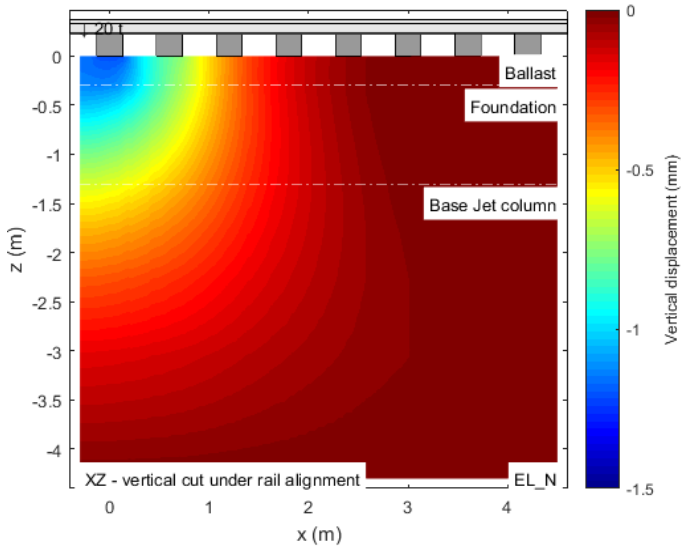

Figure 5.55 - Vertical displacement distribution with depth under the rail, in pattern N

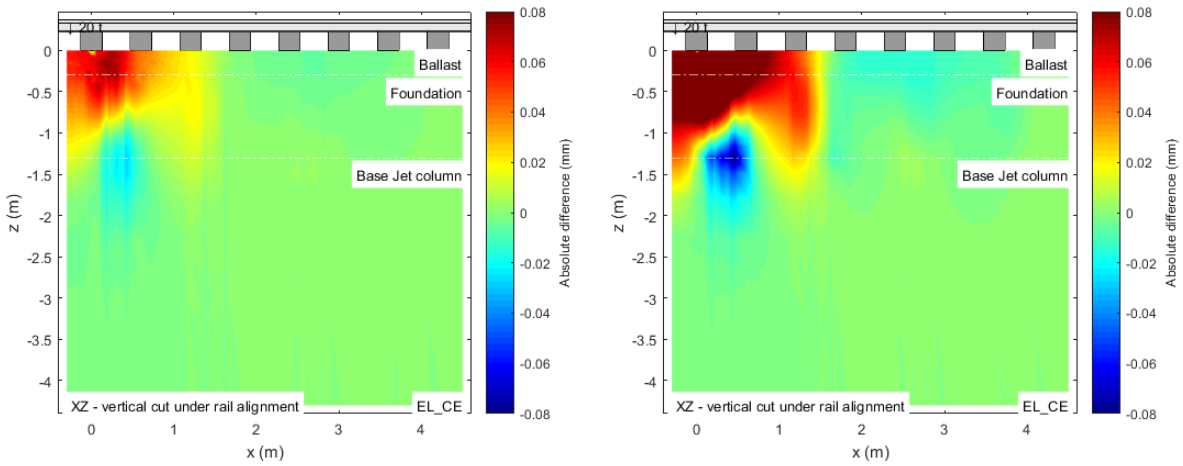

Figure 5.56 - Difference of vertical displacement distribution with depth under the rail, between models CE and N, for a) D=0.3 m and b) D=0.6 m

5.2.3 INFLUENCE OF THE AXLE LOADING POSITION

In this analysis, it was assessed the influence of the axle loading position on the railway track response. To do so, a comparison was established between models with the load being applied at a section where there is no Jet-column in the subgrade beneath the loading point and with the load being applied at a section with improved substructure under the loading point. Figure 5.57 depicts a schematic representation of the comparison being made between the results of the different models, denoting the models taken as reference and the ones under comparison.

Results of the comparison made with the larger diameter and model CE will be presented in this subchapter since the observations made are somewhat valid for both diameters and all models. The remaining results are presented in the digital annexes.

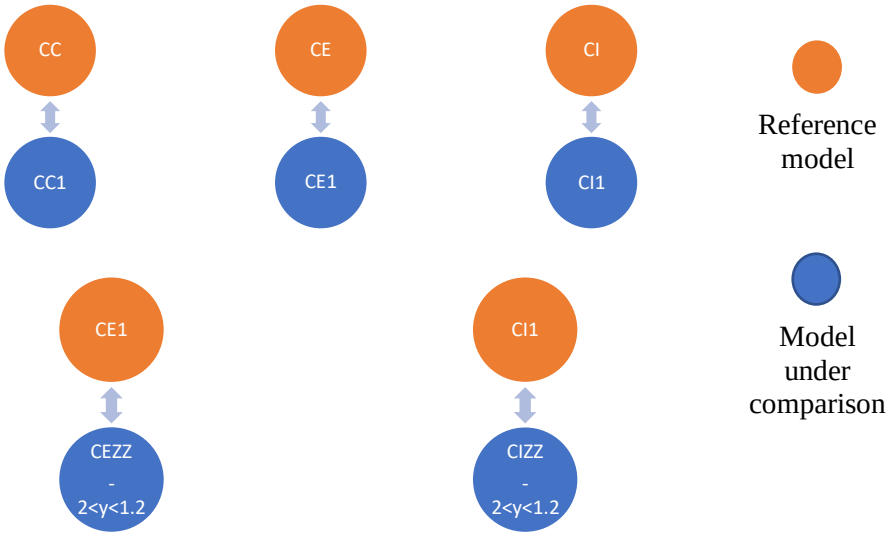

Figure 5.57 - Scheme of comparison established to analyse loading response of the track, under different model configurations (for model nomenclature see Figure 4.1)

5.2.3.1 Vertical stresses and vertical displacements at the XY planes

The vertical displacement contour plot on top of the ballast layer is shown in Figure 5.7-b) for model CE and in Figure 5.58 for model CE1. The difference between these loading responses is not very high, as can be seen in the difference plot in Figure 5.59, not reaching more than 0.1 mm for all the other models being compared. At the beginning of the model closer to the load point, smaller deflections are obtained for the model CE1 in comparison with model CE, since there is a Jet-grout column on the first span between sleepers at model CE1, a material of stiffer nature, thus undergoing smaller deflections. The opposite occurs in the middle of the first two sleepers, where displacements in that position are higher for model CE1 in comparison with the displacements for model CE.

The previous remarks are valid for the analysis of the displacements on top of the foundation, as can be seen in Figure 5.60. In this contour plot, it is observable in the circular regions, where there are higher/smaller displacements, two sets of colours. This might be related to the fact that the column is composed of two distinct materials, one stiffer from the other, being that smaller deflections should be experienced in the region where there is a stiffer material, thus the darker colour in the contour, in the centre of the circles.

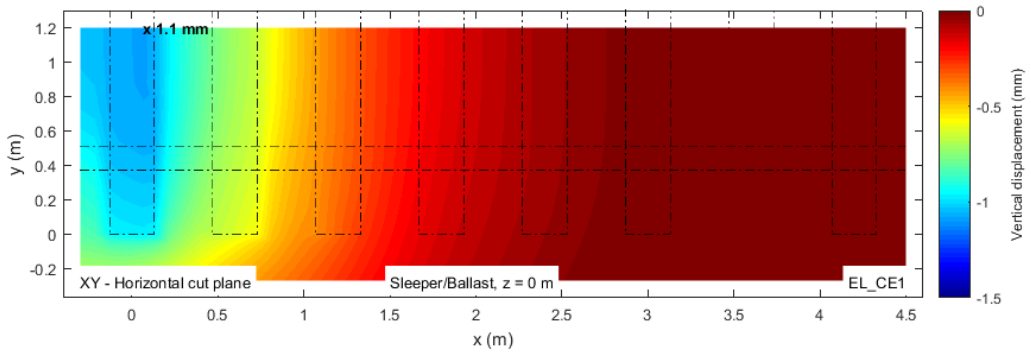

Figure 5.58 - Vertical displacement distribution on top of the ballast layer in pattern CE1, for a diameter of 0.6 m

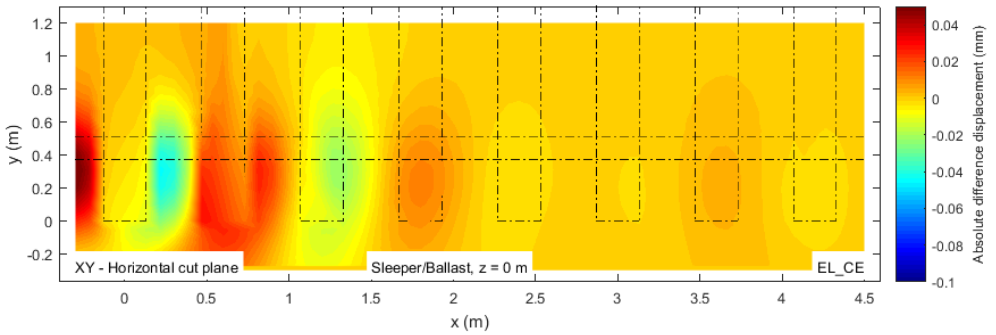

Figure 5.59 - Difference of vertical displacement distribution on top of the ballast layer, between model CE and CE1 with reference the CE model

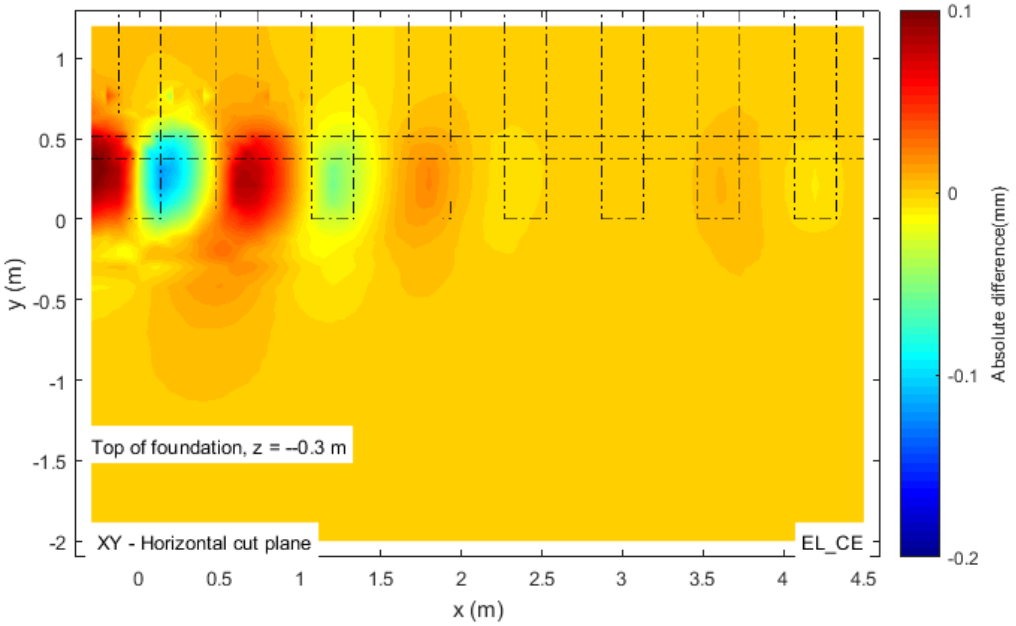

Figure 5.60 - Difference of vertical displacement distribution on top of the foundation, between model CE and CE1 with reference the CE model

For a depth just under the Jet column, the difference plot is shown in Figure 5.61. It is observable that higher displacements occur under a column, regardless of its position relatively to the loading point. In the difference plot, we can see that for model CE1 in comparison to model CE, higher displacements are occurring at the first span in between sleepers and the opposite is happening in between the first two sleepers.

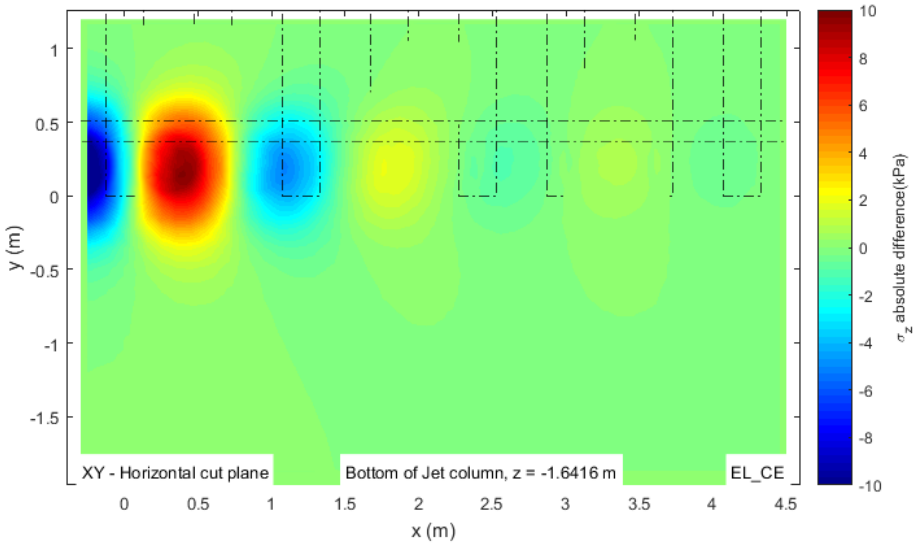

Figure 5.61 - Difference of vertical displacement distribution at a depth slightly under the Jet-grout column, between model CE and CE1 with reference the CE model

Regarding the vertical stress developed at the level of ballast layer, foundation and beneath the jet column, the following observations, regarding the contour plots, are valid for all levels. The contour plots of vertical stresses on top and bottom of the ballast layer, on top of the foundation and beneath the Jet-grout column, for model CE1, are presented in Figure 5.62. The corresponding plots of differences are shown in Figure 5.63.

In the difference plot, it is visible that higher stresses develop at the beginning of the model, at x= -0.3 m, for the model CE1, due to the presence of a column in this position. This stress concentration happens whenever there is a column, despite the model considered. The presence of a column may lead to a higher stress concentration, due to a loading path of stress transference to stiffer zones that is possibly being created. The opposite is occurring for model CE, in comparison to model CE1, where we can see stress concentrations in the middle of the first two sleepers, once more, at the column's position.

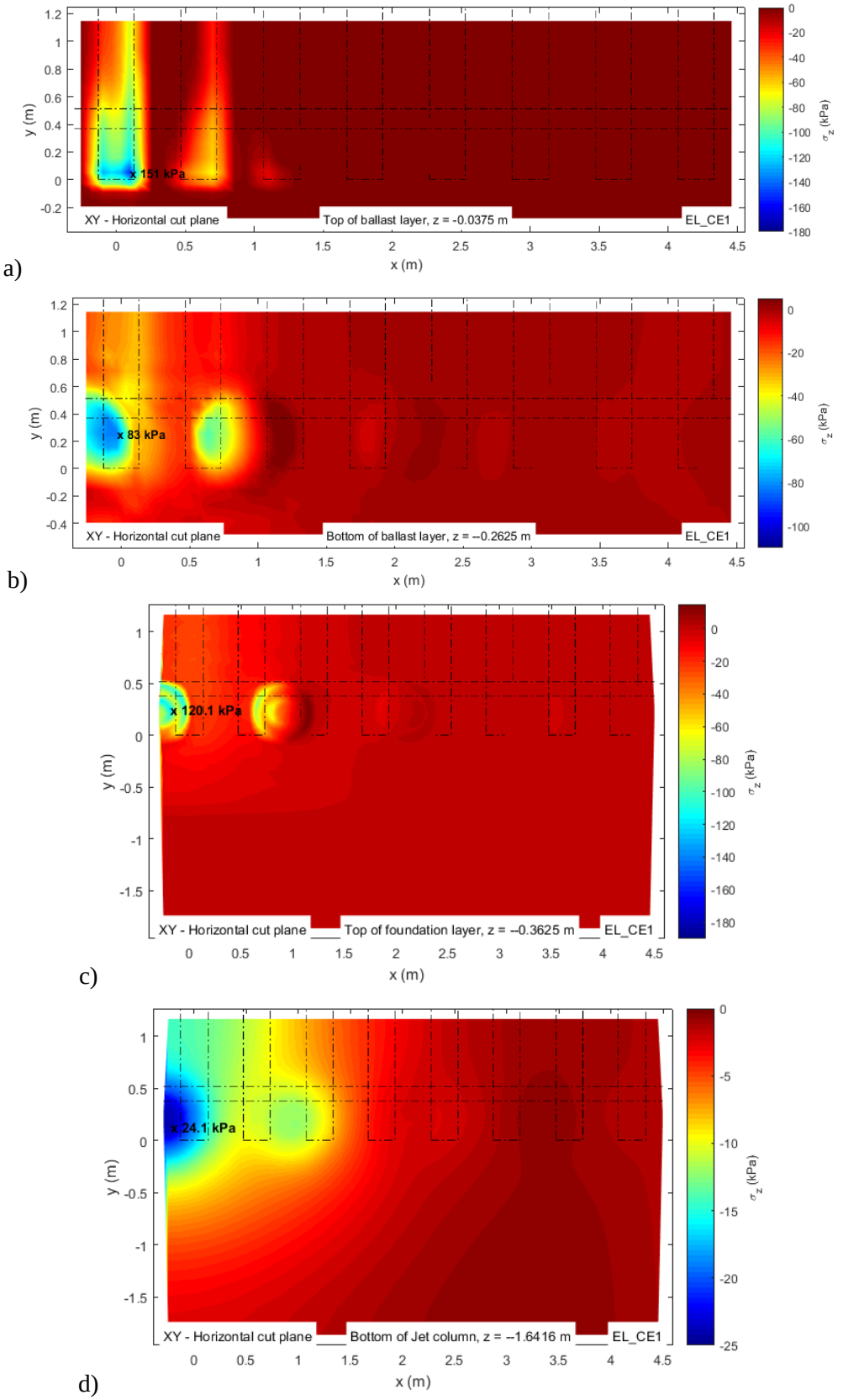

Figure 5.62 - Vertical stress distribution on a) top of the ballast, b) bottom of the ballast, c) top of foundation and d) beneath the Jet-grout columns in pattern CE1, for a diameter of 0.6 m

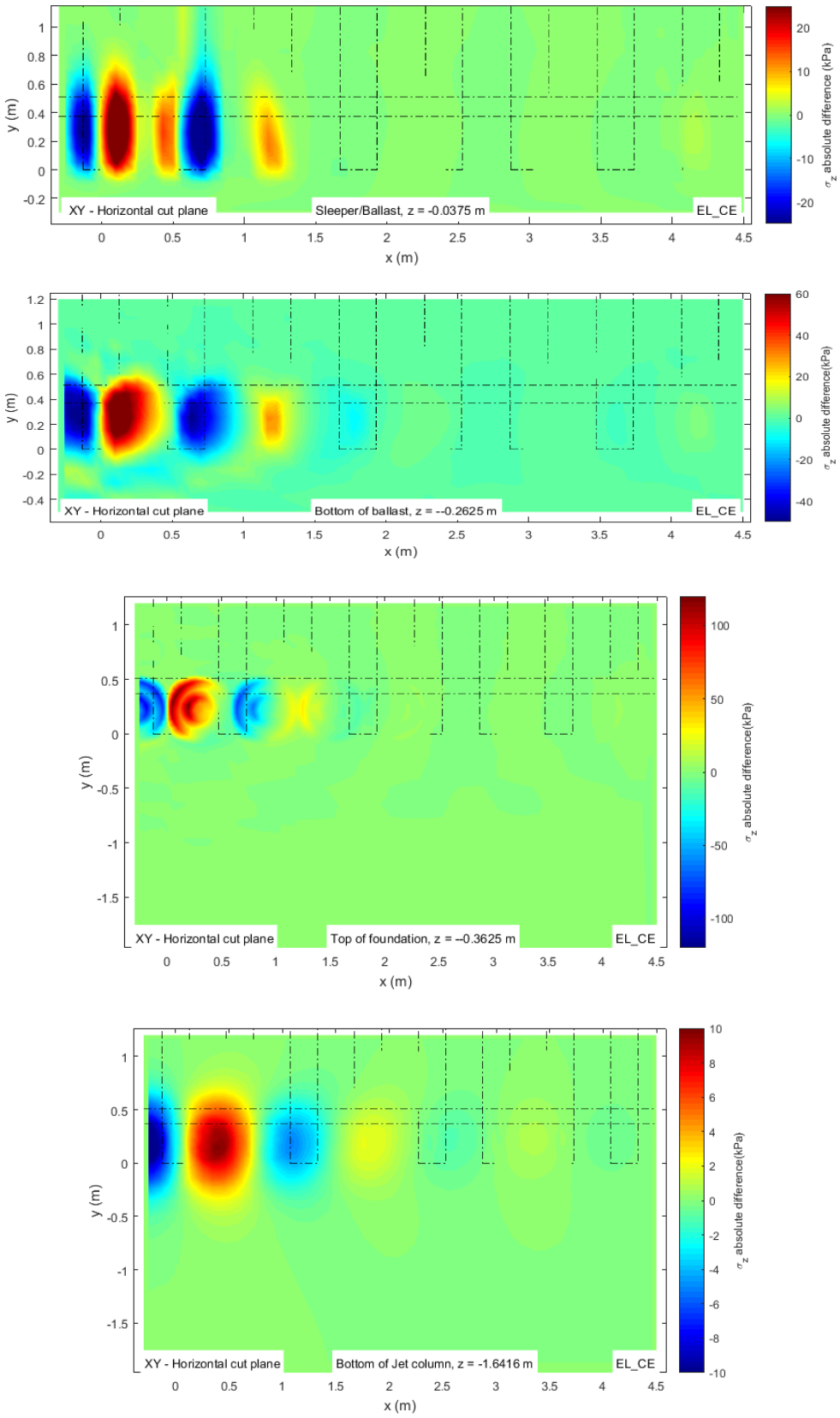

Figure 5.63 - Difference of vertical stress distribution on a) top of the ballast, b) bottom of the ballast, c) top of foundation and d) beneath Jet-grout columns between model CE and CE1 with reference the CE model

5.2.3.2 Vertical stresses and vertical displacements at the XZ plane aligned with the rail

In Figure 5.64 the difference plot of rail vertical displacement results in the longitudinal alignment, for the models mentioned before, is presented. By analysing this plot, we can see that the models with a column placed in the vertical loading plane present slightly higher displacements when compared with the ones with the loading on the adjacent sleeper span, possibly due to the vertical displacement that the Jet columns undergo, as mentioned in previous observations. However, these differences between the loading responses, for the rail displacement, are minimal as we can see by the interval of values of the difference.

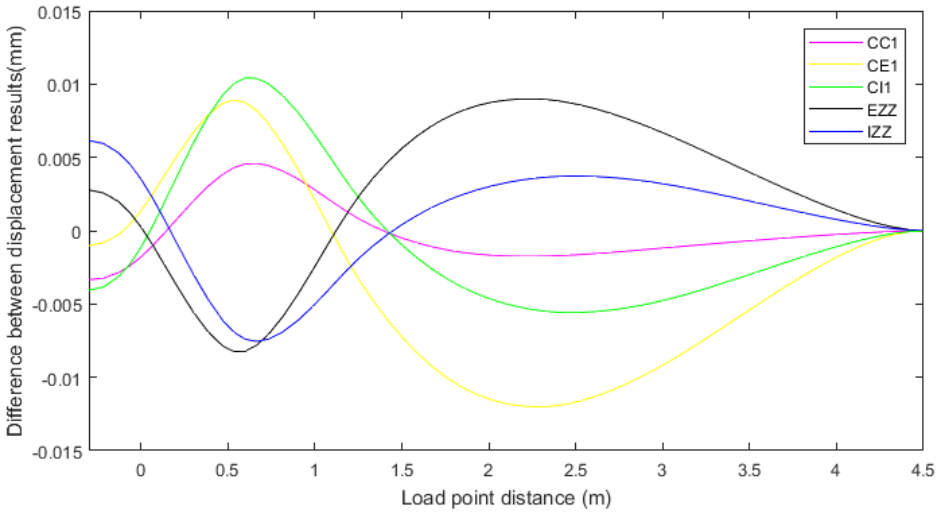

Figure 5.64 - Difference of longitudinal rail displacement results, for different loading configurations (train load at x=-0.3 m)

The vertical stress distribution with depth under the rail for model CE1 is shown in Figure 5.65. An analysis of the contour results and stress paths show that the conclusions made for model CE (see Figure 5.32-b)) are valid as well. To compare the loading response in both models, in Figure 5.66 the difference of results is presented. As observed before for the analysis in XY plane, higher stresses appear at a column's position. The vertical stress values for model CE1 are higher than for model CE, at the same position. Despite the big contrast in stress values at positions where columns are placed, stress values do not differ very much between models for the rail and foundation and ballast.

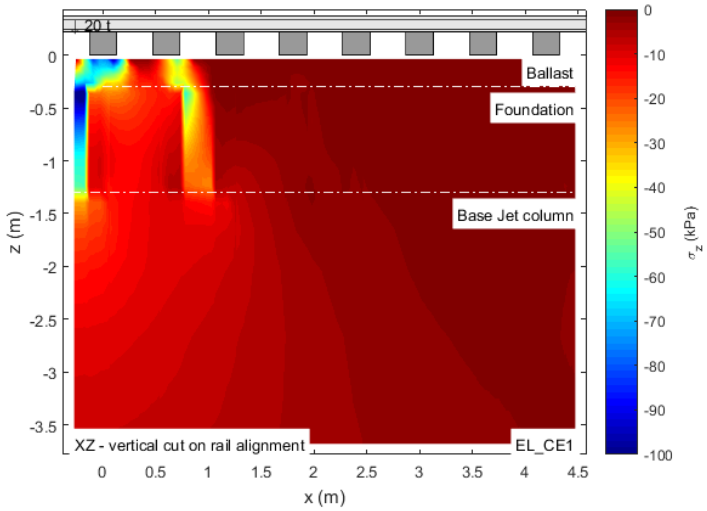

Figure 5.65 – Vertical stress distribution with depth under the rail, in pattern CE1, for a diameter of 0.6 m

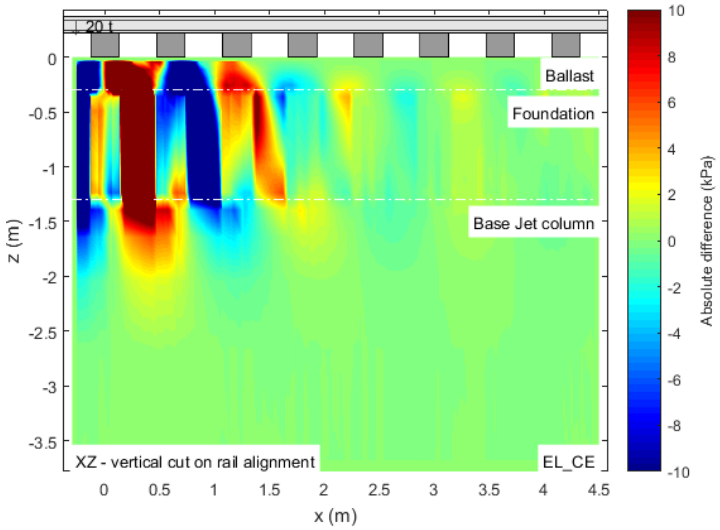

Figure 5.66 - Difference of vertical stress distribution with depth under the rail, between model CE and CE1 with reference the CE model

Regarding vertical displacements with depth, the contour plot for model CE1 is shown in Figure 5.67. Once more, to compare loading responses, a comparison between Figure 5.67 and Figure 5.34-b) was made by the difference plot in Figure 5.68. As expected, the behaviour demonstrated throughout this analysis is confirmed. We can see that, for model CE1, smaller displacements appear underneath the first sleeper, in comparison to model CE at that position. Again, this might have to do with the fact that, for model CE1, there is a Jet column placed in the vertical loading plane. Due to this, the presence of stiffer substructure, right under the loading plane will lead to smaller displacements. Right under the column, displacements in the foundation, are higher for the CE1 model than for the CE model.

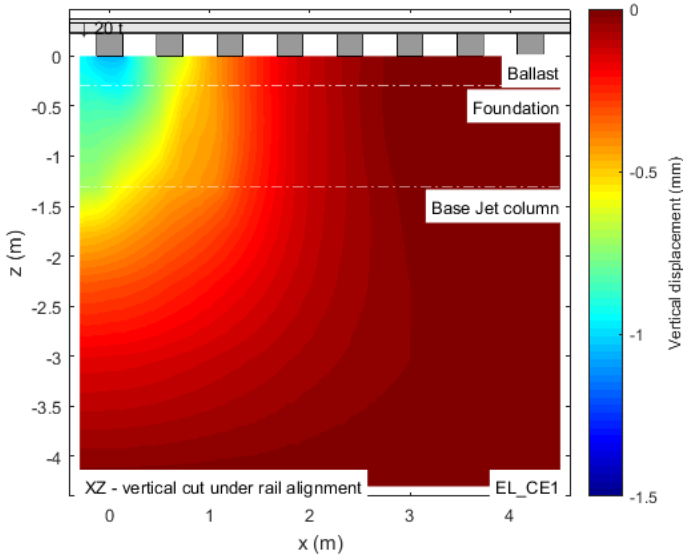

Figure 5.67 - Vertical displacement distribution with depth under the rail, in pattern CE1, for a diameter of 0.6 m

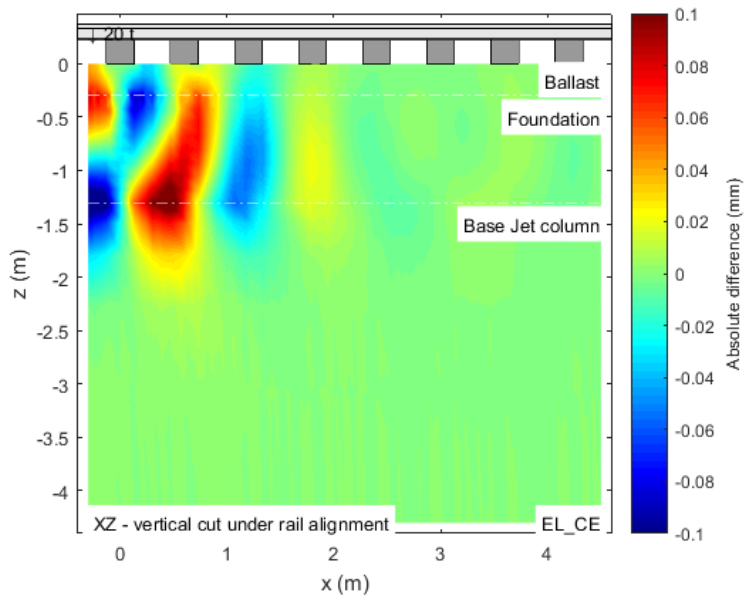

Figure 5.68 - Difference of vertical displacement distribution with depth under the rail, between model CE and CE1 with reference the CE model

5.2.3.3 Summary of vertical stresses at relevant locations

The purpose of the following analysis was to summarise the results and assess whether there was a relevant decrease in vertical stresses on the substructure, compared with the stresses in the Jet-grout columns. As mentioned before, two types of positioning of the Jet columns relatively to the loading point were studied. To fully understand this phenomenon, vertical stress values at the points indicated in Figure 5.69 were queried and analysed.

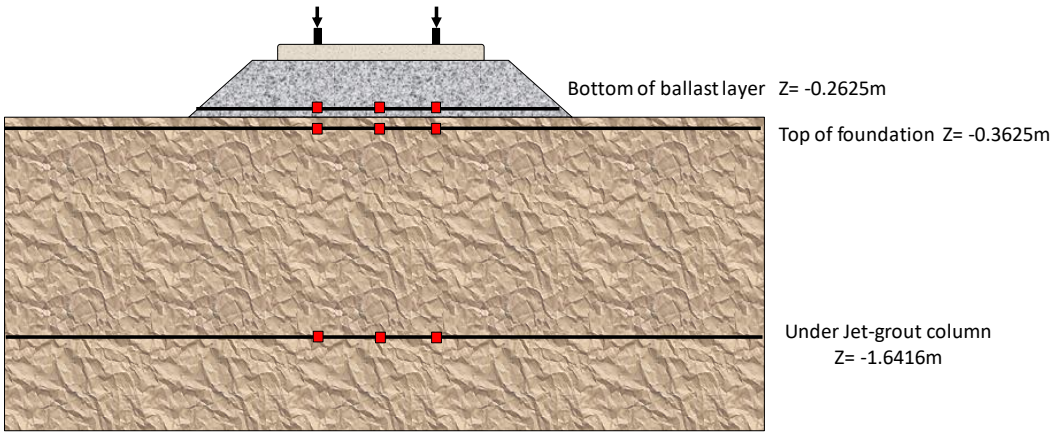

Figure 5.69 -Queried points for stress analysis in red

In Figure 5.70 is presented the vertical stress values at the bottom of the ballast layer, for both column diameters. Overall, by implementing the Jet-grout columns in the foundation, there is a reduction in the stress values in comparison to the stresses without substructure improvement, which is one of the main goals to apply this type of reinforcement.

In general, it is observable that, for the models where there is no Jet column under the loading point, the stress value is smaller than for the non-improved ground. This might mean that the stresses instead of spreading uniformly in the substructure, with the presence of the columns are now being directed into its direction, concentrating higher values at its positions and relieving the stress applied to the soil in the surrounding. By comparing the results of models CE and CE1 we can observe the explained behaviour.

With the presence of a Jet-grout column under the loading point in model CE1, in comparison with CE, there is a higher stress concentration at the column. For the exterior and interior configurations, higher stress levels are occurring under the rail, since the column's position relatively to the rail allows a better directing of the applied loads into the columns. The exterior layout presents higher stresses than the interior layout since, at the top of the ballast layer, stresses are higher at the outer extremities of the sleepers, thus the columns placed externally to the rail receives higher loads than one placed internally to the rail. These observations are valid for CIZZ and CEZZ models. Regarding configuration CC and CC1, due to the columns' positions on this configuration stresses are higher at the middle of the sleepers, as would be expected.

Comparing Figure 5.70-a) and Figure 5.70-b), with the increase of the column's diameter, stress values amplified for the exterior and interior layout models. This might be related to the increase of the area of stiffer soil (Jet-grout column) that can support higher stress levels, thus concentrating higher values. The central column models did not experience a big variation in the stress value, however, this might be due to the query points position since for the other models the query points sometimes partially catch the column, but with the central models, it does not (see Figure 5.71).

The observations made for the top of the ballast layer are analogous to those concerning the results at the top of the foundation (see Figure 5.72). Still, we can see that the range of the maximum stress increases.

a)

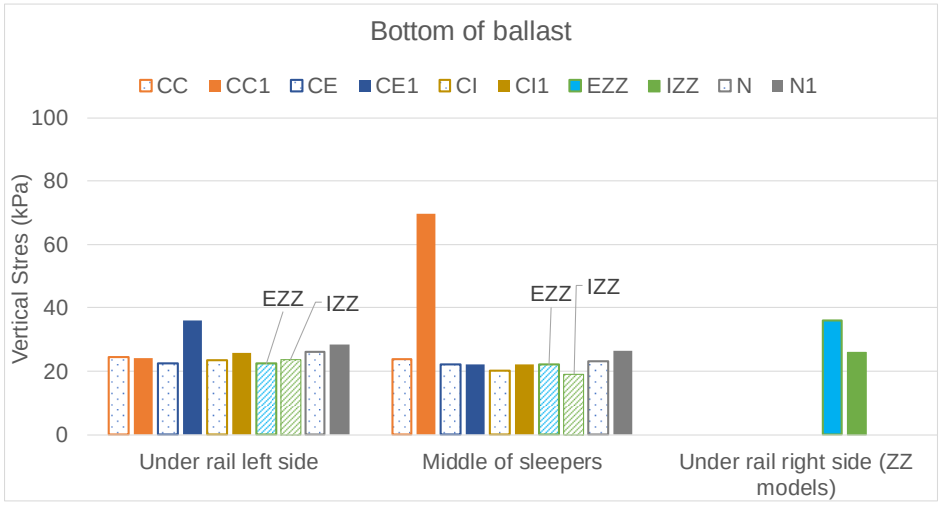

b)

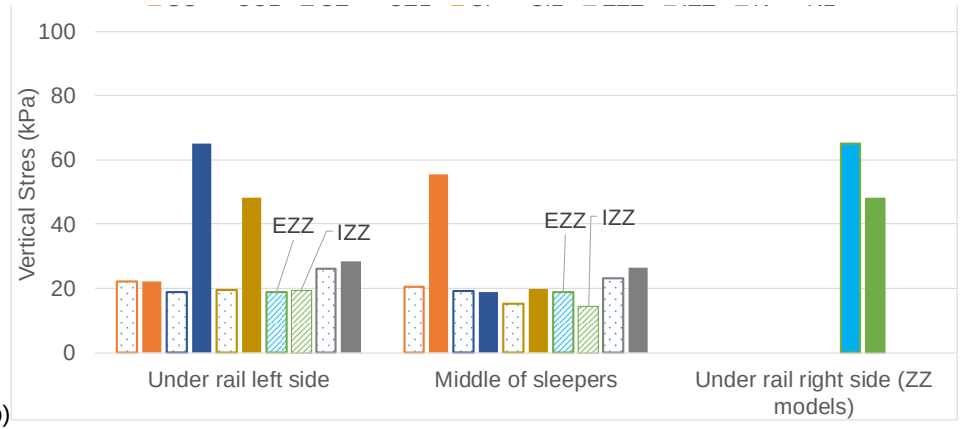

Figure 5.70 – Vertical stress values at the bottom of the ballast layer, for the different column layouts, at the query points specified in Figure 5.69 for a) 0.3 m diameter and b) 0.6 m diameter.

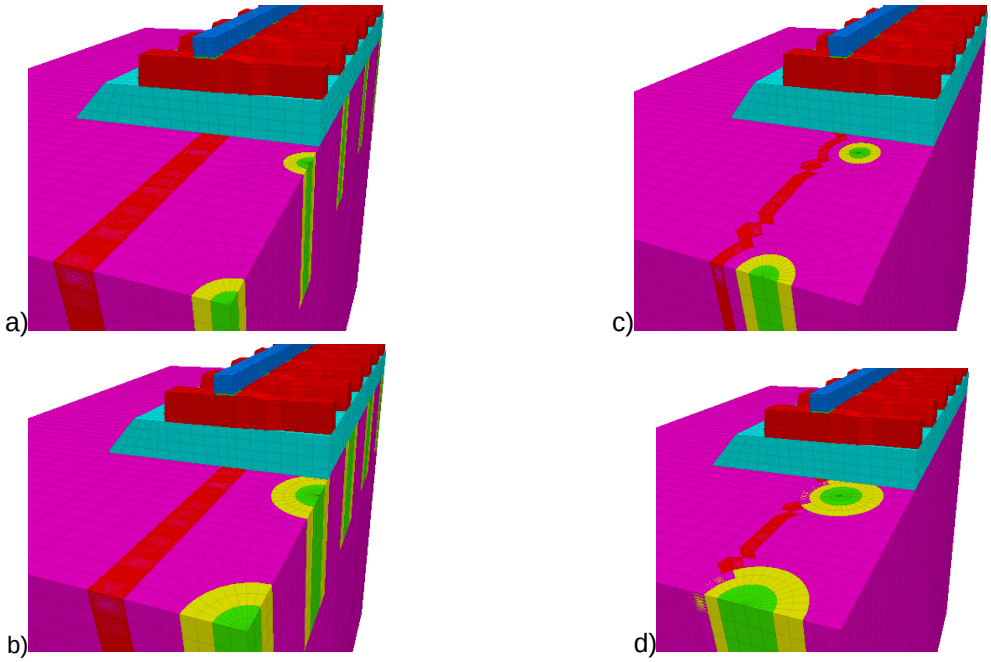

Figure 5.71 – Query points range under the rail for models a) CC1 D = 0.3 m, b) CC1 D = 0.6 m, c) CI D = 0.3 m and d) CI D = 0.6 m

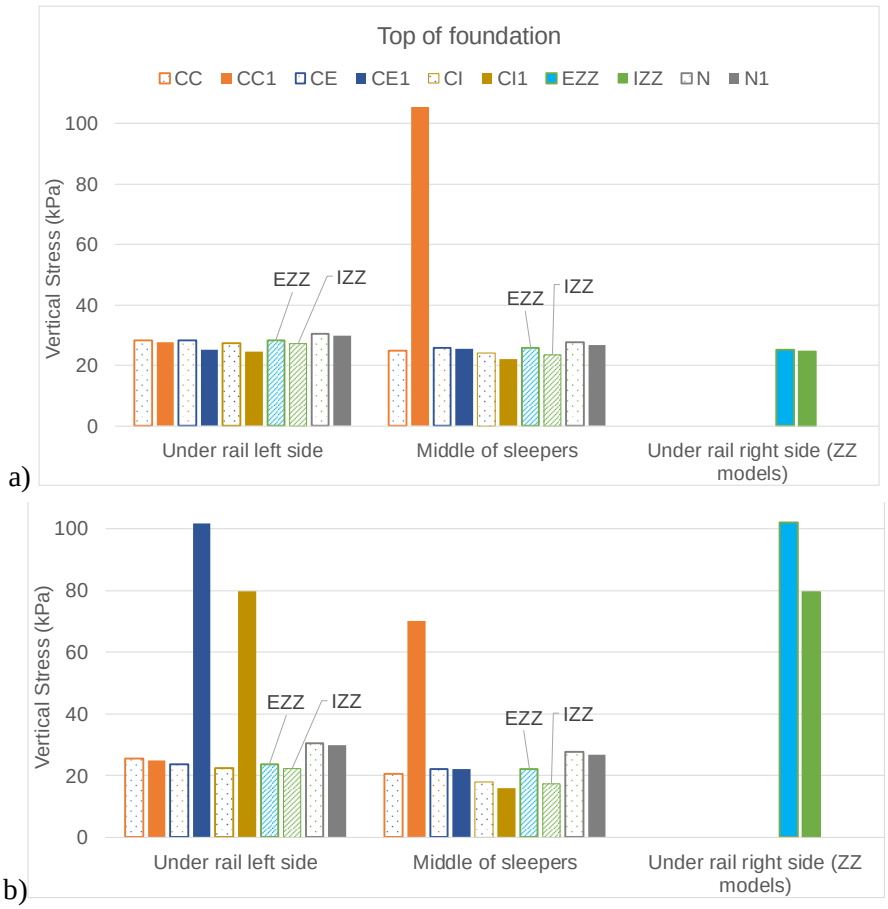

Figure 5.72 - Vertical stress values at the top of the foundation, for the different column layouts, at the query points specified in Figure 5.69 for a) 0.3 m diameter and b) 0.6 m diameter.

For a level beneath the column, the vertical stress values at different query points are presented in Figure 5.73. It is visible that in general, the stress values decrease at this depth in comparison to the level on top of the foundation.

Between no substructure improvement and substructure improvement models, where there is no column under the loading point, the stress values are not very different, suggesting that at this depth, the influence of the ground improvement technique on the reduction of the stresses on the soil that surrounds the column somewhat loses relevance. When there is a column underneath the loading point, at the query point underneath the rail, stresses are slightly higher than the ones for the non-improved substructure for the CE1 and CI1 models. This could be due to the pressure bulb that is possibly being created underneath each column. For the CI1 model, stresses are slightly higher than for the CE1, under the rail and in the middle of the sleepers. This may perhaps be due to the interior positions of the CI columns relatively to the rail: by being placed internally to the rail, columns are closer to one another and a similar effect to the installation of a group of piles is being possibly obtained, creating a pressure bulb of larger dimensions.

a)

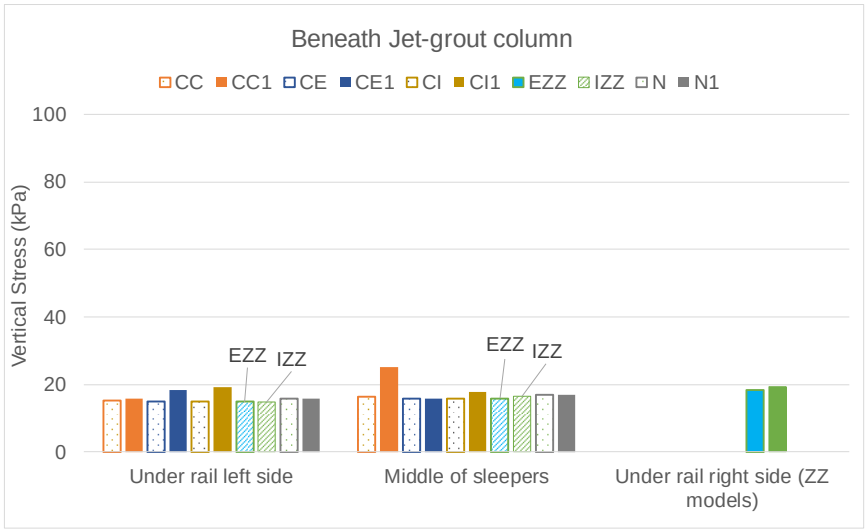

b)

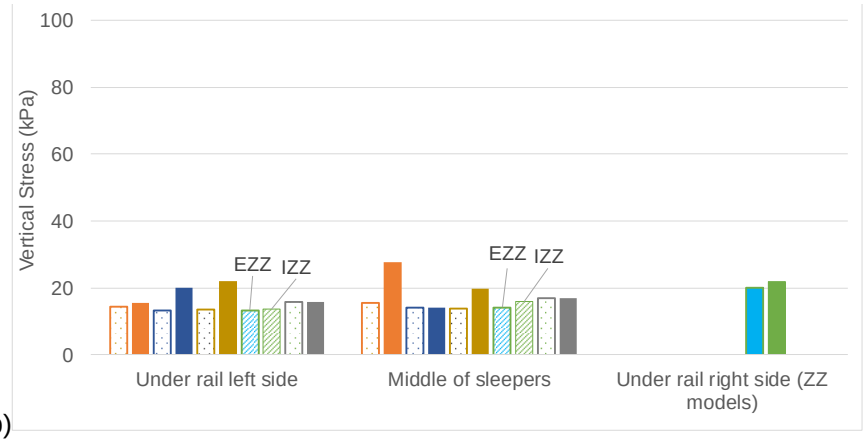

Figure 5.73- Vertical stress values beneath the Jet-grout column, for the different column layouts, at the query points specified in Figure 5.69 for a) 0.3 m diameter and b) 0.6 m diameter.

5.2.4 IMPACT ON THE TRACK VERTICAL STIFFNESS

The vertical stiffness coefficient is able to quantify the track's stiffness as it is perceived by the transiting vehicles (Teixeira, 2004). This coefficient is quantified by the following formula:

$$K_v = \frac{Q}{\delta_{max}} \tag{6}$$

where K_v is the vertical stiffness coefficient, Q is wheel load acting upon the rail and δ_{max} is the maximum vertical rail displacement.

In Figure 5.74 is presented the vertical stiffness coefficients for each model designed, calculated with the displacement values in Table 5.1. The wheel load considered in the calculations was 100 kN.

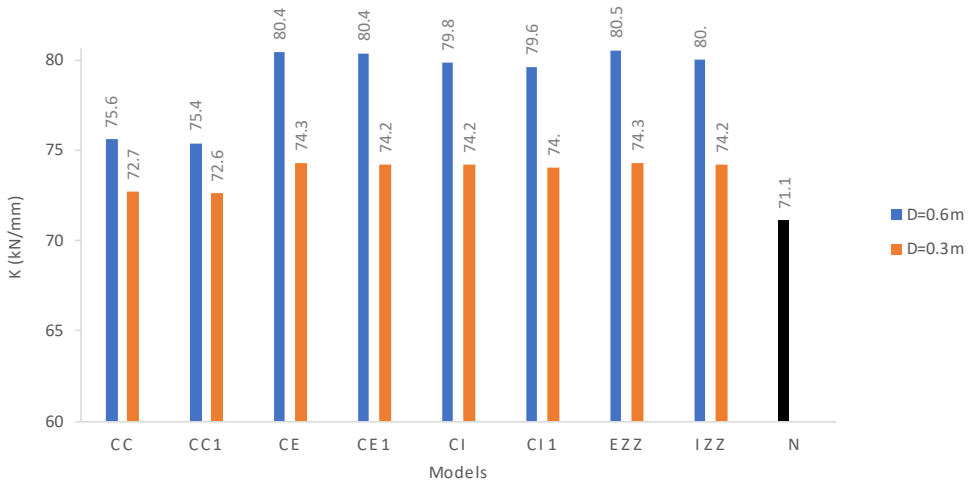

Figure 5.74 – Vertical stiffness coefficients for different model types and column diameter size

In comparison with the N model, all models that included substructure improvement increased the track's vertical stiffness. With the increase of diameter, a higher vertical stiffness parameter is obtained for all models. In the models with two columns per pair of sleepers (all except CC and CC1), the vertical stiffness increases from about 74 kN/mm to about 80 kN/mm when the column's diameter is increased from 0.3 to 0.6 m.

The layouts where the columns are placed closer to the rail, whether internally or externally to it, were the ones that showed slightly higher values for the vertical stiffness: less than 1 kN/mm of difference. It is also noted a very small decrease in the vertical stiffness (less than 1 kN/mm) when the load is applied in the sleeper spans where a column is present, compared to the situation where the wheel load acts on the same vertical plane where the column is. The model that presents the higher vertical stiffness value, for both diameters, is CEZZ with K_v = 80.5 kN/mm and 74.3 kN/mm, respectively for D = 0.6 and D = 0.3 m. As expected, the model that presents the lowest vertical stiffness, for both diameters, is CC1 with K_v = 75.3 kN/mm and 72.6 kN/mm, respectively for D = 0.6 and D = 0.3 m, because it has only 1 column per pair of sleepers – half of the number of columns the other modelled structures have.

5.3 NON-LINEAR ELASTIC BEHAVIOUR

The non-linear elastic behaviour was applied exclusively to the ballast layer. The reason for this was explained in more detail in Chapter 4. Since the sleepers are the superstructure elements that transmit the train load to the underlying layers, the substructure located right beneath them will be subjected to higher stresses than the surrounding ground. As the ballast layer is the layer that immediately underlies the sleepers, it means that higher stresses will develop at the ballast, right under the sleepers. With the non-linear model, the elements that are experiencing higher loading condition, have higher stresses and will undergo higher stiffness variations (Paixão [et al.], 2016b).

With the introduction of the column reinforcements in the foundation, the support conditions of the ballast layer become uneven in the longitudinal and transverse directions. This aspect adds to the increase in spatial stiffness variation within the ballast layer mentioned above, which in turn may yield different load distributions between sleepers and onto the column reinforcements. Thus, this section aims at shedding light on the effect of the non-linear elastic behaviour of ballasted tracks with columns reinforcements, in comparison with the linear elastic scenario presented in the previous section.

In the non-linear elastic models, the gravitational force was activated before the load was applied to the system, as mentioned in Chapter 4. This procedure is related to the way the k- θ model operates, as mentioned before. As the materials of the superstructure were provided with density, with the gravitational force the self-weight of the materials will originate initial stresses in the substructure, creating stiffer areas.

Due to the previous observations, all the results obtained with non-linear elastic behaviour had the overlapping of two effects: the effect of the gravitational force and the effect of the applied train load. In Figure 5.75 is presented the results of vertical stress distribution with depth under the rail for model CI, with linear elastic behaviour (Figure 5.75-a)) and non-linear elastic behaviour (Figure 5.75-b)). It is visible that the difference is quite significant between contour plot results. Comparing both figures, we can see that, for the non-linear elastic behaviour, there is a higher definition of the columns position and the stresses being directed to them are higher than for the elastic behaviour. However, for an adequate comparison between the linear elastic models and the non-linear elastic models, it is necessary to remove gravitational effect from the results to compare the effects only due to the train load. Figure 5.75-c) is the contour plot that results from the non-linear analysis, however, without the contribution of the gravitational effect. We can now see that the results for the linear elastic and non-linear elastic are closer to one another.

The following analysis will be made without the contribution of the gravitational force, and the results of the non-linear elastic behaviour with the contribution of the gravity are presented in the digital annexes.

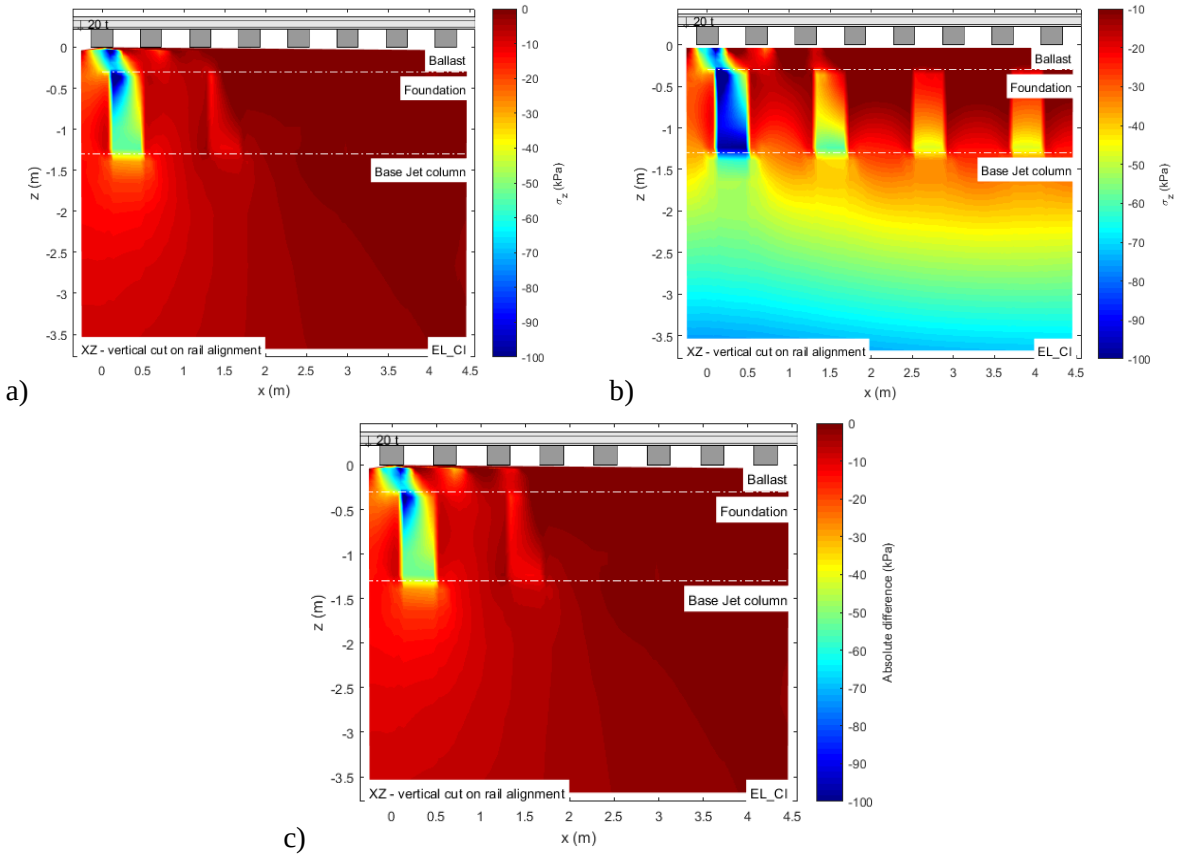

Figure 5.75 - Vertical stress distribution with depth under the rail, in pattern CE, for a diameter of 0.6 m, with a) linear elastic behaviour; b) non-linear elastic behaviour of the ballast layer; c) non-linear elastic behaviour of the ballast layer after removing the gravitational effect.

5.3.1 INFLUENCE OF THE COLUMN DIAMETER

5.3.1.1 Vertical displacements and vertical stresses at the XY planes

In general, as observed for the linear elastic behaviour, with a larger diameter, smaller vertical displacements are obtained, both for the top of the ballast or foundation, and larger displacements at the bottom of the Jet column. Since this observation is valid for most column layouts, results for the model CE will be analysed and the remaining ones are presented in the digital annexes.

Concerning the vertical displacements on top of the ballast layer, displacements are larger under the first sleeper, regardless of column size. With the increase of the column's diameter, the magnitude of the maximum displacement decreases from 1.3 mm to 1.2 mm (see Figure 5.76). The maximum vertical displacement's location, for both diameters, is in the middle of the sleepers, in similarity to the linear behaviour.

The difference plot is shown in Figure 5.77. It is observable that the higher difference remains on the displacements under the first sleeper, having the smaller diameter, larger displacements. If we care to compare the difference plots in Figure 5.8 and Figure 5.77, for the linear elastic model and the non-linear elastic model, it is visible that, by considering the non-linearity of the ballast layer, higher displacements occur for the smaller diameter and the range where those higher deflections appear is larger. Nevertheless, the comparison between considering linear or non-linear elastic behaviour will be made further on.

The maximum displacement values and their positions, for different column layouts and column diameter, are presented in Figure 5.78.

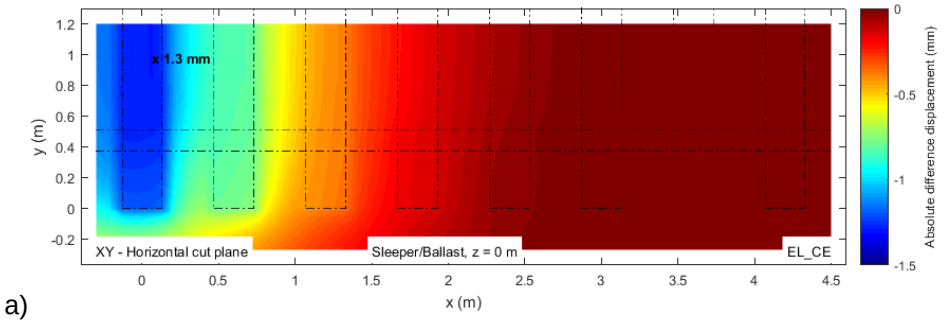

a)

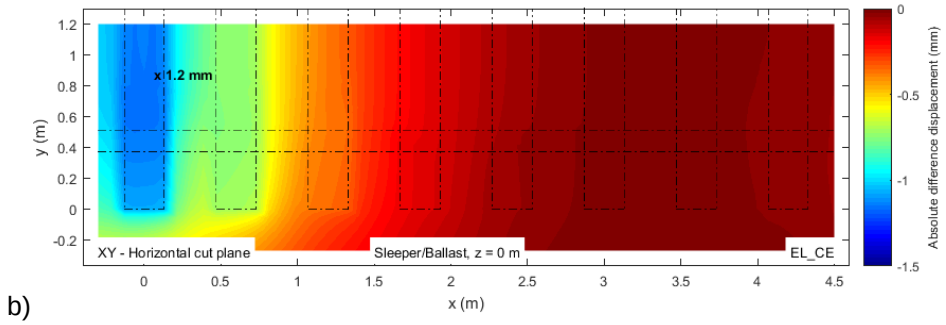

b)

Figure 5.76 - Vertical displacement distribution on top of the ballast layer in pattern CE for a diameter of 0.3 m a) and 0.6 m b), for non-linear behaviour

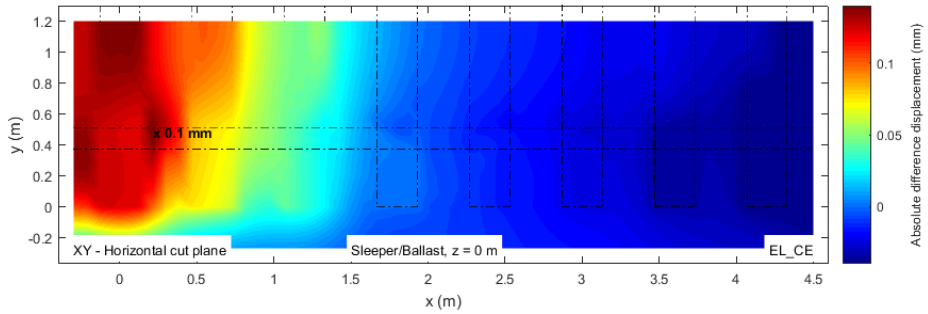

Figure 5.77 - Difference of vertical displacement distribution on top of the ballast layer between different diameters in pattern CE, for the non-linear behaviour

On top of the foundation, the observations are analogous to the ones for the top of ballast layer and like the ones for the elastic behaviour. Displacements are higher for the smaller diameter model under the first sleeper, closer to the loading point, and become similar to the displacements of the larger radius along the longitudinal direction of the track, as we can observe from the difference plot in Figure 5.79. It is visible a circular zone between the first two sleepers, exterior to the rail, where displacements diminish when the column diameter increases. This could be due to the increase of the area of improved substructure under the first sleeper. Regarding the maximum displacement, by increasing the column's diameter there is no significant improvement.

The maximum displacement and its position on top of the foundation, for different column layouts and column diameter, are presented in Figure 5.80.

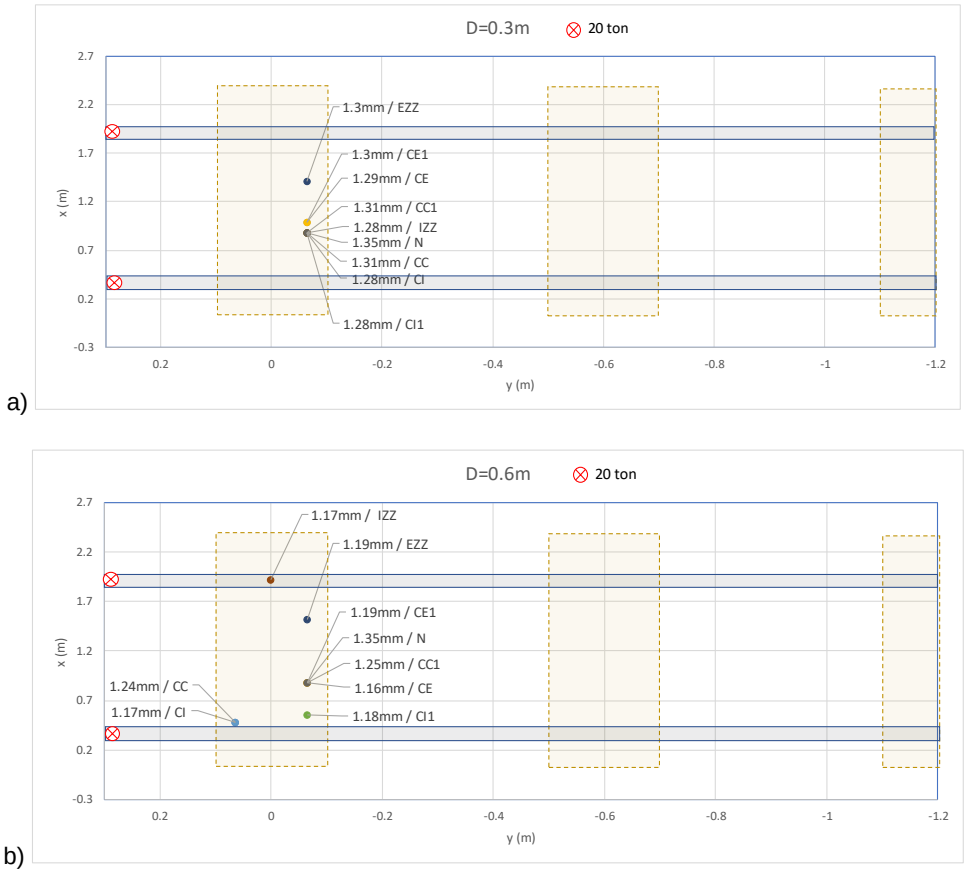

Figure 5.78 - Maximum displacement values and their position for different column layouts and diameters (a) D=0.3m and b) D=0.6m) on top of the ballast layer, for a non-linear behaviour.

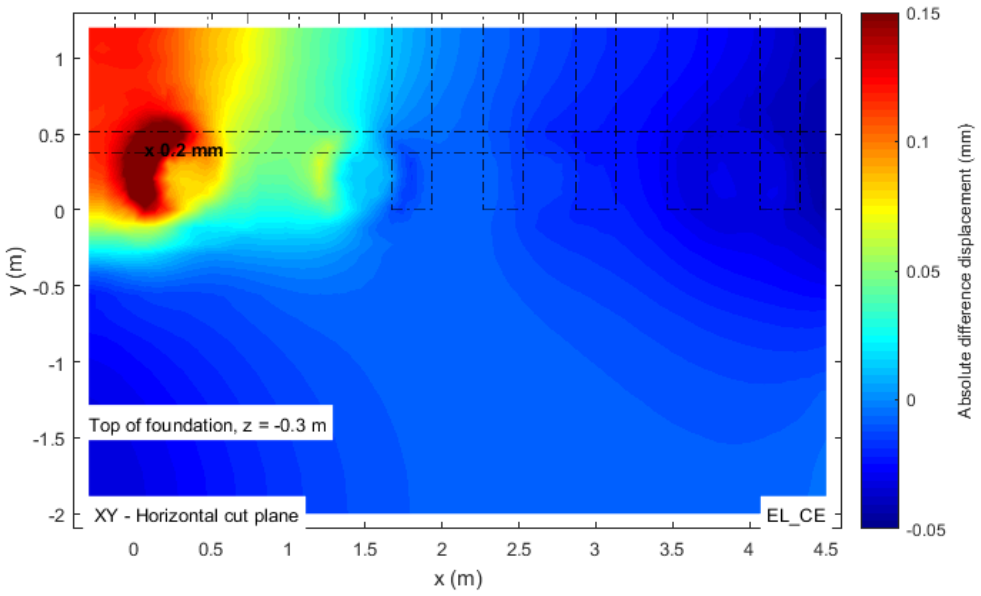

Figure 5.79 - Difference of vertical displacement distribution on top of the foundation between different diameters in pattern CE, for non-linear behaviour

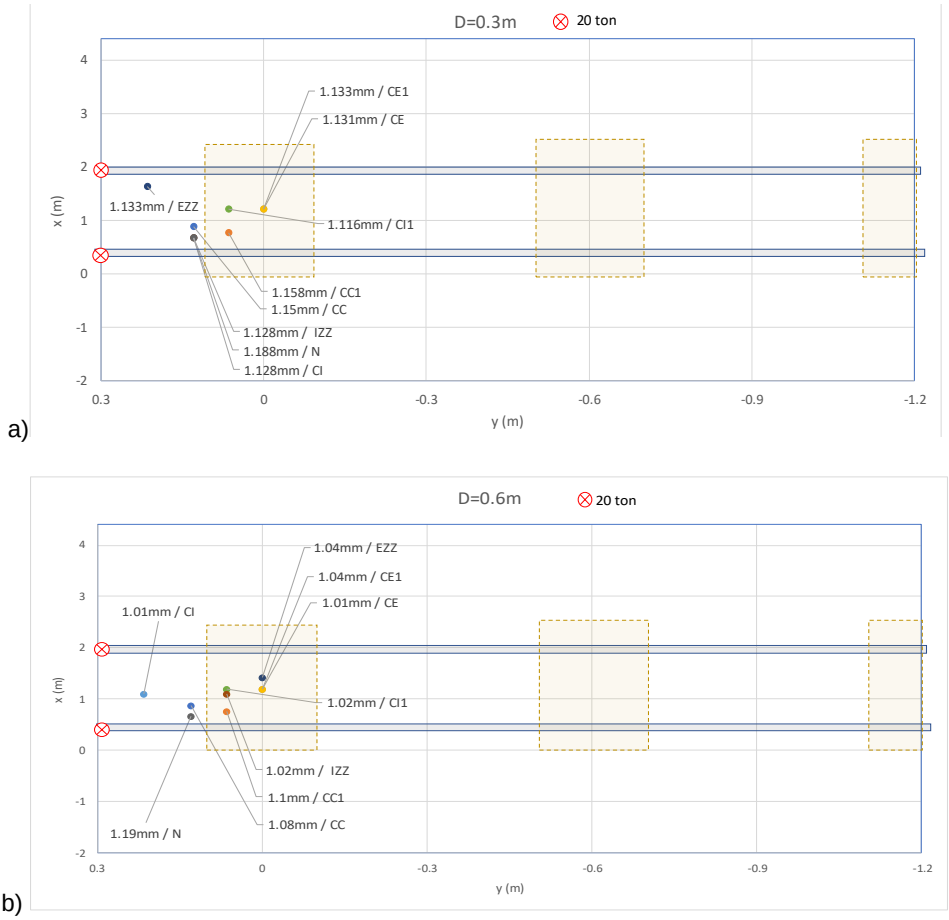

Figure 5.80 - Maximum displacement values and their position for different column layouts and diameters (a) D=0.3m and b) D=0.6m) on top of the foundation, for non-linear behaviour

At a depth, just under the Jet column, the displacements are slightly higher for the 0.6 m diameter. This is apparent when analysing the plot of difference in Figure 5.81, where it is visible circular regions, where the columns are placed, showing that for the D=0.6 m, in those positions, displacements underneath the column are higher than for the smaller diameter. Between sleepers, smaller displacements are visible, for a larger diameter. Comparing the results for the linear elastic behaviour with the non-linear elastic behaviour, the difference between deflections for each diameter becomes much smaller, when applying the non-linear elastic behaviour for the ballast layer (close to zero).

The maximum displacement values and the position of those maxima at a level beneath the Jet-grout column, for different column layouts and column diameter, are presented in Figure 5.82.

Regarding the comparison of vertical stresses on top of the ballast layer for different diameters, the observations made for the linear elastic behaviour are valid for the non-linear. A slight reduction in the maximum stress value is seen, when the column diameter increases and the exterior of the sleeper is where this maximum value is positioned. When comparing the difference plots in Figure 5.18 and Figure 5.83, we can see that by considering the k-θ model, with a larger diameter, a larger amount of stresses is being directed into the first column's direction. Also, the stresses in the outline of the second sleeper are higher for the larger diameter model and non-linear elastic behaviour.

The maximum vertical stress values and the position of those maxima on top of the ballast layer, for different column layouts and column diameter, are presented in Figure 5.84.

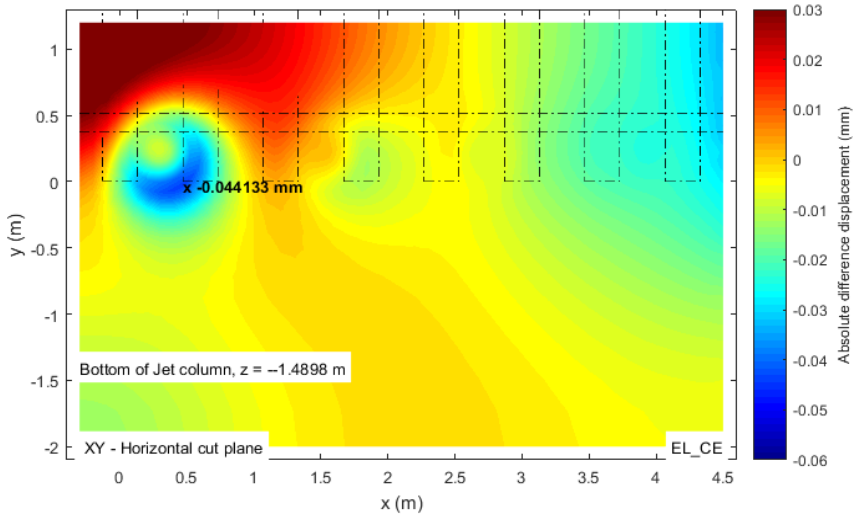

Figure 5.81 - Difference of vertical displacement at the base of the Jet column in pattern CE, for non-linear behaviour

a)

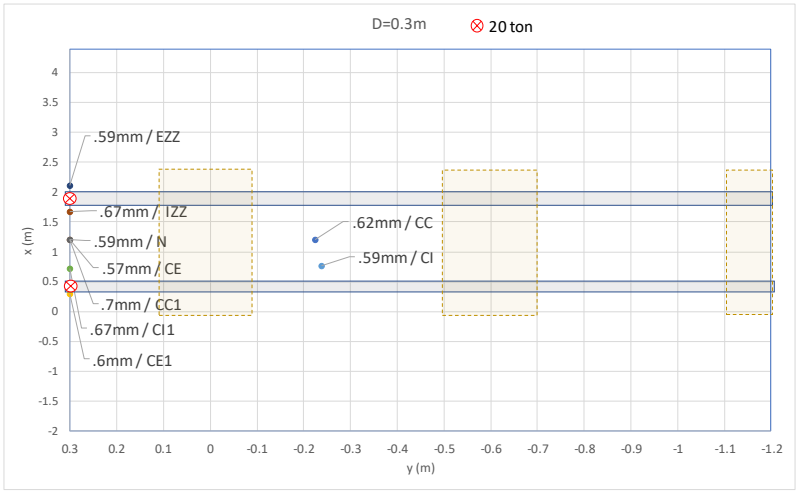

b)

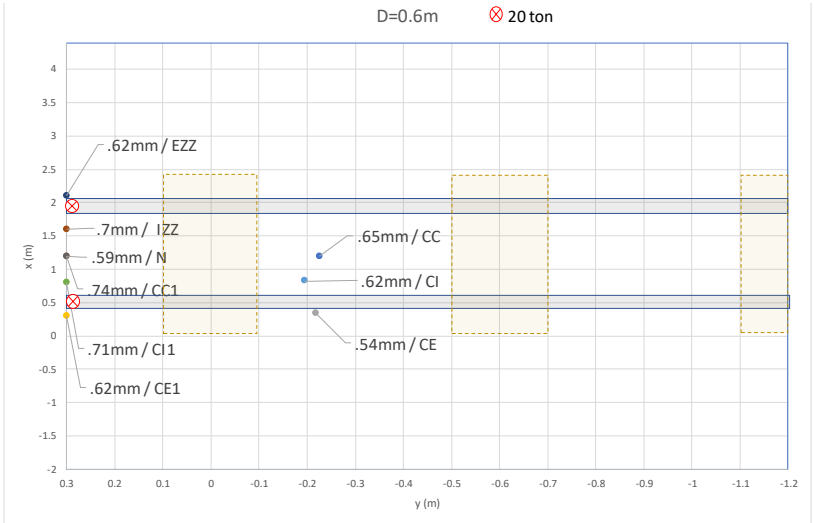

Figure 5.82 - Maximum displacement values and their position for different column layouts and diameters (a) D=0.3m and b) D=0.6m) at a position beneath the Jet-grout column, for non-linear behaviour

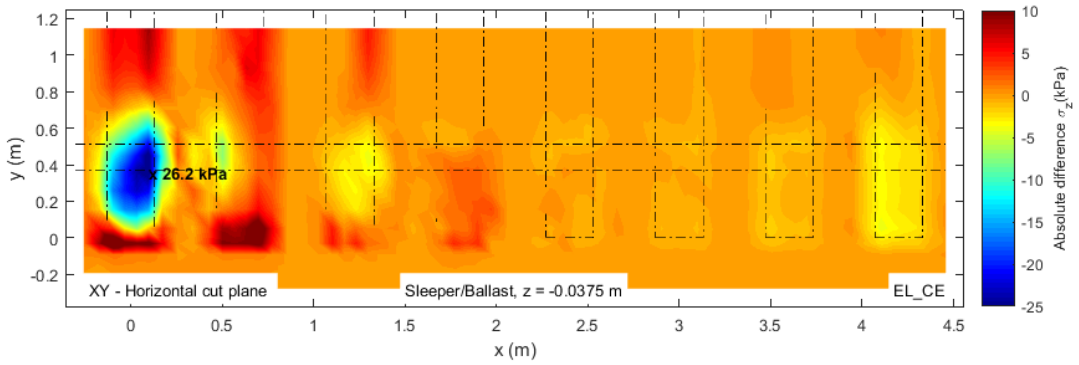

Figure 5.83 - Difference of vertical stress distribution on top of the ballast layer between different diameters in pattern CE, for non-linear behaviour

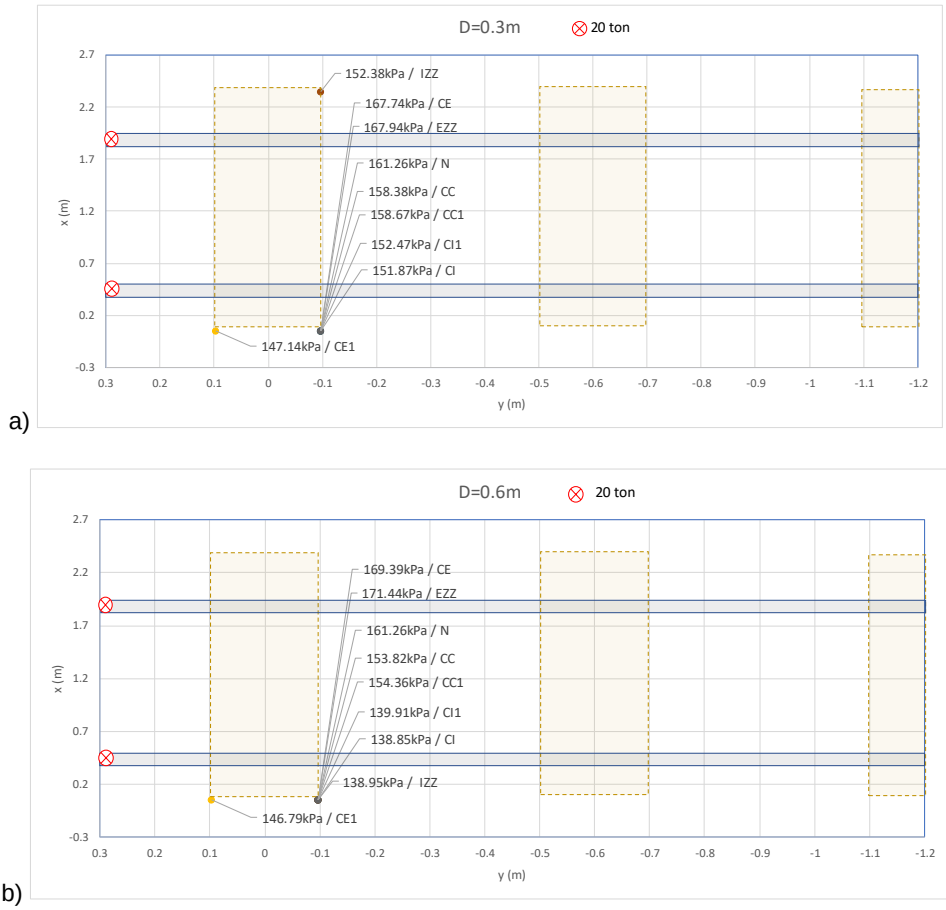

Figure 5.84 - Maximum vertical stress values and their position for different column layouts and diameters (a) D=0.3m and b) D=0.6m) on top of the ballast layer, for non-linear behaviour

When examining the vertical stress at the bottom of the ballast layer, by analysing Figure 5.85, it is visible the approximate location of the columns, suggesting a difference in the stress values for different diameters. By choosing a larger diameter, higher stresses develop at the column's positions, like in the linear elastic models. For the non-linear model, the region where stresses are higher in the models D=0.6 m than in model D=0.3 m, shown in Figure 5.85, is slightly smaller than for the elastic model. Despite this, for each material behaviour, the maximum difference between stress values for different diameters is the same. The position and value of the maximum vertical stress on the bottom of the ballast layer, for different column layouts and column diameter, are presented in Figure 5.86.

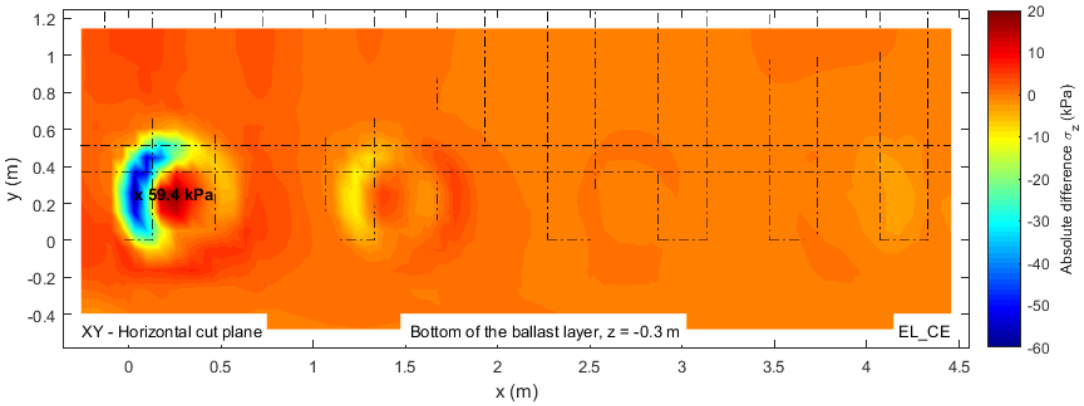

Figure 5.85 - Difference of vertical stress distribution at the bottom of the ballast layer for different diameters in pattern CE, for non-linear behaviour

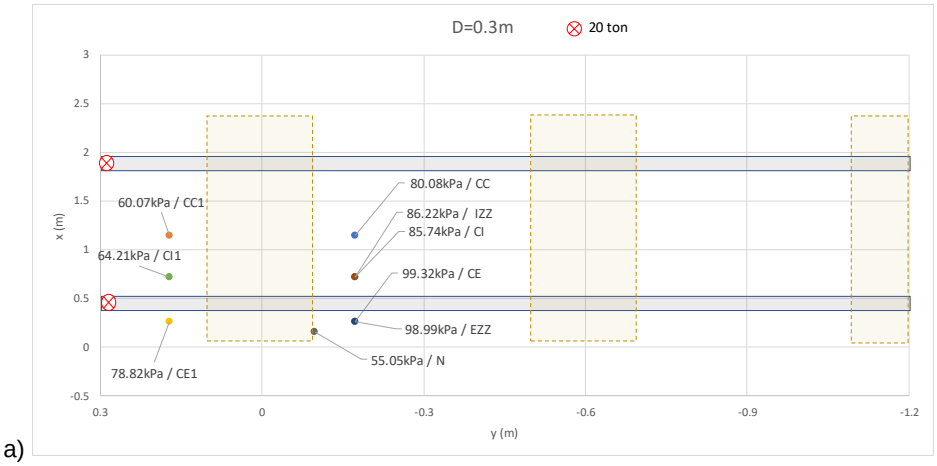

a)

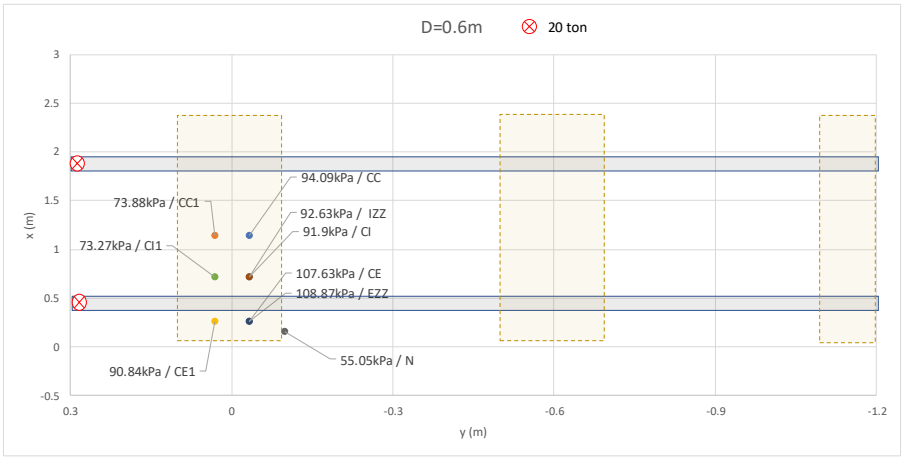

b)

Figure 5.86 - Maximum vertical stress values and their position for different column layouts and diameters (a) D=0.3m and b) D=0.6m) on bottom of the ballast layer, for non-linear behaviour

The analysis of the contour plots of vertical stress on top of the foundation, for non-linear elastic behaviour, is analogous to the linear elastic models. The difference plot for the non-linear elastic behaviour is shown in Figure 5.87. The larger difference in stress values remains at the column's position. A larger stress spreading for the larger diameter is seen, whereas at the centre of the column stresses are higher for the smaller diameter model. Comparing linear and non-linear plots in Figure 5.24 and Figure 5.87, we can see that the difference between stress values decreases by almost half when adopting a non-linear elastic law for the ballast layer.

The maximum vertical stress values and the position of those maxima on top of the foundation, for different column layouts and column diameter, are presented in Figure 5.25.

Regarding the vertical stress distribution under the Jet column, by analysing Figure 5.89, it is possible to say that with a larger diameter, there are slightly higher stress concentrations at the first column's position, likely due to the increase in the size of the pressure bulb under the column with the column's diameter. The scale for the difference plot in Figure 5.89 is different than the scale in Figure 5.27, because, when adopting a non-linear elastic behaviour, the differences in the stress values for different diameters become much higher.

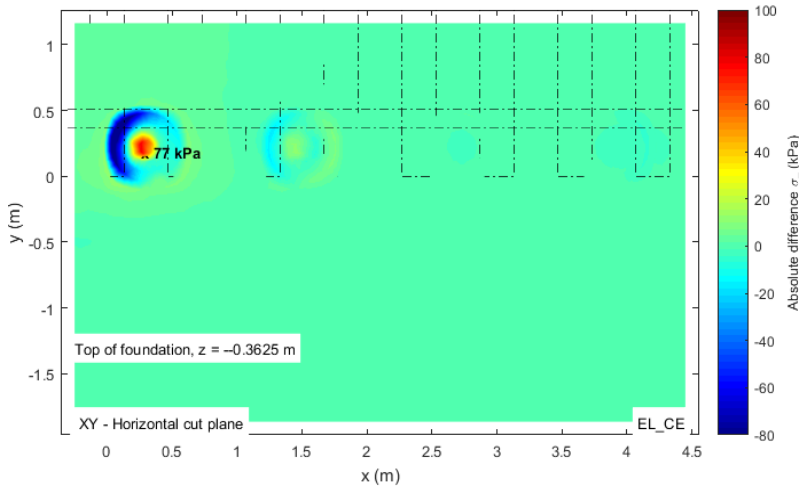

Figure 5.87 - Difference of vertical stress distribution on top of the foundation for different diameters in pattern CE, for non-linear behaviour

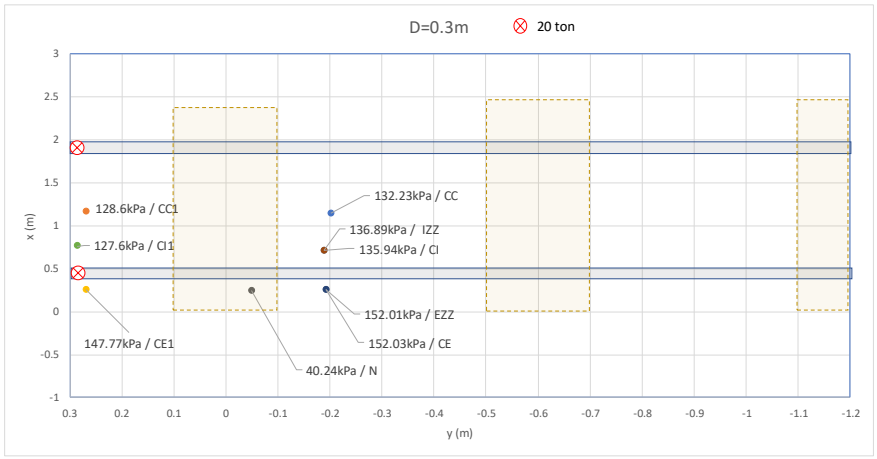

a)

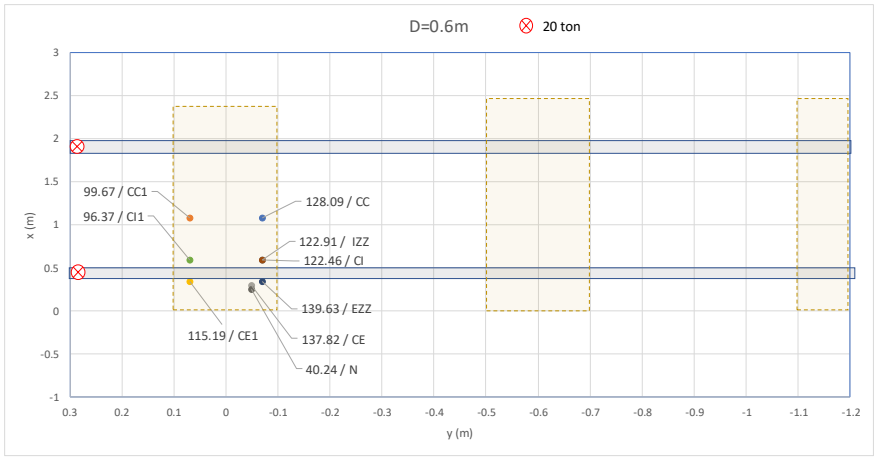

b)

Figure 5.88 - Maximum vertical stress values and their position for different column layouts and diameters (a) D=0.3m and b) D=0.6m) on top of the foundation, for the non-linear behaviour

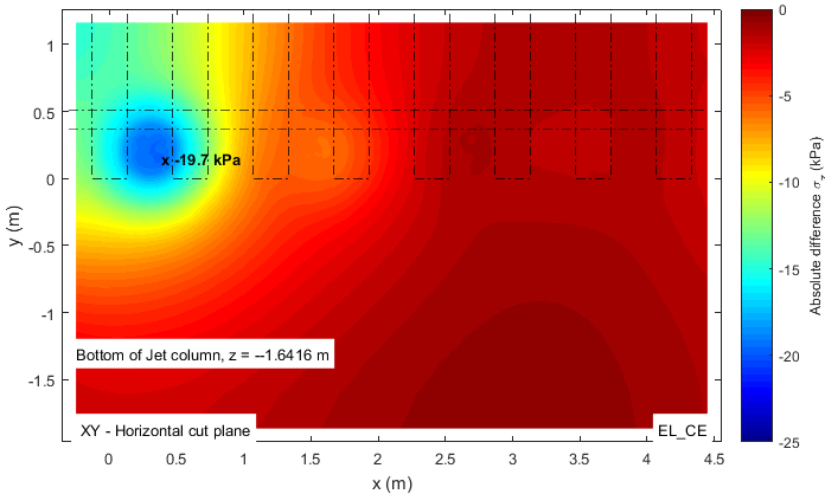

Figure 5.89 - Difference of vertical stress distribution at the bottom of the Jet-grout column for different diameters in pattern CE, for non-linear behaviour.

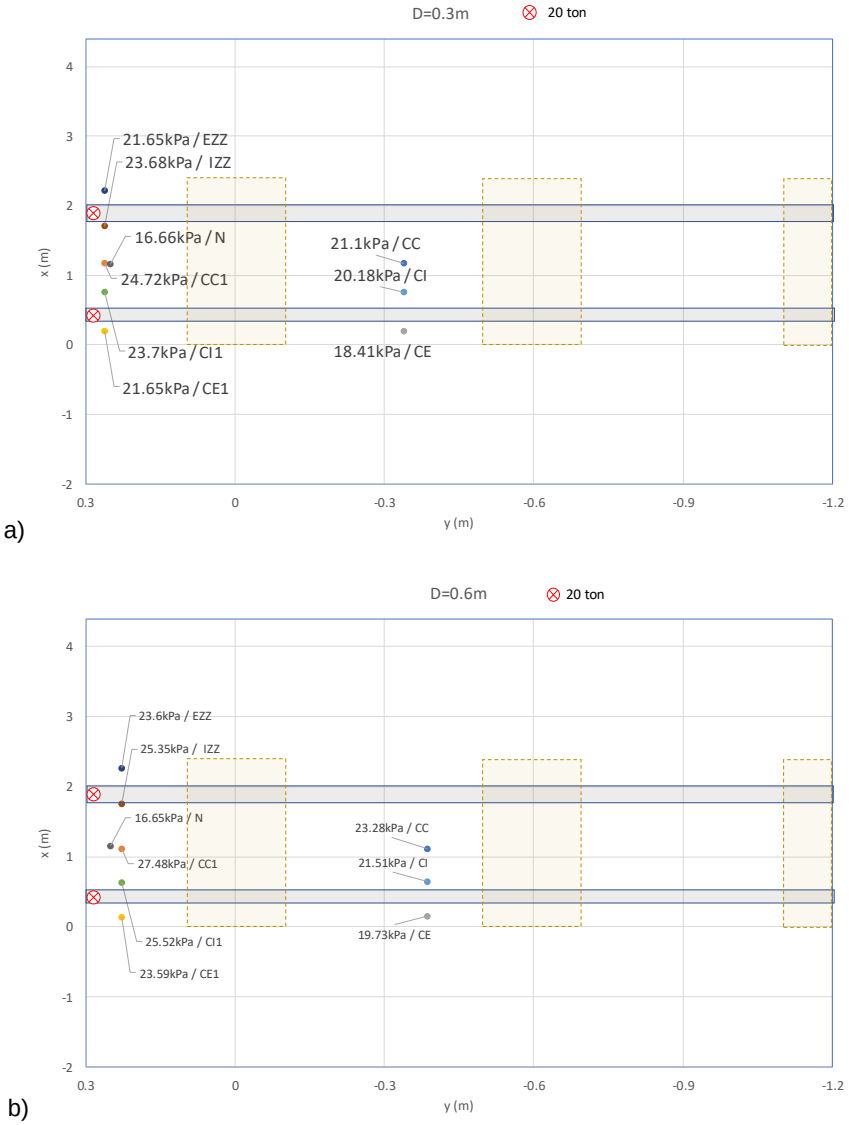

Figure 5.90 - Maximum vertical stress values and their position for different column layouts and diameters (a) D=0.3m and b) D=0.6m) at the bottom of the Jet-grout column, for non-linear behaviour

5.3.1.2 Results at the XZ plane aligned with the rail

The rail's vertical displacement in longitudinal alignment, for column diameters of 0.3 m and 0.6 m, is shown in Figure 5.91. As in the linear elastic behaviour, for all model configurations, the increase of the columns' diameter led to a reduction of the rail's maximum displacement. The upward vertical displacement of the rail, visible between point load distance of 2.5 m and 3.5 m for the linear elastic model, is no longer present in this non-linear analysis. That upper movement of the rail, that was visible in the linear elastic models, could possibly be related to the different support conditions provided by the non-linear behaviour of the ballast and the consequent unrealistic stress distribution in the structure in the linear elastic models. The maximum rail displacements obtained for each model type are shown in Table 5.2.

To compare the rail displacement obtained by the different diameters, the differences of results are presented in Figure 5.92. As in the linear elastic models, the one that showed the least amount of deflection reduction was model CC, due to its internal position of the columns relatively to the rail. The model that presented the best improvement by increasing the column's radius was model CE.

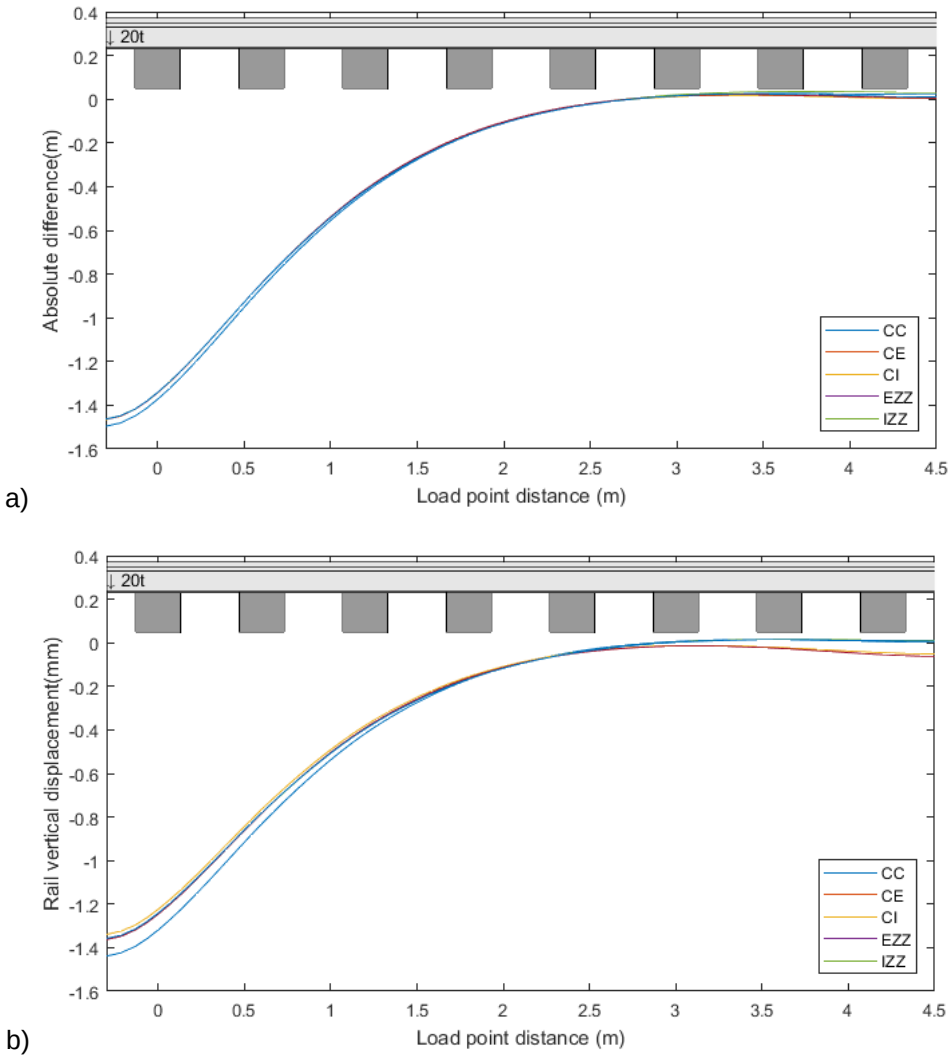

Figure 5.91 - Longitudinal rail displacement for the different models with diameter of a) 0.3 m and b) 0.6 m, for non-linear behaviour

Table 5.2- Maximum rail displacement for different models and diameters, for non-linear behaviour

	Diameter	Unit	CC	CC1	CE	CE1	CI	CI1	CEZZ	CIZZ	N
Rail displacement	0.3 m	mm	1.50	1.50	1.47	1.47	1.46	1.47	1.47	1.46	1.53
	0.6 m		1.44	1.45	1.34	1.37	1.36	1.37	1.36	1.36	1.53

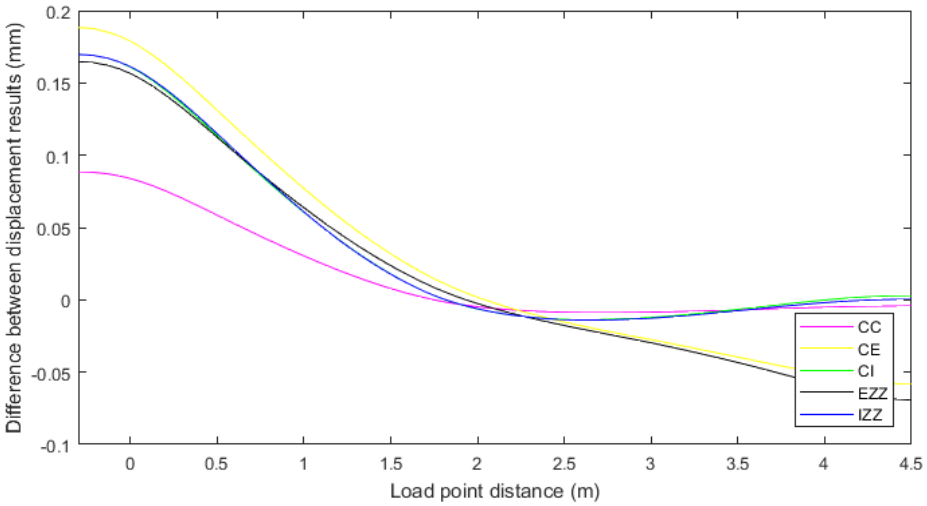

Figure 5.92 - Difference plot between different diameters for results of longitudinal rail displacement, for non-linear behaviour

The difference plot of vertical stress with depth under the rail, between different diameters, is shown in Figure 5.93. Analogously to the elastic model, greater stress concentrations are visible at the columns positions when a larger diameter is chosen, in comparison with D=0.3 m. It is observable how the left side of the column presents higher stress levels, given that by modelling a larger column, stresses are more easily directed to it, since part of the column's cross section is placed under the sleeper.

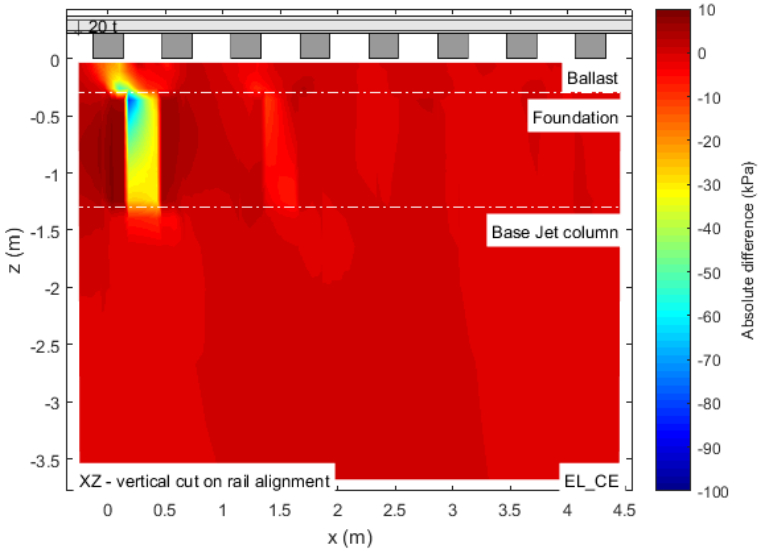

Figure 5.93 - Difference of vertical stress distribution with depth under the rail between different diameters in pattern CE, for a non-linear behaviour

Analysing Figure 5.94, regarding the difference of results for displacement values with depth under the rail, for different diameters, we can see that with a larger diameter, there is a decrease of the vertical deflections underneath the first sleeper

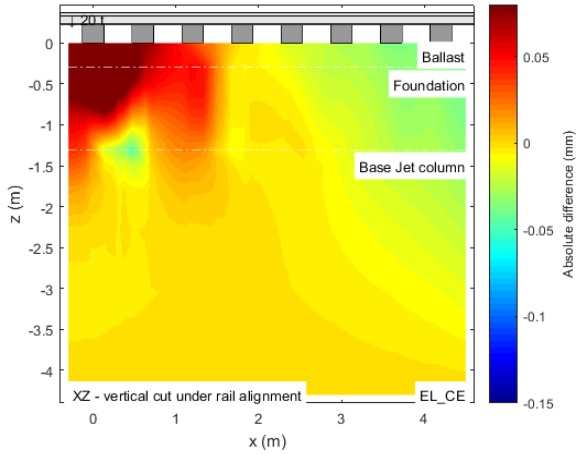

Figure 5.94 - Difference of vertical displacement distribution with depth under the rail, between different diameters in pattern CE, for non-linear behaviour

5.3.2 REINFORCED SUBSTRUCTURE VS NO REINFORCEMENT

In similarity to the linear elastic model, five different patterns for column layout were analysed and compared with a model where no substructure improvement was applied to the foundation. Considering that the observations made in the next sub-sections are generally applicable for all layout types, only the results for the CE model are presented in this section and the remaining ones are presented in the digital annexes.

5.3.2.1 Vertical stresses and vertical displacements at the XY planes

By analysing the vertical displacement results for the non-linear elastic behaviour, the general observations made for the linear elastic model are also applicable to this case. With an improved substructure, somewhat smaller displacements are attained at the top of the ballast and foundation. Beneath the columns, vertical displacements for the improved substructure are slightly higher than the non-improved structure.

With regard to the vertical displacements of the ballast layer, by improving the substructure with a larger column diameter, a stronger reduction of the vertical deflection values is seen in comparison to applying a smaller column. By analysing Figure 5.95, for the difference of results between the N model (reference for all difference plots) and CE model, it is visible the difference of applying a larger or smaller column. With the non-linear elastic behaviour applied to the ballast layer, the reduction of the deflections under the first sleeper covers a larger area, in comparison with Figure 5.38-b), comprising an upgrade of the deflections beneath the second sleeper.

For the displacements on top of the foundation, by applying Jet columns, there is a reduction at its positions, being clear a larger difference for the area underneath the first sleeper, when a larger column is placed, as can be seen in Figure 5.96. However, the improvement attained by employing Jet-columns is not very large, maintaining like the linear elastic model, a maximum reduction of only 0.15 mm, for the greater diameter.

Like the linear elastic behaviour, in the non-linear models, just beneath the Jet-grout columns, the vertical deflection results are higher at the columns' positions for the improved substructure models, as can be seen for the difference plot in Figure 5.97. Comparing the difference plots in Figure 5.42 and Figure 5.97, there is almost no difference, meaning that considering the non-linear elastic behaviour does not reproduce very different results from the linear elastic behaviour at this level.

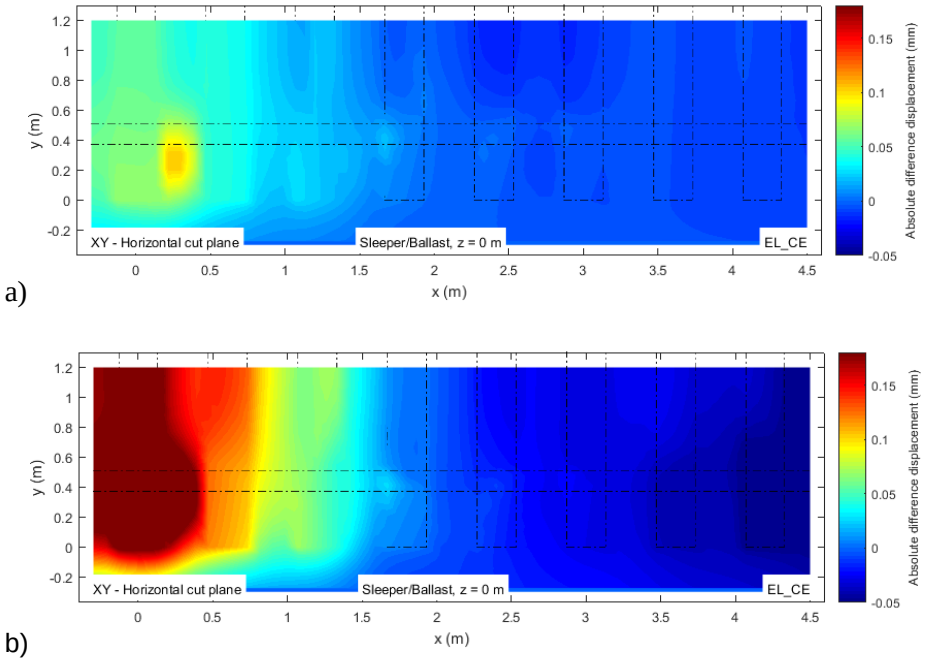

Figure 5.95 - Difference of vertical displacement distribution on top of the ballast layer between models CE and N, for a) D=0.3 m and b) D=0.6 m, for non-linear behaviour

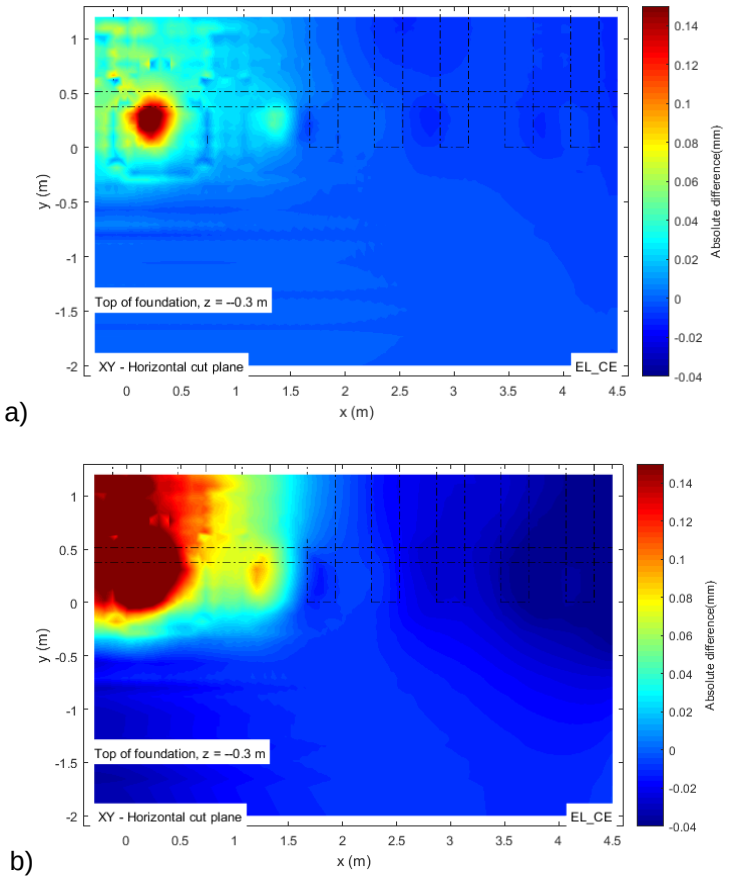

Figure 5.96 - Difference of vertical displacement distribution on top of the foundation between models CE and N, for a) D=0.3 m and b) D=0.6 m, for non-linear behaviour

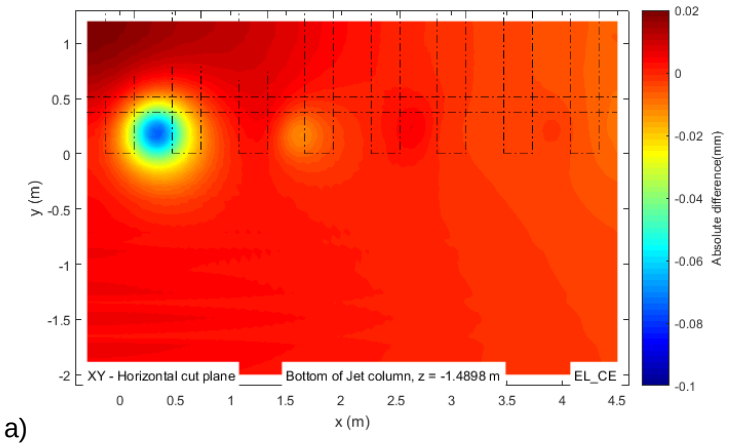

a)

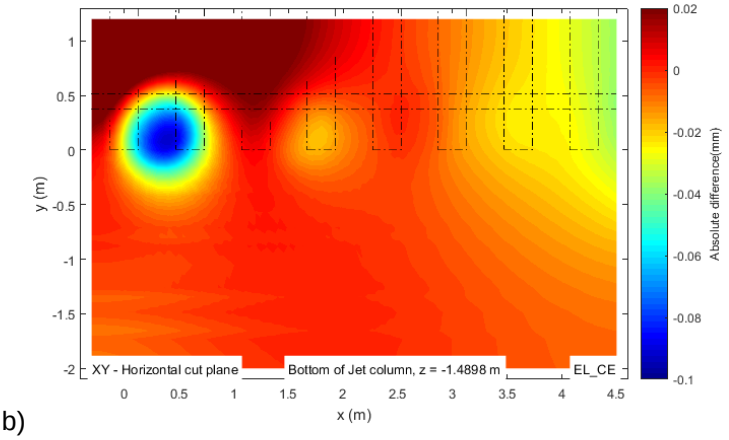

b)

Figure 5.97 - Difference of vertical displacement distribution at the bottom of the Jet-grout column between models CE and N, for a) D=0.3 m and b) D=0.6 m, for non-linear behaviour

The plot of differences of vertical stress on top of the ballast layer is shown in Figure 5.98. Most of the general observations made for the linear models are valid for the non-linear models. By implementing the columns, we can see there is a difference in the stress values. There is a stress reduction at the edges and middle of the first sleepers, in comparison to the stresses developed in a model without substructure improvement. Under the first sleepers we can see an increase in stress, in a circular region, possibly meaning that a load path is being formed, concentrating higher stresses in positions closer to the columns for model CE comparatively to model N. If we compare the plot in Figure 5.98 with that in Figure 5.44, it is observable that, for the non-linear elastic behaviour, at the sleepers' edges slightly higher stresses are appearing in an improved substructure model, especially in the second sleeper. Also, the first circular region where larger stresses are appearing, for both diameters, is apparently more loaded and the second circle of stress concentration beneath the second sleeper is slightly smaller than in the linear elastic models.

As regards stresses at the bottom of the ballast, comparing the non-improved substructure with improved one in Figure 5.99, it is visible that larger stresses are concentrating at the columns' positions and that the stresses throughout the foundation are nearly the same for models with improvement or without. Between the elastic and the non-linear elastic, there are no significant differences in overall appearance of the contour plot. For the elastic behaviour, by analysing Figure 5.46, the circular regions where higher stresses concentrate, are slightly wider and comprise slightly higher stresses than the k-θ models. Also, in the ballast soil surrounding the column, slightly higher stresses are concentrating in that area, for the linear elastic models in comparison with the non-linear ones.

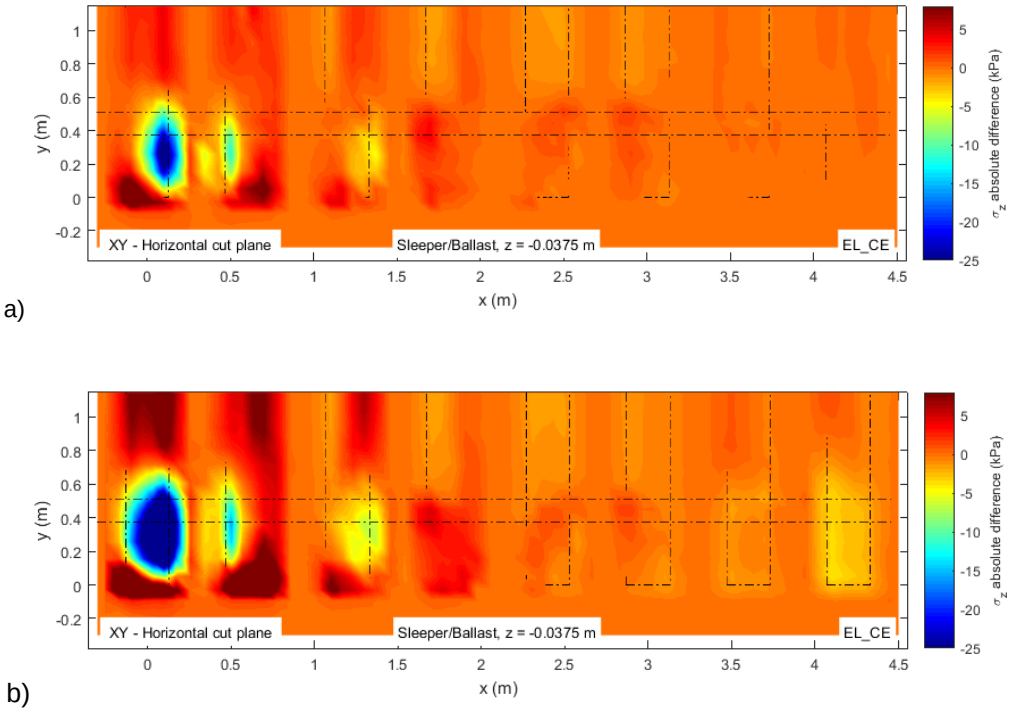

Figure 5.98 - Difference of vertical stress distribution at the top of the ballast layer between models CE and N, for a) D=0.3 m and b) D=0.6 m, for non-linear behaviour

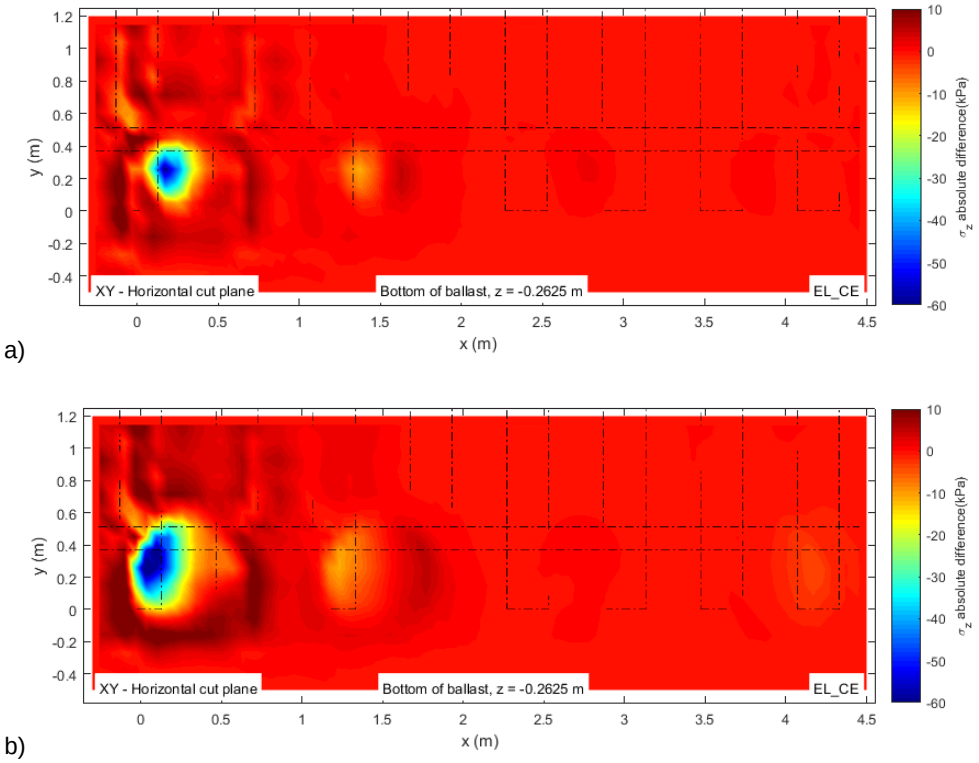

Figure 5.99 - Difference of vertical stress distribution on bottom of the ballast layer between models CE and N, for a) D=0.3 m and b) D=0.6 m, for non-linear behaviour

Analysing the difference plot for the stresses developed on top of the foundation in Figure 5.100, it is visible, in resemblance to the linear elastic models, that higher stresses develop in the columns' locations, in comparison to model N. In the rest of the layer, stress values maintained nearly equal to the N model. When comparing a non-improved substructure with an improved substructure, for the k-θ models, there is a smaller stress concentration in the columns' positions, in comparison with the linear elastic models. This observation is clear by comparing Figure 5.48 with Figure 5.100.

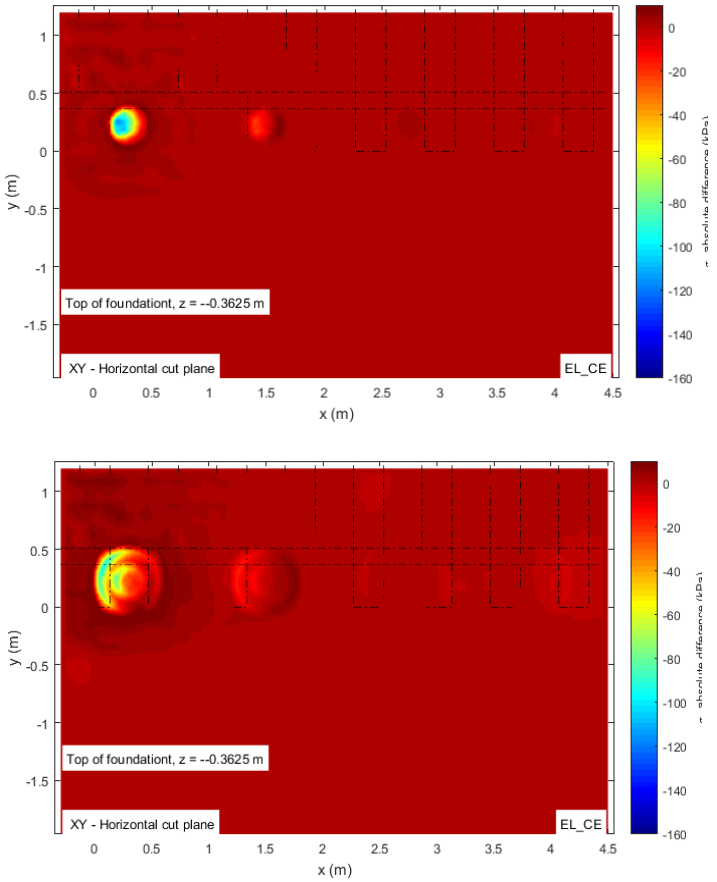

Figure 5.100 - Difference of vertical stress distribution on the top of the foundation between models CE and N, for a) D=0.3 m and b) D=0.6 m, for non-linear behaviour

The difference plots between model CE and model N for vertical stress results at a depth underneath the Jet-grout column are presented in Figure 5.101. By analysing this figure and comparing with Figure 5.50, it is visible that the behaviour is quite similar between the non-linear and linear models. In both pictures, it is visible the circular regions that are originated underneath the column's position, suggesting higher stresses when Jet-grout columns are placed. Between both material models, we can see that slightly higher stresses are developing beneath the Jet column when the linear elastic model is chosen.

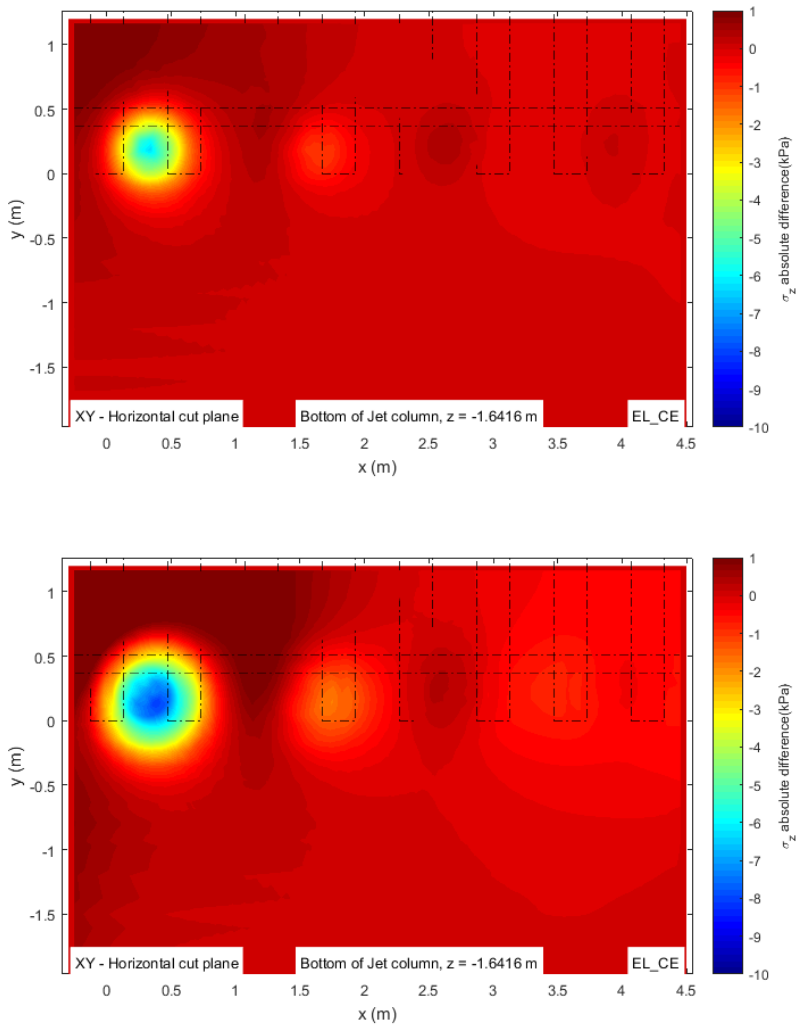

Figure 5.101 - Difference of vertical stress distribution on the top of the foundation between models CE and N, for a) D=0.3 m and b) D=0.6 m, for non-linear behaviour

5.3.2.2 Vertical stresses and vertical displacements at the XZ plane aligned with the rail

Regarding the rail's vertical displacement in the longitudinal alignment, whether we consider a non-linear or linear law for the ballast's behaviour, by implementing the Jet-grout columns, smaller rail displacements were obtained for all models. In the non-linear models, there is a slight difference, performance-wise, if we chose different column diameters. When opting for a smaller column, the interior placed layouts (CI and CIZZ) showed a higher reduction in rail displacement, compared with no improvement at all. By increasing the column's diameter, the one that showed better performance was the model CE, reducing rail displacement in almost 0.2 mm, as we can see in Figure 5.102.

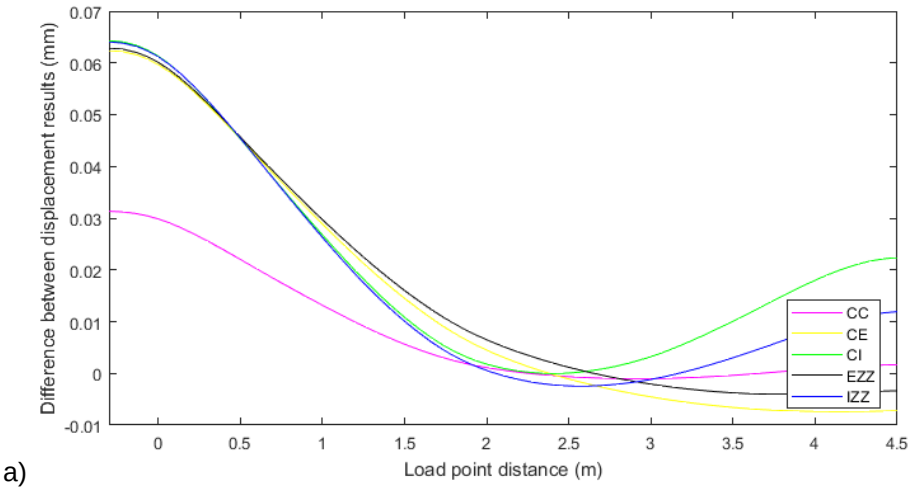

a)

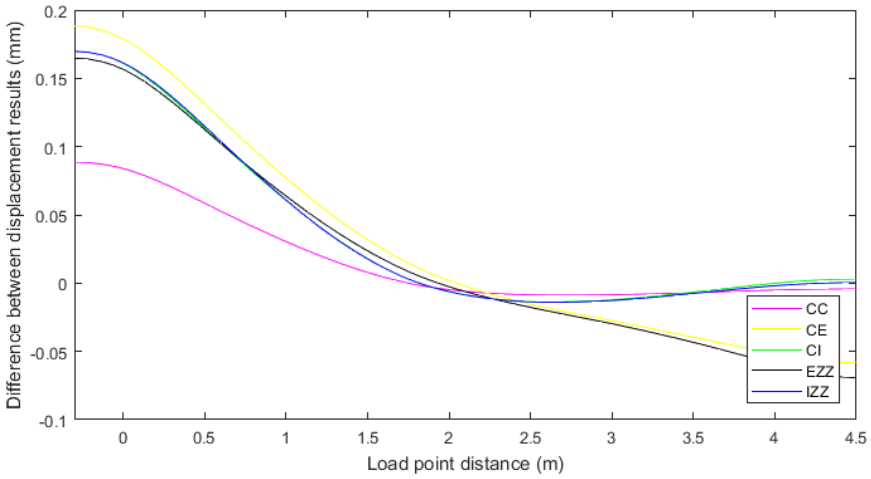

b)

Figure 5.102 - Difference plot between models with substructure improvement and model without improvement, for results of longitudinal rail displacement, for a) D=0.3 m and b) D=0.6 m, for non-linear behaviour

For the vertical stress distribution with depth, under the rail, the general observations made for the linear elastic behaviour are also valid for the non-linear elastic behaviour, as can be seen by comparing Figure 5.54 and Figure 5.103. Apparently, a larger amount of load are being led to the column, in the linear models. With the non-linear elastic model, the stress values on the surrounding soil of the column are higher for the N model, in comparison with the CE model. This difference in stress values is even larger when the elastic linear behaviour for the ballast layer is chosen.

When analysing the vertical displacements with depth, once more, most of the observations made for the elastic behaviour are valid for the k- θ models. As mentioned before, a zone of larger displacements underneath the first sleeper occurs and displacements decrease with depth. By improving the substructure, deflections reduce under the first sleeper. Beneath the Jet-grout column, a zone of higher displacements appears, when placing a column. The k-θ model, in comparison to the linear elastic model, presents a higher difference between displacement values for the CE model and N model, under the first sleeper.

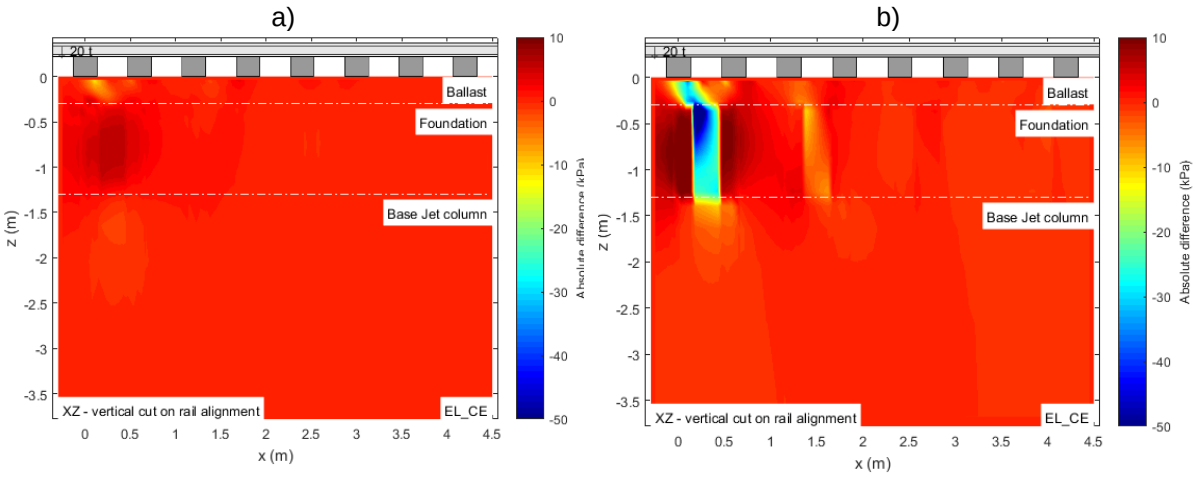

Figure 5.103 - Difference of vertical stress distribution with depth under the rail, between models CE and N, for a) D=0.3 m and b) D=0.6 m

5.3.3 SUMMARY OF VERTICAL STRESSES AT IMPERATIVE LOCATIONS

Considering that, for this analysis, the contour plots shown in the previous subchapter only demonstrated that displacements and stresses are smaller/higher when a column is present and that the behaviour explained is also valid for the non-linear analysis, whether for the XY or XZ planes, only the query points of stresses as referenced in Figure 5.69 will be analysed herein.

Comparing the plots in Figure 5.70, Figure 5.72 and Figure 5.73, for the linear elastic behaviour, with the plots in Figure 5.104, Figure 5.105 and Figure 5.106, for the non-linear elastic behaviour, there is quite some resemblance in the behaviour demonstrated in all plots. For instance, by querying a point where there is a column nearby, the vertical stress is higher than in other query points, meaning that stresses are being directed to the columns. Also, most of the queried points demonstrated that, by implementing Jet columns on the substructure, there is a stress reduction in the substructure surrounding the column, in comparison with the original stresses.

However, the overall magnitude of stresses, for the bottom of the ballast layer and top of the foundation, are smaller for the non-linear models. At a depth just beneath the base of the Jet-grout columns, the amplitude of vertical stresses is somewhat the same for both material behaviours. This could mean that, even when a non-linear elastic behaviour is implemented to the ballast layer, there is practically no significant influence in stress values at deeper layers when changing material behaviour. Moreover, it is visible that the stress levels are significantly lower at deeper layers, and in that situations, it is reasonable to consider the substructure behaviour as linear elastic (Paixão & Fortunato, 2010, Paixão [et al.], 2016b).

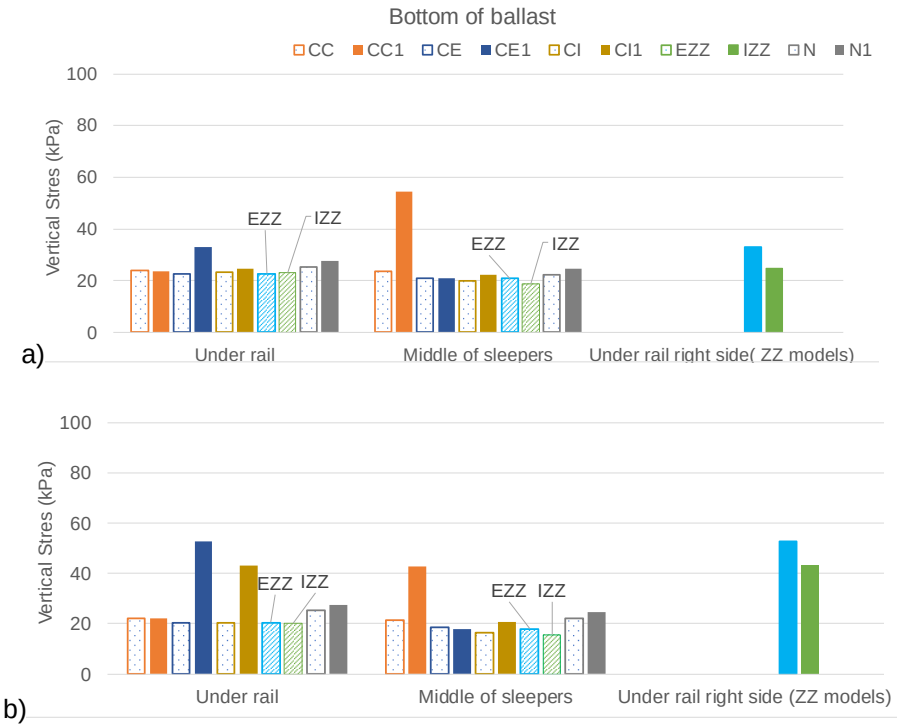

Figure 5.104 - Vertical stress values at the bottom of the ballast layer, for the different column layouts, at the query points specified in Figure 5.69 for a) 0.3 m diameter and b) 0.6 m diameter, for non-linear behaviour

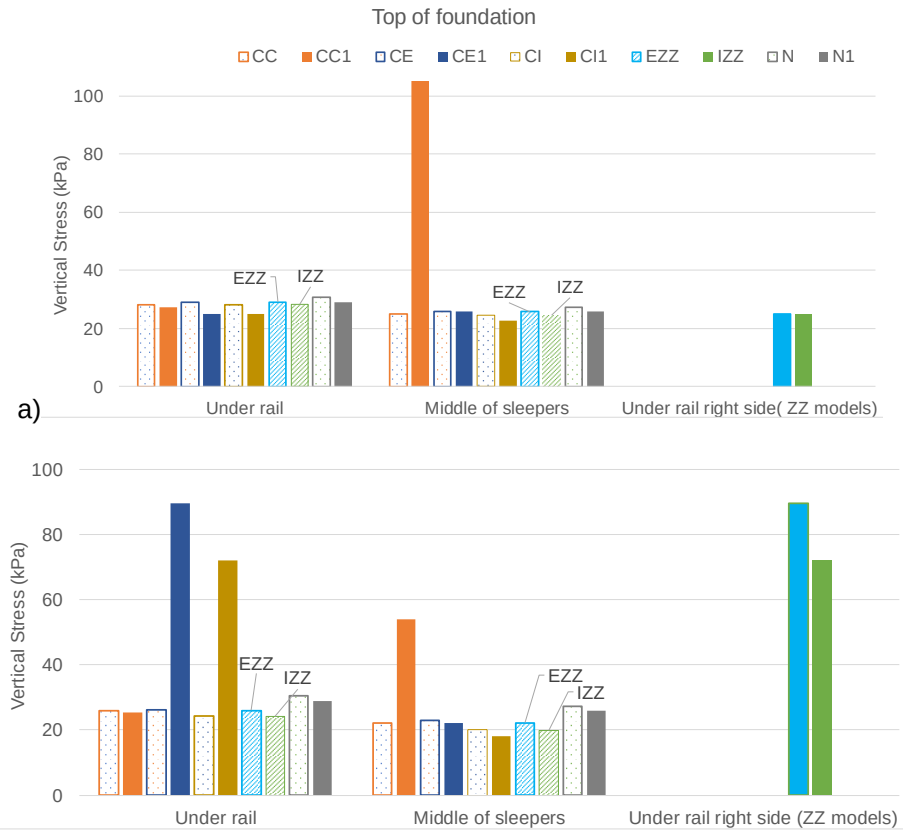

Figure 5.105 - Vertical stress values at the top of the foundation, for the different column layouts, at the query points specified in Figure 5.69 for a) 0.3 m diameter and b) 0.6 m diameter, for non-linear behaviour

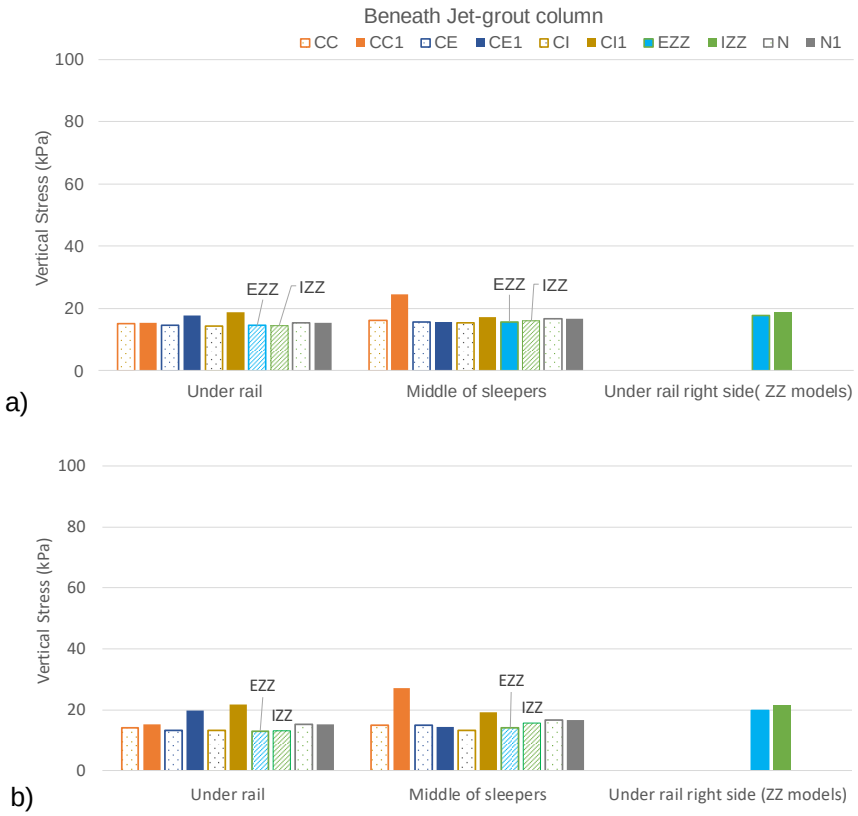

Figure 5.106 - Vertical stress values beneath the Jet-grout column, for the different column layouts, at the query points specified in Figure 5.69 for a) 0.3 m diameter and b) 0.6 m diameter, for non-linear behaviour.

5.3.4 IMPACT ON THE TRACK VERTICAL STIFFNESS

For the non-linear elastic analysis, the vertical stiffness coefficient was also calculated by Eq. (6), considering the same wheel load value as in the linear elastic calculations (100 kN) and maximum deflection values shown in Table 5.2. Results for vertical stiffness coefficients, for each model designed, are presented in Figure 5.107.

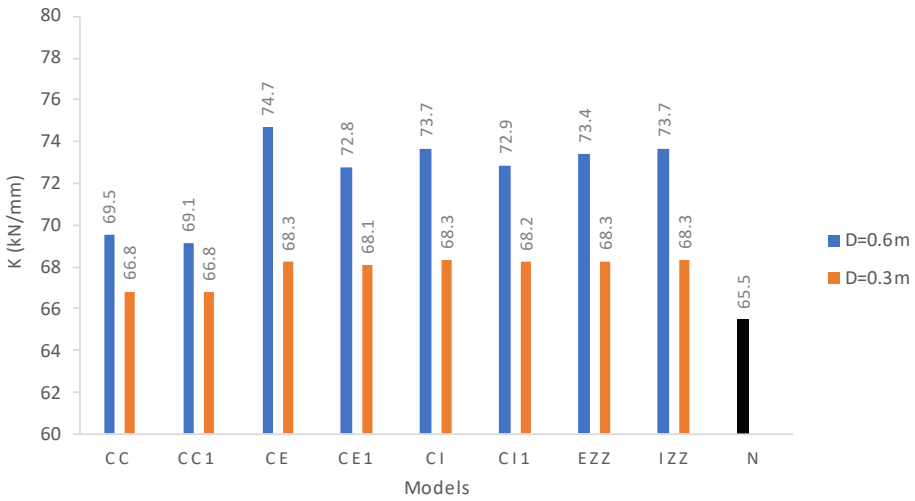

Figure 5.107 - Vertical stiffness coefficients for different model types and column diameter size, for non-linear behaviour

Similar to the linear elastic response, by improving the substructure, the track's vertical stiffness coefficient increased. With the diameter's increase, so did the coefficient. In the models with two columns per pair of sleepers (all except CC and CC1), the vertical stiffness increases from about 68 kN/mm to about 73 kN/mm when the column's diameter is increased from 0.3 to 0.6 m. Again, it is also noted a very small decrease in the vertical stiffness (less than 1 kN/mm) when the load is applied in the sleeper spans where a column is present, compared to the situation where the wheel load acts on the same vertical plane where the column is. The model that showed the highest vertical stiffness coefficient was model CE, for the largest diameter (K_v = 74.7 kN/mm), and model CI, for the smallest diameter (68.3 kN/mm). Once more and as expected, the model that presents the lowest vertical stiffness, for both diameters, is CC1 with K_v = 69.1 kN/mm and 66.8 kN/mm, respectively for D = 0.6 and D = 0.3 m

5.4 LINEAR ELASTIC BEHAVIOUR VS NON-LINEAR ELASTIC BEHAVIOUR IN THE BALLAST LAYER

After analysing the influence of the load position, the column diameter and the difference of having or not having substructure improvement for the different material behaviours assigned to the ballast layer, one must compare the response obtained for each material behaviour.

For this comparison, since the observations made here were verified throughout all models, the results for the CE model and larger diameter will be presented and analysed, being that the remaining are shown in the digital annexes. Once more, the comparison between the two types of ballast material behaviours was made with contour plots of differences, where the linear elastic behaviour was considered as reference.

5.4.1 VERTICAL STRESSES AND VERTICAL DISPLACEMENTS AT THE XY PLANES

To examine the difference in vertical displacements occurring on top of the ballast layer between the different model behaviours, Figure 5.108 presents the plot of differences between results. It is visible that, for the non-linear model, displacements under the first three sleepers are generally higher in comparison with the linear elastic results. However, that difference is not so relevant, reaching a maximum of around 0.1 mm. In between sleepers, vertical deflections are generally lower for the non-linear model, especially between the first two.

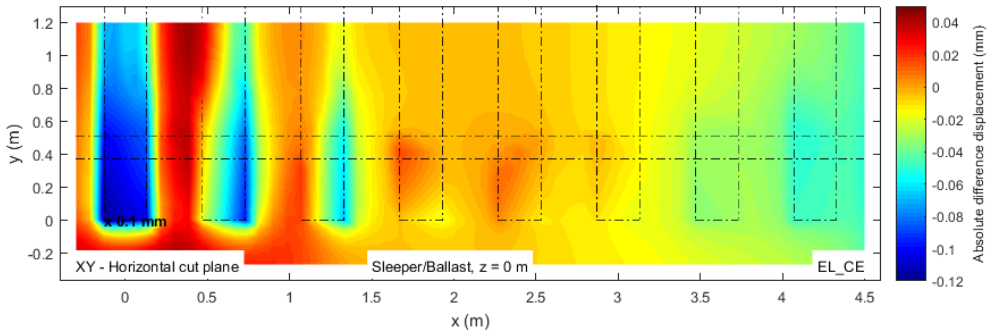

Figure 5.108 - Difference of vertical displacement distribution at the top of the ballast layer between non-linear elastic behaviour and linear elastic behaviour, for model CE

Regarding the plot of differences for vertical displacements on top of the foundation in Figure 5.109, it is noticeable that the region comprehended between the first two sleepers has lower displacements in the non-linear model, in comparison with the one with linear behaviour. Since the configuration presented is the one where the Jet-grout columns are placed externally to the rail, in between sleepers, it is observable that the reduction of the deflections, in the non-linear model, has sort of a circular region, positioned where there is a column. Throughout the rest of the foundation, in general, displacements are slightly larger for the non-linear model. Still, it should be noticed that the difference between the linear

elastic and the non-linear elastic displacement results is minimal, ranging from 0.06 mm less to 0.04 mm more.

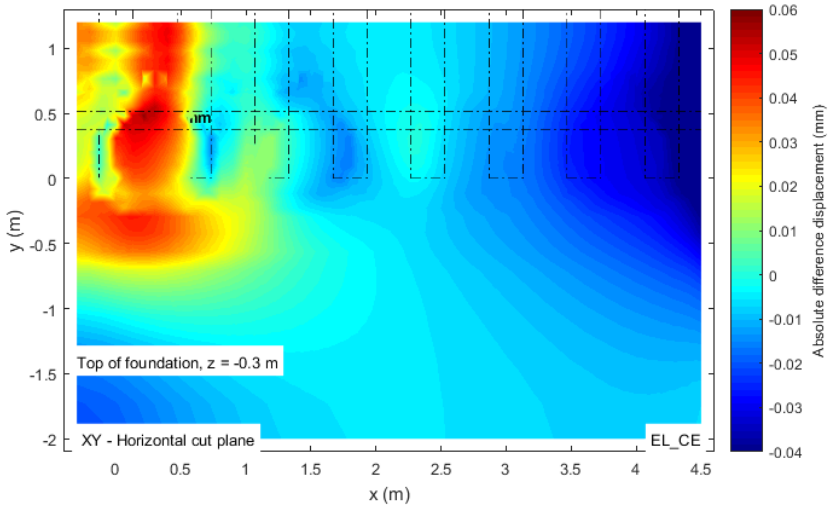

Figure 5.109 - Difference of vertical displacement distribution at the top of the foundation between non-linear elastic behaviour and linear elastic behaviour, for model CE

Concerning vertical displacements at a level beneath the Jet-grout column, Figure 5.110 shows the difference between results for non-linear and linear elastic behaviour. Once more, the difference between displacement results is not very high. Lower displacements are occurring in an area just beneath the Jet column, under the first two sleepers, in comparison to the linear elastic model. Most of the extension of the foundation, in general, shows slightly larger displacements for the non-linear model.

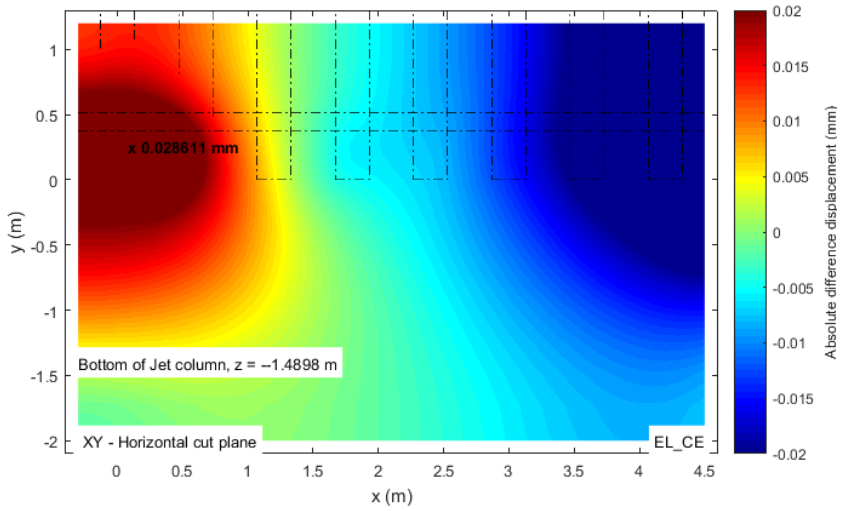

Figure 5.110 - Difference of vertical displacement distribution at a depth beneath the Jet-grout column between non-linear elastic behaviour and linear elastic behaviour, for model CE

To examine the vertical stresses on top of the ballast layer, the plot of differences between stress values is shown in Figure 5.111. By analysing this contour plot, we can see that the major stress differences are concentrated beneath the first three sleepers' edges. One side of the first sleeper's transverse edge presents around 20 kPa higher stress values for the model with non-linearity. On the other hand, the other side of the sleeper presents higher stress values on the linear elastic model by approximately the same amount. For the following two sleepers, the opposite occurs at their edges. The first sleeper's stress distribution may suggest that, in the non-linear analysis, the first sleeper might be suffering some

rotation due to the loading and that the remaining sleepers are stressing the ballast under them more than in the linear elastic analysis.

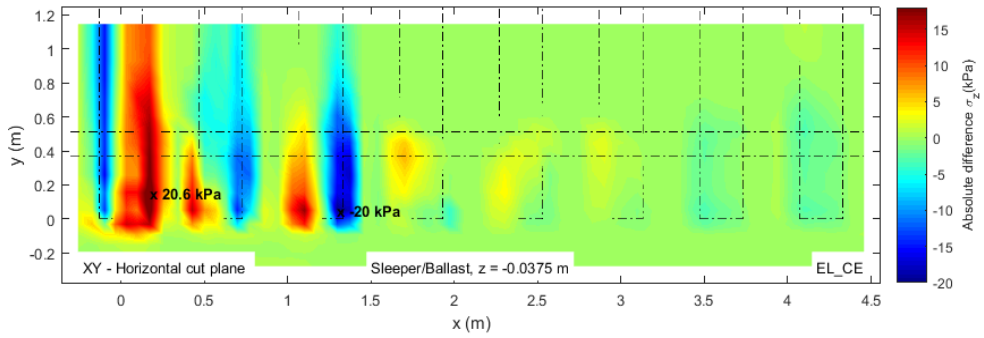

Figure 5.111 - Difference of vertical stress distribution at the top of the ballast layer between non-linear elastic behaviour and linear elastic behaviour, for model CE

Regarding the vertical stress on top of the ballast layer, Figure 5.112 shows the contour plots both for the linear and non-linear elastic behaviour. Despite the fact that for this model, by chance, the maximum stress value for both behaviours is the same, it is observable a difference in the shape of the highly stressed circular area, where a column is positioned. Comparing both plots, we can see that for the linear elastic behaviour the area of stress spreading is somewhat larger than in Figure 5.112-b). In the non-linear elastic, stresses are concentrating mainly beneath the first sleeper but in the linear elastic, the stress spreading reaches the middle of the span between the first two sleepers. Also, it is visible that the second column has slightly smaller stresses, in the non-linear model.

The plot of differences for vertical stress values is shown in Figure 5.113. It is visible a circular region where the first column is positioned suggesting smaller stresses at that location for the non-linear model. This difference in the stress value is somewhat substantial, surpassing 20 kPa for some models. At the rest of this layer, in general, stresses are slightly higher for the non-linear elastic behaviour. At the position of the second column (x = 1.5), we can see that stresses are slightly higher at that location, in the non-linear elastic behaviour. This could mean that, in the non-linear elastic behaviour, the stresses are being more redistributed throughout the adjacent columns, instead of concentrating them at the first columns as in the linear elastic model. This behaviour will be addressed in more detail later in the next sub-section.

The observations made for Figure 5.113 are valid for Figure 5.114, which concerns the comparison of vertical stress values for the top of the foundation.

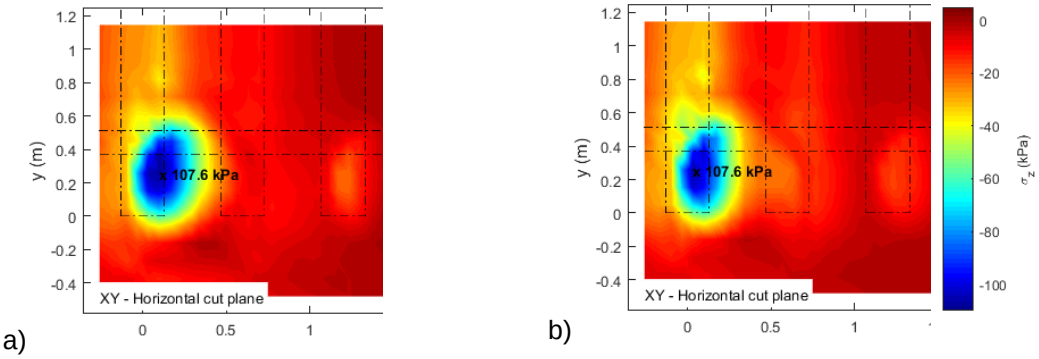

Figure 5.112 - Vertical stress distribution on bottom of the ballast layer in pattern CE, for a) linear elastic and b) non-linear elastic behaviour.

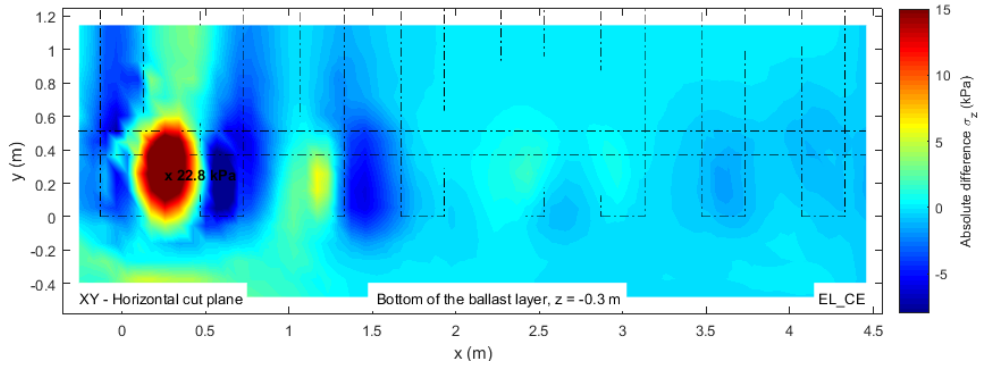

Figure 5.113 - Difference of vertical stress distribution at the bottom of the ballast layer between non-linear elastic behaviour and linear elastic behaviour, for model CE

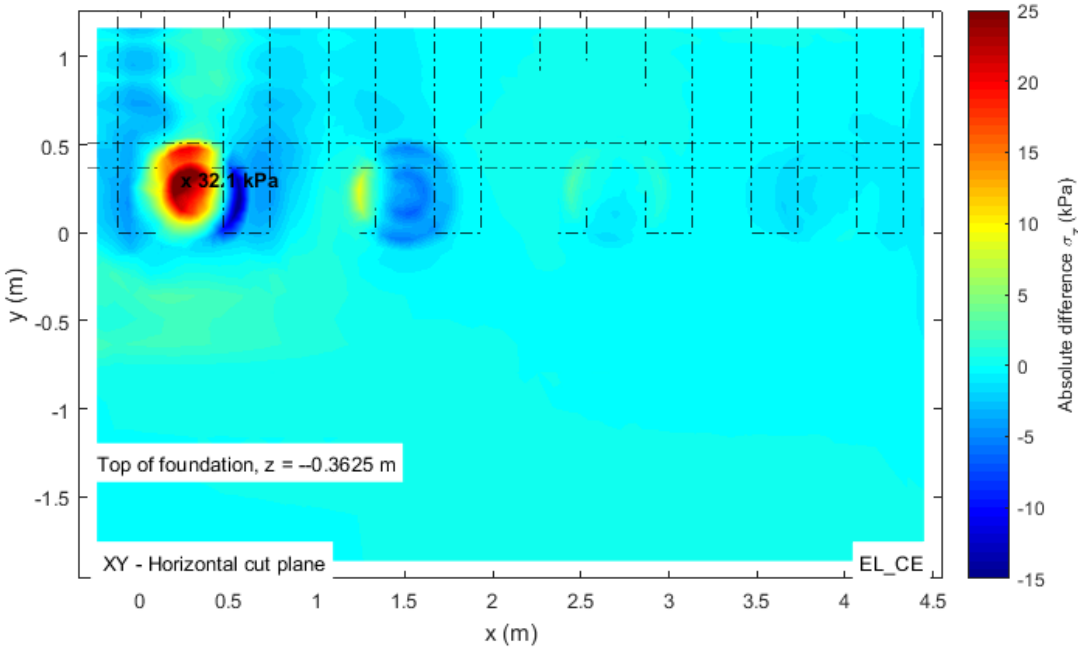

Figure 5.114 - Difference of vertical stress distribution at the top of the foundation between non-linear elastic behaviour and linear elastic behaviour, for model CE

Regarding the vertical stress distribution beneath the Jet-grout column, the plot of differences of stress results between the different material behaviours is shown in Figure 5.115. It is visible that, beneath the first column, stresses are slightly smaller for the model with the non-linear elastic behaviour at the ballast layer. Underneath the second column, the opposite occurs. However, this difference between stress results is very small, as mentioned previously in other analysis.

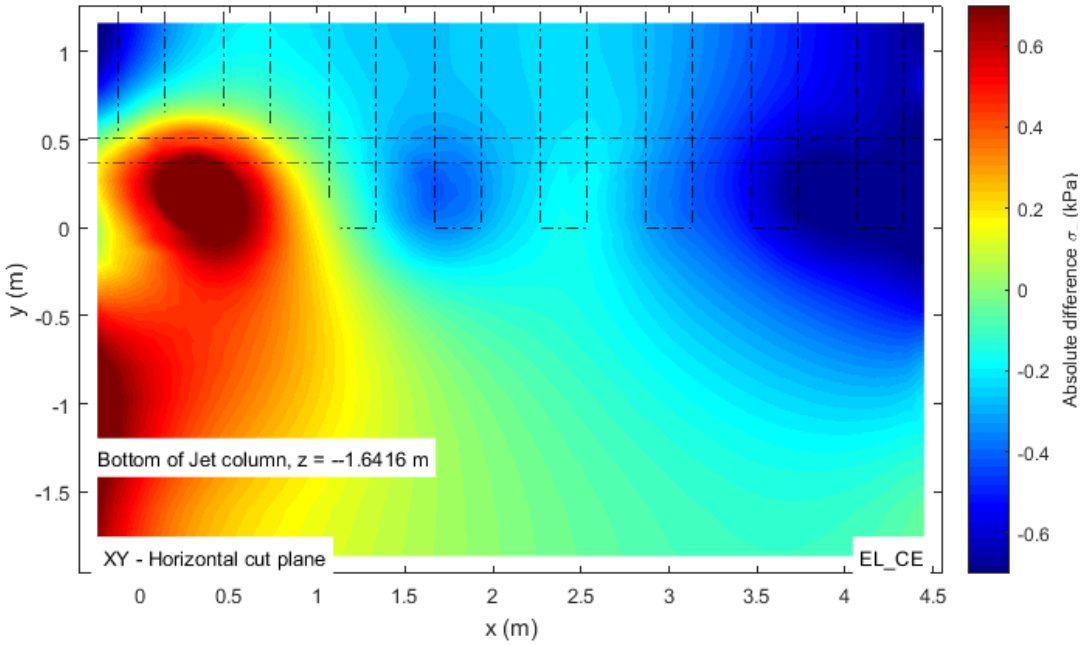

Figure 5.115 - Difference of vertical stress distribution at a depth beneath the Jet-grout column between non-linear elastic behaviour and linear elastic behaviour, for model CE

5.4.2 VERTICAL STRESSES AND VERTICAL DISPLACEMENTS AT THE XZ PLANE ALIGNED WITH THE RAIL

To compare the vertical rail displacement undergone by the different models, Figure 5.116 presents the plot of differences between results for linear elastic and non-linear elastic behaviour. By adopting a non-linear elastic behaviour for the ballast layer, higher maximum rail displacements were obtained, particularly for model CEZZ. Once more, the differences between displacement results are quite small.

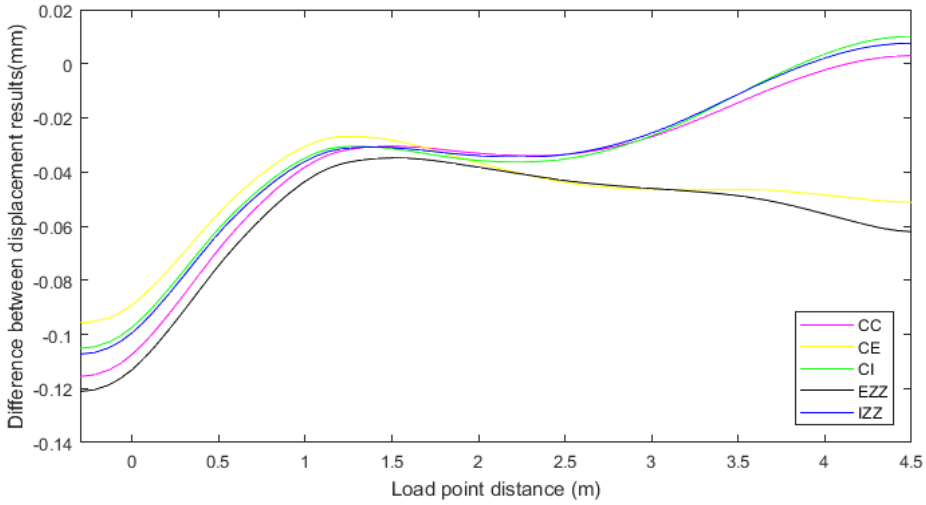

Figure 5.116 - Difference plot between models with linear elastic and non-linear elastic, for results of longitudinal rail displacement

Analysing the differences between the non-linear and linear elastic models in Figure 5.117, it is visible that, for the vertical displacements with depth, under the rail, the differences between plot a) and b) are not very large. The main difference is beneath the first three sleepers, inside the ballast layer, where displacements are larger for the non-linear elastic model as it is visible in Figure 5.118. At a column's

position, there are also some differences in the results, existing smaller displacement for the non-linear elastic behaviour. Nevertheless, this difference is quite small.

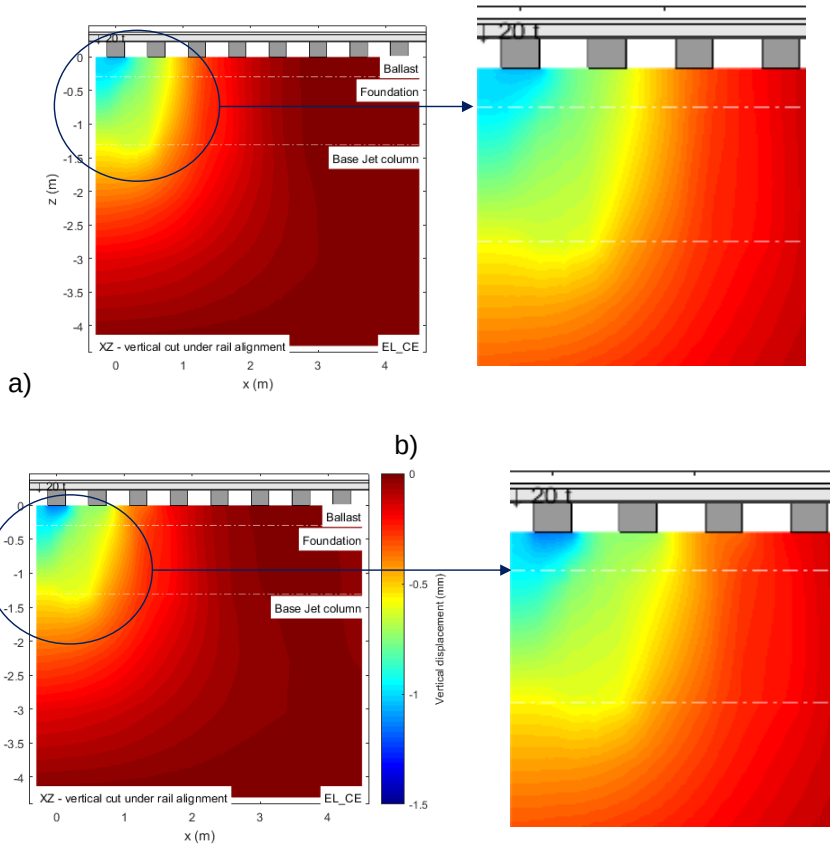

Figure 5.117 - Vertical displacement distribution with depth under the rail, in pattern CE, for a) linear elastic and b) non-linear elastic behaviour.

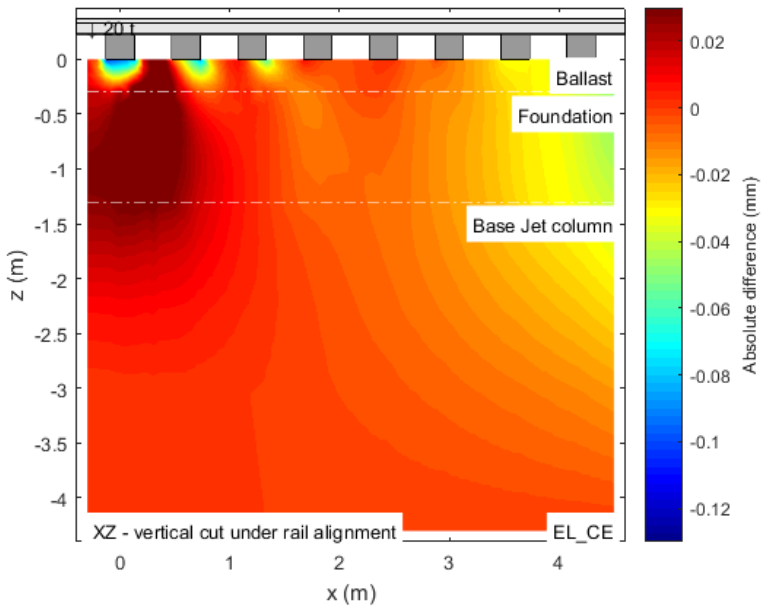

Figure 5.118 - Difference of vertical displacement with depth, under the rail, between non-linear elastic behaviour and linear elastic behaviour, for model CE

Figure 5.119 presents a zoom in on the location of the first two columns, regarding the plots of vertical stress with depth, for different behaviours attributed to the ballast layer. Comparing the plots a) and b), it is visible that the first column is being less loaded at its left side, in the non-linear model, in comparison with plot a). Another remark is that, right beneath the first sleeper, the zone where higher stresses are concentrating seems narrower in the linear model. In the non-linear model, the blue region envelops entirely the base of the first sleeper; however, the load path to the column becomes narrower at the bottom of the ballast layer. Also, in the non-linear elastic behaviour, beneath the remaining sleepers there is an increase on the vertical stress value, in comparison to the linear behaviour. Regarding the loading at the columns, it seems that by considering a non-linear elastic behaviour for the ballast layer, the second column is slightly more loaded than in the linear-elastic models.

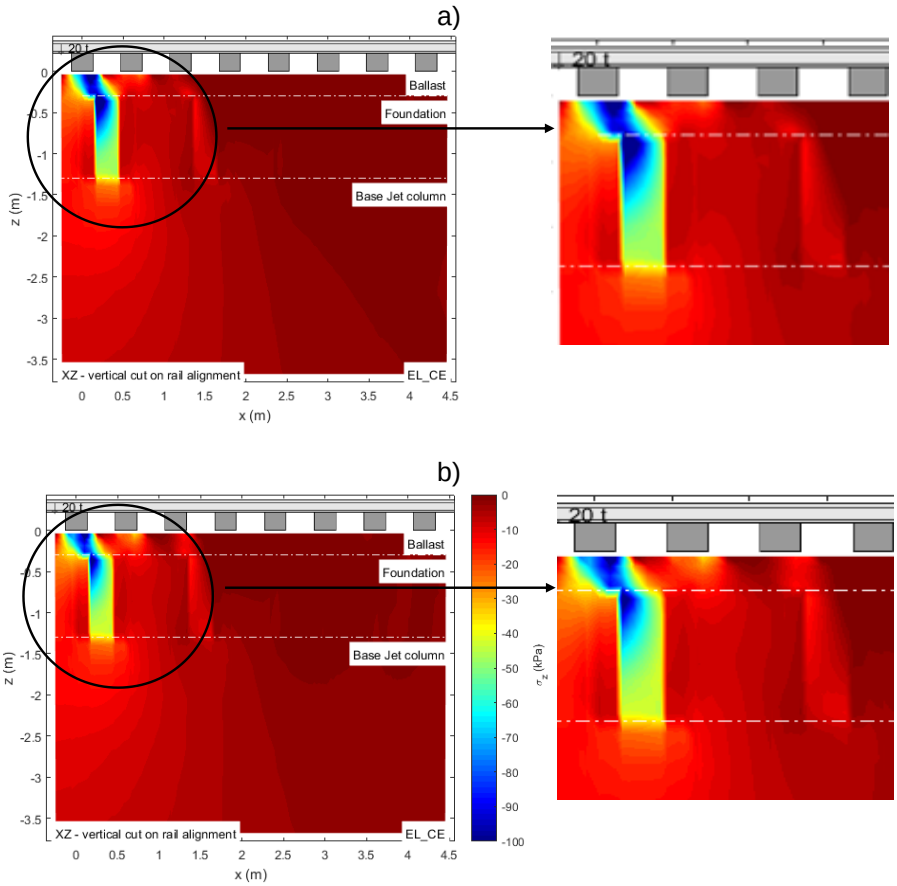

Figure 5.119 - Vertical stress distribution with depth under the rail, in pattern CE, for a) linear elastic and b) non-linear elastic behaviour.

To better understand these variances, the plot of difference between different behaviours for the ballast layer is shown in Figure 5.120. The main differences between the linear and non-linear elastic behaviour are in the stresses developed beneath the sleepers at the ballast layer, the load path created and the stresses generated at the column. At the ballast layer, it is visible how larger stresses are being generated beneath each sleeper, for the non-linear analysis. This is an expected behaviour, since elements that suffer higher loading conditions, such as the ballast particles beneath the sleepers, undergo higher elastic modulus increments, due to the k-θ law, concentrating higher stresses. In this difference plot, it is visible how the right side of the second column presents higher stresses, thus is more loaded when a non-linear elastic law is adopted for the ballast layer. The stresses developed in the first column are higher when the linear behaviour is chosen for the ballast layer, possibly meaning that with that elastic law, the load is being more directly transmitted to the column.

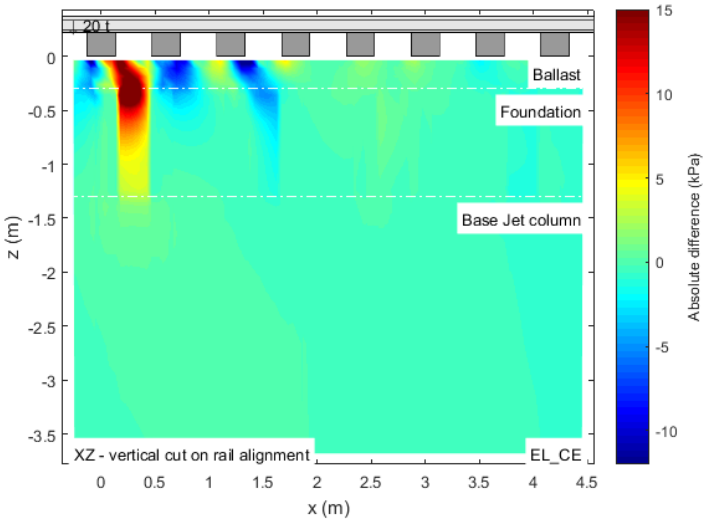

Figure 5.120 - Difference of vertical stress with depth, under the rail, between non-linear elastic behaviour and linear elastic behaviour, for model CE

Despite the previous statements, it was expected that the stresses in the columns would be higher when adopting a non-linear elastic behaviour for the ballast layer, in comparison to the linear elastic models. To better understand this three-dimensional phenomenon of stress spreading into the ballast, the tensors of principal stresses inside the mesh were analysed. Figure 5.121 shows the principal stress tensors, inside the ballast layer, for model CI. It is noted that the principal stresses represented in Figure 5.121-b) have the contribution of the gravitational load, which at this depth is somewhat neglectable.

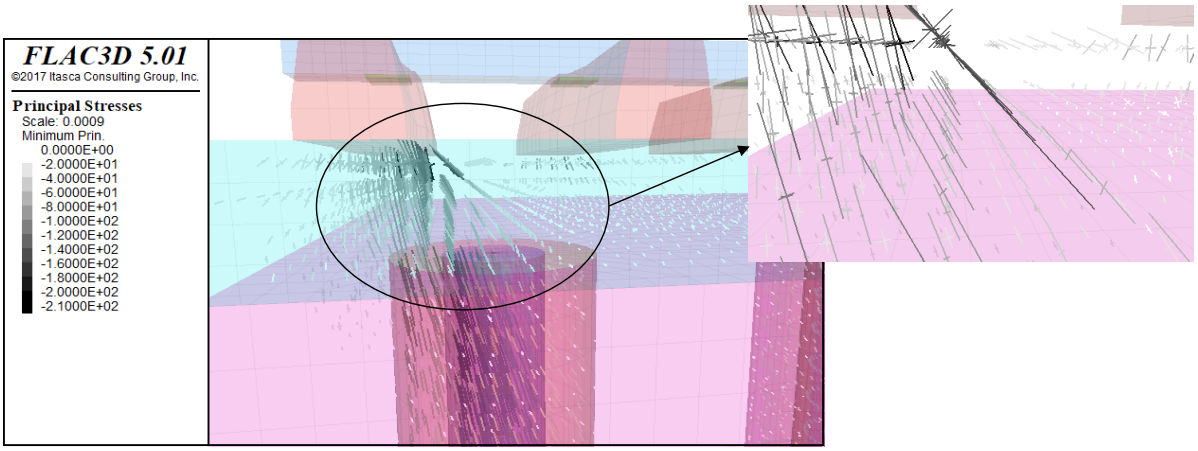

a)

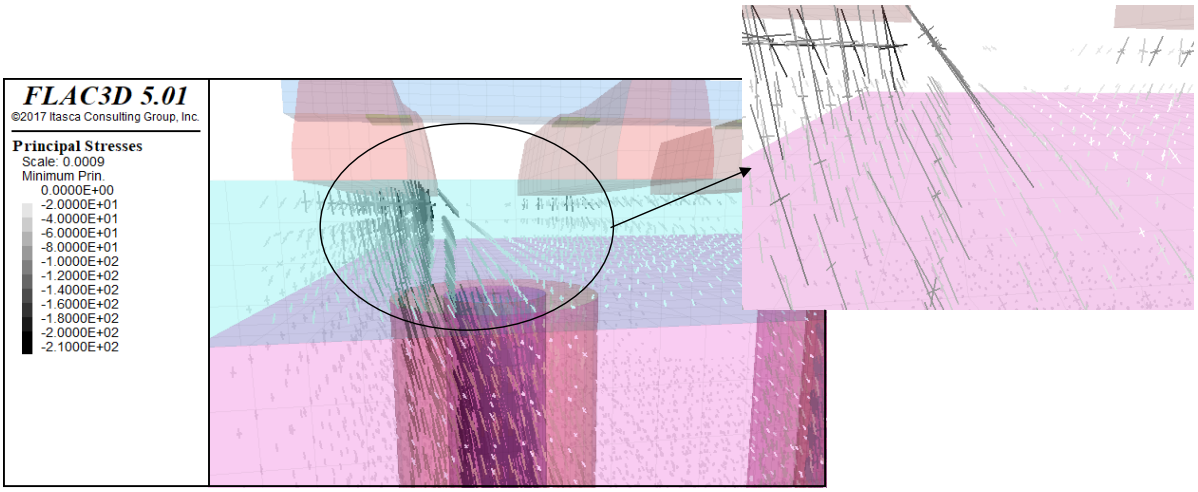

b)

Figure 5.121 -Principal stress tensor vectors, inside the ballast layer, for model CI regarding a) linear elastic and b) non-linear elastic behaviour

Analysing and comparing the previous plots, there are slight differences that help to justify the behaviour mentioned before for the non-linear models. The main difference is the angle that the tensor vectors are making in each model behaviour. For the non-linear model in Figure 5.121-b), the vector has a steeper inclination than in the elastic model. This suggests that the load is being transmitted in a more vertical alignment, concentrating higher stresses in the ballast layer. In the linear elastic models, the loading path has a smaller inclination and the stresses being transmitted by the first sleeper are being spread over a larger area and are even able to reach the second column, as can be seen in Figure 5.122, for model CI1.

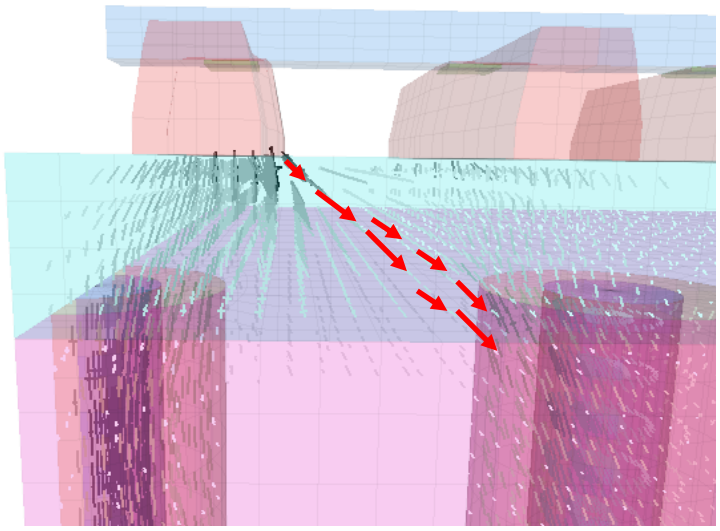

Figure 5.122 - Principal stress tensor vectors, inside the ballast layer, for model CI regarding linear elastic behaviour

As the stresses generated in the ballast are correlated with the elastic modulus assigned calculated for the elements in this layer, it is important to assess the variation of this parameter. As mentioned before, by applying the k-θ model to the ballast layer due to its iterative nature, the composing elements will suffer variations of Young modulus according to the loading they are being submitted to, reaching an ultimate value at different points along the ballast. Previous studies (Paixão [et al.], 2016b, Varandas, 2013) have focused on determining the adequate Young modulus of the ballast material that better reproduce the overall non-linear behaviour of this layer, for a given train load. Those authors verified that, for well performing substructures in plain track and for typical loads of 140-200 kN/axle, adopting a Young modulus between 130 MPa and 160 MPa for the ballast layer, in a linear elastic analysis, will normally yield good approximations to the ballast's actual behaviour.

Therefore, Figure 5.123 was prepared to assess the actual Young modulus that was being calculated by the k-θ model and assigned to the ballast in the present case studies.

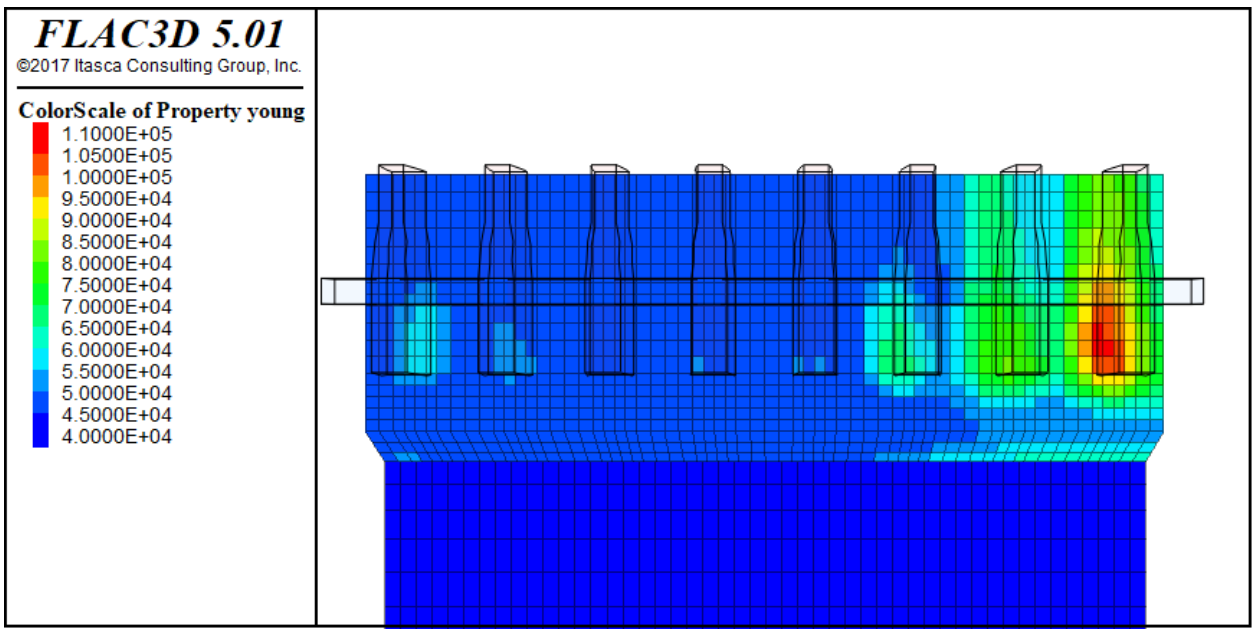

Figure 5.123 -Young modulus' variation on top the ballast layer, for the non-linear analysis in model CE

By analysing the plot in Figure 5.123, it is visible that the Young modulus achieved by this calculation and implemented by the k-θ FISH script, did not reach the expected value mentioned before and attributed to the ballast layer in the linear elastic model (160 MPa). Instead, only a maximum value of $E_r = 105$ MPa was achieved. This could mean that the Young modulus assigned to the linear elastic model is somewhat overestimated and might need to be calibrated taking into consideration that the substructure of the current case studies aims to represent a foundation with poor bearing conditions.

Another remark should be made concerning the studies mentioned before by other authors (Paixão [et al.], 2016b, Varandas, 2013) where it was studied if a constant value of the Young modulus (linear elastic) may reproduce, with enough precision, the overall track behaviour instead of considering the non-linear behaviour of the ballast layer. In the studies presented herein, the axle loads were placed at the transverse vertical plane of symmetry that was located at the centre of a sleeper span. Thus, the axle loads were acting on the rails between two consecutive sleepers, and not directly above a single sleeper. However, the conclusions obtained by the other authors correspond to the results where the axle load was being applied directly above a single sleeper. If the current study considered the axle load directly above a single sleeper, higher stresses would be expected in the ballast layer and, consequently, the k-θ model would yield higher resilient deformation modulus for the ballast under that sleeper. However, if we were to design the model with a sleeper under the loading point, it would not be possible to consider the transverse symmetry and, therefore, it would be necessary to design a model with much larger dimensions, leading to an extensive additional computational effort and model complexity.

5.4.3 IMPACT ON THE TRACK VERTICAL STIFFNESS

To compare the vertical stiffness coefficients obtained for each constitutive model scenario, a ratio between the results for the coefficients was made and is shown in Figure 5.124. It is visible that, by considering the non-linear elastic behaviour of the ballast layer, the magnitude of this coefficient reduced around 8 % from the values obtained with the linear elastic analysis. This result is probably the consequence of the fact that the elastic behaviour of the ballast in the linear elastic models is stiffer than the maximum stiffness achieved for the ballast by the k-θ law in the non-linear elastic models, as discussed above. Another result was that by reducing the vertical stiffness of the track in the non-linear models, more load was being transferred to the adjacent columns further away from the loading area.

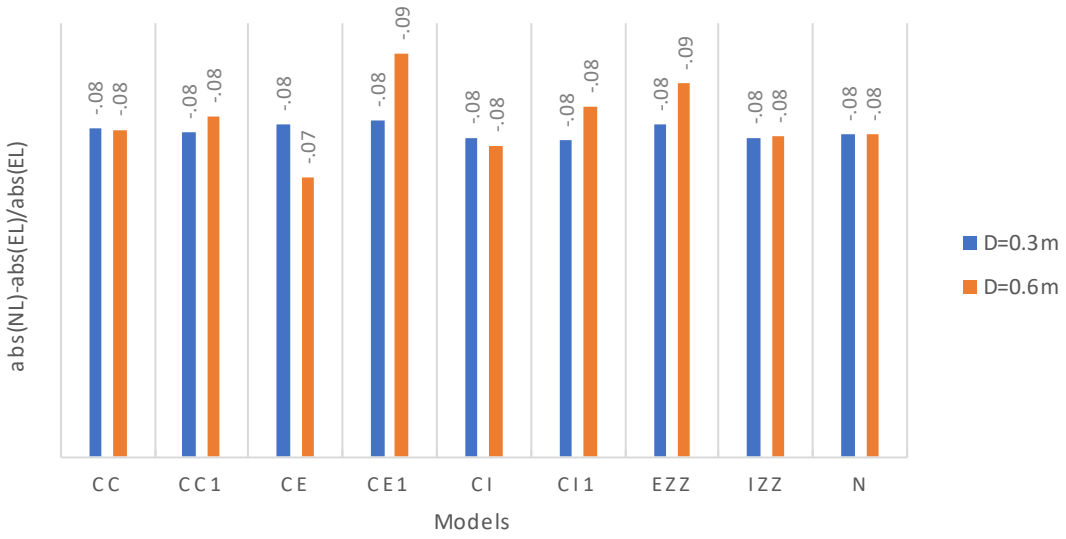

Figure 5.124 -Relative difference between results of vertical stiffness coefficient, between the two model types

6

CONCLUSIONS AND FUTURE DEVELOPMENTS

This closing chapter seeks to present the major conclusions attained in this study and to suggest future developments and research, considering the observations made throughout this analysis.

The present work focused on the elaboration of parametric studies regarding the improvement of the railway track's subgrade resorting to Jet-grout columns, laying them out in various patterns. The scope of this study was the railway's response to such intervention, in what regards stresses and displacements generated by a static train load. The numerical modelling in these studies was made with a finite-difference method (FDM) software - FLAC3D - and the post-processing and analysis of results was carried out with MATLAB.

6.1 MAIN CONCLUSIONS

Due to the subgrade's importance in the overall track behaviour it is very important to properly design it, to perform inspection and maintenance operations and, when necessary, to intervene with appropriate technologies, when track performance is below the expected. Railway track substructure reinforcement with Jet-grout columns is one of many possible ways to intervene and improve the subgrade performance. Since those track operations are very costly, time consuming and disrupt normal railway operation, it becomes imperative to verify their effectiveness. For that purpose, numerical software that use continuous element methods, like FEM or FDM software, are very appropriate tools that allow to simulate, with enough accuracy, various aspects of the structural behaviour before and after such geotechnical interventions.

Since the railway is made up of various elements, when modelling such system, it is essential that all elements are modelled correctly and that the interconnection between the various elements is represented properly. Modelling the track system using continuous element methods entails a compromise between generating a very refined mesh and calculation time (computational effort). Thus, it is necessary to generate an adequate mesh that can yield results as precise as required for the given problem. In some situations, for example due to the geometric complexity of the structures under analysis, it may be advantageous to apply specific numerical techniques to merge different mesh layouts. The numerical modelling studies presented in this thesis, focusing on railway track substructure reinforcement using different column patterns, is one of those situations. In Chapter 3, a series of parametric studies were made comprising FLAC3D commands "ATTACH" and "INTERFACE" that are used to adjoin different mesh types, allowing a deeper insight on how to implement these commands.

The first parametric study allowed to draw conclusions concerning the assignment of the nature of an interface, that depends on the stiffness of the adjacent materials, calculated by Eq. (1), according to the

software's manual. If an interface has two similar materials adjoining it, choosing between a stiff or soft behaviour interface is almost irrelevant, being advised to opt for an interface behaviour based in the stiffer material adjacent to the interface. Nevertheless, if the properties of those adjacent materials differ significantly, as proposed in the software manual, soft interface behaviour should be chosen, to avoid significantly increasing computational effort and calculation times.

The second parametric study had the purpose to compare and distinguish the commands mentioned above, when applied to adjoin distinct types of sub-grids. Results suggested that choosing between the "ATTACH" or "INTERFACE" command will not affect results considerably, suggesting that the application of the "ATTACH" command is satisfactory and more efficient, in terms of calculation effort. Weighing both commands, if no slip or separation is expected at the location where an interface might be placed, it is prudent to choose the "ATTACH" command due to its easier implementation comparing with the "INTERFACE" command, that involves complicated geometric generation and assignment of interface attributes. These parametric studies were made to better understand how to apply these tools when designing a complex model of the railway track system.

Later on, a parametric study on the structural behaviour of the railway track with reinforced substructure was made. The complex model studied was designed as mentioned in Chapter 4, where two types of behaviours were adopted for the ballast layer: i) linear elastic and ii) non-linear elastic using the k-θ model (Brown & Pell, 1967). It was analysed the influence of the Jet-grout column's diameter, column placement and loading position.

In general, both material behaviours yielded comparable results in what concerns the reinforced track's behaviour. However, some differences were found.

When analysing the influence of the column's diameter size, it was seen that, in general, by increasing the column's diameter smaller displacements are obtained for the top of the ballast and foundation and higher displacements occur beneath the Jet column. However, the improvement obtained, displacement-wise, was not very significant when increasing the column's diameter.

Concerning vertical stresses, results demonstrated that an increase in column size leads to higher stress concentrations at the ballast layer, beneath the sleepers. At the foundation level, when a smaller diameter was adopted, higher stress concentrations would occur at a column's position, whereas, with a larger diameter smaller stresses would arise, since there is a larger area for stress spreading. Beneath the Jet-grout columns, higher stresses would develop under the column, for the larger diameter, which could mean that a pressure bulb was created under it. With a larger column diameter, larger pressure bulbs are created as it was seen in these results.

The results of the rail's vertical displacement demonstrated that an increase of the columns radius led to a reduction of the rail's displacement, having the models where the columns are placed closer to the rail a slight better performance.

In the XZ vertical plane, it was observed that with a larger radius, vertical deflections underneath the first sleeper are reduced and that the columns placed in the foundation, might undergo some differential settlements. Regarding vertical stress with depth, it was visible a clear stress path from the bottom of the sleepers to the column, where possibly stresses are being more efficiently directed to with a larger column diameter.

In what regards the influence of reinforcing the substructure, an analysis of the vertical displacements results showed that, in general, with an improved substructure, slightly smaller displacements are obtained under the first sleeper extending till the third sleeper, at the top of the ballast and foundation. At the bottom of the columns, displacements of the improved substructure at that level are roughly higher than the non-improved model. In general, as expected, the reinforced structures under study showed slightly lower vertical displacements assessed at the rail level, having the external column layouts reinforcement showed a better performance.

By analysing the vertical stress results, at the positions where a column is placed, higher stresses are developed at the ballast layer and foundation, possibly due to the presence of the stiffer substructure which directs stresses into that region, creating a clear loading path.

By installing Jet-grout columns in the foundation, the stresses being developed by the train load with depth, instead of spreading evenly throughout the foundation, are being concentrated in limited zones of stiffer nature, being a stress path created from the base of the sleepers to the column. In the XZ plane, lower vertical displacements are observed under the first sleeper however, not so significant.

What regards the influence of the axle load position, with the contour plots it was possible to perceive that displacements are smaller and stresses higher when a column is present beneath the loading point, as expected. By querying vertical stress results at pertinent positions of the track, it was demonstrated that, by applying Jet columns to the substructure, there is a stress reduction in the substructure surrounding the column, in comparison with the original stresses, being most of the load induced stresses now directed to the columns, relieving the surrounding ground.

In terms of vertical stiffness coefficient, with the improved substructure and diameter increase, the track stiffness increased. Column patterns placed externally to the rail showed the highest increase in vertical stiffness. With the diameter increase, the coefficient's value increased constantly, independently of the layout used, except for the CC model.

In general, the main differences between the linear elastic and the non-linear elastic model lay in the stress values, since the consideration of the linear-elastic behaviour for the ballast layer somewhat reproduced the global track behaviour, analysed in terms of vertical displacements.

At the top of the ballast layer, displacements under the first three sleepers are higher, for the non-linear behaviour of the ballast layer. On top of the foundation, the *k-θ* model presented smaller displacements where columns were placed, in comparison to the linear elastic. Beneath the Jet columns, vertical displacements are smaller for the non-linear behaviour, meaning that the columns suffer smaller differential settlements with this analysis. However, these differences mentioned are not very significant.

Rail vertical displacements were demonstrated to be slightly higher for the non-linear elastic behaviour.

Referring to vertical stresses, it was seen that, for a non-linear elastic behaviour, on top of the ballast layer, the first sleeper presented some stress differences at its edges suggesting that sleeper rotation is happening due to the train load. This behaviour was not visible in the linear elastic models. It was also visible that larger stresses were generated beneath each sleeper, for the non-linear analyses. This was an expected behaviour since elements that suffer higher loading experience higher elastic modulus increments, concentrating higher stresses. In general, it was demonstrated that, by opting for a non-linear behaviour for the ballast layer, higher stresses would accumulate at this level.

At the bottom of the ballast layer and top of the foundation, it was visible that, by considering the non-linear behaviour for the ballast, a wider stress redistribution over the columns was happening, not concentrating stresses mainly in the first column, as in the linear elastic models. Despite this, the amount of stress being directed at each column was smaller, when a non-linear behaviour was adopted for the ballast layer, occurring higher stresses in the columns with the linear behaviour, possibly meaning that with the elastic law, the load was being transmitted more directly to the column.

Beneath the Jet-grout columns stress results demonstrated, for a non-linear behaviour, smaller values beneath the first column and higher beneath the remaining ones, corroborating the statement that the other columns are being more loaded in the non-linear analysis. An analysis of the results in the XZ planes also showed that the second column is more loaded in the non-linear analysis.

The results of stress distribuition with depth, under the rail, showed that, for the non-linear analysis, the load path is narrower. By analysing the stress tensor vectors it was seen that inside the ballast layer,

there was a difference in the vectors inclinations, due to different material behaviour. The non-linear model showed steeper inclination in comparison with the elastic one, meaning that loads were being trasmitted in a more vertical manner, thus concentrating higher stresses at the ballast layer under the loading region. It was also visible that the elastic models had the ability of spreading stresses over a larger area, inclusively, being able to directly load other columns adjacent to the one that was right bellow the axle load.

The value of the Young modulus assigned to the linear elastic behaviour of the ballast layer was based in previous studies performed by Paixão [et al.] (2016b) and Varandas (2013). However, when analysing the actual Young modulus that was being calculated by the k- θ model, it was seen that the achieved value was quite lower than the one assigned to the ballast layer in the linear elastic approach, meaning that an overestimation of this parameter was made for this study's conditions. It should be pointed out that the studies mentioned above were made considering a well-performing railway track substructure and that the axle loads were acting in the vertical alignment of a sleeper. This was not case of the studies presented here, where it was intended to simulate a poor-performing substructure and the axle load was applied at mid-span between sleepers.

6.2 FUTURE WORKS AND RECOMMENDATIONS

These parametric studies allowed a better understanding of the railway track's behaviour when its substructure is improved. However, some suggestions for future developments can be made that might allow a deeper and better understanding of this ground improvement methodology.

Results demonstrated that the value achieved for the Young modulus in the ballast layer, in non-linear calculations, was quite lower than the one assigned to the ballast in linear elastic calculations. So, to achieve more realistic results with the linear elastic approach, it is recommended that a calibration of the ballast's Young modulus should be made for linear elastic calculations considering the axle load position and the poor bearing characteristics of the substructure.

This study was made considering the train load as static, however to achieve more realistic results, moving and dynamic train loads should be considered in future studies since it has a very high influence in the stress paths inside the upper layers of the track.

A simplification that was made in this study was the assumption of a perfect bond between the columns and the foundation soil. However, it might be interesting to introduce interface elements surrounding the Jet-grout columns, to investigate the interaction forces that may surge when the railway is loaded and if slip is occurring between the columns and surrounding soil.

Nevertheless, it is recommended that more layout patterns for the columns should be studied, since there are many possible combinations. With this study, it can be advised to study patterns where columns are placed in positions closer to the rail.

REFERENCES

Adam, D.; Vogel, A.; Zimmermann, A. - Ground improvement techniques beneath existing rail tracks. 6th International Conference on Ground Improvement Techniques. Coimbra, Portugal. 18-19 July 2005. (2005).

Adegoke, Clement W.; Chang, Ching S.; Selig, Ernest T. - Study of analytical models for track support systems. 58th Annual Meeting of the Transportation Research Board. Washington District of Columbia, United States. 15-19 January 1979. (1979). p. 12-20.

Allaart, Albert Pieter - Design principles for flexible pavements: a computational model for granular bases. Technische Universiteit Delft. Delft, (1992). Ph.D.

Alves Ribeiro, A.C. - Transições aterro-estrutura em linhas ferroviárias de alta velocidade: análise experimental e numérica. Faculty of Engineering, University of Porto (FEUP). Porto, (2014). Ph.D.

Arulrajah, A.; Abdullah, A.; Bo, M. W.; Bouazza, A. - Ground improvement techniques for railway embankments. *Proceedings of the Institution of Civil Engineers: Ground Improvement*. Vol. 162. n.º 1 (2009). p. 3-14. ISSN: DOI: 10.1680/grim.2009.162.1.3.

Berthelot, P; Pezot, B; Liausu, Ph - Amélioration des sols naturels ou anthropiques par colonnes semi-rigides: Le procédé CMC. 13th European Conf. on Soil Mechanics and Geotehnical Engineering (XIII ECSMGE). Prague, Czech Republic. (2003). p. 25-29.

Brecciaroli, Fabrizio; Kolisoja, Pauli - Deformation behaviour of railway embankment materials under repeated loading - Literature review. Helsinki: Finish Rail Admnistration A 5/2006, (2006). ISBN: 952-445-147-6

Broms, B B - Design of lime, lime/cement and cement columns. Keynote lecture. International Conference on Dry Mix Methods for Deep Soil Stabilization. Stockholm, Sweden 13-15 October 1999. Balkema. (1999). p. 125-153. ISBN:

Brown, SF; Pell, PS - An experimental investigation of the stresses, strains and deflections in a layered pavement structure subjected to dynamic loads. Intl Conf Structural Design Asphalt Pavements. Michigan, Ann Arbor. (1967). p. 487-504.

Burrow, MPN; Bowness, D; Ghataora, GS - A comparison of railway track foundation design methods. *Proceedings of the Institution of Mechanical Engineers, Part F: Journal of Rail and Rapid Transit*. Vol. 221. n.º 1 (2007). p. 1-12. ISSN: 0954-4097. DOI:

Calon, Nicolas; Robinet, Alain; Mosser, JF; Reiffsteck, Philippe; Guilloux, Alain; Cui, Yu-Jun - Improvement of railroad platforms by column of soil mixing. 9th WCRR. Lille, France. May 22-26 2011. (2011).

CEN - 12715: Execution of special geotechnical work: Grouting. 2000). ISBN/ISSN:

CEN - 14679: Execution of special geotechnical works–Deep Mixing. 2005). ISBN/ISSN:

Chang, Ching S; Adegoke, Clement W; Selig, Ernest T - GEOTRACK model for railroad track performance. *Journal of Geotechnical and Geoenvironmental Engineering*. Vol. 106. n.º 11 (1980). ISSN: 1090-0241. DOI:

Chrismer, SM; Read, DM - Examining ballast and subgrade conditions. *Railway Track and Struct., AREA*. (1994). p. 39-42. ISSN: DOI:

Chu, Jian; Varaksin, Serge; Klotz, Ulrich; Mengé, Patrick - Construction processes. Proceedings of the 17th International Conference on Soil Mechanics and Geotechnical Engineering. Alexandria, Egypt. 5-9 October 2009. (2009). p. 3066-3135.

Correia, A Gomes; Loizos, A. - Evaluation of mechanical properties of unbound granular materials for pavements and rail tracks. Proceedings of the International Seminar on Geotechnics in Pavement and Railway Design and Construction. Athens, Greece. Millpress. (2004). p. 35-60. ISBN: 90-5966-038-2

Dahlberg, Tore - Railway track dynamics-a survey. *Linköping University*. (2003). ISSN: DOI:

Denies, N; Van Lysebetten, G - General Report Session 4–SOIL MIXING 2–DEEP MIXING. Proceedings of the International Symposium of ISSMGE-TC211. Recent research, advances & execution aspects of ground improvement works. 31 May-1 June 2012, Brussels, Belgium (2012). ISBN:

EC - Panorama of transport- Statistical overview of transport in the European Union Theme 7 -Transport. Luxembourg: Office for Official Publications of the European Communities, (2003). ISBN: 92-894-4993-4

EC - White Paper on transport :Roadmap to a single European transport area :Towards a competitive and RESOURCE-EFFICIENT transport system Luxembourg Publications Office of the European Union, (2011). ISBN: 978-92-79-18270-9

EC - EU transport in figures General and regional statistics-Statistical books. Brussels: 2014). ISBN:

EC - Key figures on Europe. Luxembourg: Publications Office of the European Union, (2017). ISBN: 978-92-79-63348-5

Ekberg, Anders; Paulsson, Björn - INNOTRACK: concluding technical report. International Union of Railways (UIC), (2010). ISBN: 2746118505

Esmaeili, Morteza; Hakimpour, Seyed Mehrab - Three Dimensional Numerical Modelling of Stone Column to Mitigate Liquefaction Potential of Sands. *Journal of Seismology and Earthquake Engineering*. Vol. 17. n.º 2 (2015). ISSN: DOI:

Esmaeili, Morteza; Zakeri, Jabbar Ali; Babaei, Mohammad - Laboratory and field investigation of the effect of geogrid-reinforced ballast on railway track lateral resistance. *Geotextiles and Geomembranes*. Vol. 45. n.º 2 (2017). p. 23-33. ISSN: 0266-1144. DOI: http://dx.doi.org/10.1016/j.geotexmem.2016.11.003.

Essler, R - Application of Ground Improvement: Jet Grouting. ISSMGE TC211. International Society for Soil Mechanics and Geotechnical EngineeringApplication of Ground Improvement: Jet Grouting.-(2008).

Essler, R; Kitazume, M - Application of Ground Improvement: Deep Mixing. ISSMGE TC211 International Society for Soil Mechanics and Geotechnical EngineeringApplication of Ground Improvement: Deep Mixing.-(2008).

Fatahi, Behzad; Khabbaz, Hadi - Optimising The Pattern Of Semi-Rigid Columns To Improve Performance Of Rail Tracks Overlying Soft Soil Formation. *Australian Geomechanics Journal*. Vol. 48. n.º 3 (2013). p. 89-97. ISSN: 0818-9110. DOI:

Fatahi, Behzad; Khabbaz, Hadi; Liem Ho, Huu - Effects of geotextiles on drainage performance of ballasted rail tracks. *Australian Geomechanics*. Vol. 46. n.º 4 (2011). p. 91-102. ISSN: 0818-9110. DOI:

Fortunato, Eduardo - Renovação de Plataformas Rodoviárias. Estudos relativos à capacidade de carga. Universidade do Porto. (2005). Ph.D.

Fortunato, Eduardo; Paixão, André - Novas soluções de superestrutura de via para Alta Velocidade Ferroviária. Lisboa: LNEC, (2009). ISBN/ISSN: 978-972-49-2173-0.

Fortunato, Eduardo; Resende, Ricardo - Mechanical behaviour of railway track structure and foundation-Three dimensional numerical modelling. Proc. of RailFound 06 - International Conference on Railway Track Foundations. Birmingham, UK. 11-13 September 2006. University of Birmingham Press. (2006). p. 217-227. ISBN: 0704426005

HaywardBakerInc. - Jet Grouting. Keller Worlwide, (2011). ISBN/ISSN:

Huang, Yang Hsien - Pavement analysis and design. 2nd. Englewood Cliffs, NJ: Pearson Prentice Hall, (1993). ISBN: 0-13-142473- 4

Hughes-Hallet, Deborah; McCallum, William G; Gleason, Andrew M - Calculus:Single and Multivariable. 6. John Wiley & Sons., (2013). ISBN: 978-0470-88861-2

INNOTRACK - D 2.2.1 State of the art report on soil improvement methods and experience. D 2.2.1 State of the art report on soil improvement methods and experience.-(2008).

INNOTRACK - D 2.2.5 Subgrade reinforcement with columns. Part 1 Vertical columns, Part 2 Inclined columns. D 2.2.5 Subgrade reinforcement with columns. Part 1 Vertical columns, Part 2 Inclined columns.-(2009).

Itasca - FLAC 3D: User Manual. Minneapolis, MN, USA: Itasca Consulting Group, (2015). ISBN/ISSN:

Jardine, RJ - Some observations on the kinematic nature of soil stiffness. *Soils and foundations*. Vol. 32. n.º 2 (1992). p. 111-124. ISSN: 0385-1621. DOI:

Jenck, Orianne; Dias, Daniel; Kastner, Richard - Three-dimensional numerical modeling of a piled embankment. *International Journal of Geomechanics*. Vol. 9. n.º 3 (2009). p. 102-112. ISSN: 1532-3641. DOI:

Jianmin, Z - Modelling and optimizing track maintenance and renewal. University of Birmingham. (2007). Ph.D.

Kempfert, Hans-Georg; Raithel, Marc - Chapter 21 - Soil Improvement and Foundation Systems with Encased Columns and Reinforced Bearing Layers -Ground Improvement Case Histories. San Diego: Butterworth-Heinemann, 2015. - Chapter 21 - Soil Improvement and Foundation Systems with Encased Columns and Reinforced Bearing Layers ISBN: 978-0-08-100698-6.

Koch, E; Szepesházi, R - Laboratory tests and numerical modeling for embankment foundation on soft chalky silt using deep-mixing. Proc. of the 18 th Intern. Conf. on Soil Mechanics and Geotechnical Engineering.–Paris. (2013). p. 2521-2524. ISBN:

Koerner, Robert M - Designing with geosynthetics 1. Xlibris Corporation, (2012). ISBN: 978-1-4628-8290-8

Le Kouby, Alain; Bourgeois, Emmanuel; Rocher-Lacoste, Frédéric - Subgrade improvement method for existing railway lines–an experimental and numerical study. *Electronic Journal of Geotechnical Engineering*. Vol. 15. n.º E (2010). p. pp 461-494. ISSN: DOI:

Lekarp, Fredrick; Isacsson, Ulf; Dawson, Andrew - State of the art. I: Resilient response of unbound aggregates. *Journal of transportation engineering*. Vol. 126. n.º 1 (2000). p. 66-75. ISSN: 0733-947X. DOI:

Li, Dingqing; Selig, Ernest T - Method for railroad track foundation design. I: Development. *Journal of Geotechnical and Geoenvironmental Engineering*. Vol. 124. n.º 4 (1998). p. 316-322. ISSN: 1090-0241. DOI:

Madhavi Latha, G; Rajagopal, K; Krishnaswamy, NR - Experimental and theoretical investigations on geocell-supported embankments. *International Journal of Geomechanics*. Vol. 6. n.º 1 (2006). p. 30-35. ISSN: 1532-3641. DOI:

McGown, A; Brown, SF - Applications of reinforced soil for transport infrastructure. Proc. of the 1st Int. Conference on Transportation, Geotechnics, Nottingham, UK., Advances

in Transportation Geotechnics–E. Ellis, HS Yu, G. McDowell, A. Dawson, N. Thom (Eds), CRC Press, Taylor & Francis Group, London. (2008). p. 27-36. ISBN:

Montenegro, Pedro - A methodology for the assessment of the train running safety on bridges. Faculty of Engineering of University of Porto. Porto, (2015). Ph.D.

Moreno, Javier; González, Javier; Santos, Antonio; Cuéllar, Vicente - SUPERTRACK:Retrofitting of track sections by hydraulic fracture injections. Laboratorio de Geotecnia, CEDEXSUPERTRACK:Retrofitting of track sections by hydraulic fracture injections.-(2005).

Morteza, Esmaeli; Mosayebi, Seyed Ali - Factors affecting jet grouting applicability in stabilizing loose railway subgrades. Proceedings of the 43rd Symposium on Engineering Geology and Geotechnical Engineering:water, soils and sustainability in the intermountain West. Las Vegas, Nevada, USA. 23-25 March 2011. Engineering Geology and Geotechnical Engineering Symposium (EGGES). (2011). p. 87-101. ISBN: 9781622762491

Moseley, Michael P; Kirsch, Klaus - Ground improvement Spon Press, (2004). ISBN: 0203305205

Nimbalkar, Sanjay; Indraratna, Buddhima - Field Assessment of Ballasted Railroads Using Geosynthetics and Shock Mats. *Procedia Engineering*. Vol. 143. (2016). p. 1485-1494. ISSN: 1877-7058. DOI: http://dx.doi.org/10.1016/j.proeng.2016.06.175.

Okada, Hiroshi - High-speed railways in China. *Japan Railway & Transport Review*. n.º 48 (2007). p. 22-29. ISSN: DOI:

Paixão, André - Transition zones in railway tracks-An experimental and numerical study on the structural behaviour. Faculty of Engineering of University of Porto. Porto,Portugal, (2014). Ph.D.

Paixão, André; Fortunato, Eduardo - Análise estrutural de via-férrea com recurso a um modelo numérico tridimensional. 3as Jornadas Hispano Portuguesas sobre Geotecnia en las Infraestructuras Ferroviarias. Madrid. 25-26 June. (2009).

Paixão, André; Fortunato, Eduardo - Rail track structural analysis using three-dimensional numerical models. 7th European Conference on Numerical Methods in Geotechnical Engineering (NUMGE2010). Trondheim. 02-04 Jun. 2010. (2010). p. 575-580.

Paixão, André; Fortunato, Eduardo; Calçada, Rui - A numerical study on the influence of backfill settlements in the train/track interaction at transition zones to railway bridges. *Proceedings of the Institution of Mechanical Engineers, Part F: Journal of Rail and Rapid Transit*. Vol. 230. n.º 3 (2016a). p. 866-878. ISSN: 0954-4097. DOI:

Paixão, André; Varandas, José N.; Fortunato, Eduardo; Calçada, Rui - Non-Linear Behaviour of Geomaterials in Railway Tracks under Different Loading Conditions. *Procedia Engineering*. Vol. 143. (2016b). p. 1128-1135. ISSN: 18777058. DOI: 10.1016/j.proeng.2016.06.147.

Pirapakaran, K.; Sivakugan, N. - Numerical and experimental studies of arching effects within mine fill slopes. Proceedings of the 6th International Conference on Physical

Modelling in Geotechnics - Physical Modelling in Geotechnics - 6th ICPMG '06. Hong Kong. (2006). p. 1519-1525. ISBN: 0415415861

Pires, J.; Phuong, H.T.M.; Dumont, A.G.; Vajdić, M.; Lenart, S.; Oslaković, I. Stipanović - SMARTRAIL – DEL 3.2 Rehabilitation of Open Tracks and Transition Zones. SMARTRAIL – DEL 3.2 Rehabilitation of Open Tracks and Transition Zones.-(2014).

Poorooshasb, H. B.; Meyerhof, G. G. - Analysis of behavior of stone columns and lime columns. *Computers and Geotechnics*. Vol. 20. n.º 1 (1997). p. 47-70. ISSN: 0266-352X. DOI: http://dx.doi.org/10.1016/S0266-352X(96)00013-4.

Potts, David M; Zdravkovic, Lidija; Zdravković, Lidija - Finite element analysis in geotechnical engineering: application. Thomas Telford, (2001). ISBN: 0727727834

Powrie, W; Yang, LA; Clayton, Chris RI - Stress changes in the ground below ballasted railway track during train passage. *Proceedings of the Institution of Mechanical Engineers, Part F: Journal of Rail and Rapid Transit*. Vol. 221. n.º 2 (2007). p. 247-262. ISSN: 0954-4097. DOI:

Prause, Robert H; Kennedy, James C - Parametric study of track response. Parametric study of track response.-(1977).

Priebe, H. J. - The design of vibro replacement. *Ground Engineering*. Vol. 28. n.º 10 (1995). p. 31-37. ISSN: 0017-4653. DOI:

Profillidis, Vassilios A - Railway engineering. Ashgate, (2000). ISBN: 9780754612797

Raju, V.R. - Ground improvement techniques for railway embankments. Railtech Conference. (2003). ISBN:

Ribeiro, Ana - Técnica de tratamento de solos–Jet Grouting. Universidade Técnica de Lisboa. (2010). MSc

Ribeiro, Viviana - Estudos sobre métodos não destrutivos de caracterização do comportamento dinâmico da viaférrea com diversos tipos de fundação. Faculty of Engineering of Univeristy of Porto. Porto, (2015). MSc

Selig, E. T.; Waters, J. M. - Track geotechnology and substructure management. London: Thomas Telford Publications, (1994). ISBN: 0727720139

Stewart, Harry - The prediction of track performance under dynamic traffic loading. University of Massachusetts Amherst. (1982). Ph.D.

Sunaga, Makoto; Hifumi, AOKI - Development of slab tracks for Hokuriku Shinkansen line. *Quarterly Report of RTRI*. Vol. 42. n.º 1 (2001). p. 35-41. ISSN: 0033-9008. DOI:

Taciroglu, Ertugrul - Constitutive modeling of the resilient response of granular solids. University of Illinois at Urbana-Champaign. Urbana, Illinois, (1998). Ph.D.

Tarabji, SD; Thompson, MR - PROGRAM ILLI-TRACK: Finite Element Analysis of a Railway Track Support System,User's Manual. PROGRAM ILLI-TRACK: Finite Element Analysis of a Railway Track Support System,User's Manual.-(1976).

Teixeira, Paulo - Contribución a la reducción de los costes de mantenimiento de vías de alta velocidad mediante la opitimización de su rigidez vertical. Universitat Politècnica de Catalunya. (2004). Ph.D.

Townsend, Frank C; Anderson, J Brian - A compendium of ground modification techniques. Florida Department of Transportation. A compendium of ground modification techniques.-(2004).

UIC - Track-Bed Layers for Railway Lines (UIC Code 719 R). International Union of Railways, Paris, France. Track-Bed Layers for Railway Lines (UIC Code 719 R).-(2008).

Varandas, J.N. - Long-term behaviour of railway transitions under dynamic loading application to soft soil sites. Faculdade de Ciências e Tecnologia da Universidade Nova de Lisboa- FCT/UNL. Lisboa, (2013). Ph.D.

Varandas, J.N.; Paixão, André; Fortunato, Eduardo - A study on the dynamic train-track interaction over cut-fill transitions on buried culverts. *Computers & Structures*. Vol. 189. (2017). p. 49-61. ISSN: 0045-7949. DOI:

Varandas, J.N.; Paixão, André; Fortunato, Eduardo; Hölscher, Paul - A Numerical Study on the Stress Changes in the Ballast Due to Train Passages. *Procedia Engineering*. Vol. 143. (2016). p. 1169-1176. ISSN: 18777058. DOI: 10.1016/j.proeng.2016.06.127.

Varandas, J.N.; Paixão, André; Fortunato, Eduardo; Hölscher, Paul; Calçada, Rui - Numerical modelling of railway bridge approaches: influence of soil non-linearity. *The Int. J. of Railway Technology*. Vol. 3. n.º 4 (2014). p. 73-95. ISSN: DOI:

Wu, Jiu-Jiang; Li, Yan; Cheng, Qian-Gong; Wen, Hua; Liang, Xin - A simplified method for the determination of vertically loaded pile-soil interface parameters in layered soil based on FLAC3D. *Frontiers of Structural and Civil Engineering*. Vol. 10. n.º 1 (2016). p. 103-111. ISSN: 2095-2449. DOI: 10.1007/s11709-015-0328-4.

Zeghal, Morched - Discrete-element method investigation of the resilient behavior of granular materials. *Journal of Transportation Engineering*. Vol. 130. n.º 4 (2004). p. 503-509. ISSN: 0733-947X. DOI: